Late Quaternary Volcano-Tectonic Evolution

of the

Mono Basin, Eastern California

Thesis by

Marcus Ivan Bursik

In Partial Fulfillment of the Requirements

for the Degree of

Doctor of Philosophy

California Institute of Technology

Pasadena, California

1989

(submitted June 9, 1988)

ACKNOWLEDGEMENTS

Creek Campground ever pleasant.

Mark Fahnestock, Jan Mayne, Niki Cervantes and the people in Graphic Arts lent invaluable assistance with the mechanical production of the thesis. The generosity of Jim Westphal and Pat Cuccaro is also greatly appreciated.

I thank Niki for consistently believing in me as I struggled through various stages of the dissertation blues.

ABSTRACT

The Mono Basin of eastern California provides an ideal laboratory in which to study the interaction of volcanic and tectonic processes. The late Quaternary geological record of volcanic activity and range-front faulting is relatively complete in the basin. Range-front faults of the Sierra Nevada offset dateable late Pleistocene glacial moraines, thus affording the opportunity to estimate range-front slip rates. The first two chapters concern dating of moraines that are offset by range-front faults.

In Chapter One, I discuss the ages of the glacial moraines of the Mono Basin and their correlation between canyons. I dated the moraines by studying their morphology and the relative weathering of granitic boulders atop their crests, and by use of the clast-sound velocity (CSV) dating technique. The CSV technique consists of measuring the p-wave speed (V_p) in morainal boulders. V_p decreases with age as boulders weather. Clast-sound velocities enabled statistical division of moraines in each canyon into differently weathered deposits. Relative weathering features of boulder surfaces further helped discern age differences between moraines in a single canyon. Finally, CSV, relative weathering and moraine morphology, considered together, allowed correlation of moraines to an established glacial sequence, and therefore, correlation between canyons. Regression of mean V_p against best estimates of glaciation ages within the glacial sequence provided a further check on the validity of the correlations.

Moraines in all major canyons from Lee Vining south were correlative with the standard late Pleistocene sequence of Tioga, Tenaya, Tahoe and Mono Basin deposits. At Lundy Canyon, however, Tahoe and Tenaya moraines are poorly, if at all, preserved. The prominent moraines extending into the basin are probably

of Tioga age. Poor preservation of Tenaya and Tahoe deposits may be due to the narrow, steep-sided morphology of Lundy Canyon, and rapid down-dropping on the range-front fault.

In Chapter Two, I discuss the application of a new quantitative dating technique to the moraines of Lee Vining Canyon. At Lee Vining Canyon, I measured cross-sectional profiles of lateral moraines of different ages to determine whether the degree to which they have been degraded could be used as a relative-dating method. Correlation of the degree of moraine degradation against an independent measure of age suggested that relative ages of late Pleistocene lateral moraines can be inferred from moraine profiles.

Analysis of the degradation of moraine profiles with a diffusion model resulted in equations that relate profile width and maximum slope angle to age. In accordance with the diffusion model, the functional relationship between profile width and estimated age was found to be nearly linear for the moraines of Lee Vining Canyon. Fits of model to data were good, despite evidence of transport of material by non-linear diffusive processes along some of the profiles.

Maximum slope angle is inversely proportional to age according to the diffusion model. Regression of mean maximum slope angle against inverse age for the group of moraines from Lee Vining Canyon suggested that the relationship between the two variables is expressed by the diffusion model.

Deviations of model profile shapes from true shapes suggested that in addition to moraine age, initial profile shape and non-diffusive degradation processes are important in controlling the relationship between slope parameters and age over spans of 10^4 years.

In Chapter Three, I use moraine ages determined in Chapter One to

estimate slip rates of range-front faults. For Chapter Three, I measured fault-scarp profiles on the dated lateral moraines of the Mono Basin to determine fault slip rates. I compared these data with what can be deduced about the extension rate due to dike intrusion underneath the Mono Craters. I then considered extension rates in the context of regional strain patterns to infer the mode of deformation and strain relief in the Mono Basin during late Quaternary time.

The extension-rate data indicate that dikes are being intruded underneath the Mono Craters in response to crustal stretching, and because of this, are now accommodating elastic strain that was once accommodated by range-front normal faulting. The section of the range front near the craters accommodated as much as 1 mm/yr of extension until 40,000 to 70,000 years ago. For the past 40,000 to 70,000 years, this section of range front has become inactive, even though extension along the range front to north and south has continued at up to 0.9 mm/yr. Dikes have been intruding underneath the Mono Craters for the past 40,000 years. Depending upon the assumptions used to calculate dike intrusion rates, the dikes accommodate 1 mm/yr of tectonic extension that was previously accommodated by range-front faulting.

Consideration of the extension rates in the context of regional tectonic strain patterns suggests that the Mono Craters are forming along one of the extensional boundary structures of a pull-apart basin, the other extensional boundary of which is the deactivated range-front segment.

If the Mono Craters represent an early stage of caldera formation, then their formation within a pull-apart zone may indicate that this is an ideal tectonic environment in which to form certain types of calderas.

TABLE OF CONTENTS

CHAPTER 2: Determination of Ages of Moraines at Lee Vining Canyon from Landform Degradation

Chapter 3: Evolution of the Sierra Nevada Range Front in the Mono Basin and the Relationship of Range-Front Faulting to Volcanism

CHAPTER 1

LATE PLEISTOCENE GLACIAL CHRONOLOGY OF THE MONO BASIN

INTRODUCTION

Reason for the Present Work

This study of the glacial moraines in the Mono Basin of eastern California (Figure 1-1) was undertaken as part of a larger work to determine late Quaternary slip rates of range-front faults of the Sierra Nevada in the Mono Basin. Glacial moraines are important to understanding the tectonic history of the basin because they are the most readily dated late Quaternary deposits along the range front, and because fault scarps are best preserved where they cross moraine crests.

Another goal, secondary to the above for my own purposes, but equally as important in its own respect, was to determine the degree to which moraines could be differentiated on the basis of weathering features and, therefore, to determine the number of separate glaciations represented by the moraines, which are so prominent in the basin. The number and timing of differentiable glacial stages represented by Sierran moraines has been a point of great controversy in the community of glacial geologists, as the next section outlines.

Previous Work

Discussions or maps of the Pleistocene glacial geology of parts of the Mono Basin appear in Russell (1889), Blackwelder (1931), Putnam (1949; 1950),
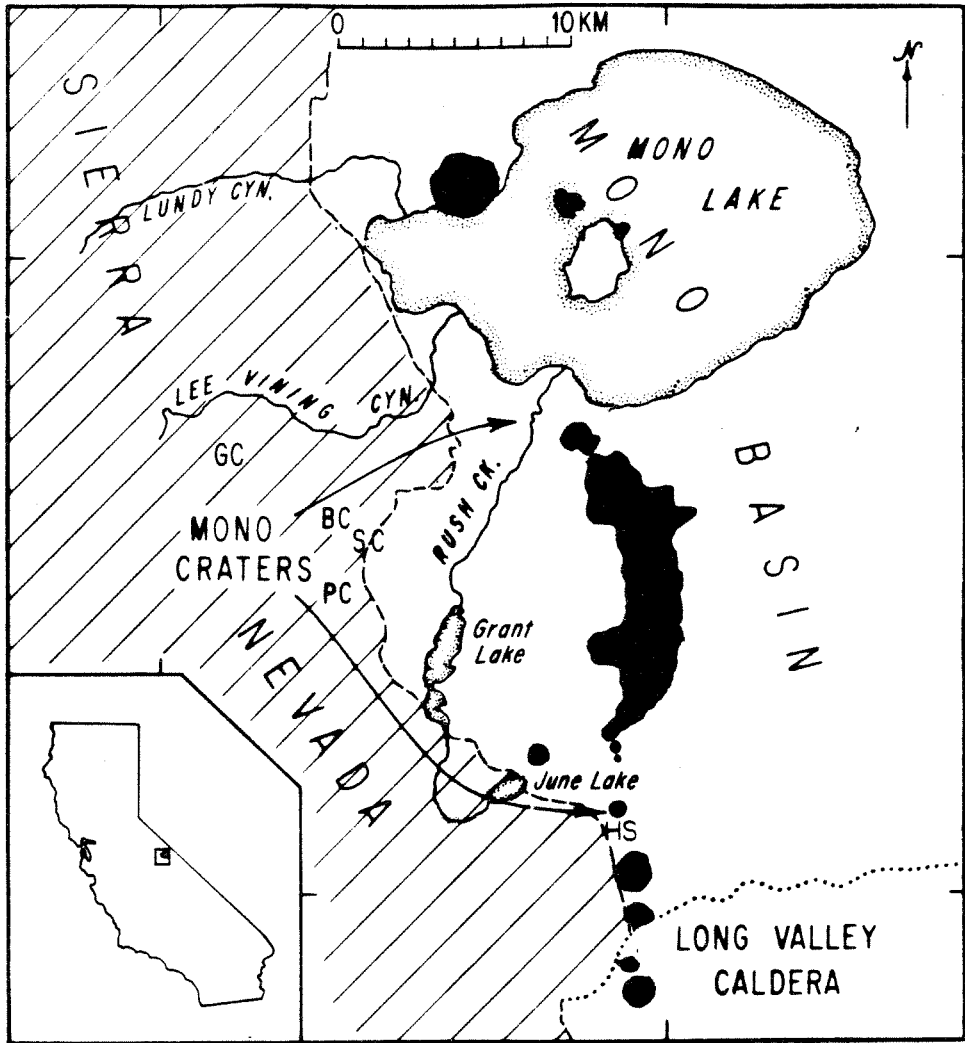
Figure 1-1. Location of the Mono Basin and geographic features. GC = Gibbs Canyon, PC = Parker Canyon, BC = Bloody Canyon, SC = Sawmill Canyon, HS = Hartley Springs. Piedmont moraines were studied at June and Grant Lakes, Hartley Springs, Parker Canyon, Lee Vining Canyon and Lundy Canyon. Moraines at Bloody Canyon have been studied extensively by other workers. Moraines within the Sierra Nevada at Gibbs Canyon were mapped by Sharp and Birman (1963).

Kistler (1966a), Sharp and Birman (1963), Birman (1964), Chesterman and Gray (1975), Lachmar (1977), Bailey and Koeppen (1977), Clark (1979), Burke and Birkeland (1979), Gillespie (1982) and Mathieson (1984).

Russell (1889) convincingly argued the existence of glacial deposits of two different ages at June and Grant Lakes, and showed evidence for deposits of at least three glaciations at Parker and Bloody Canyons. Blackwelder (1931) used weathering features of glacial deposits as criteria to distinguish till of different ages along the eastern Sierra Nevada and throughout the Basin Ranges. He divided late Quaternary glacial deposits -- those characterized by prominent lateral and terminal moraines --into Tioga (younger) and Tahoe (older) glaciations (Table 1-1). He also found tills which, he believed, were deposited during mid-Pleistocene (Sherwin) and early Pleistocene (McGee) glaciations. Putnam (1949; 1950), Chesterman and Gray (1975) and Kistler (1966a) used Blackwelder's nomenclature, and mapped Tioga, Tahoe and Sherwin deposits throughout the Mono Basin.

Sharp and Birman (1963) refined Blackwelder's methods for quantifying differential weathering features and were able to distinguish Mono Basin and Tenaya moraines from Tioga and Tahoe moraines at Bloody Canyon. Bailey and Koeppen (1977) used Sharp and Birman's nomenclature and mapped Tioga, Tenaya, Tahoe and Mono Basin deposits at June and Grant Lakes.

Although Burke and Birkeland (1979) argued against the additions to Blackwelder's glacial sequence made by Sharp and Birman (1963), Gillespie (1982) found evidence that the Tahoe moraines of Sharp and Birman (1963) at Bloody Canyon were formed during two separate advances (Tahoe I and Tahoe II). He suggested (Gillespie, 1984) that the earlier, Tahoe I, moraine be assigned to the Mono Basin glaciation, since he was unable to differentiate it from the

Table 1-1. Ages of glaciations of the Mono Basin.

Glacial stage names used in this study	Oxygen isotope stage	Age[a], best estimate	Age range for CSV regression	Pertinent bracketing ages
Hilgard	End 2			10,060+/-130 [1] c. 14,000 [2]
Tioga	2	14,000	11,000-21,000	c. 11,000 [3] 12,000-14,000 [4] c. 14,100 [5] 13,900-18,900 [6] 21,000+/-130 [7] 24,000-26,000 [4]
Tenaya	2+	40,000	34,000-43,000	34,000-36,000 [4] 34,000-40,000 [8]
Tahoe	4	66,000	60,000-85,000	60,000-85,000 [8] 65,000-79,000 [9] 118,000+/-7,000 [10]
Mono Basin	6+	130,000	130,000-198,000	130,000+/-1,000 [11] 131,000+/-10,000 [12] 132,000-198,000 [13] 185,000+/-90,000 [14]
Sherwin	18-22?	750,000	708,000-900,000	708,000+/-15,000 [15] 900,000 [16]

[a] Except for Hilgard, these are ages which Crook and Gillespie
(1986) found to correlate well with mean V_p.

Sources for age data:
(1) ^{14}C date on overlying peat (Mezger, 1986).
(2) Two youngest ^{14}C dates on Tioga stage (Dorn et al., 1987;
Marchand and Allwardt, 1981), which predates Hilgard stage.
(3) Cluster of ^{14}C ages in overlying peat (Fullerton, 1986; Mezger, 1986).
(4) ^{14}C age of highstands in Mono Lake which may follow glacial maximum by
up to 7,000 years (Lajoie and Robinson, 1982).
(5) Wood in Tioga age deposits (Marchand and Allwardt, 1981).
(6) Range of ^{14}C rock varnish ages on Tioga (?) boulders (Dorn et al., 1987).
(7) ^{14}C on tufa in beach deposit overlain by Tioga fan (Lubetkin, 1980).
(8) ^{14}C and sed. rate on highstands in Searles Lake (Smith, 1979).
(9) Oxygen isotope stage 4 (Richmond and Fullerton, 1986).
(10) Ar-Ar on basalt underlying Tahoe till (Gillespie, 1982).
(11) U-Th on beginning of sea-level highstand (stage 5(?)) (Edwards et al., 1987)
(12) Ar-Ar on basalt overlying pre-Tahoe (Mono Basin ?) till (Gillespie, 1982).
(13) Oxygen isotope stage 6 (Richmond and Fullerton, 1986).

Mono Basin moraines of Sharp and Birman (1963). Gillespie also showed that two pre-Mono Basin moraine remnants lay outboard of the Mono Basin moraines at Bloody Canyon.

When the present study was begun, then, moraines at Bloody Canyon had been studied carefully by several workers, who came to seemingly incompatible conclusions. No thorough studies of moraines in other canyons had been undertaken.

Description of Present Work

As stated above, the foremost goal of this research was to compare offset rates of faults that cut moraines issuing from the canyons of the Mono Basin. In order to do this, it was important to be able to correlate moraines of the same age between canyons. I did this by studying the moraines in each canyon separately to determine which moraines were deposited at significantly different times, as shown by differences in weathering features. I then correlated moraines to established glacial stages by using weathering and morphological criteria that are thought to be diagnostic of age. Blackwelder (1931) and Birman (1964) have probably compiled the most useful information for correlating deposits to glacial stages. Some of their criteria are shown in Figure 1-2 and are discussed more fully in later sections.

Outline of Present Work

In the discussion that follows, I first present the methods used to date and correlate moraines. Next, I discuss the glacial geology within each canyon and suggest correlations to the standard glacial sequence shown in Table 1-1. I conclude with a discussion of the late Pleistocene glacial

Figure 1-2. a) Schematic diagram of nested moraines showing morphological features diagnostic of age. View is oblique aerial view looking down moraine, b) Relative weathering features of boulders on moraines of different ages. These features have been used to determine ages of moraines relative to one another and to correlate moraines between canyons.

MORPHOLOGICAL FEATURES OF MORAINES
USEFUL FOR RELATIVE DATING

MONO BASIN has broad crest, shallow-sloping flanks

TIOGA grades to late Pleistocene lake terrace; older moraines cut by terrace

TAHOE most extensive

TAHOE higher than TENAYA and TIOGA

MONO BASIN deeply dissected by gullies

TIOGA moraine slightly breached by axial stream

TIOGA to TAHOE progressively broader crests, shallower flanks

MONO BASIN buried by TAHOE

gullies in TAHOE, few in TENAYA and TIOGA

7

Figure   1-2 a

SHARP
CREST

STEEP
FLANK

fresh surfaces;
shallow or no
weathering pits;
unburied

Glacial
striae

UNWEATHERED

BOULDERS

"YOUNG" MORAINE

deep weathering pit

BROAD CREST

fretted surface

GENTLE
FLANK

buried

WEATHERED

BOULDERS

"OLD" MORAINE

RELATIVE WEATHERING OF
BOULDERS ON MORAINES

Figure   1-2b

history of the Mono Basin.

DATING METHODS

General Statement

Glacial moraines are composed of poorly sorted till and are difficult to date unless they contain organic material for radiocarbon dating or are interbedded with lava flows that can be dated with K-Ar or Ar-Ar techniques. None of the moraines in the Mono Basin contain material that has been dated with the above absolute dating methods.

Glacial geologists, encountering the lack of dateable material, established non-absolute dating techniques to obtain an idea of the relative ages of moraines. These techniques consist of observations of features on moraines that weather and change appearance with age. If non-biased observations of these features are made, they can serve as the basis for differentiating moraines within a canyon, and for correlating moraines between canyons, in spite of the fact that absolute ages are unobtainable.

I used three non-absolute dating techniques. These techniques were: 1) semiquantitative or relative dating (RD) techniques based on those of Birman (1964), Sharp (1969) and Burke and Birkeland (1979), 2) the clast-sound velocity (CSV) technique of Crook (1986), and 3) moraine morphology and topographic relationships (Blackwelder, 1931; Figure 1-2a). RD techniques consist of visual (and sometimes chemical) estimates of the amount of weathering of boulders and soils on moraine crests. The CSV technique is based on the assumption that the speed of sound in weathering boulders

decreases monotonically with age because of the formation of microcracks. Moraine morphology is useful because the form of a moraine changes with age, as erosion and redeposition degrade initial glacial landforms.

Following is a more detailed discussion of each of the above methods.

Clast-sound velocity

I used the clast-sound velocity (CSV) technique of dating Quaternary clastic deposits developed by Crook (1986), Crook and Gillespie (1986) and Gillespie (1982), who have shown that it is an operator-independent measure of the degree of mechanical weathering of boulders in the weathering zone of clastic deposits.

The technique is based on the assumption that p-wave or sound speed (V_p) through a boulder in the weathering zone decreases with time as microcracks form in it during mechanical weathering. Boulders on an older deposit, therefore, should have lower mean V_p than boulders on a younger deposit because they have been exposed longer to weathering processes.

The abbreviation CSV will be used throughout to refer to the clast-sound velocity technique. V_p will be used to refer to p-wave speed.

CSV data consist of measurements of p-wave speed in a statistically useful sample of boulders. One measurement is made on each boulder in the sample. Measurements are made with a microsecond timer to which a piezoelectric transducer and a seismic source are linked. The transducer is affixed to each boulder surface with putty and has a lead into the timer. Another lead from the timer connects with the seismic source, which is two ball-peen hammers. The peen of one hammer is held against the boulder surface at a measured distance from the transducer. The observer strikes the heads of

the two hammers together, which both opens a circuit to start the timer, and also sends a sound wave into the boulder. When the transducer senses the wave, it closes a circuit which stops the timer.

On each boulder, the hammer is held at five, fifteen and twenty-five centimeters from the transducer. The p-wave speed, V_p, is recorded as:

$$V_p = \{(d_3-d_2)/(t_3-t_2)+(d_2-d_1)/(t_2-t_1)\}/2,$$

where d_3 = 25 cm, d_2 = 15 cm, d_1 = 5 cm, and t_3, t_2 and t_1 are the times recorded at these distances.

V_p was generally measured in at least forty-five boulders on each moraine. The mean, standard deviation and other statistical parameters of the samples were computed and analyzed to test hypotheses about moraine ages and correlations with other moraines.

I refer the reader to Gillespie (1982) and Crook (1986) for thorough introductions to the CSV technique.

Moraine morphology

Certain characteristics of moraine morphology are useful relative age indicators. Useful characteristics include the degree of rounding of moraine crests, height or bulk of a moraine relative to other moraines, down-valley extent, steepness and amount of gullying of moraine flanks, degree of breeching of terminal moraines by axial streams, preservation of original depositional form, and topographic position relative to other moraines and to present-day base level (Figure 1-2).

Each of the major glacial stages of Blackwelder (1931) is defined

primarily in terms of morphological features of moraines. Tioga moraines are
sharp-crested and little eroded. Axial streams only narrowly breach Tioga
terminal moraines. Tahoe moraines have rounded crests and gullied slopes but
are more extensive than Tioga moraines. Sherwin till covers a greater area
than any other glacial deposit, yet almost completely lacks primary
depositional features. McGee deposits sit high above Sherwin and later
deposits. McGee till may have been deposited when the canyons of the east
side of the Sierra Nevada were less deeply incised than during Sherwin time.

No landforms are widely accepted as diagnostic of the Tenaya, Mono Basin,
or other glaciations that have been proposed since Blackwelder (1931),
although Birman (1964) lists several diagnostic features.

Relative-dating techniques

Blackwelder (1931) noted that the number of boulders and the degree of
weathering of boulders and soils on a moraine crest were useful indicators of
moraine age. Quaternary geologists since then have sought to refine
observations of these weathering features to yield greater amounts of
information about relative ages.

I will call the collection of semiquantitative observations of weathering
features of boulders, soils or landforms relative or relative-weathering
dating (RD) techniques (Burke and Birkeland, 1979). RD techniques have been
referred to as semiquantitative (Sharp, 1969) because, although data are
numerical, they cannot be related directly to age or even, in most instances,
statistically treated because they are somewhat subjective.

Several geologists working in the Sierra Nevada have added new RD
techniques or increased their capability to differentiate more closely spaced

depositional ages. Particularly useful advances were made by Birman (1964), Sharp and Birman (1963), Birkeland (1964), Sharp (1969; 1972), Clark (1967) and Burke and Birkeland (1979).

When the RD literature is reviewed, one discovers that the particular weathering features studied, and the manner in which they were studied, are dependent on the worker and on weathering phenomena peculiar to a field area. There is therefore no "correct" relative dating method. Experience dictates that one remain open to the observation of any feature that could be used to differentiate or correlate deposits.

The results of different workers at one locale depend on sampling methods and on emphasis placed on various deposit characteristics. The problem of different results following from different methods is illustrated by the interpretation made of the Bloody Canyon moraines by Sharp and Birman (1963) contrasted with that made by Burke and Birkeland (1979). Sharp and Birman (1963) concluded that the moraines were divisible into four deposits weathered to significantly different degrees. Burke and Birkeland (1979) concluded that they were divisible into only two distinct deposits. Sharp and Birman (1963) collected data at a larger number of sites on each moraine than did Burke and Birkeland (1979). Burke and Birkeland (1979) put a greater emphasis on soil development and measured a greater number of boulder-weathering features than did Sharp and Birman (1963). Although the greater amount of data collected meant that Burke and Birkeland (1979) more thoroughly characterized each site, differences between sites on the same moraine are frequently as large as differences between sites on different moraines. Therefore, Sharp and Birman (1963) were perhaps better able to average their observations on each moraine and distinguish differences between moraines rather than sites. For maximum

age resolution, therefore, data should be collected at a number of sites on each moraine.

Another problem with RD samples is that they usually consist of qualitative observations that cannot be statistically treated or applied rigorously over a large area. The problem is especially acute with older till. For example, no adequate bases of comparison founded on RD have yet been established to correlate Sherwin till between the type locality and other proposed Sierran outcrops (Birkeland *et al.*, 1980).

If relative dating techniques are used with an understanding of their limitations, they can be powerful tools. RD techniques are most useful when they are applied by one observer to discern age differences between moraines in one canyon, or between adjoining, similar canyons.

My RD studies focused on the degree of weathering of granitic boulder surfaces. Boulders of acidic- through intermediate-intrusive igneous composition were randomly chosen at sites atop moraine crests to characterize their weathering features.

To understand which aspects of boulder surfaces might be particularly diagnostic of age among the moraines of the Mono Basin, I inspected boulder surface features on several moraines before collecting RD data that would be used to differentiate moraines. I concluded that the grain-scale surface roughness, the depth of weathering pits or pans and the depth of burial of boulders were the most useful features available for RD.

Weathering pits are depressions on boulder surfaces, which range from grain-scale to several meters across and up to a meter deep. I measured the depth of the deepest weathering pit on every boulder at each site, excluding those pits that were formed by the coalescence of a number of smaller pits, or

that were anomolously deep because of unusually vigorous weathering along cracks. Measurements were made by holding a straightedge across each pit mouth, supported by the highest local projections above the mouth, then measuring perpendicular to this to the deepest part of the pit. For pits having a diameter greater than the length of the straightedge, I supported the straightedge on one side of the pit mouth and sighted across to the other. When the error in this process was possibly greater than an estimated average one centimeter error, an estimate of the error was recorded. A boulder was classified as "unpitted" if the deepest pit was less than 0.5 cm deep, that is, about the average grain-size for many rock types in the area.

Grain-scale roughness or "fretting" of boulder surfaces was also useful. I categorized a boulder as "fresh" if fifty percent or more of its surface was weathered to a depth less than the average grain size. Boulders were "weathered" if fifty percent or more of the surface was weathered to a depth equal to or greater than the average grain size. These criteria are identical to those of Birman (1964) and are similar to those of Gillespie (1982). They are not the same as those of Sharp (1969) -- it is possible in his classification to find a single boulder that is both abraded (fresh) and weathered --nor are they the same as those of Blackwelder (1931).

A boulder was classified as "buried" if most of the angles between it and the ground surface were obtuse, and "unburied" if the angles were mostly acute or if the boulder could be lifted easily from the ground and fully inspected for depth of burial.

In presenting the relative-weathering data, I generally plot fraction of fresh or weathered boulders at each site against a diagnostic percentile of the frequency distribution of weathering pit depths, or against fraction of

buried boulders. Some plots are of one parameter versus stratigraphic position in the morainal sequence. Clustering of data indicates relative age equivalence and is not meant to imply any correlation between the two variables being plotted.

Data collection

All RD and CSV measurements were made on a random sample of granitic boulders over thirty centimeters in diameter, in longest dimension.

Measurements were collected at sites, which I defined as a group of boulders near one another. I ensured random site selection by choosing sites with reference to factors other than the appearance of boulders within an area. Some potential sites were rejected if they had been affected by an anomolous degree of redeposition or erosion that either covered boulders completely or exposed boulders beneath the weathering zone.

I minimized sample bias -- the tendency to pick one measurement over another -- within each site by taking measurements on the first fifteen or more granitic boulders encountered and flagged for study, regardless of appearance, accessibility or degree of burial. I measured RD parameters on all flagged boulders, but rejected some boulders when making CSV measurements if 1) they broke under testing, or 2) V_p was computed to be faster than 4.5 km/s, since V_p in unweathered granite is 4.5 km/s and above (Press, 1966), or 3) t_2 was less than t_3. The last two situations are impossible if p-waves are travelling through homogeneous layers of weathered granite, and are assumed to have been caused by operator error when they arose.

In the following discussion, any grouping of measurements from sites will be referred to as a sample or subsample. The entire number of CSV

measurements that could be made on a moraine will be referred to as the population. These definitions are conformable to standard statistical usage (Dixon and Massey, 1957).

Statistical testing of CSV samples

Brief introduction to statistical hypothesis testing

Decisions on whether to group moraines together as deposits of one glacial stage or to separate them were based primarily on statistical hypothesis testing performed on CSV samples, which is the testing of premisses about the populations from which the samples were drawn.

One begins a statistical testing procedure by setting up a premiss, called the null hypothesis and symbolized H_0, that two samples to be compared were drawn from the same or identically distributed populations.

Dixon and Massey (1957) discuss the standard format for testing this hypothesis. One begins by assuming that H_0 is true, that is, that the two samples being compared were drawn from identically distributed populations. To test the validity of the hypothesis, one chooses a test statistic, a number that characterizes the comparison between the samples. There is a probability that the null hypothesis is true for every value of the test statistic. If the probability is less than a previously chosen critical amount, called the significance level and symbolized by $\propto$ (Greek alpha), then it is concluded that there is sufficient reason to reject the null hypothesis, and that the samples were drawn from differently distributed populations. If the probability is greater than the significance level, then there is insufficient information to conclude that the underlying populations are differently distributed. For this study, a reasonable significance level was 10%, that

is, if the probability that the null hypothesis was true was less than 10%, I concluded that samples were drawn from differently distributed populations. I will therefore refer to a probability as "significant" if it is less than 10%, and as "highly significant" if it is less than 1%.

Statistical analysis of CSV samples

Statistical testing of CSV samples followed the procedure outlined in the flowchart in Figure 1-3.

As the flowchart shows, the main goal was to test the hypothesis that samples from different moraines were drawn from differently distributed populations. If it was probable that samples were not drawn from similar populations, then I concluded that the moraines from which the samples came were of significantly different ages. I was almost always able to hold constant other factors besides time -- such as vegetation and lithology -- that might affect the CSV samples.

Three statistical tests were used: 1) the Kolmogorov-Smirnov one-sample test to examine the hypothesis that a CSV sample was drawn from a normally distributed population; 2) the Kolmogorov-Smirnov two-sample test or the Student's t-test, to test whether two CSV samples were drawn from similarly distributed populations; and 3) the two-sample F-test to verify whether sample variances were different. This determined which of two versions of the t-test to use. All tests were "two-tailed" (Dixon and Massey, 1957).

The Kolmogorov-Smirnov (K-S) test is a common non-parametric statistical test (Bradley, 1968) and can be envisioned as follows. Two cumulative frequency distributions to be compared are plotted together. The K-S test statistic, D_{max}, is the maximum distance along the abscissa between the two

FLOWCHART FOR CSV STATISTICAL TESTING
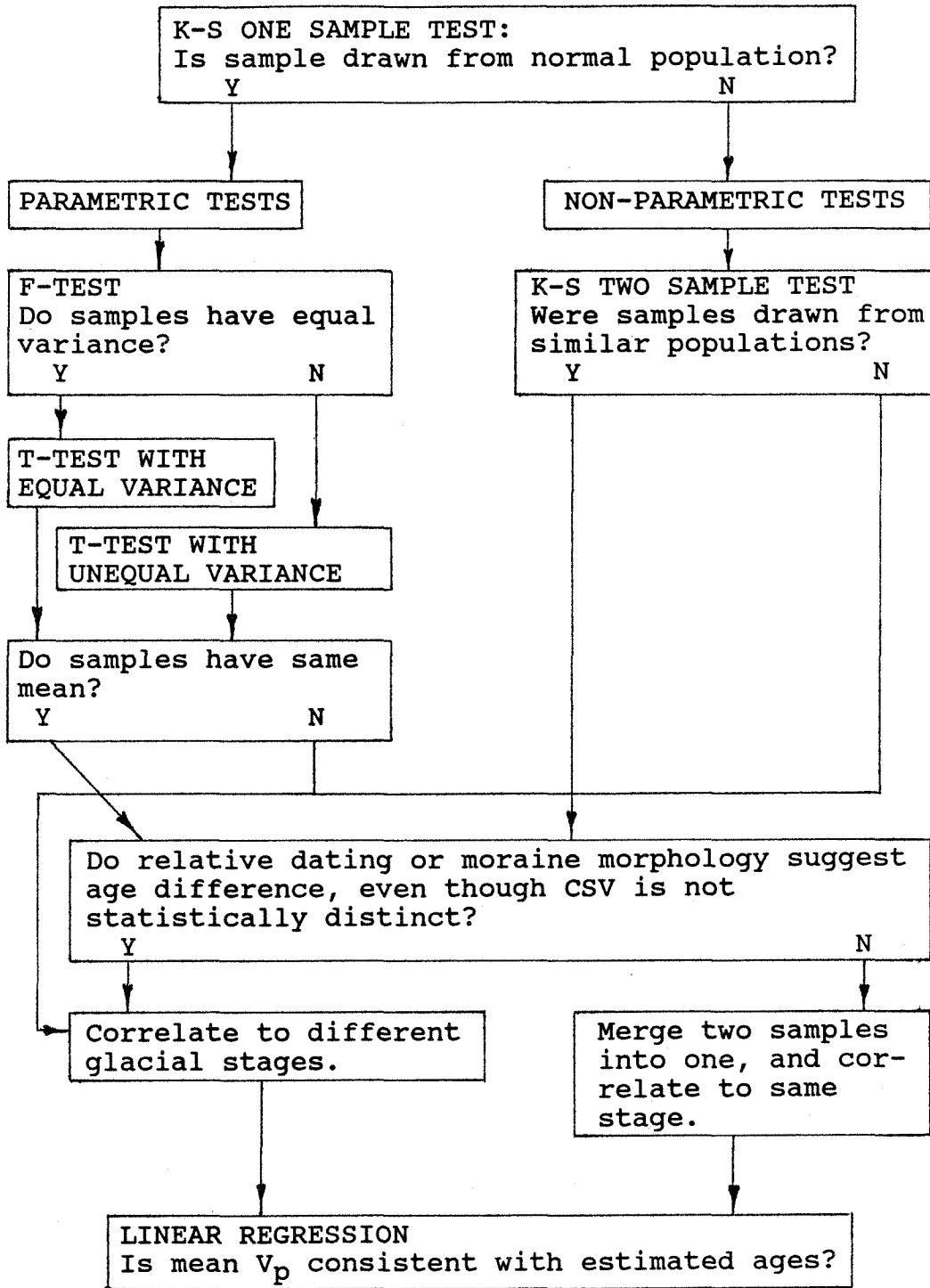
Figure 1-3. Flowchart of statistical testing procedure used on CSV.

distributions, that is:

$$D_{max} = max|S_1 - S_2|,$$

where S_1 and S_2 are the two distributions. The probability is low that D_{max} will be large if the two samples were drawn from similarly distributed populations. D_{max} is likely to be near zero if the null hypothesis is true. The probability that D_{max} could assume its value if H_0 is true is dependent on sample size, since, for constant D_{max}, one can be more confident that two large samples, as opposed to two small samples were drawn from different populations.

The Kolmogorov-Smirnov test was useful at two points in the analysis. I first used it to decide whether a CSV sample was drawn from a normally distributed population by comparing the CSV sample with a cumulative-normal distribution having the same mean and variance as the sample. Table 1-2 shows that some samples were probably not drawn from normally distributed populations, although most may have been.

I also used the test to decide whether two CSV samples were drawn from similar populations in case one or both samples had been shown in the previous step to be non-normally distributed. The standard parametric test used for comparing two samples, the t-test, becomes less valid as samples diverge from normality (Gillespie, 1982).

When both samples were probably normally distributed as determined by the one-sample K-S test, I used two common parametric statistical tests (Dixon and Massey, 1957) to decide whether they were drawn from similar populations.

First, the F-test determined whether the variances of two normally

Table 1-2. Results of K-S test. Are samples from normal populations?

Canyon	Moraine	D_{max}	Probability[a]	Reject H_o?[b]
Parker	I	0.147	28.3%	N
	II	0.150	26.1%	N
	III	0.168	22.0%	N
	IV	0.091	96.4%	N
	III+IV	0.087	66.8%	N
Grant Lake	I	0.079	94.4%	N
	II	0.111	63.8%	N
	I+II	0.084	55.0%	N
	III	0.131	70.6%	N
	IV	0.102	72.1%	N
	III+IV	0.103	40.5%	N
	V	0.102	91.1%	N
	III+V	0.112	45.1%	N
	VI*	0.146	48.1%	N
	VI**	0.139	63.1%	N
	VI	0.244	97.1%	N
	V+VI	0.110	43.5%	N
June Lake	Ia	0.141	59.3%	N
	Ib	0.130	71.4%	N
	II	0.076	87.7%	N
	Ia+II	0.093	42.4%	N
	III	0.208	1.1%	Y
	Ia+II+III	0.133	1.0%	Y
	V	0.128	21.5%	N
	VI	0.094	42.0%	N
	V+VI	0.079	28.8%	N
Lee Vining	I	0.085	89.9%	N
	III	0.135	38.8%	N
	IV	0.187	8.6%	Y
	III+IV	0.137	6.9%	Y
	V	0.188	8.4%	Y
	VI	0.120	35.4%	N
	V+VI	0.098	27.0%	N
Lundy	Ia	0.175	74.7%	N
	Ib	0.109	86.7%	N
	II	0.139	60.8%	N
	III	0.233	7.6%	Y
	Ib+II+III	0.123	13.1%	N
	IV	0.143	31.9%	N
	V*	0.164	17.8%	N
	V***	0.189	21.6%	N
	V	0.207	54.0%	N
	IV+V	0.144	4.8%	Y

[a] Probability is the likelihood that D_{max} could be as large as it is if the null hypothesis is true.

[b] H_o is the (null) hypothesis that the sample was drawn from a normally distributed population.

* Normally weathering boulders only.

** Case-hardened boulders only.

*** Resistant granitic boulders only.

distributed CSV samples were significantly different. The outcome of this test determined which of two versions of the next test, the t-test, should be used. The F-statistic is simply:

$$F = (variance\ of\ sample\ 1)/(variance\ of\ sample\ 2).$$

If the F-ratio is very different from one, then the probability is low that two samples were drawn from populations with similar variances, and the difference in the degree to which the samples are "spread out" will have to be accounted for when using the t-test.

Student's t-test for the difference of sample means was used to test whether average CSV was different for two normally distributed samples. The Student's t-test statistic, t, is the difference of the means of two samples normalized by a measure of their variance. The normalization is important because samples with large variances must have means that differ by a large amount before it can be shown that they were probably drawn from different populations. If two samples were drawn from different populations, then Student's t is likely to be large in absolute value. As t approaches zero, it becomes less likely that the samples were drawn from different populations. A different version of the test was used depending on whether it could be assumed that sample variances were the same, as determined by the F-test (Dixon and Massey, 1957).

All statistics and their probabilities were computed with the algorithms in Press *et al.* (1986).

Comparison of mean V_p with estimated deposit age

Gillespie (1982) and Crook and Gillespie (1986) argued on both theoretical and empirical grounds that V_p decreases with the logarithm of deposit age. They hypothesized that V_p is proportional to the density of microcracks in a rock, and that the rate at which microcrack density increases is proportional to the fraction of uncracked rock present at any time, for example, the rate at which microcrack density increases in a relatively unweathered rock is high, since microcrack density is low. The mathematical formulation of the relationship leads to an equation of the form:

$$V_p[\sigma(t)] = a + b \, log_{10}(1 + t),$$

where σ = microcrack density, t = time since deposition, and a and b are constants. Crook and Gillespie (1986) presented data from many localities in southern California and the eastern Sierra Nevada that corroborate the validity of this relationship.

To compare CSV results from this study with the estimated ages of glacial stages represented by moraines, I regressed means of the CSV samples against the logarithms of estimated ages from Table 1-1. I calculated the coefficient of determination, r^2, for each linear regression and compared results with those of Crook and Gillespie (1986) to determine how well my data fit the estimated ages. In most cases r^2 was greater than 0.9, indicating that the two variables -- mean V_p and time -- correlated, and therefore that the CSV were compatible with the glacial stage correlations.

AGES OF PIEDMONT MORAINES

General Statement

The following discussion of glacial geology is arranged canyon-by-canyon. For each canyon, I first discuss statistically significant differences in weathering between moraines as determined by CSV. Next, evidence from moraine morphology and relative dating studies are used to reinforce conclusions based on CSV or to show further differences between moraines that may not have been statistically separable with CSV. CSV, relative dating and morphological evidence are then used to correlate the moraines to the sequence of glacial stages shown in Table 1-1. As a final check, I test whether average V_p is compatible with the estimated ages.

Before discussing my work, it is important to discuss previous work done at Bloody Canyon to clarify certain points. The moraines in Bloody Canyon (Figure 1-4) have been extensively studied by Sharp and Birman (1963), Burke and Birkeland (1979), Gillespie (1982) and Mathieson (1984). Not all data presented by the above workers are inconsistent with each other, in spite of the disparity in conclusions of the particular authors. A consensus interpretation of the sequence -- based on all available data except that used by Mathieson (1984), but in agreement with his conclusions -- is that all moraines in the northeast-trending group, except the outermost lateral moraines, are Wisconsin age (or post-oxygen isotope stage 5), and that the outermost, northeast-trending moraines, as well as the east-trending moraines of Sawmill Canyon, are Illinoisan age (or oxygen isotope stage 6). This interpretation fits the data, assuming only that the small number of sites used by Burke and Birkeland (1979) allowed them to discern age differences

Figure 1-4. Previous work at Bloody and Sawmill Canyons: a) Data sites sampled by previous workers. Filled circles are sites of Gillespie (1982), open circles sites of Burke and Birkeland (1979), north-trending lines are areas used by Sharp and Birman (1963) to differentiate Tenaya moraines, east-trending lines to differentiate Mono Basin moraines (Sharp, pers. comm., 1987). Dotted lines show ways in which moraines have been correlated downstream by different workers. Gillespie (1982) clearly has the most complete data set; b) The most reasonable interpretation of the moraines, from Gillespie (1982; 1984). Although Burke and Birkeland (1979) correlated their site on the Tahoe II moraine of Gillespie (1982) to their sites on his Tahoe I moraine, it had an anomolously low degree of weathering for this correlation. Gillespie's more thorough sampling suggested that the Tahoe II moraine was closer in age to the moraines inboard from it. Thus, the data of Burke and Birkeland and Gillespie are not incompatible, if it is only assumed that Burke and Birkeland were unable to differentiate among Tioga through Tahoe moraines because of the small number of sites per moraine. Sharp and Birman (1963) correlated the Tenaya lateral moraine of Gillespie to his Tahoe II terminal moraine and Gillespie's Tahoe II lateral moraine to his Tahoe I terminal moraine. However, Sharp and Birman did not study the terminal moraines, therefore, their data are not incompatible with the interpretation of Gillespie even though their conclusions were.

MORAINES OF
SAWMILL AND BLOODY
CANYONS

(a)

SAWMILL
CANYON

Walker Lake

BLOODY
CANYON

(b)

"TAHOE I" ≡ MONO BASIN
"TAHOE II" ≡ TAHOE

"TAHOE I"

MONO BASIN

MONO BASIN

"TAHOE II"

TIOGA
TENAYA

PRE-MONO
BASIN II

PRE-MONO
BASIN I

1 km

N
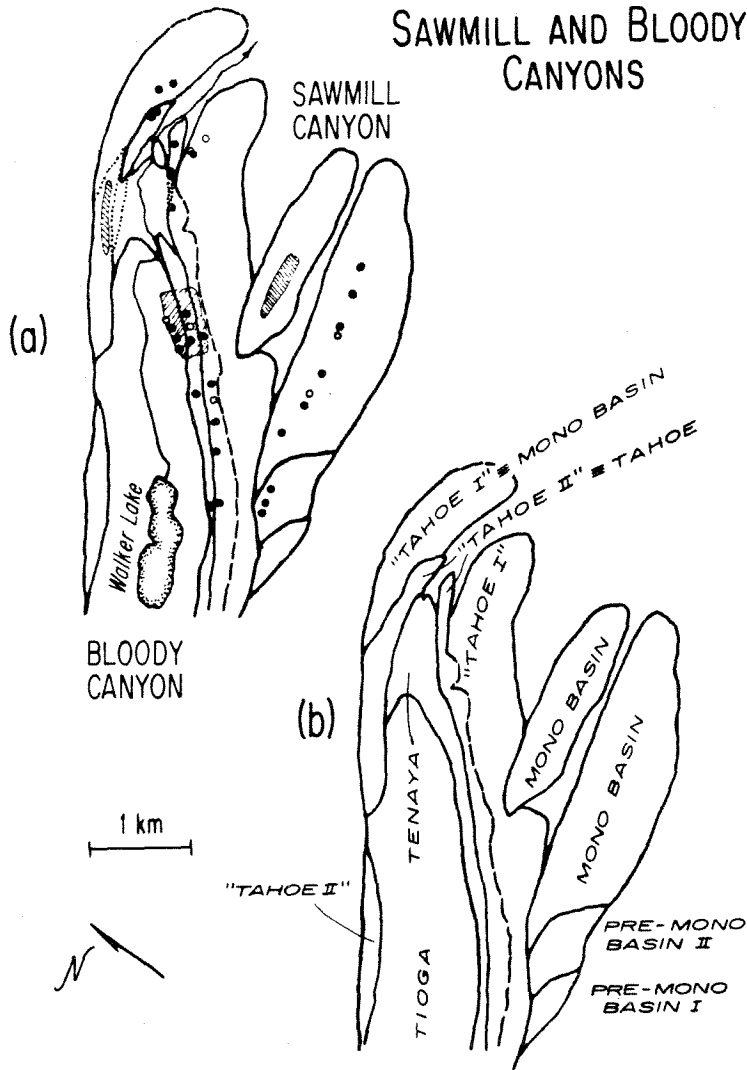
Figure   1-4

only so great as those arising from deposition separated by complete interglacial conditions, such as occurred during oxygen-isotope stage 5.

Parker Canyon

General statement

There are four prominent right-lateral moraines at Parker Canyon, as opposed to only three prominent left-lateral moraines (Figure 1-5a). I therefore collected clast-sound velocity and relative-weathering data on the right-lateral moraines. Most of the granitic boulders on these moraines are medium-grained granite of Lee Vining Canyon (Kistler, 1966a; Kistler and Swanson, 1981), but a small percentage are quartz monzonite of Aeolian Buttes.

Moraine I has a prominent terminal loop and was deposited directly on top of moraine II. Two closely spaced, extensive moraines (III and IV) enclose moraine II.

South of Parker Canyon, a young rock-glacial moraine issues from a cirque that was probably linked with Parker Canyon during earlier glaciations.

The moraines of Parker Canyon have gained little attention from glacial geologists, probably because they consist of so few separate landforms. Clark (1979) briefly discussed some of the geomorphic features. The only recently published map of the moraines is that of Kistler (1966a), who was not interested primarily in glacial geology.

Clast-sound velocity

Mean V_p decreases monotonically from inner to outer moraines at Parker Canyon (Table 1-3; Figure 1-6). The t-test clearly distinguished only three separate glacial stages within the Parker Canyon moraines. Moraines III and

Figure 1-5. Moraines of Parker Canyon: a) Moraines, numbered as in text, and sites. Dotted lines are moraine crests; b) Interpretation of moraine ages. Correlation to glacial stages is based on very consistent CSV and RD data. Mono Basin and earlier moraines are probably buried underneath the Tahoe moraines. Correlation to left-lateral moraines is based on similar down-valley extents.

MORAINES
OF
PARKER
CANYON

N

II

III

17
14
16
15
13
7
11
12
18
19
IV
10
I

Parker Lk

Parker Ck

Rock glacial moraine

(a) Numbered Moraines and sites

0   1   2
kilometers

TAHOE

TENAYA

TIOGA

TAHOE

TAHOE

TIOGA
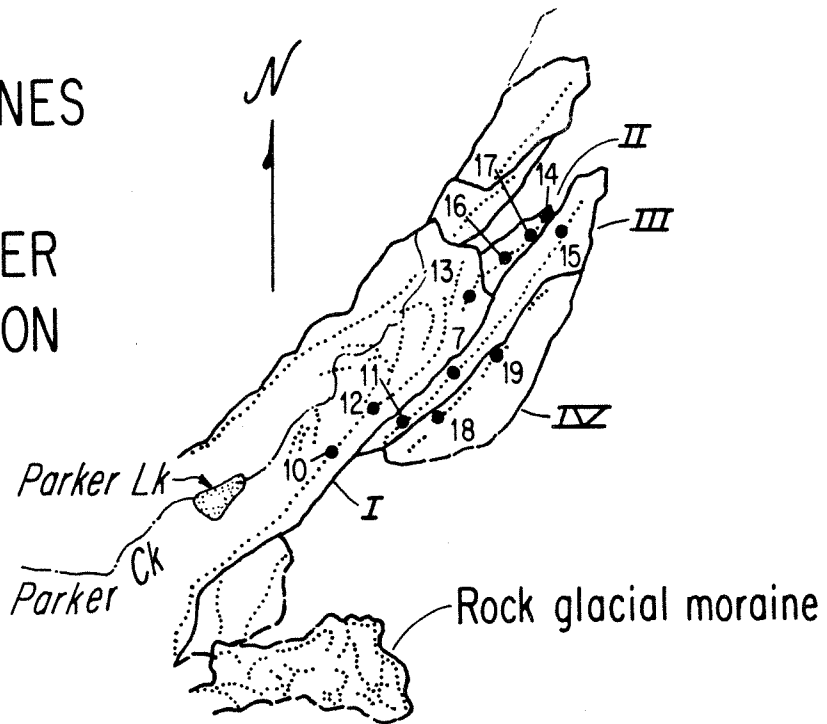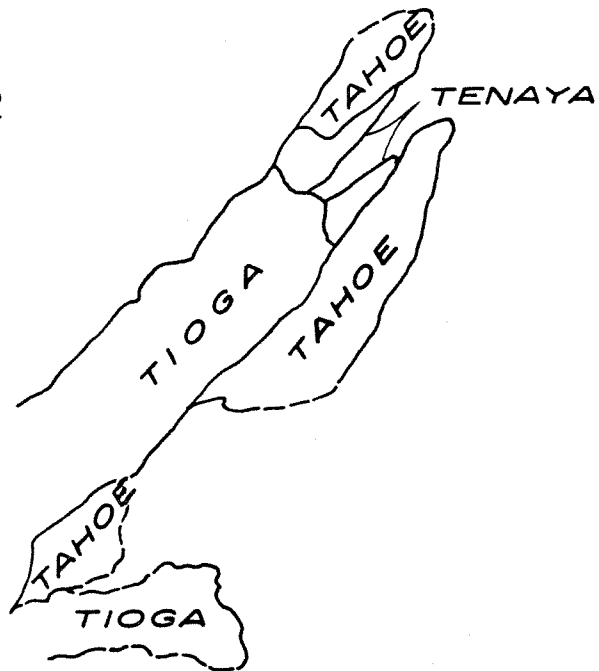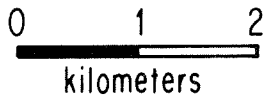
(b) Interpretation

Figure   1-5

Table 1-3. CSV data for Parker Canyon right-lateral moraines.

Moraine	Site	No. of boulders	$\overline{V_p}$[a]	S_{V_p}	$S_{\overline{V_p}}$
I	10	15	2.025	0.589	0.152
	12	15	1.933	0.417	0.108
	13	15	2.036	0.395	0.102
	All sites	45	1.998	0.466	0.070
II	14	15	1.908	0.219	0.057
	16	15	1.624	0.327	0.084
	17	15	1.696	0.575	0.148
	All sites	45	1.742	0.412	0.061
III	7	15	1.407	0.435	0.112
	11	9[*]	1.737	0.489	0.163
	15	15	1.646	0.531	0.137
	All sites	39	1.575	0.493	0.079
IV	18	15	1.592	0.392	0.101
	19	15	1.350	0.521	0.135
	All sites	30	1.471	0.469	0.086
III+IV	All sites	69	1.530	0.482	0.058

[a] $\overline{V_p}$ = Sample mean, S_{V_p} = Sample std. dev., $S_{\overline{V_p}}$ = Std. dev. of mean.

[*] Some measurements rejected.
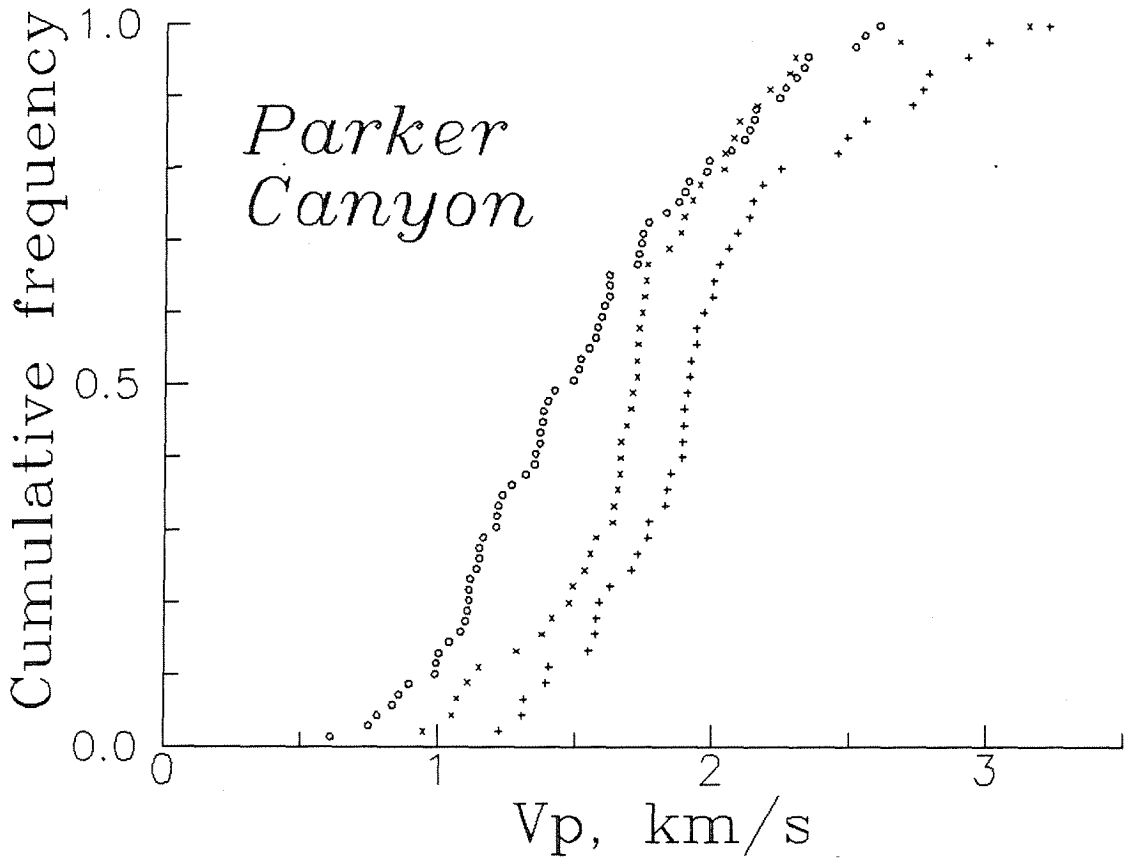
Figure 1-6. Cumulative frequency distributions of Parker Canyon CSV data. Circles = moraines III+IV; crosses = moraine II; plusses = moraine I. Difference in locations of distributions indicates samples were drawn from different populations. V_p from moraines III and IV are combined because samples were statistically indistinguishable.

IV are not significantly different in V_p (Table 1-4).

Morphological features of the moraines

The most obvious and important morphological feature of the moraines is that the older ones are more extensive than the younger. Moraine I is the shortest and moraines III and IV are the longest.

The crests of the moraines become progressively broader and more rounded as one proceeds from moraine I to moraines III and IV. Moraine I and all the recessional moraines which it encloses have very sharp crests, on the order of a few meters wide. Moraine crest II is slightly wider, and moraines III and IV have broad crests.

The flanks of moraine I are extremely steep and locally are near the angle of repose. The flanks of moraines II through IV are shallower, except where they have been resteepened by stream-cutting.

Parker Creek has cut a narrow canyon through moraine I at the left side of its terminus. The termini of moraines II through IV have been completely removed by erosion.

Based on moraine morphology alone, one could argue that the moraines were deposited during at least three separate glaciations.

Relative weathering

Almost no boulders on moraine I have weathering pits (Figure 1-7a). Moraine II has only slightly more pitted boulders. Boulders on moraines III and IV are considerably more pitted.

Grain-scale surfaces of boulders are noticeably different between each moraine (Figure 1-7). The great number of weathered boulders at site 19 on

Table 1-4. Statistical test of Parker Cyn CSV data.
Crests numbered as in Table 1-3.

Crests compared	F-ratio	Probability[a]	t-test stat.,t	Probability[b]	Reject H_0?
I--II	1.284	41.0%	2.754	0.7%	Y
II--III	1.435	24.7%	1.697	9.4%	Y
III--IV	1.105	79.0%	0.889	37.7%	N
II--III+IV	1.372	26.4%	2.437	1.6%	Y

[a] Probability that "F" could assume the tabled value if the two samples were drawn from populations of equal variance.

[b] Probability that "t" could assume the tabled value if the population means are the same (H_0 true).
H_0 is the hypothesis that the populations from which the samples were drawn are the same.

Parker Canyon

Relative dating
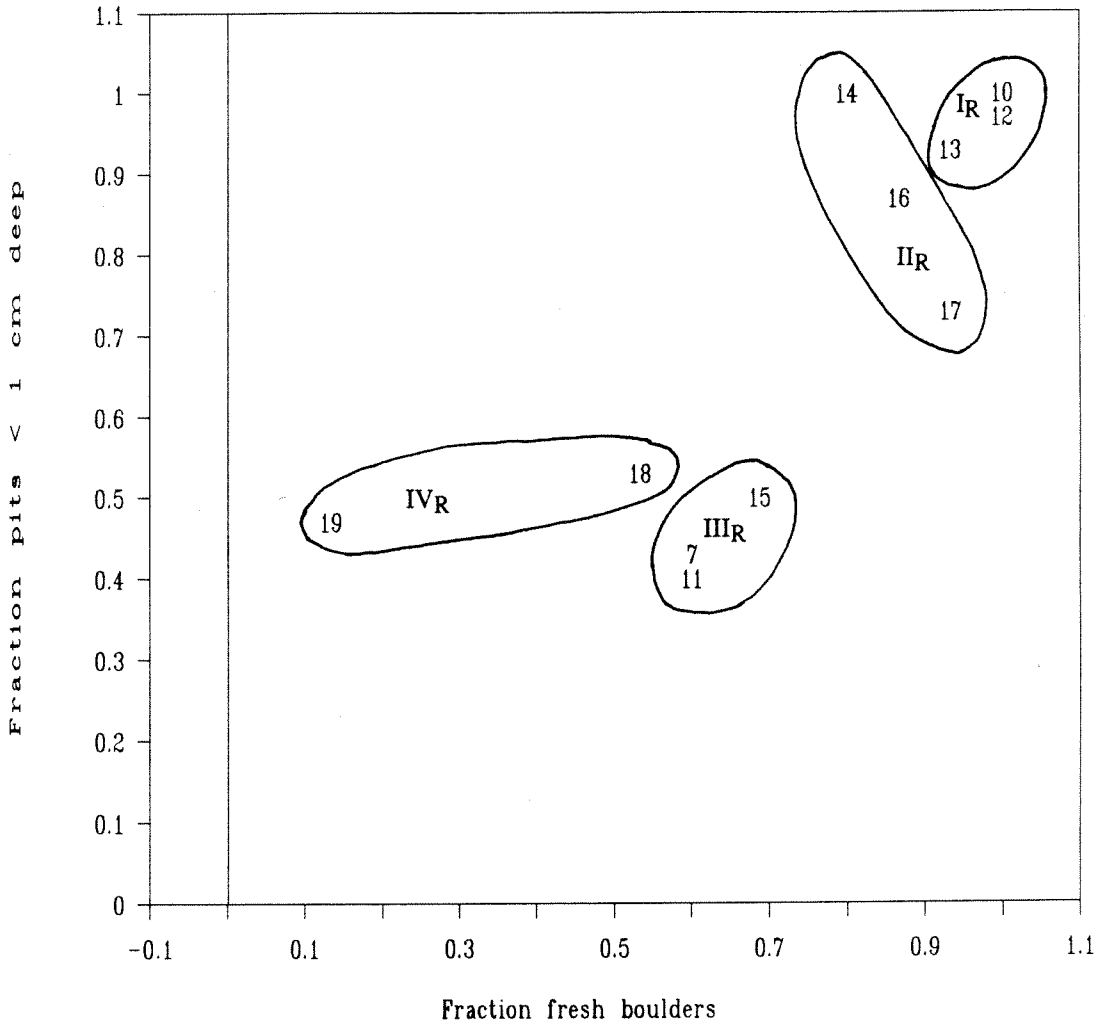
Figure   1-7a

Figure 1-7. Relative weathering of boulders on Parker Canyon moraines: a) Fraction of boulders with weathering pits less than 1 cm deep vs. fraction of boulders with fresh grain-scale surfaces. Older moraines plot to lower-left corner; b) Fraction of boulders more than half-buried vs. fraction of boulders with weathered surfaces. Older moraines plot to upper right corner. All moraines are clearly differentiated only by their grain-scale surfaces. Moraines III and IV have similar weathering pit depths and fractions of buried boulders. There are, therefore, insufficient data to differentiate moraine IV from moraine III.

Parker Canyon

Relative dating
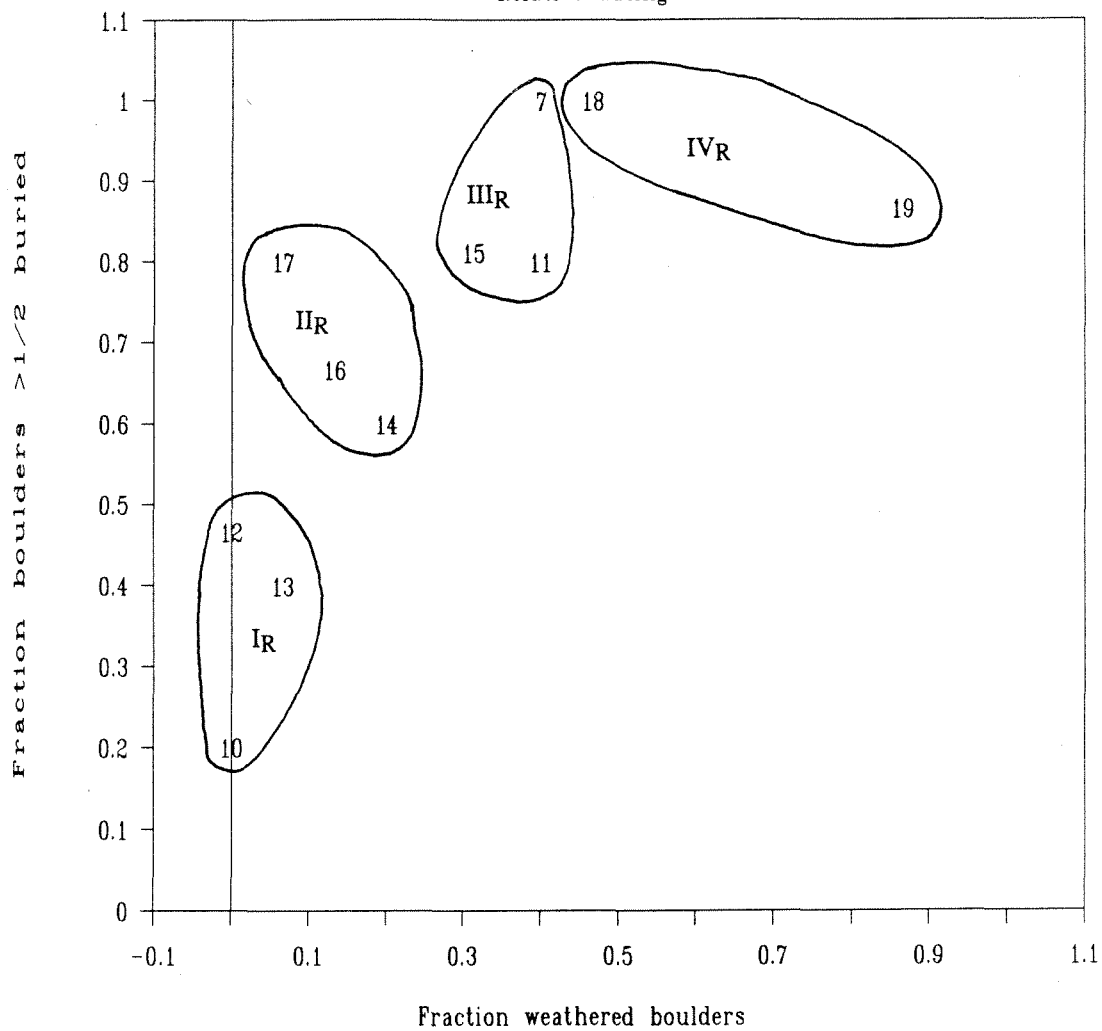
Figure   1-7b

moraine IV gives some hint that more data may reveal it to be noticeably more weathered than moraine III.

Fewer boulders on moraine I are buried than on moraine II (Figure 1-7b), and fewer on moraine II than on moraines III and IV.

The relative-weathering data alone suggest that the moraines were deposited during three separate glaciations, but also hint that moraine IV may be distinctly older than moraine III.

Rock-glacial moraine south of Parker Canyon

What is the age of the rock-glacial moraine south of Parker Canyon (Figure 1-5)? The moraine issues from a cirque at an elevation of about 3300 m near the foot of Mt. Wood. The surface of the moraine is a confusion of crests with no coherent pattern. Small, nearly conical depressions on the surface -- probably kettle holes -- and sharp ridges are well-preserved, like small amplitude features on moraine I and unlike features on any of the older moraines. The moraine apparently cross-cuts moraines that are probably the up-canyon extensions of moraines II through IV.

Most of the boulders on the moraine surface are fresh in appearance. The boulders are not, however, precariously stacked in such a way that any slopes within the deposit are at their angle of repose. This suggests thatthe moraine was not formed during a Holocene neoglaciation, since some bouldery slopes on Holocene moraines are above the angle of repose (Birman, 1964).

All evidence suggests that this rock glacier formed and was active at the same time as moraine I.

Conclusions

The steep flanks, narrow crest, well-defined terminal loop, high fresh-to-weathered ratio, small weathering pits and good exposure of surface boulders of moraine I suggest that it was deposited during the Tioga glaciation. The down-valley extent of moraines III and IV, and the weathered and buried boulders on their surfaces suggest that they are of Tahoe age. However, additional work may reveal that moraine IV correlates to a pre-Tahoe glaciation. Moraine II occupies the same stratigraphic position between distinct Tioga and Tahoe moraines that Tenaya moraines occupy elsewhere. Boulder-weathering features are compatible with this correlation. Figure 1-5b shows this interpretation of the glacial geology of Parker Canyon.

The mean p-wave speeds show excellent agreement with the estimated ages for Tioga, Tenaya and Tahoe deposits (Figure 1-8), thus reinforcing the validity of the stage assignments.

Grant Lake

General statement

The glacial stratigraphy around Grant Lake is complex. Perhaps because the Rush Creek glacier was deep and was fed by a large ice field, it was more persistent and transported more debris than glaciers in other canyons. No fewer than six separate moraines flank Grant Lake (Figure 1-9).

The innermost moraines consist of numerous, sharp-crested, discontinuous lateral moraines and nested terminal loops. Somewhat older material consists of bulky lateral moraines that grade to subdued remnants of a terminal loop. Still older lateral moraines with rounded crests grade directly into shorelines of Pleistocene Lake Russell.
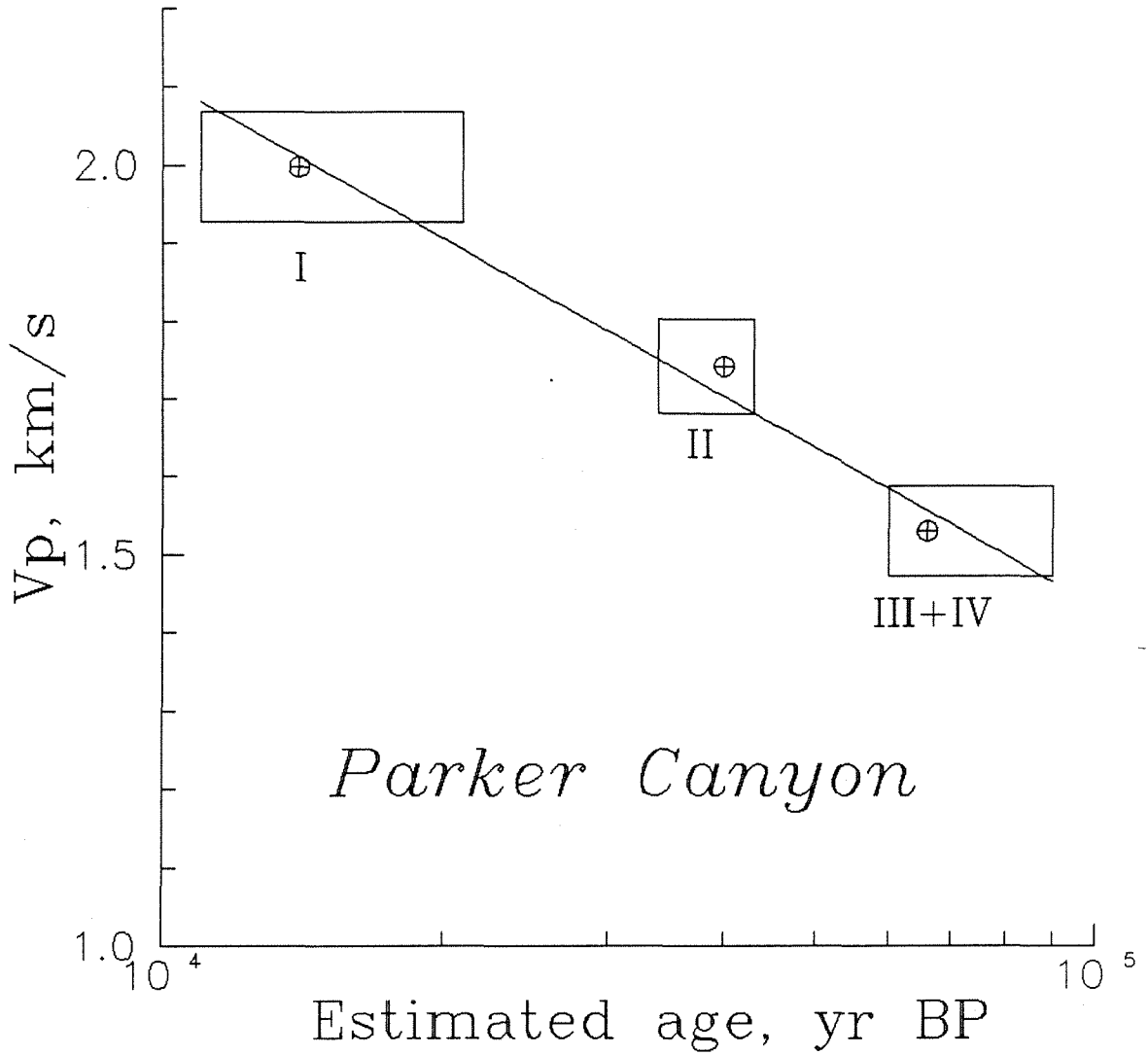
Figure 1-8. V$_p$-age regression, Parker Canyon. Horizontal error bars are ranges of estimated ages from Table 1-1; vertical error bars are one standard deviation of the mean (68% confidence interval). The correlations of glacial stages to estimated ages are reasonable since a straight line can be fit through all error boxes.

Figure 1-9. Moraines of Grant and June Lakes, numbered as in text, and sites.
Site symbols mean the following: filled circles = CSV and RD data collected;
half-filled circles = CSV data collected; triangles = RD data collected.
Dotted lines are moraine crests. Levees on northeast lobe of June Lake basalt
are cross-hatched. Moraines up-canyon from June and Grant Lakes are not
shown. Glacial geometry is complicated in center of figure because glaciers
flowed around Reversed Peak then merged on downstream side. Complex geometry
of June Lake right-lateral moraines is caused by faulting.

MORAINES OF
JUNE AND GRANT LAKES

Figure   1-9

40

Blackwelder (1931), Putnam (1949; 1950), Kistler (1966a) and Bailey and Koeppen (1977) mapped at least parts of the moraines around Grant Lake. Russell (1889) discussed some important relationships. In spite of the excellent exposure of numerous geomorphically separate landforms, the Grant Lake moraines have not been studied in much detail except by Putnam (1949; 1950).

The right-lateral moraines are broken by range-front faults, and therefore, determination of their ages was more important to this study than ages of the left-lateral moraines. However, I collected only relative-weathering data on the right-lateral moraines. It was necessary to measure clast-sound velocities on the left-lateral moraines because the rock type on the right-lateral moraines produced poor results when tested at June Lake.

Granitic boulders on the right-lateral moraines are coarse-grained, porphyritic Wheeler Crest Quartz Monzonite. Granitic boulders on the left-lateral moraines are mostly medium-grained quartz monzonite of Aeolian Buttes (?) and granite of Lee Vining Canyon.

Clast-sound velocity

CSV data collected on the left-lateral moraines indicate the presence of four distinct glacial deposits (Tables 1-5, 1-6; Figure 1-10a).

Moraines I-L and II-L seem to be of the same age (-L and -R refer to left- and right-lateral moraines). They are not distinct from moraine IV-L in V_p, but their morphology is distinct from that of moraine IV-L, as discussed in the next section, therefore they are not correlated with it.

Moraine III-L can be correlated to either moraine IV-L or moraine V-L, which are both possible downstream continuations of moraine III-L. Moraines

Table 1-5. CSV data for left-lateral moraines of Grant Lake.

Moraine	Site	No. of boulders	$\overline{V_p}{}^a$	S_{V_p}	$S_{\overline{V_p}}$
I	ud	15	1.942	0.493	0.127
	uh	15	2.049	0.421	0.108
	ui	15	1.747	0.296	0.076
	All sites	45	1.912	0.407	0.061
II	ue	15	2.089	0.667	0.172
	uk	15	1.890	0.375	0.097
	ul	15	1.869	0.440	0.114
	All sites	45	1.950	0.508	0.076
III	ug	14	1.673	0.364	0.097
	uj	15	1.544	0.642	0.166
	All sites	29	1.606	0.522	0.097
IV	un	15	1.596	0.487	0.126
	uo	16	1.893	0.845	0.211
	up	15	1.801	0.611	0.158
	All sites	46	1.766	0.666	0.098
V	uc	15	1.575	0.420	0.108
	vb	15	1.253	0.452	0.117
	All sites	30	1.414	0.459	0.084
VI	uf	18	1.439	0.619	0.146
	um	15	1.410	0.514	0.133
	All sites	33	1.426	0.563	0.098
	Non-case-hardened boulders	29	1.303	0.463	0.086
	Case-hardened boulders	4	2.315	0.417	0.208
I+II		90	1.931	0.458	0.048
III+IV		75	1.704	0.616	0.071

a V_p = Sample mean; S_{V_p} = sample std. dev.; $S_{\overline{V_p}}$ = Std. error of mean.

Table 1-6. Statistical test of Grant Lake CSV data.
Crests numbered as in Table 1-5.

Crests compared	F-ratio	Proba-bility[a]	t-test stat.,t	Proba-bility[b]	Reject H_0?
I--II	1.557	14.6%	-0.382	70.3%	N
II--III	1.054	85.8%	2.811	0.6%	Y
II--IV	1.719	7.5%	1.480	14.3%	N
I+II--III	1.296	36.0%	3.211	0.2%	Y
I+II--IV	2.114	0.3%	1.508	13.6%	N
III-IV	1.631	17.2%	1.098	27.6%	N
I+II--III+IV	1.805	0.8%	2.640	0.9%	Y
III--V	1.291	49.8%	1.501	13.9%	N
III+IV--V	1.797	8.0%	2.638	1.0%	Y
III+IV--VI	1.197	58.3%	2.219	2.9%	Y
V--VI	1.502	27.1%	-0.090	92.8%	N
III+IV--V+VI	1.446	13.6%	2.910	0.4%	Y

[a] Probability that "F" could assume the tabled value if the
two samples were drawn from populations of equal variance.
[b] Probability that "t" could assume the tabled value if the
population means are the same (H_0 true).
H_0 is the hypothesis that the populations from which the
samples were drawn are the same.
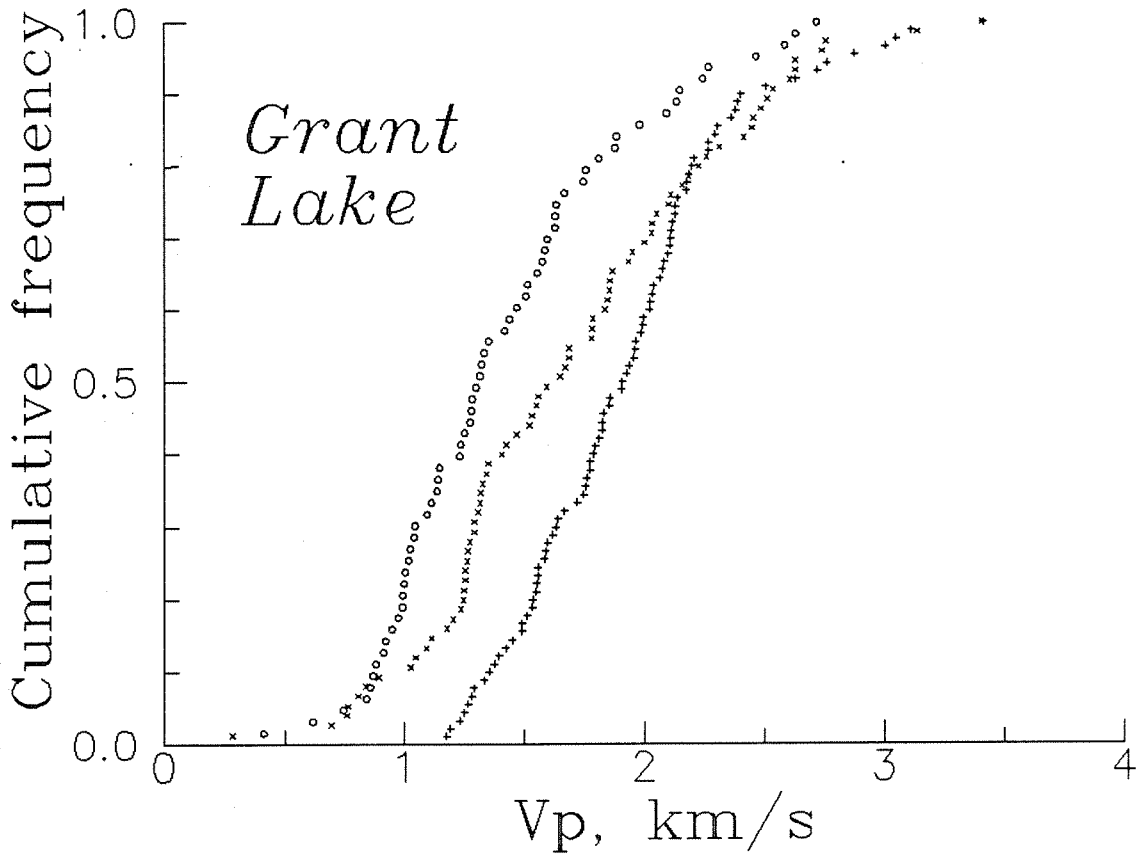
Figure 1-10. Cumulative frequency distributions of CSV data, Grant Lake moraines: a) All moraines. Moraines that are statistically indistinguishable have been grouped together. Circles = moraines V-L and VI-L; crosses = moraines III-L and IV-L; plusses = moraines I-L and II-L. The lower slope of the moraine III+IV-L sample is caused by large sample variance; b) Cumulative frequency distributions of CSV subsamples, moraine VI-L. Plusses = normally weathering boulders; circles = case-hardened boulders. Case-hardened boulders generally "ring" rather than "thud" when hit with a hammer, making them easy to distinguish from normally weathering boulders. The separation of samples and subsamples in both plots suggests that they were drawn from different populations and therefore from moraines of different ages.
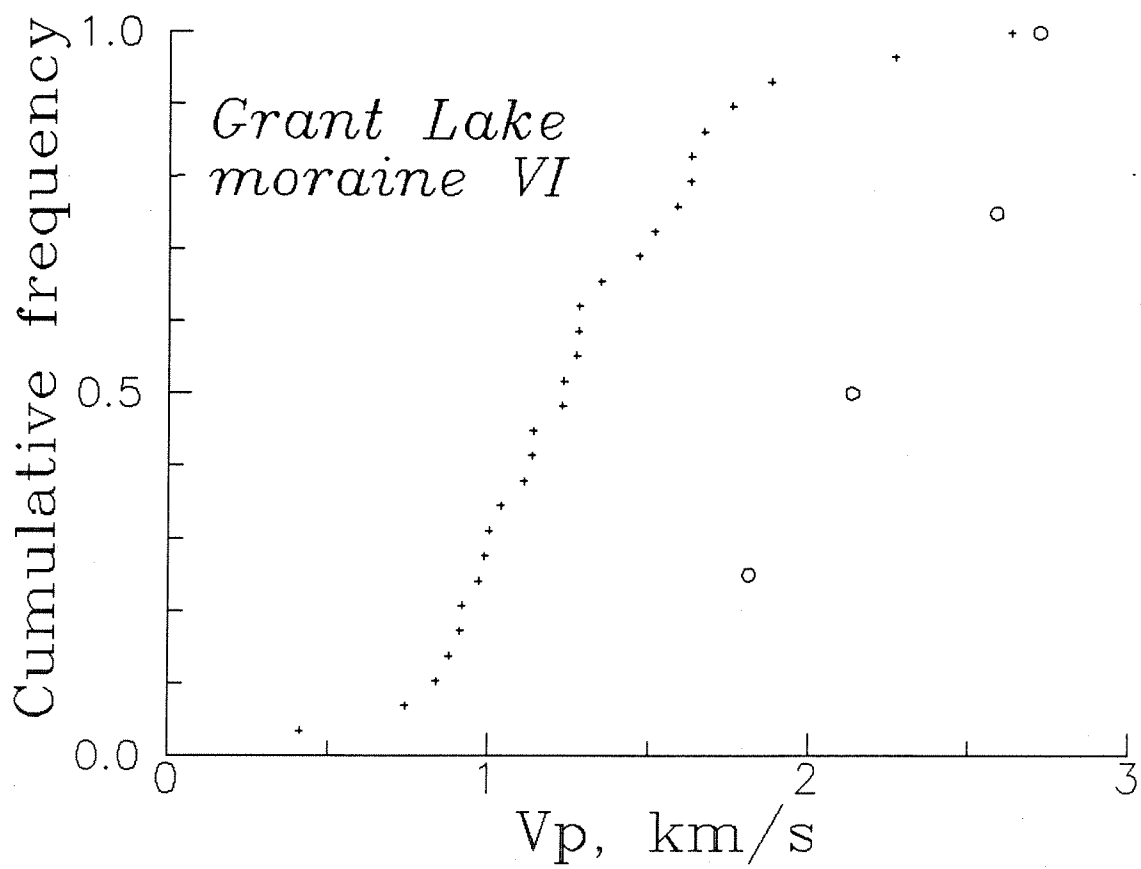
Figure   1-10 b

IV-L and V-L are statistically distinct from each other. Because of geomorphological relationships discussed in the next section, I correlate moraine III-L to moraine IV-L rather than moraine V-L.

Moraine VI-L is distinct from moraines III-L and IV-L, but is not distinct from moraine V-L. However, moraine VI-L contains a small, statistically distinct subsample of case-hardened boulders with high V_p (Figure 1-10b). None of the moraines that are inboard of moraine VI-L contains significant fractions of case-hardened boulders. The presence of this subsample suggests that moraine VI-L is significantly more weathered than moraine V-L and therefore the moraines are not grouped together.

The most reasonable grouping for the moraines, then, is moraines I+II-L, III+IV-L, V-L and VI-L, where the plus sign indicates CSV and age equivalence.

Moraine morphology

Lateral moraines I-L and II-L are sharp-crested and steep-sided. They both grade into the bulky terminal loop north of Grant Lake. This loop is only slightly breached by Rush Creek.

Moraine III-L seems to grade into both moraines IV-L and V-L. The critical region in which moraine III-L actually joins to IV-L or V-L is covered by moraine II-L, making it impossible to ascertain which of moraines IV-L and V-L is the downstream continuation of moraine III-L. However, it is most likely that moraine III-L consists of moraine-IV-L-age material veneering a more bulky moraine-V-L-age landform. This is strongly supported by the observation that for a small part of its length, moraine III-L clearly has separate inner and outer crests, which appear on aerial photographs to be weathered to different degrees. Therefore, it seems likely that moraine IV-L

is the downstream equivalent of a veneer deposit atop moraine III-L, the bulk

of which is the same age as moraine V-L. This is in fact a situation

frequently encountered among groups of nested lateral moraines.

Moraine V-L is the most extensive left-lateral moraine. It becomes quite

subdued in relief near its present termination, possibly because it merges

with moraines III and IV of Parker Canyon to form a medial moraine or glacio-

lacustrine deposit rather than a lateral moraine.

Relative weathering

Relative-weathering data were collected on the right-lateral moraines of

Grant Lake, north of Reversed Peak. Relative weathering features suggest that

the seven right-lateral moraines studied can be grouped into three differently

weathered groups of moraines.

The innermost group, comprising moraines I-R, IV-R and V-R, grades into

the terminal loop to which moraines I-L and II-L also grade. Boulders on

moraines I-R, IV-R and V-R typically have fresh surfaces and few weathering

pits (Figure 1-11a).

Boulders on moraines II-R and VI-R are weathered to similar degrees.

Slightly more than half the boulders have fresh surfaces, and there are some

rather deep weathering pits (Figure 1-11b). Moraine VI-R can be continued

through the loop of subdued terminal debris just outboard of the younger loop.

It is similar in relative bulk and stratigraphic position to moraine IV-L.

Moraines IV-L, II-R and VI-R are therefore probably correlative.

Boulders on moraines III-R and VII-R display the same amount of

weathering. Most boulder surfaces are weathered, and some weathering pits are

over twenty centimeters deep (Figure 1-11). Moraine VII-R is extremely bulky,

Grant Lake

Relative dating
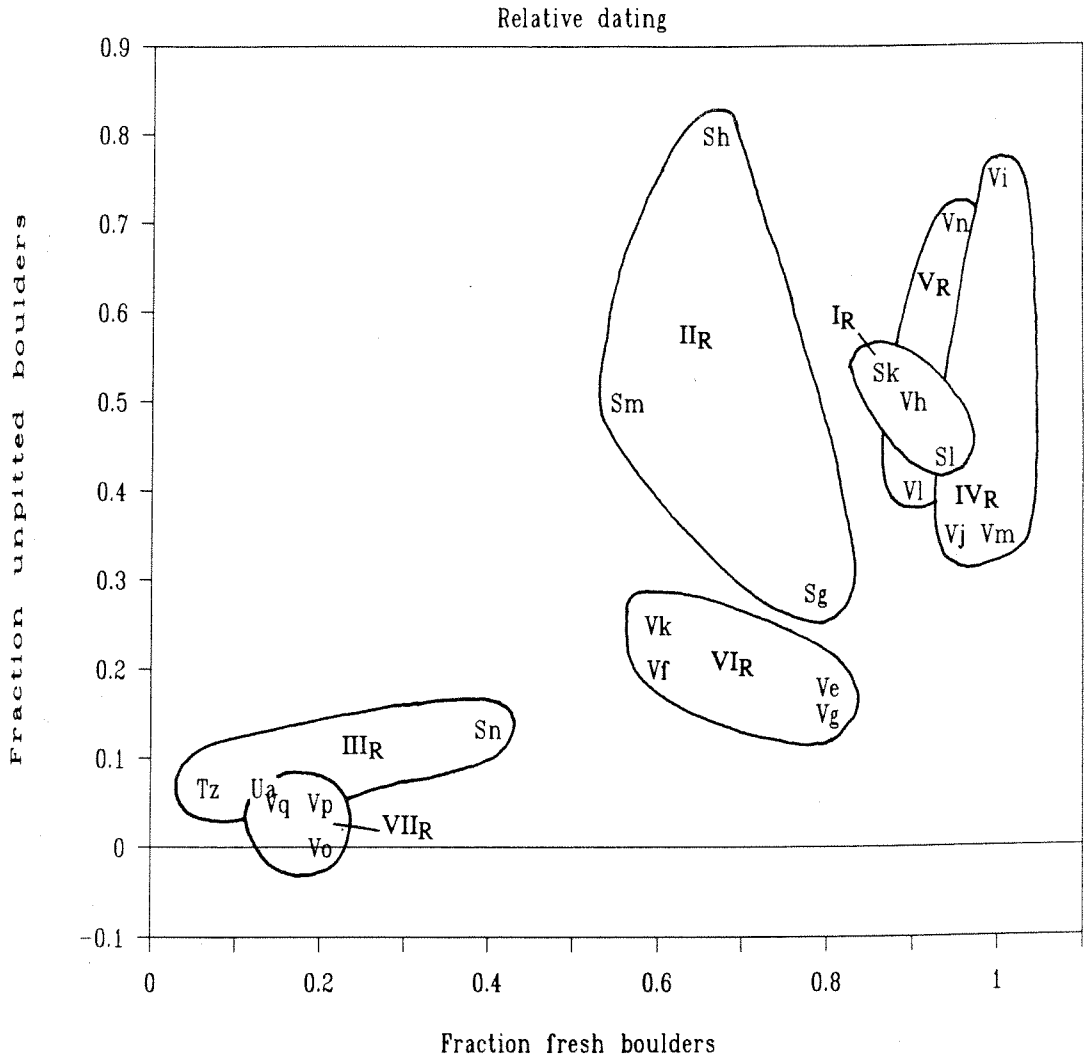
Figure 1-11 a

Figure 1-11. Relative weathering of boulders on Grant Lake right-lateral moraines. RD data were collected on the right-lateral moraines, whereas CSV data were collected on the left-lateral moraines, to avoid problems caused by lithology. More advanced weathering is to the lower left in (a), to upper right in (b). a) Fraction unpitted boulders vs. fraction boulders with fresh surfaces on grain scale, b) Fraction of boulders with weathering pits more than $1^{1/2}$ cm deep vs. fraction of boulders with weathered surfaces. These data allow correlation between looped moraines upstream and lateral moraines downstream. Moraines that seem to be of the same age are I-R, IV-R and V-R II-R and VI-R; and III-R and VII-R.

Grant Lake

Relative dating

Figure   1-11 b

and numerous recessional moraines lie between it and moraine III-R. Moraine VII-R merges with moraines of the June Lake branch of the glacier, which divided upstream around Reversed Peak (Figure 1-9). Moraine VII-R was therefore formed by an extensive glacier. In stratigraphic position and size, it is similar to moraine V-L, and therefore probably correlates with it.

Conclusions

Numerous weathering characteristics suggest that the moraines of Grant Lake were deposited during at least three distinct glacial episodes.

Fresh boulder surfaces, high V_p and nearly continuous terminal loops indicate that moraines I-L and II-L, and I-R, IV-R and V-R were deposited during the Tioga glaciation (Figure 1-12).

Moraines V-L, III-R and VII-R, and all recessional moraines between III-R and VII-R, were deposited during the most extensive glaciation. Boulders on the crests of these moraines display heavily weathered surfaces. They therefore correlate to the Tahoe glacial stage.

Moraine IV-L, II-R and VI-R, as well as the veneer deposit on moraine III-L from which CSV data were collected, can be correlated to the Tenaya glacial stage, based on stratigraphic position, intermediate amounts of weathering and partially preserved terminal moraines. However, the bulk of moraine III-L was probably deposited during the Tahoe glaciation.

Subdued morphology and presence of case-hardened boulders suggest that moraine VI-L was deposited during a pre-Tahoe glaciation, probably the Mono Basin.

The V_p-age regression (Figure 1-13) shows that the CSV data are in excellent agreement with the proposed correlations and with estimated ages.
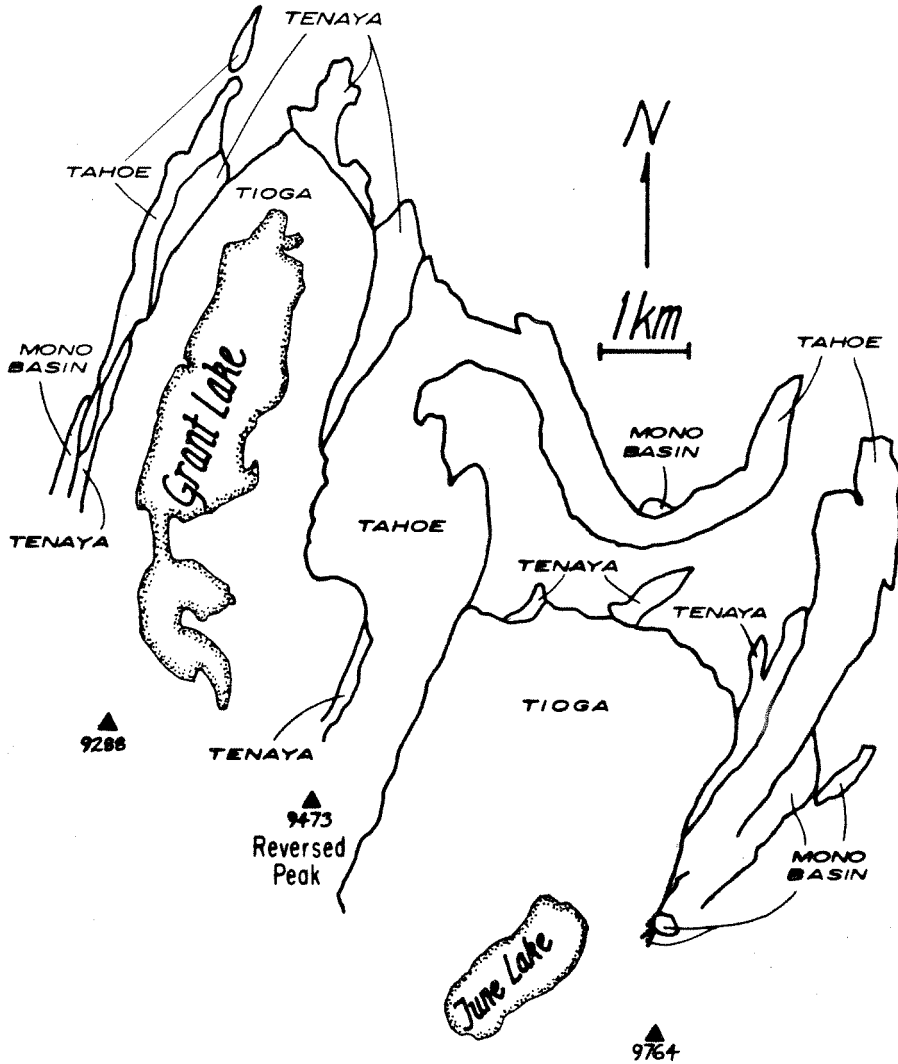
Figure 1-12. Interpretation of glacial geology, Grant and June Lakes.
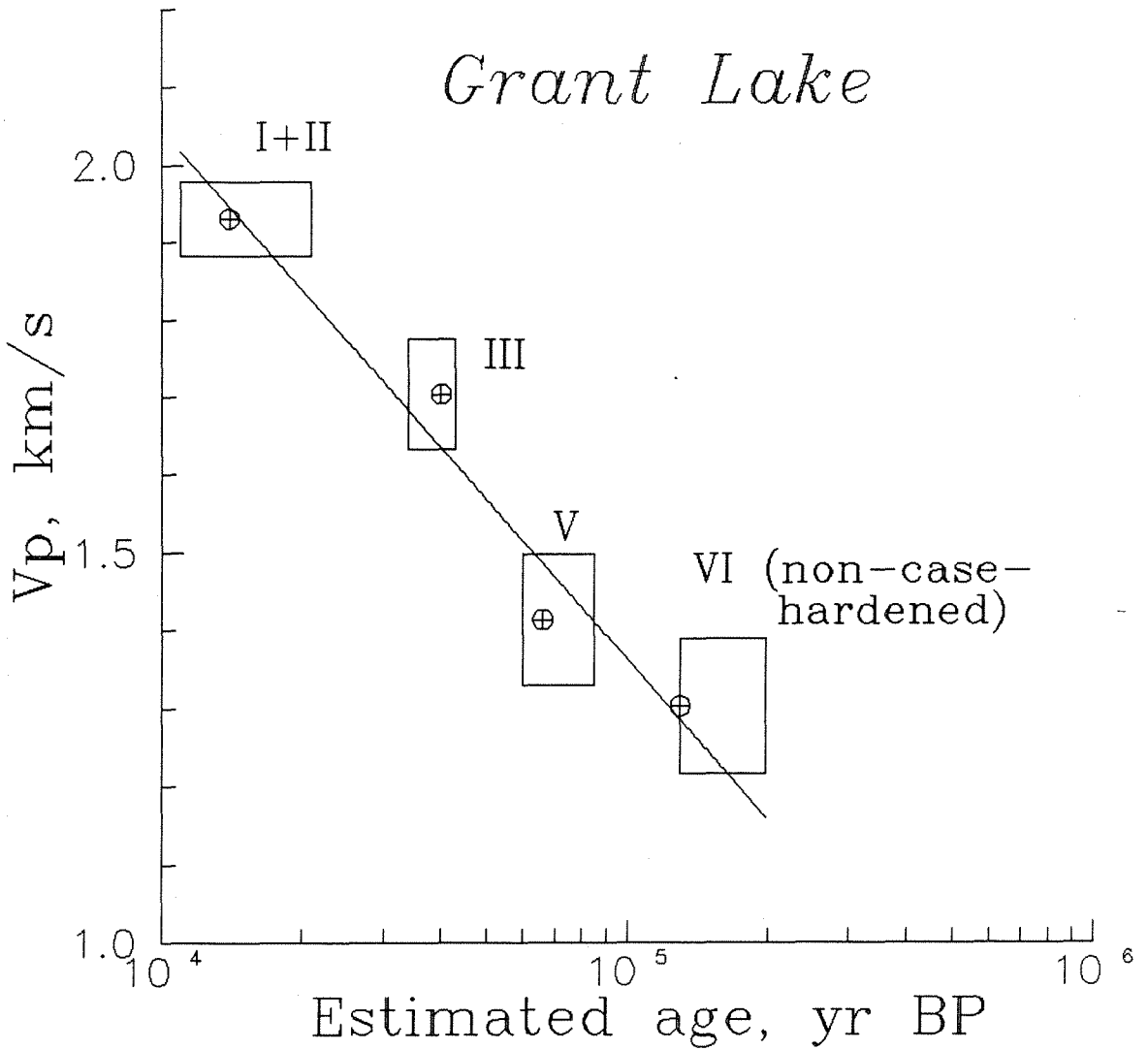
Figure 1-13. V_p-age regression, Grant Lake moraines. Horizontal error bars are range of estimated ages, vertical are one standard deviation of the mean (68% confidence interval). Case-hardened subsample from moraine VI-L has not been used. Estimated ages seem to fit CSV data reasonably well.

June Lake

General Statement

The moraines surrounding June Lake, like those surrounding Grant Lake, are large and well-preserved because of the great volume of ice that once flowed in the Reversed and Rush Creek drainage. Also, continuous headward erosion of Reversed Creek throughout glacial time contributed to preservation of ancient June Lake moraines by vertically separating them from younger moraines in a terrace-like fashion.

There are approximately ten right-lateral moraines near June Lake. The oldest and highest of these (moraine VI-R in Figure 1-9) is a thin layer resting directly atop Bishop Tuff. In the roadcut of Highway 395, it appears to consist of two tills that are not separated by substantial weathering atop the lower unit. Inboard of moraine VI-R are a number of voluminous and extensive moraines (moraine group V-R). Inboard of moraine group V-R are two less extensive moraines, IIIa-R and IV-R. Moraines I-R through III-R rest above a basaltic cinder cone and lava flows (basalt of June Lake), which were erupted after deposition of moraine IIIa-R.

Russell (1889) reasoned that the June Lake basalt separates till of two ages, which Putnam (1949) correlated to the Tioga and Tahoe glaciations. Kistler (1966a) and Bailey and Koeppen (1977) constructed more recent reconnaissance maps of the moraines. Although Bailey and Koeppen (1977) differentiated Tenaya and Mono Basin moraines on their map, they did no relative dating studies (R.A. Bailey, personal communication, 1986).

Except for moraine I-L, the left-lateral moraines are more difficult to interpret than the right-lateral moraines because of the complicated basement

topography underlying them. The following discussion therefore refers to relationships among the right-lateral moraines. I will discuss the left-lateral moraines separately.

Granitic boulders used for CSV and RD studies are monolithogic, medium- to coarse-grained porphyritic Wheeler Crest Quartz Monzonite (Kistler, 1966a), which weathers rapidly and therefore may be the cause of anomolous clast-sound velocities measured at June Lake.

The basalt interbedded with the till at June Lake plays an important role in interpreting the glacial history. Because of its importance, I begin with a discussion of the basalt.

The basalt of June Lake

Although Putnam (1949) believed that the basalt at June Lake was subaerially erupted, the position is occasionally argued that it is the product of subglacial eruptions. Below, I discuss three features that strongly suggest subaerial eruption of the June Lake basalt.

The most convincing evidence that the basalt of June Lake was subaerially erupted is the form of the vent structure, the cinder cone near June Lake. The cone is a typical subaerial cinder cone with steep outer ramparts, a nearly circular crest and a deep crater within. Glaciers of advances II-R and III-R overrode the cone and scoured it to reveal its welded interior.

If the cone had been formed by subglacial eruptions rather than subaerial eruptions, it would have the tuya or table mountain form typical of such eruptions (Mathews, 1947; Jones, 1970). Tuyas are flat-topped mountains consisting of lava flows overlying fragmental debris, with pillow lava in the deepest stratigraphic levels. In contrast to this stratigraphy, the cone at

June Lake consists entirely of cinder. Even the deepest levels of the cone revealed by glacial erosion contain only welded cinder and no pillow lava.

Two lobes of basaltic material crop out to the northeast and to the northwest of the cinder cone (Figure 1-9). The lobes are thickly mantled with rhyolitic tephra, making it difficult to decipher outcrop relationships. Therefore, it is not obvious that the material comprising the lobes emanated from the cinder cone or shared its subaerial origin.

Morphological features of the northeast lobe, however, suggest that it is a subaerial lava flow that originated from the June Lake cinder cone. Lava levees enclose the lobe on its northwest and southeast sides (Figure 1-9). Such levees are common features of subaerial lava flows (Sparks *et al.*, 1976). No levees occur on the southwest side of the lobe adjacent to terminal moraine III-R, suggesting that moraine III-R overlies the upstream extension of the lobe. Therefore, the lobe probably consists of a subaerial lava flow that originated from the June Lake cone, since the cone lies to the southwest of the flow, where the trends of the lava levees suggest that the source-vent lies.

The second most convincing piece of evidence that the basalt was erupted subaerially is the form of ejecta at the cone and within the scoria mounds on both lobes. These ejecta are almost invariably well-vesiculated, clinkery or almond-shaped cinder and bombs, with up to 80% vesicles by volume. The material in no way resembles angular, poorly vesiculated, fine-grained hyaloclasite -- as at Black Point -- which is the typical product of both subglacial and submarine eruptions.

The landforms and pyroclast types support a subaerial rather than a subglacial origin for the June Lake basalt.

Clast-sound velocity

Only three groups of moraines were statistically separable with CSV (Tables 1-7, 1-8). Moraine Ib-R was separable from moraines Ia-R and II-R. Moraines Ia-R, II-R and III-R were indistinguishable as were moraines V-R and VI-R (Figure 1-14).

Boulders on moraine Ib-R have low average V_p. Although the moraine is morphologically the downstream equivalent of moraine Ia-R, it is separated from moraine Ia-R by a bedrock knoll and a steep declivity in the moraine crest. It may be that most boulders on moraine Ib-R are derived from the knoll. If the knoll had been plucked little by the glacier that built moraine II-R (a reasonable assumption, since that glacier would have been in its ablation zone at this point), then it could be expected that the few boulders that rolled down from the knoll, or were carried supraglacially from it, would be weathered. The veracity of this hypothesis explaining anomolous CSV is reinforced by the greater degree of relative weathering observed in boulders on moraine Ib-R (Figures 1-16a and 1-16c) over those on moraines Ia-R and II-R.

V_p values on moraines V+VI-R are scattered more widely than on moraines Ia+II+III-R (Table 1-7). The greater standard deviation results from the presence of anomolously fast boulders on both moraines V-R and VI-R. Inspection of many such boulders revealed that they were "case-hardened" (Conca and Rossman, 1985), that is, hardened by deposition of secondary minerals near their surfaces. Seventy-two percent of the boulders on moraine V-R were case-hardened, based on the "thudding" or "booming" noise produced when they were struck with a hammer. Although case-hardened boulders

Table 1-7. CSV data for right-lateral moraines of June Lake.

Moraine	Site	No. of boulders	$\overline{V_p}$	V_p mode	S_{V_p}	$S_{\overline{V_p}}$
Ia	tp	15	1.672		0.349	0.090
	tq[*]	15	1.643		0.407	0.105
	All sites	30	1.658	1.712	0.373	0.068
Ib	tt[*]	14	1.523		0.465	0.120
	ub	15	1.379		0.202	0.052
	All sites	29	1.448	1.437	0.355	0.066
II	sy	15	1.675		0.289	0.075
	sz	15	1.954		0.376	0.097
	ta	15	1.789		0.450	0.116
	ob	15	1.633		0.302	0.078
	All sites	60	1.763	1.766	0.372	0.048
III	tf	15	1.739		0.636	0.164
	tg	15	1.858		0.514	0.133
	th	15	1.634		0.356	0.092
	ti	15	1.551		0.208	0.054
	All sites	60	1.696	1.592	0.461	0.060
V	tw	38	1.916		0.602	0.098
	tx	15	1.652		0.759	0.196
	ty	15	1.774		0.515	0.132
	All sites	68	1.826	1.374	0.623	0.076
VI	oe	15	1.761		0.560	0.145
	oo	15	1.524		0.502	0.130
	rp	15	1.755		0.421	0.109
	rq	26	1.880		0.535	0.105
	rr	16	1.821		0.697	0.180
	All sites	87	1.757	1.295	0.551	0.059
Ia+II+III		150	1.715	1.794	0.410	0.033
V+VI		155	1.787	1.328	0.583	0.047

[a] $\overline{V_p}$ = Sample mean, S_{V_p} = Sample std. dev., $S_{\overline{V_p}}$ = Std. dev. of mean.

[*] Second of two runs at these sites.

Table 1-8. Statistical test of June Lake CSV data.
Crests numbered as in Table 1-7.

Crests compared	F-ratio	Proba-bility[a]	t-test stat.,t	Proba-bility[b]	K-S stat., D_{max}	Proba-bility[c]	Reject H_0?
Ia--Ib	1.105	79.4%	2.206	3.1%			Y
Ia--II	1.006	95.7%	-1.262	21.0%			N
Ib--II	1.098	80.5%	3.792	0.03%			Y
II--III					0.217	12.0%	N
Ia+II--III					0.183	17.8%	N
III--V					0.226	7.6%	Y
V--VI	1.277	28.4%	0.735	46.4%			N
Ia+II+III--V+VI					0.162	3.6%	Y

[a] Probability that "F" could assume the tabled value if the two samples were drawn from populations of equal variance.

[b] Probability that "t" could assume the tabled value if the population means are the same (H_0 true).

[c] Probability that D_{max} could assume the tabled value if the samples were drawn from similarly distributed populations (H_0 true).

H_0 is the hypothesis that the populations from which the samples were drawn are the same.
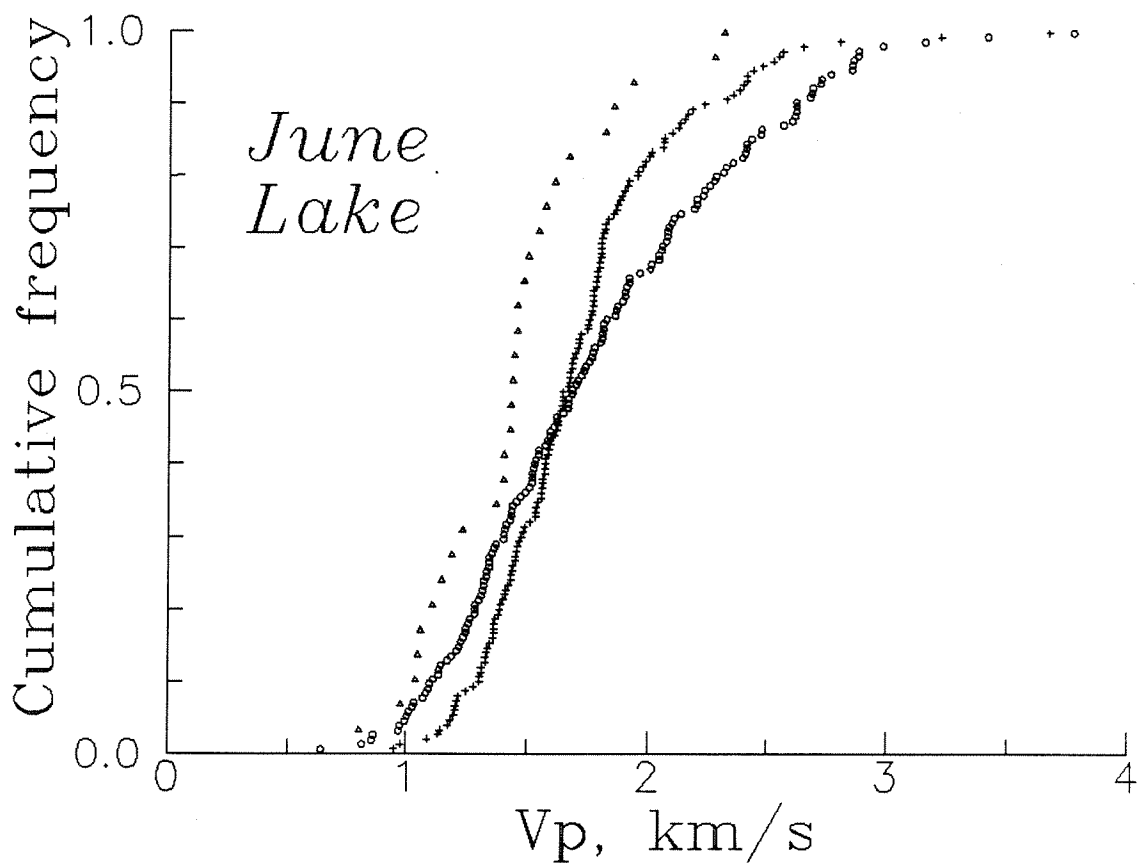
Figure 1-14. Cumulative frequency distributions of CSV data, June Lake. Trianges = moraine Ib-R; plusses = moraines Ia-R, II-R and III-R; circles = moraines V-R and VI-R. Moraine Ib-R has the slowest V_p, perhaps due to bedrock knoll upstream from moraine. Upstream of the knoll, on moraine Ia-R, boulders are weathered similarly to those on moraines II-R and III-R. Although the sample from moraines Ia+II+III-R has about the same mean as that from moraines V+VI-R, the shapes of the curves are quite different, and the samples are statistically separable.

generally have higher V_p than other boulders (Gillespie, 1982) statistical

tests were unable to divide subsamples of case-hardened boulders from the main

samples.

Accompanying the scattering of the data with age is a lack of decrease of

mean V_p. Mean V_p is (statistically) constant from moraine Ia-R to moraine VI-

R. A different measure of central tendency, the mode, does, however, decrease

monotonically from moraine Ia-R to moraine VI-R. Before discussing the

possible physical significance of the mode and justifying its use, I will

first discuss how it is found for a continuous distribution.

The mode of a continuous distribution is the value of the variable around

which measurements most tightly cluster. Figure 1-15 illustrates the search

for the mode. In this plot, the abscissa is the midpoint of an interval over

which the ordinate is proportional to the density of measurements in the

interval. The graphs were obtained by first sorting the measurements in

ascending order, then counting to the Jth V_p measurement following each V_p

measurement, where J is a previously chosen integer. The likelihood that the

next measurement of V_p will fall in any interval is then proportional to the

difference in V_p between the first and last points in the interval:

$$likelihood \approx J/N[V_{p(i+J)} - V_{p(i)}],$$

where N is the total number of measurements (Press et al., 1986). The above

equation states that the likelihood that the next measurement will fall in any

interval is approximately equal to the fraction of measurements in the

interval (J/N), divided by the length of the interval $(V_{p(i+J)} - V_{p(i)})$. The

midpoint of the interval with the highest likelihood is the mode of the

Figure 1-15. Frequency distributions of CSV data, June Lake, showing modes (peaks) in the distributions of V_p values: (a) and (b) Graphical comparison of results for different values of J, the window size; (c) General decrease in normally weathering mode with age. In (a), a window size of J=5 causes an anomolously large, slow peak. At J=10 and 20, it is easier to see that most data cluster very near 1.7 km/s. This indicates that J=5 is too narrow a window size. In (b), a window size of J=5 or 10 reveals two peaks near 1.5 km/s. Since it is known that many of the boulders are case-hardened, the faster peak probably contains data from many of them. The slower peak probably contains data from boulders that are following a "normal-weathering" trend, that is, granular disintegration by microcrack development. At J=20, the window size is so broad that the two peaks have merged, indicating that J=20 is too wide a window size. In (c), data from all moraines have been plotted together for J=10. Except for moraine Ib-R, there is a steady decrease in the highest, normal-weathering mode from top to bottom. All curves are plotted at the same scale, so lower amplitudes for moraines V-R and VI-R are caused by data being spread more widely.
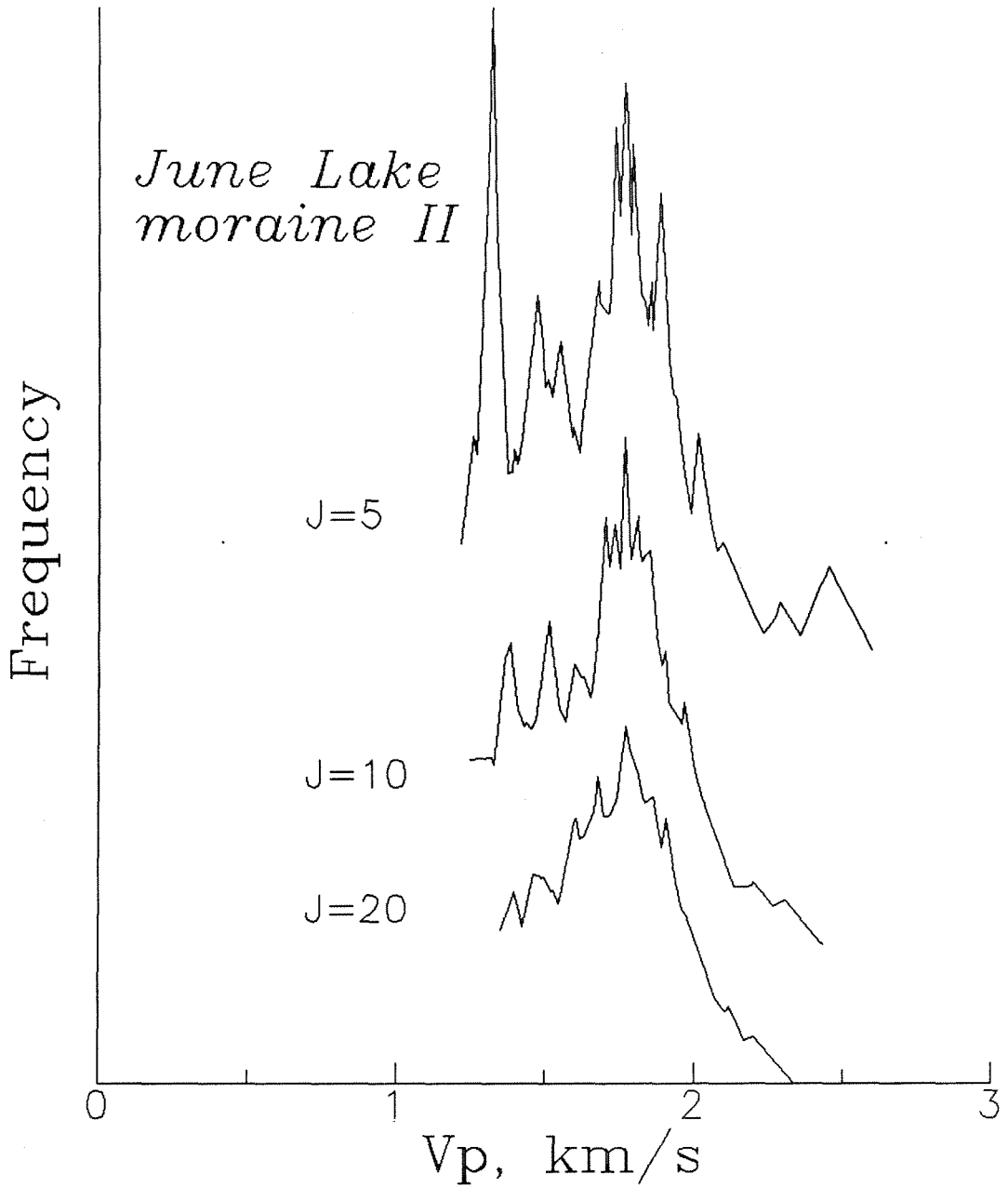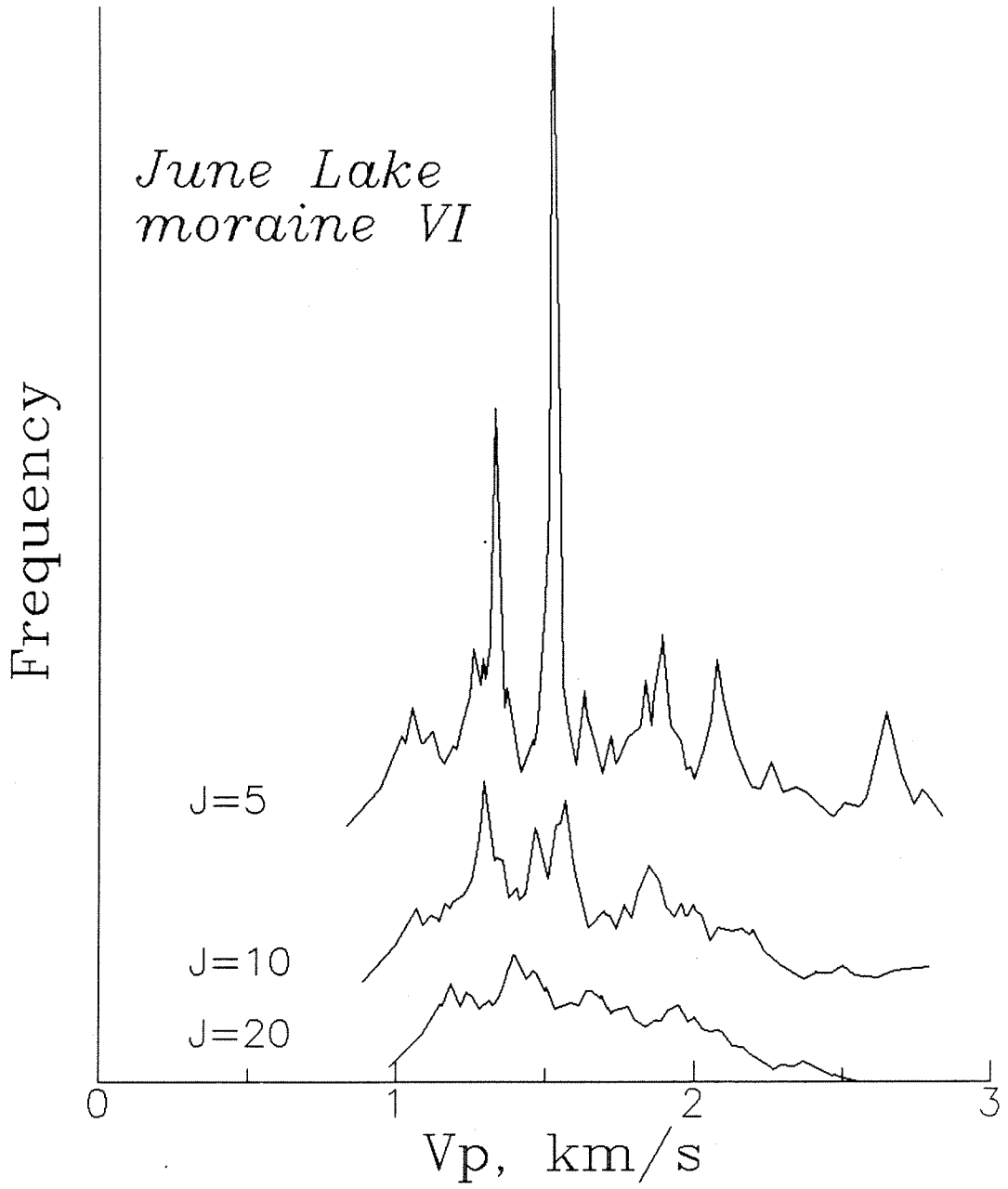
Figure   1-15a

June Lake moraine VI

J=5

J=10

J=20

Frequency

Vp, km/s

Figure 1-15b

June Lake
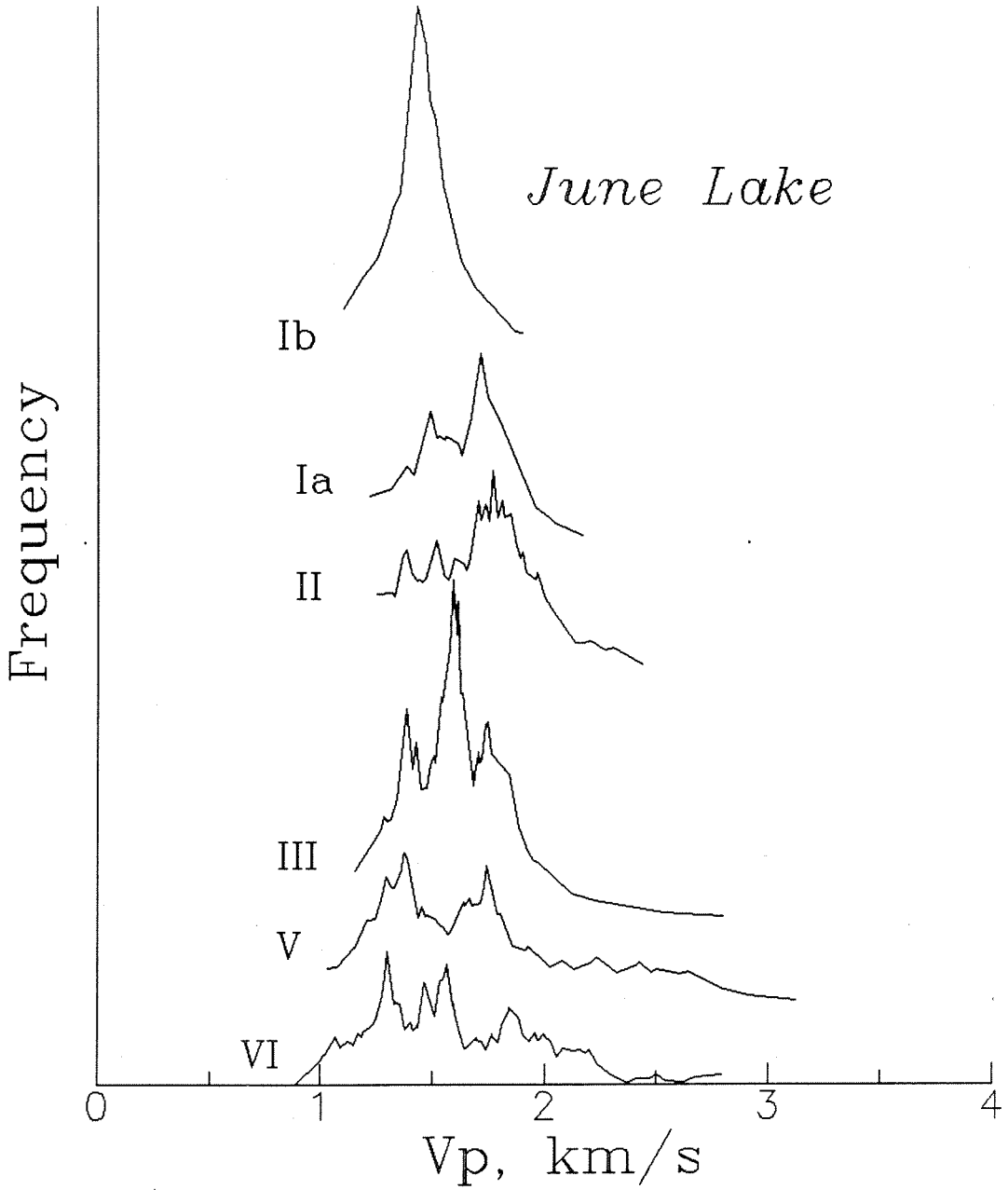
Ib

Ia

II

III

V

VI

Frequency

Vp, km/s

Figure 1-15c

sample. A sample can have secondary modes, as Figure 1-15 shows. Trials were run with J = 5, 10 and 20 (Figures 1-15a, 1-15b) to determine optimal interval length for finding physically significant modes.

Three assumptions were used to determine optimal interval length for finding modes that might correspond to means of distinct, but statistically inseparable subpopulations. The first assumption was that there were two kinds of boulders in the study: 1) normally weathering boulders, and 2) case-hardened boulders. The second assumption was that case hardening causes anomolously high V_p, just as it causes anomolous hardness (Conca and Rossman, 1985). The third assumption was that normally-weathered boulders have a tendency toward a central value different from that of case-hardened boulders. Under these assumptions, two modes should be evident in the frequency distribution of a sample containing many case-hardened boulders. Inspection of Figures 1-15a and 1-15b therefore suggest that setting J = 20 causes modes associated with two such subsamples to merge, whereas setting J = 5 causes distributions to be dependent on fluctuations more localized than those expected from assuming only two underlying subpopulations. Setting J = 10 accentuates the features that can be expected in the hypothesized underlying populations.

Figure 1-15c shows that the primary mode generally becomes slower with age (except for anomolous moraine Ib-R), and that older moraines are bimodal -- with slow, normally weathered, and fast, case-hardened peaks. The "normally weathered" modes were used as estimates of mean V_p in the V_p-age regression to obtain the additional constraint on moraine ages that true V_p means provided in other canyons.

<u>Moraine morphology</u>

Moraines I-R through III-R overlie the June Lake basalt. Not only are there fresh-looking erratics atop the June Lake cinder cone that are similar to boulders on moraines I-R to III-R , but also basaltic scoria can be found in terminal moraines II-R and III-R, and in none of the older tills. Terminal moraines II-R and III-R also overlie lateral levees of the June Lake basalt flow, as discussed above. Since there is no evidence that the basalt was erupted underneath ice, or flowed over ground saturated with glacial outflow, it was probably erupted during interglacial conditions preceding the deposition of moraines I-R to III-R.

Terminal moraines II-R to III-R consist of groups of elongate hummocks spread in a broad fan or loop (Figure 1-9). Topographic features of small amplitude are well-preserved on these hummocks. Lateral moraines I-R to III-R are relatively insubstantial compared to the terminal moraines, but nevertheless are sharp-crested.

Several features of their morphology suggest that moraines IIIa-R and IV-R and moraines I-R to III-R were deposited at significantly different times. Much of lateral moraine III-R seems to be only a veneer on moraines IIIa-R and IV-R. The crests of moraines IIIa-R and IV-R project from the flank of moraine III-R at low angles in map view (Figure 1-9), suggesting but not proving a significant age difference between them (R.P. Sharp, personal communication, 1985; Sharp and Birman, 1963). In addition, moraines IIIa-R and IV-R are crosscut by the June Lake basalt flow (Figure 1-9). Since the flow was erupted when no glacial ice lay northeast of June Lake, then the length of time between the two glaciations, corresponding to moraines I-R to III-R and IIIa-R to IV-R, included time for the glacier to retreat from the

IIIa-R and IV-R maximum at least to June Lake, then time for the basalt to erupt, and finally time for the glacier to readvance to the III-R maximum.

Moraine group V-R is the most extensive at June Lake. The morphology of these moraines is noticeably more evolved than that of moraines IIIa-R and IV-R. Moraine IV-R has a continuous crest (Figure 1-9), but moraine V-R does not, because of large amounts of erosion, deposition of pumice, faulting and redeposition that have taken place since its original deposition.

Two of the morphological features of moraine VI-R suggest that it is considerably older than moraine V-R, despite the similarity in V_p: 1) Range-front faults offset it a much greater amount than moraine V-R, and 2) it is little more than a veneer of till resting atop Bishop Tuff, indicating that most of the original volume of the moraine may have been removed by erosion.

Relative weathering

About 90% of the granitic boulders on moraines I-R to III-R have fresh surfaces, and the vast majority have no weathering pits (Figure 1-16a). Less than 10% of the weathering pits are greater than one cm deep (Figure 1-16b). The relative-weathering data are distinct from those collected on moraines IIIa-R and IV-R.

Only about 70% of the boulders on moraines IIIa-R and IV-R have fresh surfaces, in contrast to moraines I-R to III-R and to most sites on moraine V-R. Weathering pits are significantly deeper than those on moraines I-R to III-R, but not significantly less shallow than those on moraine V-R (Figures 1-16b, 1-16c).

Even though their V_p distributions are not statistically separable, the degree of weathering of boulders on moraines V-R and VI-R is significantly

June Lake

Relative dating

Figure 1-16a

Figure 1-16. Relative weathering of boulders on right-lateral moraines of June Lake: a) Fraction of unpitted boulders vs. fraction of boulders with fresh surfaces. Older material to lower left. Data from moraines Ia-R, II-R and III-R are tightly clustered; b) Fraction of boulders with weathering pits greater than 1 cm deep vs. fraction of boulders with weathered surfaces. Older material to upper right. Moraines I-R, II-R and III-R are clustered, but moraines IIIa+IV-R, V-R and VI-R are all well-separated in both parameters; c) Mean weathering pit depths on each moraine. Error bars are one standard deviation of the mean, which may not correspond to a confidence interval since the samples are probably non-normally distributed. Weathering pits are much better developed in boulders on moraine VI-R than in those on any other moraine.

June Lake

Relative dating
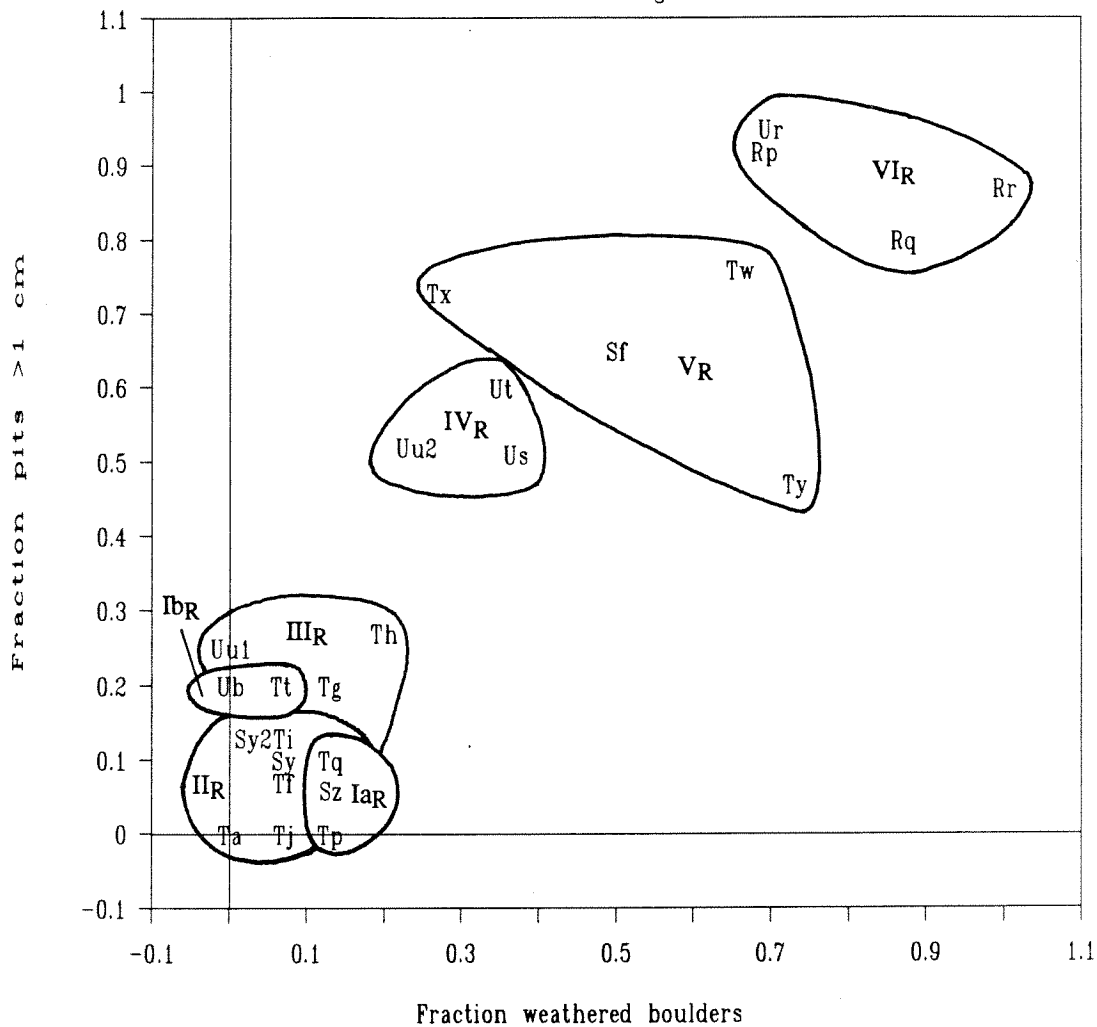
Figure 1-16 b
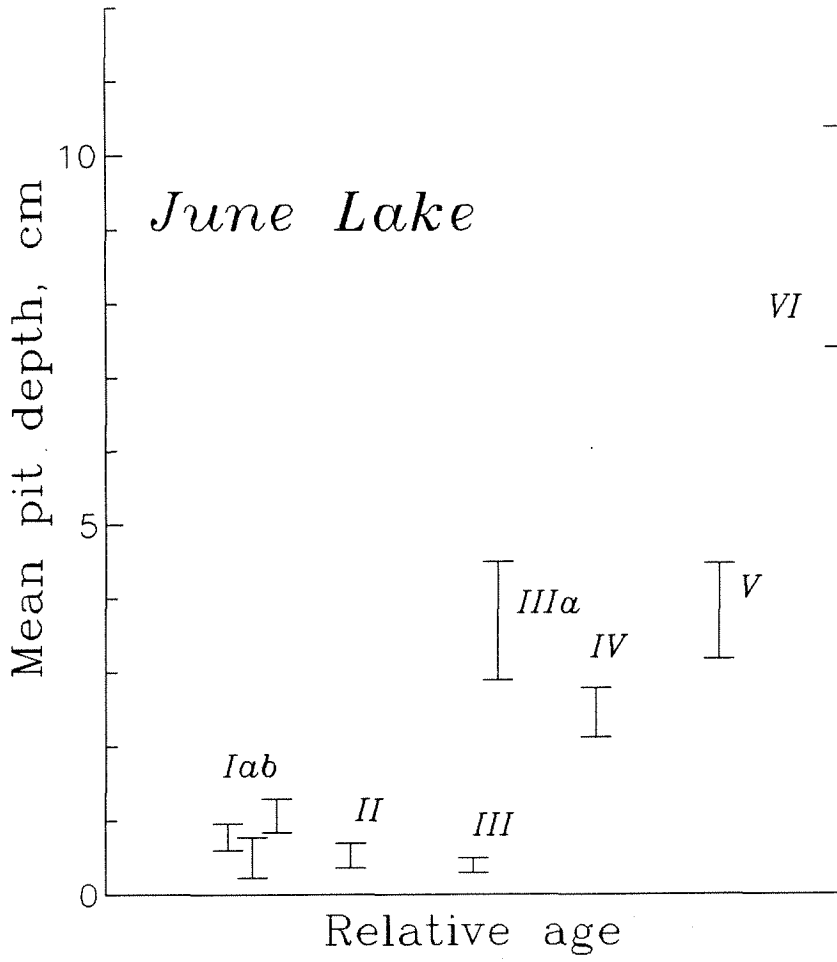
Figure 1-16 c

different.   Weathering pits on moraine V-R are considerably shallower than those on moraine VI-R (Figures 1-16b, 1-16c).   The grain-scale surfaces of boulders on moraine V-R also indicate that these boulders have been weathered less than those on moraine VI-R (Figure 1-16a).   RD data are incompatible with moraines V-R and VI-R being the same age.   The weathering-pit data especially suggest that weathering of moraine VI-R is more evolved than that of moraine V-R.   However, the surfaces of boulders on both moraines are partially sandblasted and case-hardened, unlike boulder surfaces on younger moraines. Both moraines have been exposed to episodes of aeolian attack and case-hardening to which the younger moraines have not.

Left-lateral moraines

Lateral moraine III-R can be followed through a looped terminal moraine into the complicated left-lateral moraine complex.   The maximum extent of this glaciation is clearly marked by the outcrop area of till containing cinders derived from the June Lake basalt.

The glacier that formed lateral moraine IV-L merged with the right-lateral Grant Lake glacier that formed Grant Lake moraine VII-R, to form a subdued medial moraine.   These moraines are therefore of the same age.

A prominent moraine (III-L) is similar in both relative extent and volume to lateral moraine IV-R and to moraine VI-R of Grant Lake, and locally lies just outside the most distal outcrops of till containing June Lake basalt cinders (Figure 1-9).

Boulder weathering on moraine III-L is intermediate between weathering on comparably situated right-lateral moraines VI-R and VII-R of Grant Lake (Figure 1-17a), and therefore the moraine is not directly comparable to nearby

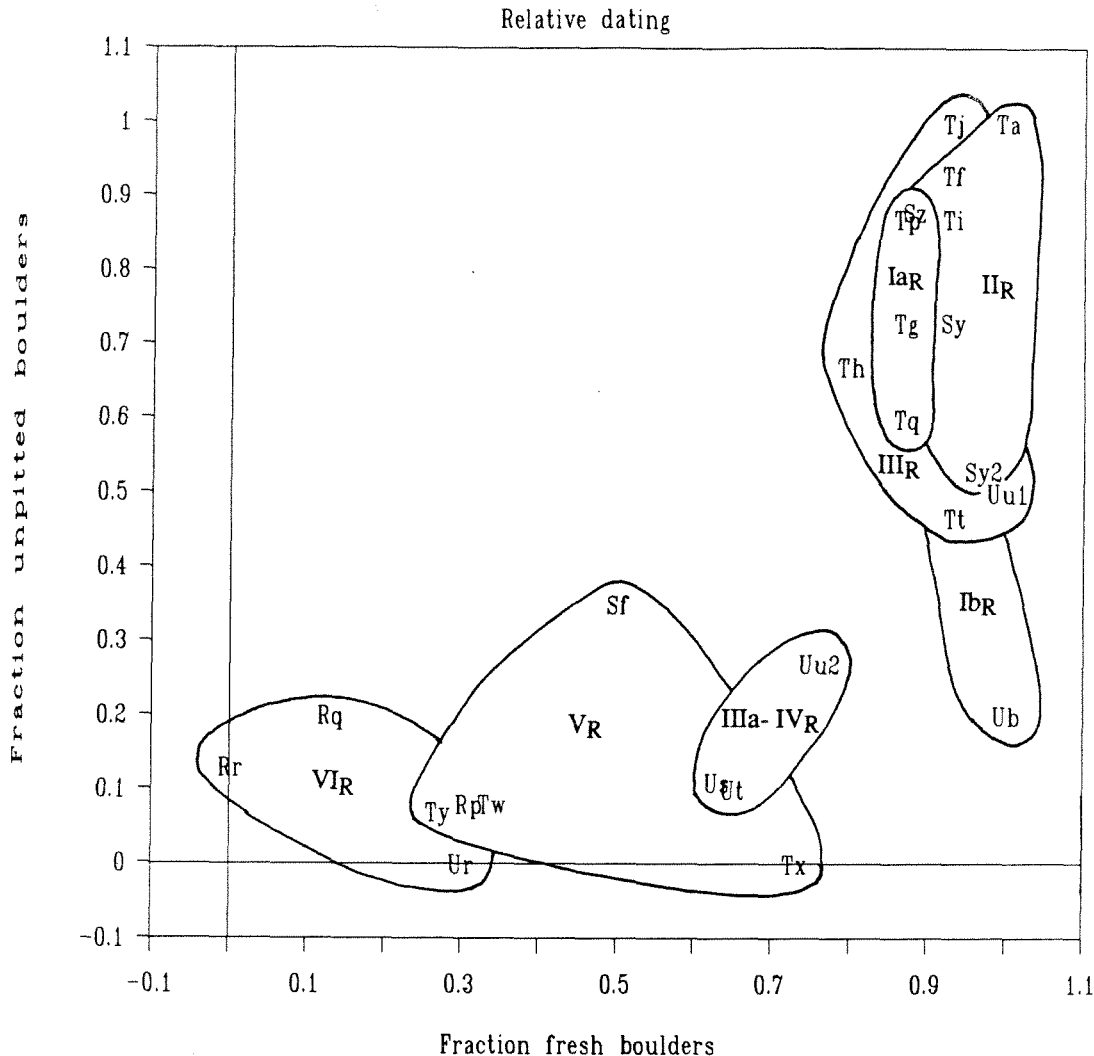*Grant Lk + Lune Lk left-lat. moraines*
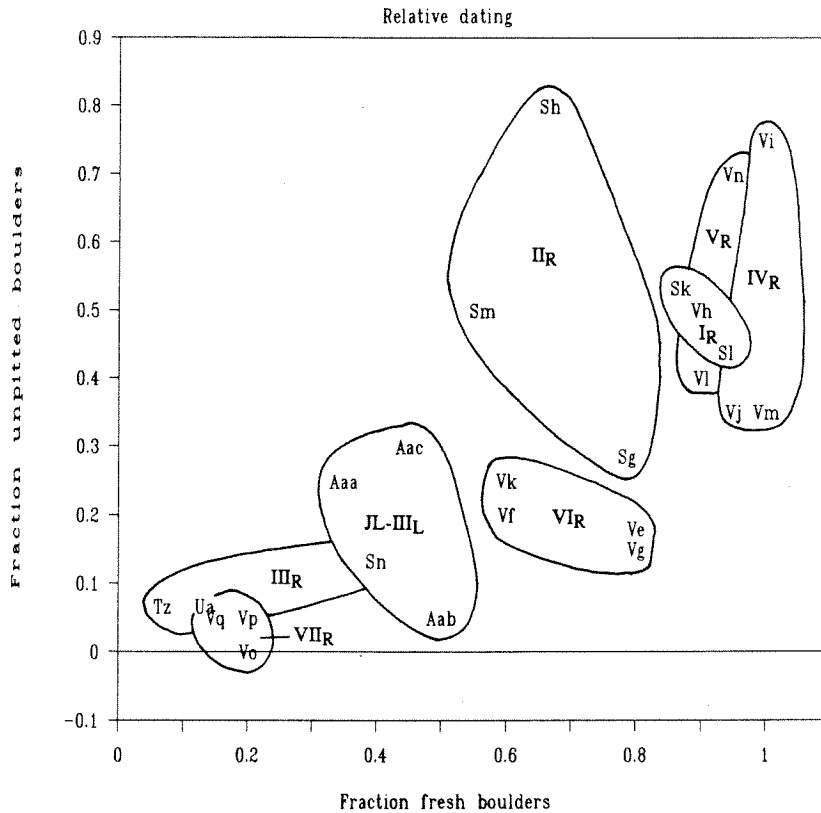
Figure   1-17a

Figure 1-17. Relative weathering of boulders on left-lateral moraines of June Lake: a) Fraction of unpitted boulders vs. fraction of boulders with fresh surfaces for June Lake moraine III-L compared with Grant Lake moraines, which have similar climate and boulder lithology. Age increases to lower left. Relative weathering of June Lake moraine III-L is similar to that of moraines III-R and VII-R of Grant Lake, and not very different from moraine VI-R; b) Fraction of unpitted boulders vs. fraction of boulders with fresh surfaces for June Lake left-lateral moraines.. Samples consist of unburied, meter-sized boulders. Age increases to lower left. Data from moraine III-L clearly clusters with data from moraine IV-L, which is correlative to moraine VII-R of Grant Lake; c) Fraction of boulders with pits > 10 cm deep vs. fraction of boulders with weathered surfaces for unburied, meter-sized boulders on June Lake left-lateral moraines. Age increases to upper right. As in (b), data from moraines III-L and IV-L are clustered, indicating that these moraines were deposited at approximately the same time. Single data point from moraine II-L indicates that it is slightly more weathered than moraine I-L. However, it contains no clasts of June Lake basalt, unlike moraine I-L. It is therefore probably correlative with moraines IIIa+IV-R.

June Lake left–lateral moraines
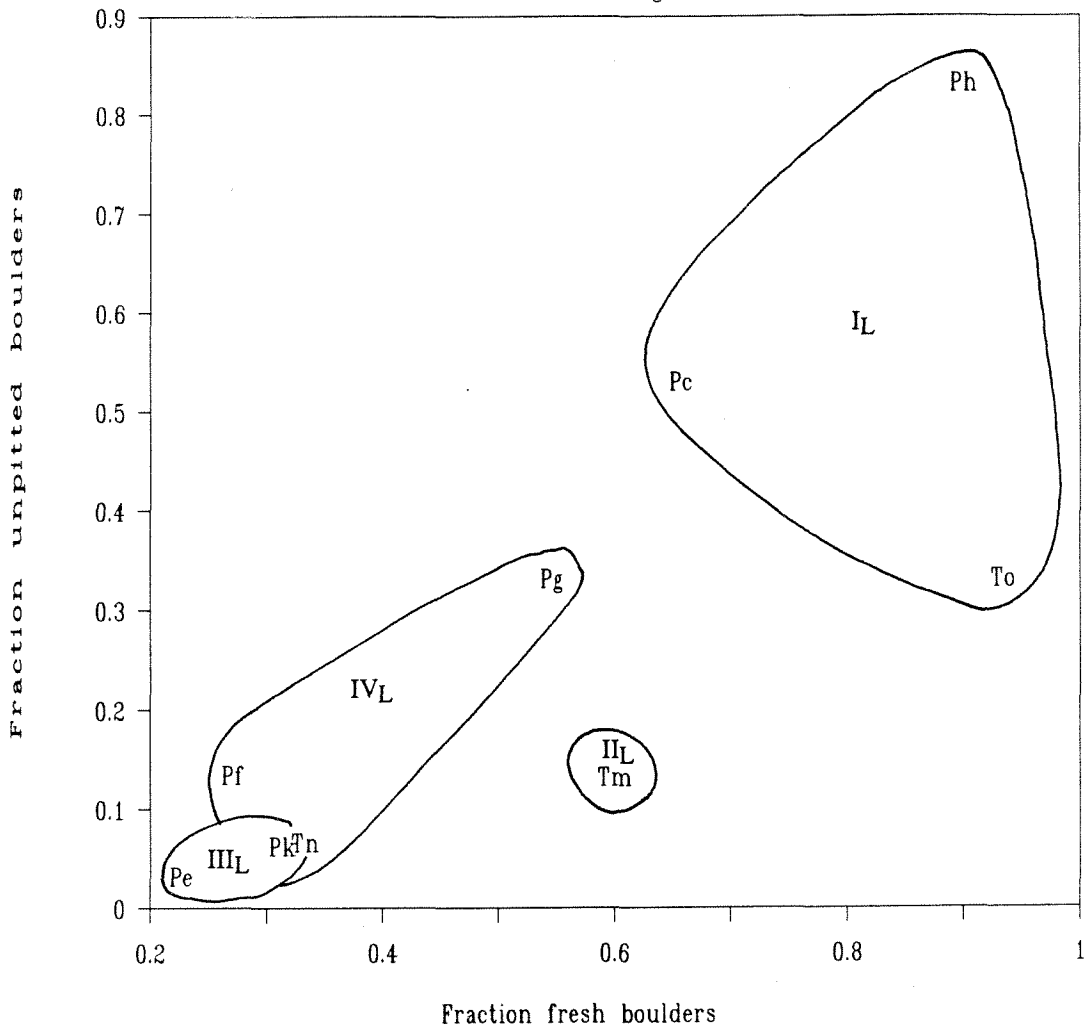
Relative dating

Figure   1-17b

June Lake left–lateral moraines

Relative dating
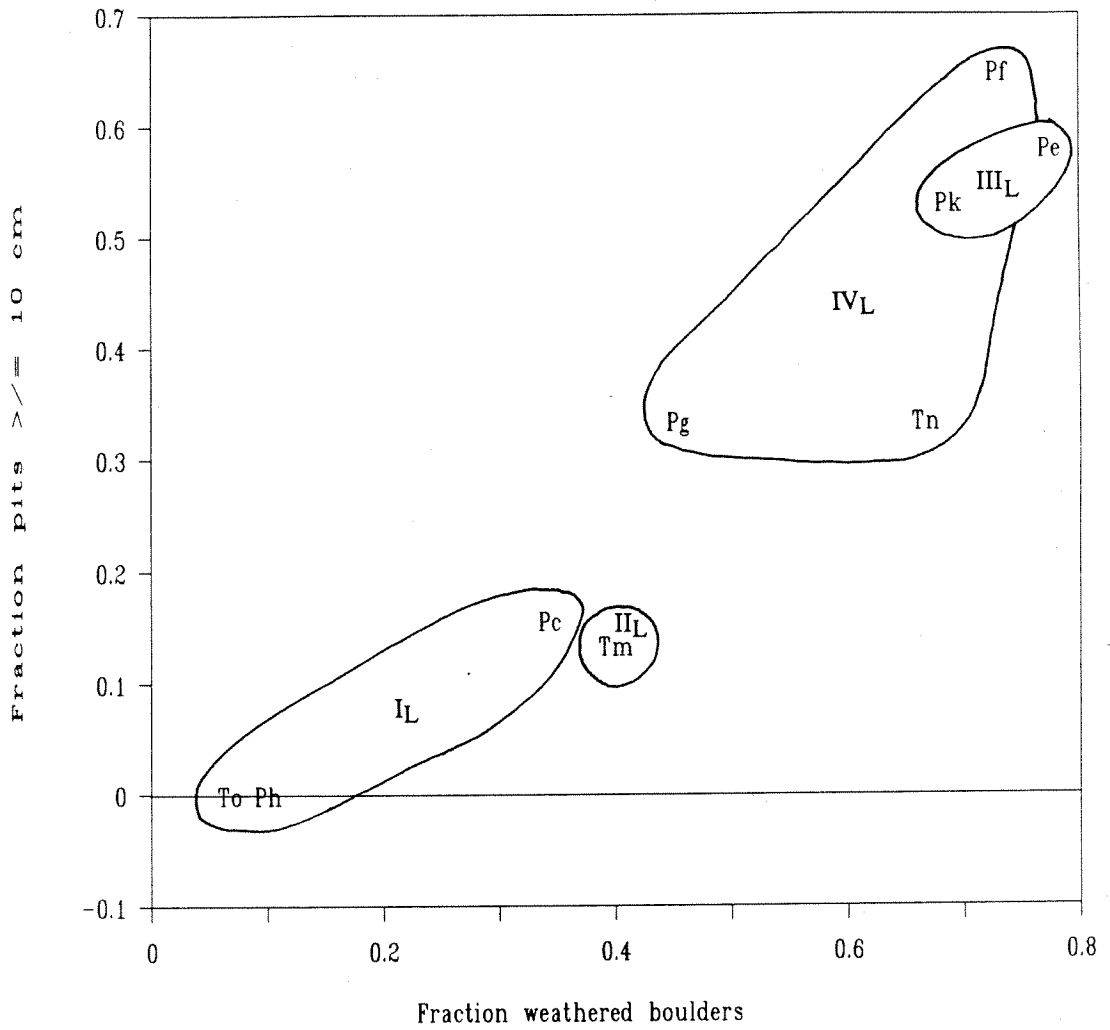
Figure   1-17c

moraines of Grant Lake. By plotting results from large, rapidly weathering boulders, Figures 1-17b and 1-17c, however, suggest that moraine III-L is correlative with moraine IV-L, which is equivalent to moraine VII-R of Grant Lake. Figures 1-17b and 1-17c suggest that moraine II-L, which, like moraines III-L and IV-L, contains no June Lake basalt cinders, is considerably younger than moraines III-L and IV-L. Moraines III-L and IV-L are therefore tentatively correlated to the same glaciation, and moraines I-L and II-L to two separate, younger glaciations.

Conclusions

Because of their well-developed terminal loops and fresh boulder surfaces, moraines I-R to III-R correlate to the Tioga glaciation. Moraines IIIa-R and IV-R probably correlate to the Tenaya glaciation, since they are still sharp-crested and have only moderately weathered boulders on their surfaces. Moraines V-R and VI-R probably correlate to the Tahoe and Mono Basin glaciations, based on their evolved landforms and the relative extent of moraine V-R (Figure 1-12). Because the Tenaya moraines are separated from the Tioga moraines by basalt that was not erupted during full glacial conditions, it seems possible that the Tenaya glaciation was not merely an early phase of the Tioga glaciation, as suggested by Fullerton (1986), but was truly a separate advance.

CSV data do not have the same systematics found in other canyons. It was not possible to fit mean V_p to estimates of age for the deposits. However, V_p modes associated with normally weathering boulders -- used as estimates of "true" mean V_p -- do become slower with age (Figure 1-18). Figure 1-18 shows the regression of the "normal-weathering" mode against estimated age with
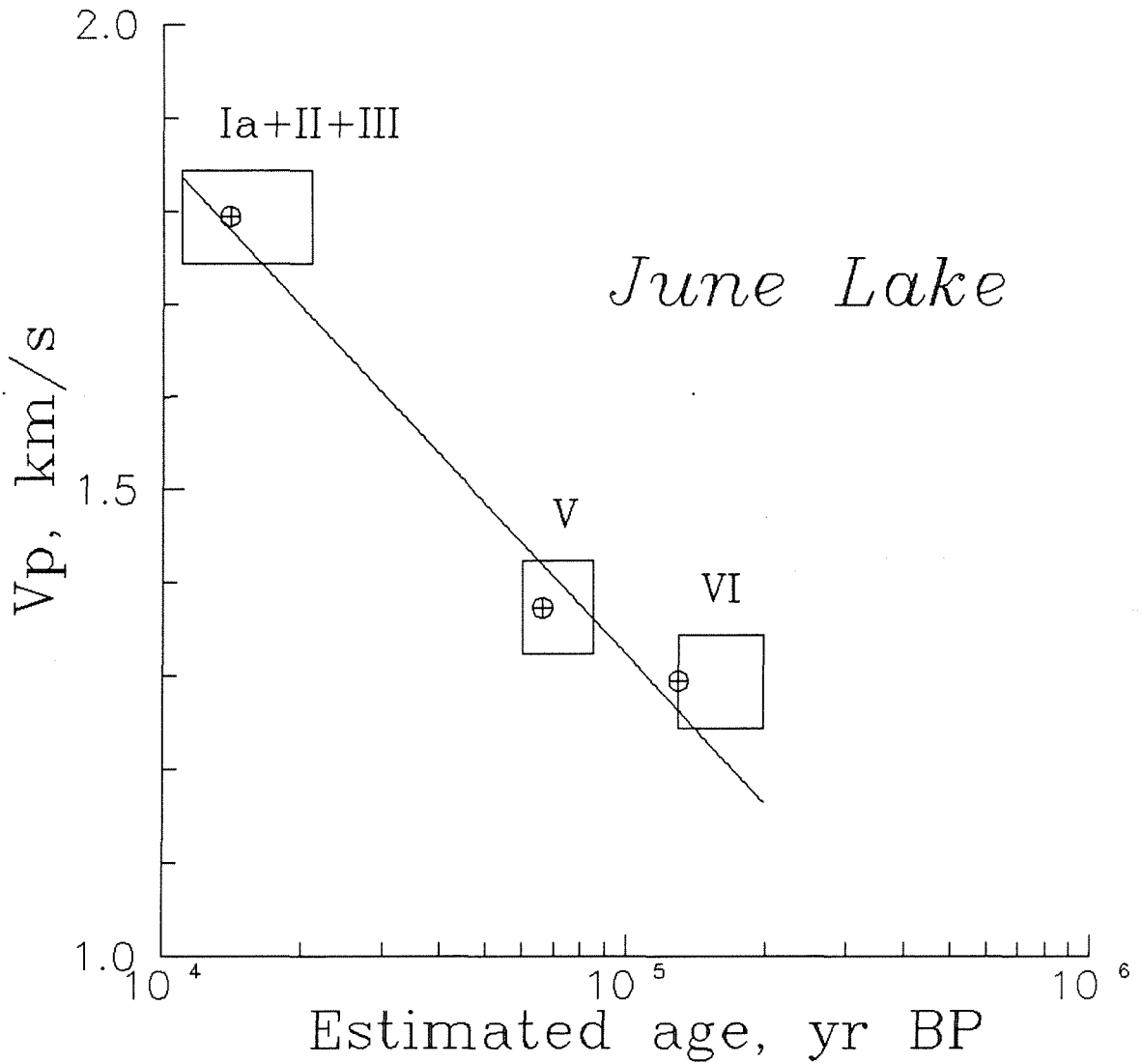
Figure 1-18. V_p-age regression, June Lake. "Normal-weathering" modes used instead of means for best-estimate points. Horizontal error bar is range of estimated age, vertical is "typical" one standard error of the mean found in most CSV samples. Data are consistent with the hypothesized ages of the moraines, if assumptions about case-hardening are correct.

"typical" error bars (sample standard deviation of mean = 0.05 km/s) on the modes. It seems reasonable to conclude that the moraines were deposited at the estimated times, if the assumptions about case-hardening are valid.

Moraine complex I-L is, like moraines I-R to III-R, of Tioga age. Moraines III-L and IV-L are both tentatively correlated to the Tahoe glaciation. Moraine II-L may therefore be the sole, small left-lateral remnant of Tenaya till.

Lee Vining Canyon

General Statement

There are six distinct right-lateral moraines at Lee Vining Canyon. There are only three distinct left-lateral moraines because a bedrock promontory that juts into the canyon from the north probably forced succeeding glaciers to conform to the same shape and, therefore, to bury deposits left by preceding glaciers.

Moraine I is steep-sided and grades to a terminal loop (Figure 1-19a). Moraine II is also steep-sided but ends abruptly about 300 m upstream from the moraine I terminus. Moraines III and IV merge upstream into the most prominent lateral moraine. The downstream termini of these moraines are cut by shorelines of Pleistocene Lake Russell. Moraines V and VI are heavily eroded and are crosscut by moraines III and IV.

Lee Vining Canyon was studied by Russell (1889) and Blackwelder (1931), who used the canyon as the type locality for his Tioga till. Moraine I is his Tioga moraine. Putnam (1950) studied the Tioga terminal and recessional moraines and correlated them to similar groups of moraines at June and Grant Lakes. Putnam (1949) and Kistler (1966a) included Lee Vining Canyon in their

Figure 1-19. Moraines of Lee Vining Canyon: a) Numbered as in text, and CSV sites. Dotted lines are moraine crests. Relative weathering of boulders on moraines I, II and III was studied by Birman (1964); b) Interpretation. Moraine II was assigned to the Tenaya glaciation by Birman (1964).

MORAINES OF
LEE VINING CANYON

(a) Numbered moraines and sites

(b) Interpretation
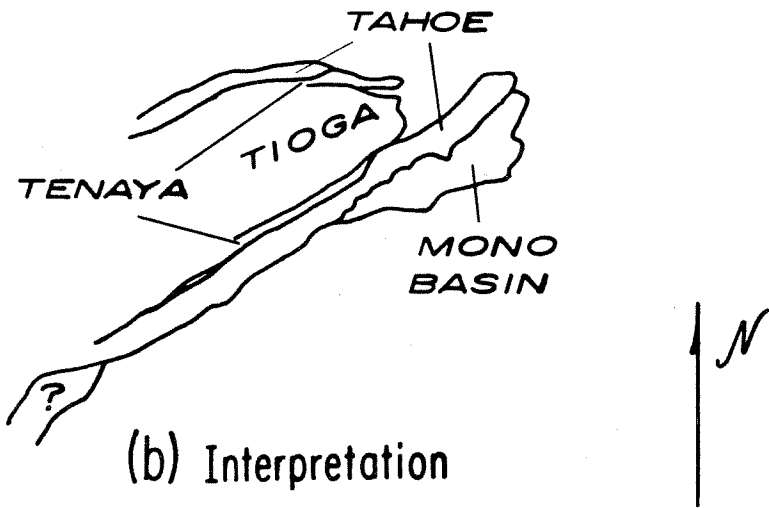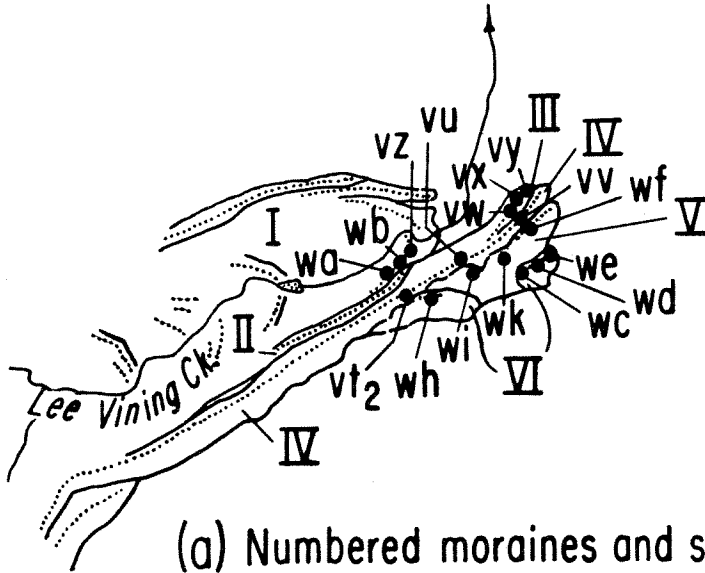
Figure   1-19

regional studies. Birman (1964) studied the relative weathering

characteristics of the Tahoe and younger moraines. He was able to

differentiate a Tenaya moraine (moraine II) from Tahoe (moraine IV) and Tioga

moraines, based on relative weathering of boulder surfaces.

I used medium-grained granite of Lee Vining Canyon for CSV studies, and

was able to distinguish three glacial stages with these data. Including the

Tenaya moraine of Birman (1964), on which I did not collect CSV data, the six

right-lateral moraines were deposited during at least four distinct

glaciations.

Clast-sound velocity

Figure 1-20 and Tables 1-9 and 1-10 show the three statistically distinct

groups of moraines in Lee Vining Canyon as determined by CSV. Moraines III

and IV and moraines V and VI were not statistically distinguishable with CSV.

Moraine morphology

Moraine I is steep-sided and grades into a prominent, well-preserved

terminal loop. Blackwelder (1931) used it as the type Tioga stage deposit,

which he named after the pass at the head of Lee Vining Canyon.

The terminal loop of moraines III+IV has been removed by erosion from Lee

Vining Creek, although part of the loop probably underlies the broad lake

terraces to the northeast of the lateral moraines. Locally, these moraines

have steep sides, especially where eroded into broad, shallow gullies. None

of the gullies are through-going.

Moraines V+VI are overlain by moraines III+IV along much of their length

(Figure 1-19a). The crests of moraines V and VI are distinctly more rounded
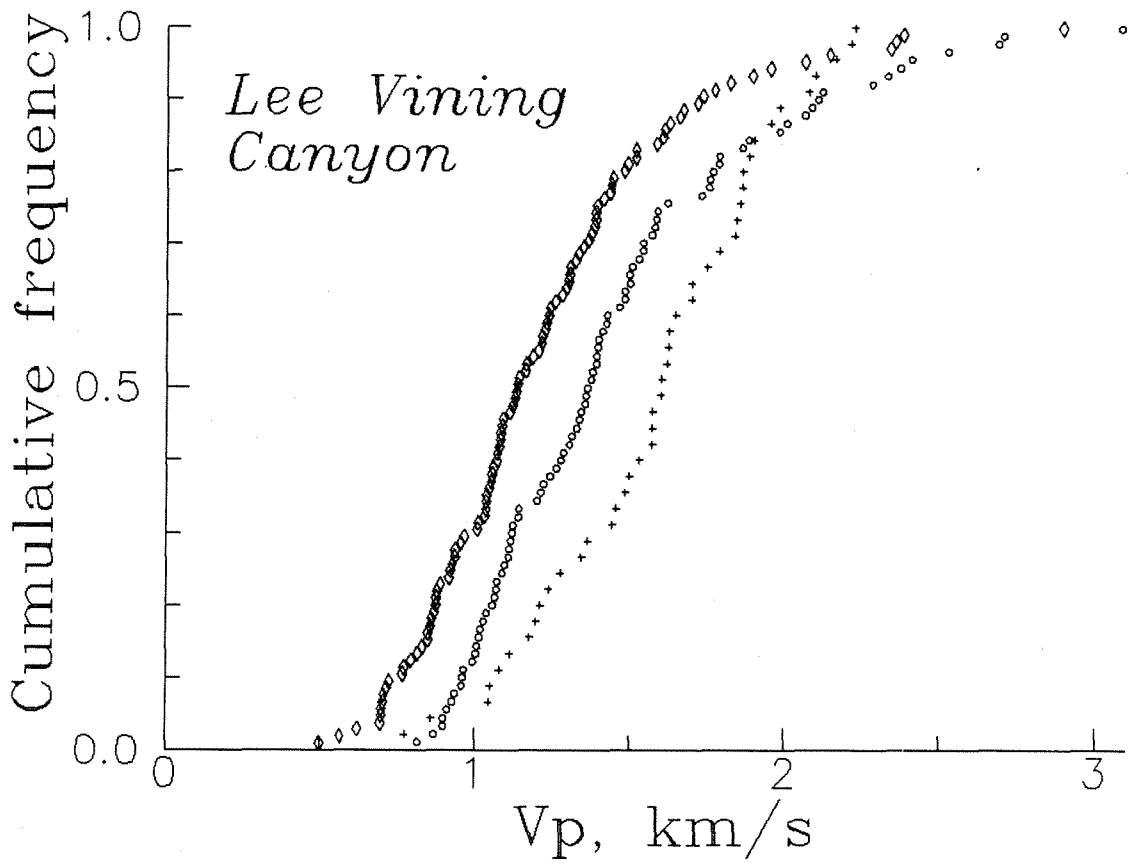
Figure 1-20. Cumulative frequency distributions of CSV data, Lee Vining Canyon. Diamonds = moraines V and VI; circles = moraines III and IV; plusses = moraine I. Samples from moraines III and IV, and V and VI are grouped together because they are statistically indistinguishable. The separation between the grouped samples suggests that they were drawn from moraines of different ages.

Table 1-9. CSV data for moraines of Lee Vining Canyon.

Moraine	Site	No. of boulders	$\overline{V_p}$a	S_{V_p}	$S_{\overline{V_p}}$
I	vz	15	1.546	0.356	0.092
	wa	15	1.781	0.238	0.061
	wb	15	1.419	0.385	0.099
	All sites	45	1.582	0.358	0.053
III	vw	15	1.388	0.544	0.141
	vx	15	1.488	0.323	0.083
	vy	15	1.473	0.436	0.122
	All sites	45	1.450	0.436	0.065
IV	vt2	15	1.352	0.407	0.105
	vu	15	1.553	0.583	0.151
	vv	15	1.478	0.533	0.138
	All sites	45	1.461	0.508	0.076
V	wf	15	1.122	0.371	0.096
	wg	15	1.378	0.555	0.143
	wi	15	1.263	0.512	0.132
	All sites	45	1.254	0.486	0.072
VI	wc	15	1.031	0.339	0.115
	wd	15	1.228	0.549	0.302
	we	15	1.248	0.198	0.039
	wh	15	1.281	0.255	0.065
	All sites	60	1.197	0.365	0.047
III+IV		90	1.455	0.471	0.050
V+VI		105	1.222	0.420	0.041

a $\overline{V_p}$ = Sample mean, S_{V_p} = Sample std. dev., $S_{\overline{V_p}}$ = Std. dev. of mean.

Table 1-10. Statistical test of Lee Vining Canyon CSV data.
Crests numbered as in Table 1-9.

Crests compared	F-ratio	Probability[a]	t-test stat.,t	Probability[b]	K-S stat., D_{max}	Probability[c]	Reject H_o?
I--III	1.480	19.8%	1.570	12.0%			N
III--IV					0.133	81.9%	N
I--III+IV					0.311	0.6%	Y
IV--V					0.289	4.7%	Y
V--VI	1.773	4.0%	0.663	51.0%			N
III+IV--V+VI					0.256	0.4%	Y

[a] Probability that "F" could assume the tabled value if the two samples were drawn from populations of equal variance.

[b] Probability that "t" could assume the tabled value if the population means are the same (H_o true).

[c] Probability that D_{max} could assume the tabled value if the samples were drawn from similarly distributed populations (H_o true).

H_o is the hypothesis that the populations from which the samples were drawn are the same.

than those of moraines III and IV. The two moraines are also cut by deep gullies, some of which are through-going. Where they are not gullied, their flanks have shallow slopes.

Conclusions

Clast-sound velocity and morphology indicate that the moraines of Lee Vining Canyon can be separated into three distinct deposits. Relative-weathering data collected by Birman (1964) indicate that moraine II was deposited during a fourth distinct glacial stage. As already mentioned, moraine I is the type Tioga moraine of Blackwelder (1931). Moraines III and IV are bulky and elongate, and boulders on their crests have intermediate values for mean p-wave speeds. They are outboard of the Tenaya moraines of Birman (1964). There is therefore good reason to correlate them to the Tahoe glaciation (Figure 1-19b). Moraines V+VI have distinctly lower p-wave speeds than moraines III+IV, and are heavily gullied. It is reasonable to correlate them to the Mono Basin glaciation of Sharp and Birman (1963). They may have been deposited by a glacier equally as extensive as the Tahoe glacier, although the ends of the moraines are truncated by the range-front fault and modified by lake terraces. That they were of equal extent corroborates the suggestion of Gillespie (1982; 1984), furthered by Mathieson (1984), that the Mono Basin glaciation was as extensive as the Tahoe glaciation.

A comparatively low value for the coefficient of determination, r^2 (Table A-1; Figure 1-21), indicates a weak correlation between the mean V_p values and estimated ages. The goodness of fit could probably be improved by separating moraines V and VI into different glacial stages. There are some morphological differences between these two moraines, in the degree of dissection and
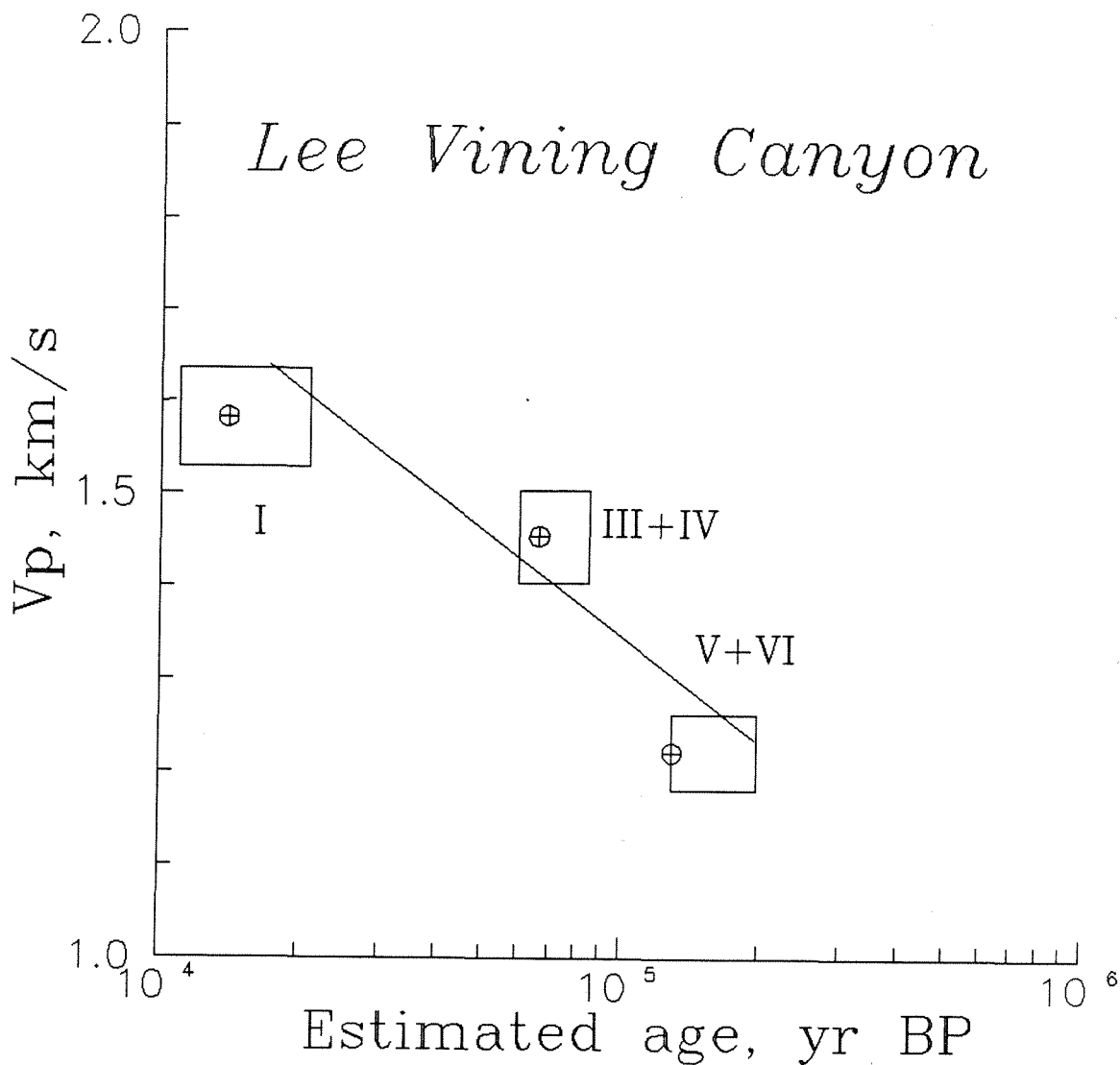
Figure 1-21. V_p-age regression, Lee Vining Canyon. Horizontal error bars are ranges in estimated age; vertical error bars are one standard deviation of the mean (68% confidence interval). Line is not least-squares fit through the sample means as it is in all other similar graphs. There is a relatively poor correlation between estimated age and V_p, perhaps caused by grouping moraines V and VI together, which may actually be significantly different in age.

rounding of crests. However, a separation of the two moraines was not warranted by the CSV statistics.

Lundy Canyon

General statement

There is only one set of lateral moraines extending past the range front at Lundy Canyon. Two other right-lateral moraines, and perhaps one left-lateral moraine, are truncated by the range-front fault. Apparently, their basin-ward extensions are now buried under younger morainal and lacustrine deposits.

The moraines of Lundy Canyon have received some attention because of their strange morphology. Immediately upon leaving the confines of Lundy Canyon, both right- and left-lateral moraines arc dramatically to the north. Russell (1889) showed that this was caused by a greater volume of tributary ice on the south side of the canyon. These tributaries contributed a large amount of medial debris to the right-lateral moraines, thus accounting for their hummocky form, which is similar to that of terminal moraines in other canyons.

Blackwelder (1931) thought that the lateral moraines in the basin were Tahoe age and that the two moraines truncated by the frontal fault, moraines IV and V, were both Sherwin age (Figure 1-22). Lachmar (1977) reached the same conclusion, but also mapped Tioga and Hilgard material farther up-canyon (moraines Ib and Ia, respectively). Sharp and Birman (1963) suggested that moraine IV was of Mono Basin age rather than of Sherwin age.

I collected CSV measurements on the Tioga and Hilgard moraines of Lachmar (1977) as well as on the supposed Tahoe and Sherwin moraines of Lachmar (1977)

MORAINES OF LUNDY CANYON
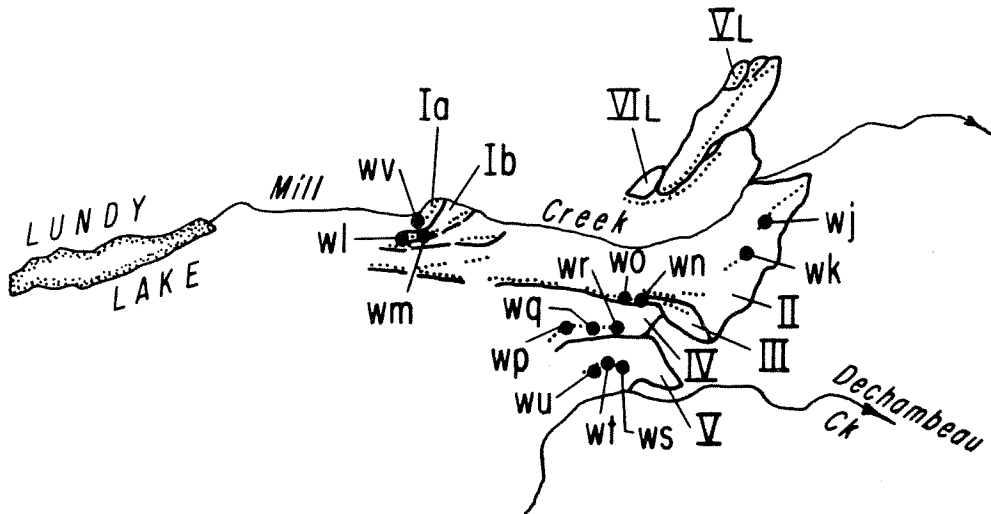
(a) Numbered moraines and sites
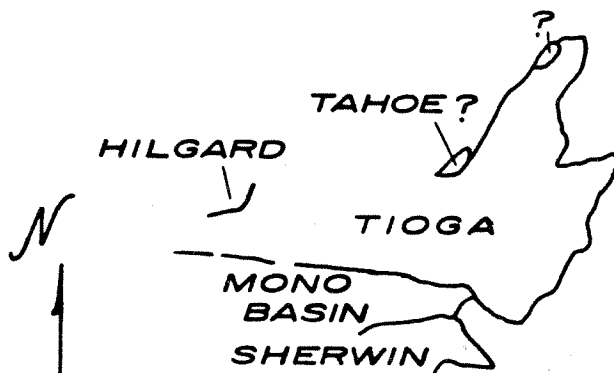
(b) Interpretation

Figure 1-22. Moraines of Lundy Canyon: a) Numbered as in text, and sites. Dotted lines are moraine crests, and b) Interpretation. Relative-weathering data were collected here by Lachmar (1977). Interpretation, which differs significantly from that of Lachmar (1977), is based on CSV measurements from this study. Lundy Canyon is noteworthy for the prominent Tioga moraines.

and Blackwelder (1931). All boulders used in the survey were of medium-grained granodiorite of Mono Dome (Chesterman and Gray, 1975). Boulders from a distinct, cataclasized facies were extremely common on the outermost moraine.

Clast-sound velocity

Moraine Ia is statistically separable from moraine Ib (Tables 1-11, 1-12; Figure 1-23a). Mean V_p on moraine Ia is lower than mean V_p on moraine Ib. This seems to corroborate the conclusion of Lachmar (1977) that boulders on moraine Ia were more heavily weathered, even though the moraine is clearly younger. Lachmar (1977) concluded that moraine Ia was a Hilgard deposit.

Moraines Ib, II and III are not statistically separable one from another (Table 1-12) and are therefore considered to be of the same age. This interpretation differs from that of Lachmar (1977), who considered moraine Ib to be younger than moraines II and III. Lachmar's (1977) RD data are actually compatible with the interpretation suggested by the CSV data. RD data collected during this study (not illustrated) suggest that moraines II and III are young. Almost all boulder surfaces on these moraines are fresh and unpitted. Moraines Ib, II and III are therefore considered to be of the same age.

The inner moraines (I-III) are all highly significantly different from moraines IV and V (Table 1-12; Figure 1-23a). Although these last two are not statistically distinct from each other, there are two distinct boulder subsamples on moraine V -- resistant, epidotized, cataclasized boulders, and normally weathered boulders (Figure 1-23b). Because the subpopulation of resistant boulders is not noticeable on moraine IV, weathering on moraine V

Table 1-11. CSV data for Lundy Canyon right-lateral moraines.

Moraine	Site	No. of boulders	$\overline{V_p}$ [a]	S_{V_p}	$S_{\overline{V_p}}$
Ia	wv	15	1.471	0.221	0.057
Ib	wl	15	1.688	0.468	0.121
	wm	15	1.785	0.279	0.072
	All sites	30	1.736	0.382	0.070
II	wj	15	1.613	0.382	0.099
	wk	15	1.662	0.266	0.069
	All sites	30	1.637	0.324	0.059
III	wn	15	1.670	0.422	0.109
	wo	15	1.712	0.439	0.113
	All sites	30	1.691	0.424	0.077
II+III		60	1.664	0.375	0.048
IV	wp	15	1.407	0.763	0.197
	wq	15	1.254	0.496	0.128
	wr	15	0.906	0.277	0.071
	All sites	45	1.189	0.577	0.086
V	ws	15	1.138	0.529	0.137
	wt	16	1.161	0.552	0.138
	wu	15	1.497	0.594	0.153
	All sites	46	1.263	0.571	0.084
	Resistant boulders only	15	1.498	0.577	0.149
	Non-resistant only	31	1.150	0.541	0.097
IV+V		91	1.227	0.572	0.060

[a] $\overline{V_p}$ = Sample mean, S_{V_p} = Sample std. dev., $S_{\overline{V_p}}$ = Std. dev. of mean.

Table 1-12. Statistical test of Lundy Canyon CSV data.
Moraines numbered as in Table 1-11.

Moraines compared	F-ratio	Proba-bility[a]	t-test stat.,t	Proba-bility[b]	K-S stat., D_{max}	Proba-bility[c]	Reject H_o?
Ia--Ib	2.977	3.5%	-2.937	0.5%			Y
Ib--II	1.389	38.1%	1.083	28.3%			N
Ib--III					0.300	13.4%	N
II--III					0.100	99.8%	N
III--IV					0.633	<<<1%	Y
I+II+III--IV					0.600	<<<1%	Y
IV--V	1.030	92.3%	-0.733	46.5%			N
IV--V[*]	1.139	71.7%	0.301	76.4%			N
IV--V[**]	1.001	100.0%	-1.797	7.8%			Y
V[*]--V[**]	1.137	73.7%	-2.007	5.1%			Y

[a] Probability that "F" could assume the tabled value if the two samples were drawn
from populations of equal variance.

[b] Probability that "t" could assume the tabled value if the population means are
the same (H_o true).

[c] Probability that D_{max} could assume the tabled value if the samples were drawn
from similarly distributed populations (H_o true).

H_o is the hypothesis that the populations from which the samples were drawn
are the same.

[*] Non-resistant boulders only.

[**] Resistant boulders only.
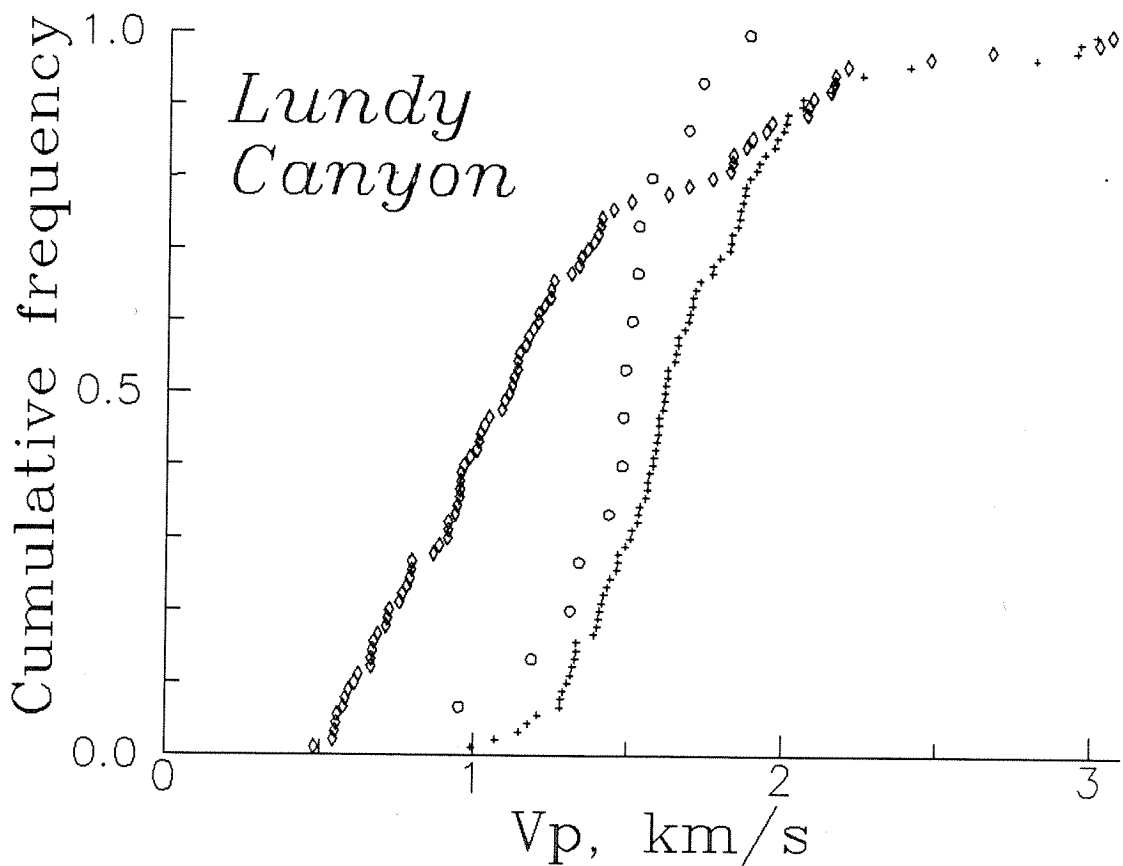
Figure 1-23a

Figure 1-23. Cumulative frequency distributions of CSV data, Lundy
Canyon. a) All moraines. Diamonds = moraines IV and V; plusses =
moraines Ib, II and III; circles = moraine Ia. Moraines Ib, II and III
are grouped together because they are statistically indistinguishable.
The anomolous degree of weathering of boulders on moraine Ia is
corroborated by the RD data of Lachmar (1977); b) Different subsamples
in moraine V. Squares = normally weathering boulders, plusses =
resistant boulders. The resistant boulders are composed of a
cataclasized facies of the same plutonic rock from which the normally
weathering boulders are derived. These two subsamples are
statistically significantly different.
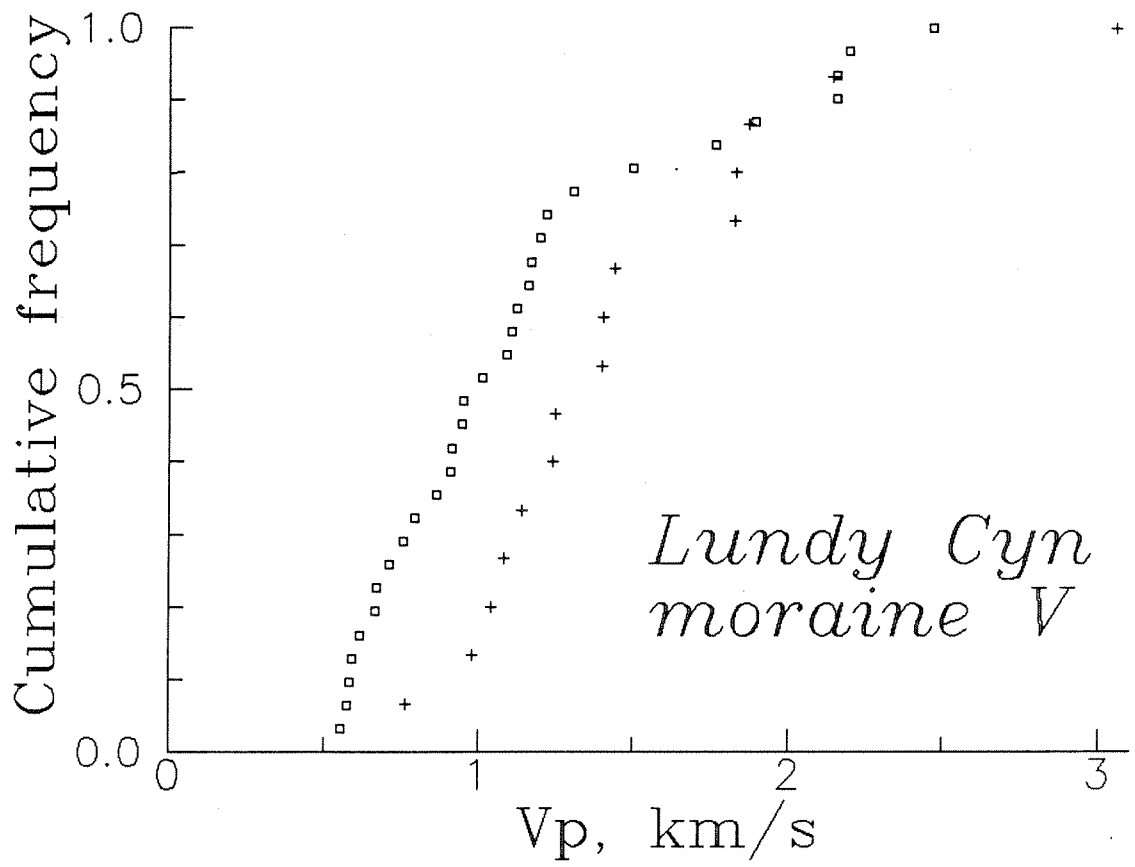
Figure 1-23b

must be more evolved, and the two moraines were probably deposited at very different times.

Moraine morphology

Moraines I-III are all sharp-crested and have low-amplitude depositional features preserved on them, such as small, separate crests.

Moraine Ia has a prominent terminal loop with a silted pond behind it, in contrast to moraine Ib, which is mostly lateral material grading to very subdued terminal moraines. The flat crest of the terminal loop of moraine Ia indicates that it was not formed as separate piles of material dumped from englacial medial moraines like moraine II, but may indicate instead that the moraine was formed by glacial bulldozing. Moraine Ia may be a push moraine formed by a short-lived advance (Rabassa *et al.*, 1979), following a glacial retreat from moraine Ib.

Right-lateral moraine II seems to be disarticulated by large gullies (Figure 1-24). However, as mentioned in the introduction, this moraine is probably composed of material dumped from englacial medial moraines and therefore the "gullies" are swales between mounds of material deposited from medial moraines that have been modified only a minor degree by erosion.

Moraine IV is cut by gullies that have eroded through the crest. It is considerably elevated above moraine III, indicating that the canyon was substantially down-cut between the two glaciations.

Similarly, moraine V is much higher than moraine IV. Bedrock knobs jut through its broad crest. Since it curves southward toward lower Dechambeau Creek rather than heads straight toward Mono Basin as do the younger moraines within the range, its present form is probably mostly erosional and not

Figure 1-24. Photograph taken from Black Point looking east at the moraines of Lundy Canyon, showing "gullies" in moraine II. The "gullies" are probably swales between piles of debris dumped by medial moraines, rather than erosional furrows. Also visible are true erosional gullies in moraine IV.

moraine IV
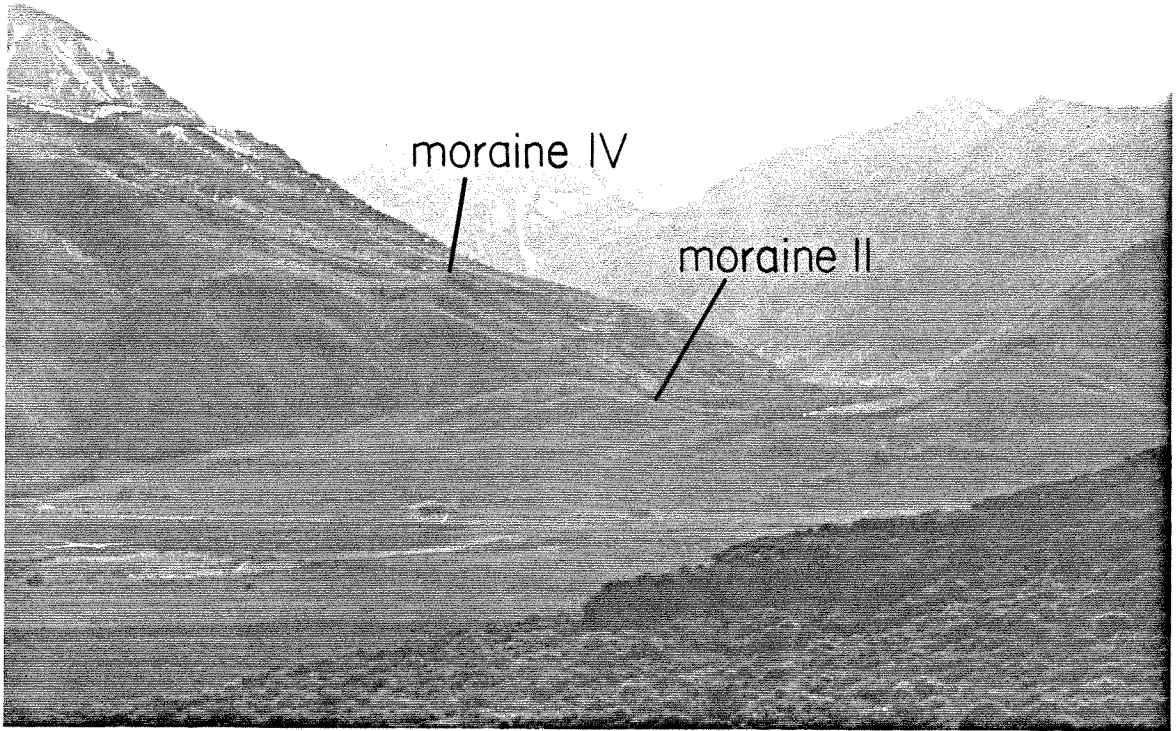
moraine II

Figure 1-24

primary.

Conclusions

Moraine Ia is distinct in morphology and CSV from moraine Ib. It could be correlated to the Hilgard glaciation, but its great extent and low terminal elevation seem anomalous for Hilgard deposits (Birman, 1964). However, the Hilgard moraines of Mammoth Creek (Curry, 1971) seem to be comparably extensive, and the possibility that the moraine was formed by a short-lived readvance argue for the Hilgard correlation.

The high V_p, fresh boulders and youthful landforms of moraines Ib-III indicate that they are deposits of the Tioga glaciation, not the Tioga and Tahoe glaciations as suggested by Lachmar (1977).

The elevation of moraine IV relative to moraines I-III and the V_p-age regression (Figure 1-25) indicate that moraine IV correlates to the Mono Basin glaciation as suggested by Sharp and Birman (1963). A correlation to the Tahoe glaciation is less satisfatory because of the low V_p and the lack of comparably large readjustment of canyon depth at other locales between Tioga and Tahoe deposits. The data allow a correlation to one of the many glaciations that have been proposed for the inter-Sherwin/ Mono Basin period (Casa Diablo of Curry (1971); pre-Mono Basin I and II of Gillespie (1982); Deep Creek and Grouse Meadow of Clark (1967), etc.), so the Mono Basin correlation is tentative.

The residual boulder population, weathered form and low V_p of moraine V are all compatible with correlation to the Sherwin stage, as suggested by Blackwelder (1931).

If moraine IV correlates to the Mono Basin glaciation, and moraines Ib-
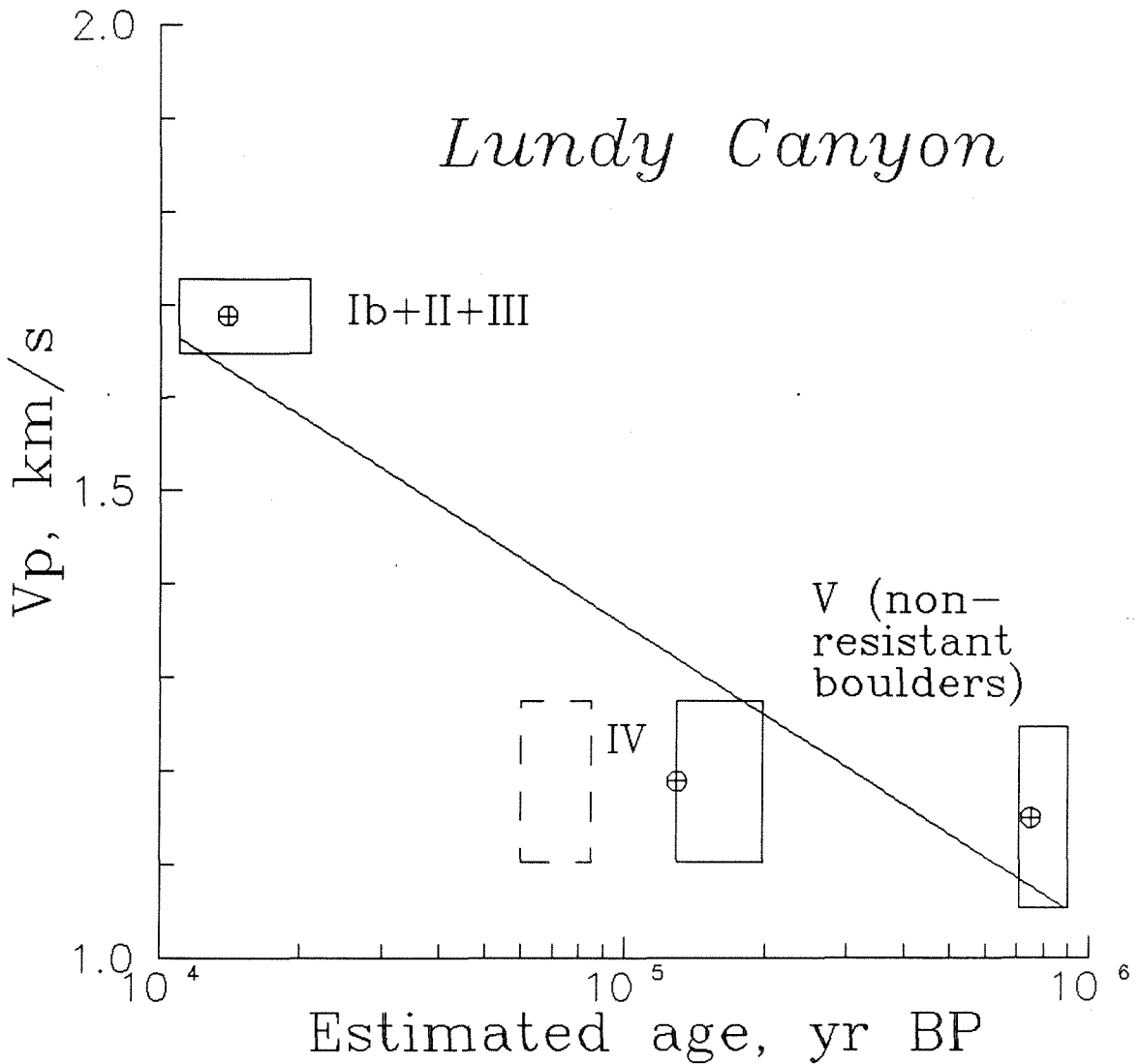
Figure 1-25. V_p-age regression, Lundy Canyon. Horizontal error bars
are range in estimated ages; vertical bars are one standard deviation
of the mean (68% confidence interval). Only non-resistant boulders on
mroaine V were used. Poor regression between estimated age and V_p may
be caused by attrition of boulders with lowest V_p from moraine V.
Dashed box shows that an alternative Tahoe age for moraine IV is less
compatible with available data than is the Mono Basin age.

III to the Tioga glaciation, then where are the Tahoe moraines, which should be more extensive than the Tioga? Lateral moraines within the range at Lundy Canyon are preserved only locally as terraces separated by episodes of extensive downcutting because of the canyon's unusually steep and confining bedrock walls. If there was insufficient time for substantial down-cutting between Tahoe and Tioga time, as is the case in most canyons, then it is reasonable that the Tahoe moraines are not preserved. Judging from the amount of downdropping of the Tioga moraines along the range front and from the lack of preservation of moraines IV and V within the basin, the Tahoe moraines within the basin are probably downdropped and buried by the Tioga moraines. The only possible remnants of Tahoe till are the moraines marked V-L and VI-L on Figure 1-22. Moraine VI-L is a veneer deposited on the range front just outboard of the left-lateral Tioga moraines. Its crest is at about the same elevation as the Tioga crest within the range, and it abruptly terminates along the range-front fault. Moraine V-L is a small remnant that is crosscut by the left-lateral Tioga moraines.

As at Lee Vining Canyon, a low coefficient of determination was found for the CSV-age regression proposed in Figure 1-25. The low coefficient of determination is probably the result of attrition of the slowest boulders from moraine V, since a large percentage of the normally weathering granitic boulders on it have turned to grus and are unavailable for testing. This therefore gives an upper age bound for the usefulness of the CSV technique in this region of approximately 750,000 years. A similar upper bound was found by Gillespie (1982) at Green Creek in the Bridgeport Basin.

Till (?) at Hartley Springs

A small body of till (?) crops out at Hartley Springs (Figure 1-26). The till may be of rock-glacial origin, based on its corrugated surface, which is reminiscent of the surface of the rock-glacial moraine at Parker Canyon. Since the till overlies Bishop Tuff and since it seems to retain original depositional morphology, it is probably post-Sherwin age.

The source region for the till is small and low in elevation, and there is no evidence that it was deposited during multiple glaciations. The lateral moraine has a rounded crest, similar to other pre-mid-Wisconsin moraines. In addition, the till has been present sufficiently long that locally it consists only of erratics flushed of matrix material.

Most granitic boulder surfaces found on the moraine were weathered (Figure 1-27). Their weathering resembles that on the Tahoe moraines at June Lake, where boulder lithology (Wheeler Crest Quartz Monzonite) and vegetation (Jeffrey Pine) are the same. Weathering pits on the boulders are shallow, but they may have been modified by fire flaking. Many rock flakes spalled from the boulders have faces that crosscut weathering fronts.

The moraine is tentatively correlated to the Tahoe glaciation.

DISCUSSION

Below, I discuss a few of the general results of this work. I begin with observations on weathering features and differentiation of the glacial deposits and end with some remarks on the ages of the moraines of the Mono Basin. A brief discussion of dating techniques is given in Appendix A.

MORAINES AT
HARTLEY SPRINGS

Campground

Hartley Springs

TAHOE?

TAHOE?

Bishop
Tuff

9568

N

OBSIDIAN

FLOW

0   1   2 km
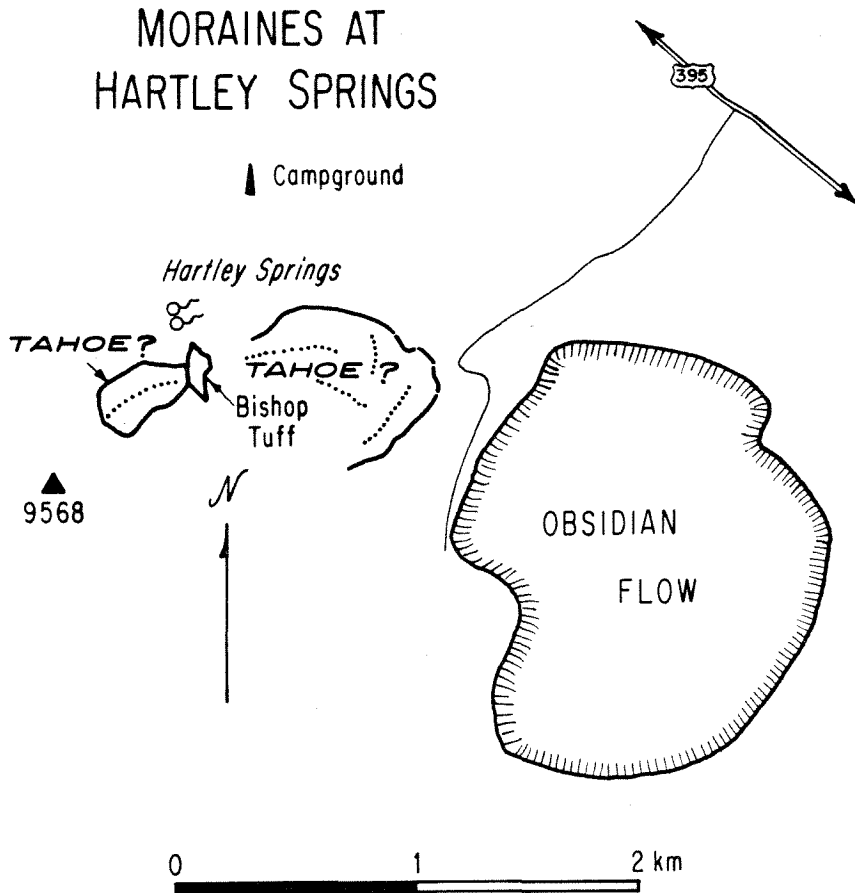
Figure 1-26. Glacial geology near Hartley Springs. Dotted lines are
moraine crests. Small moraine-like landforms lie both within and
outside of the range. The range front lies on the western edge of both
the eastern moraine and Obsidian Flow. Morphology of the eastern
moraine is similar to that of the rock-glacial moraine at Parker Canyon
in that both contain numerous short, irregular crests.

Hartley Springs and June Lake

Relative dating
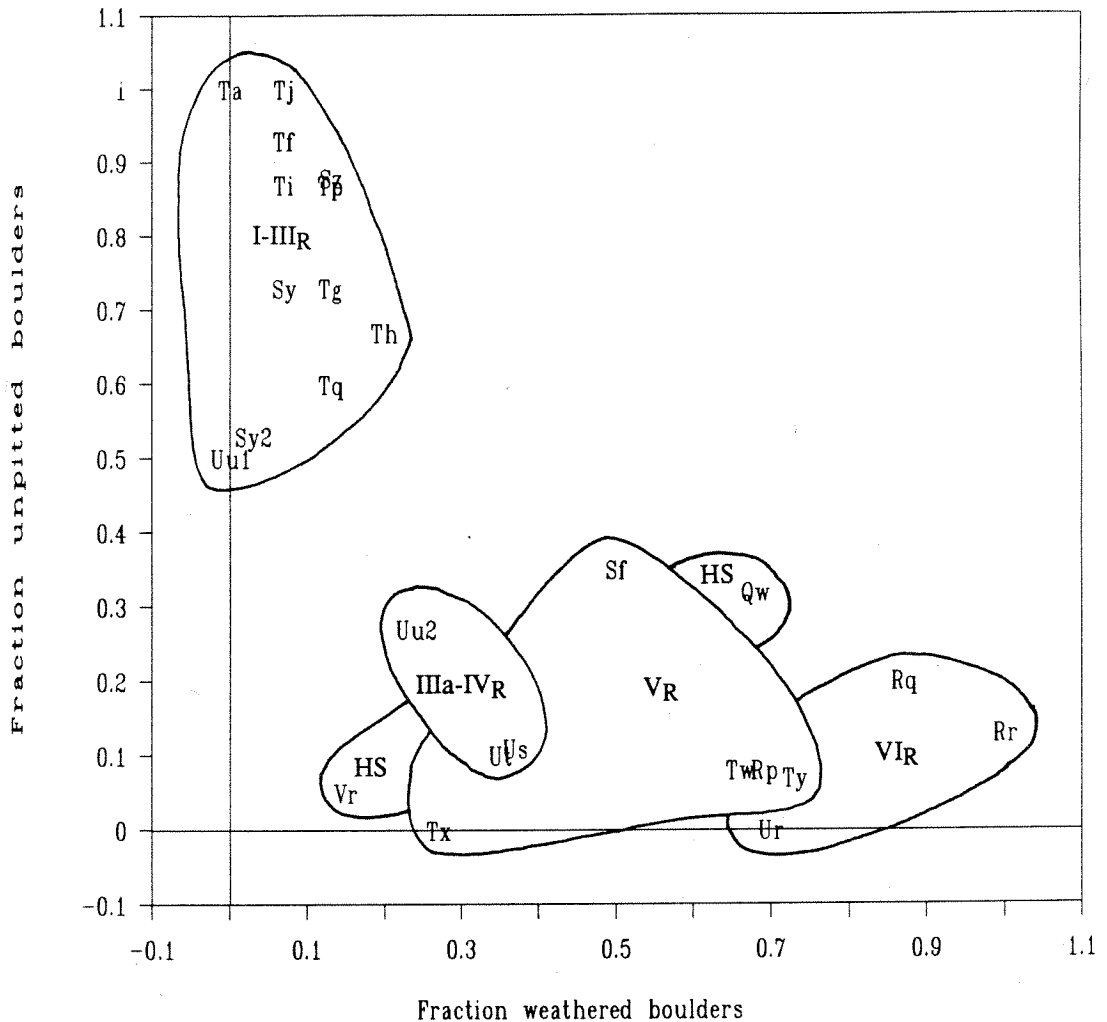
Figure 1-27. Relative weathering of boulders on moraines at Hartley Springs compared with weathering of boulders on June Lake moraines. Fraction of unpitted boulders vs. fraction weathered boulders is plotted. Age increases to lower right. The Hartley Springs moraine certainly does not correlate to moraines I-R to III-R at June Lake, and seems to correlate best to moraine V-R, which is of Tahoe age.

Differentiation of Deposits

Several generalizations about weathering features peculiar to deposits of certain ages can be drawn.

Sherwin Till (?) at Lundy Canyon appears to be a residual deposit, formed by the weathering of an earlier constructional landform. Not only is the landform modified by erosion, but also the boulder population on the surface is composed in large part of residual, slowly weathering boulders.

Only in Lee Vining Canyon were Mono Basin deposits statistically distinct from Tahoe deposits using CSV. At Grant Lake, the Mono Basin CSV sample could be split into case-hardened and non-case-hardened subsamples, suggesting a greater degree of weathering of Mono Basin till over Tahoe till. At June Lake, relative weathering criteria differentiated Mono Basin from Tahoe material, but CSV did not. At both Grant and June Lakes, Tahoe and especially Mono Basin boulders are case-hardened, whereas very few boulders on these deposits at Lee Vining Canyon are case-hardened. Case-hardening is almost certainly responsible for the poor CSV results in Tahoe and Mono Basin deposits, and may be especially well developed at June Lake because of ventifaction, coarse-grained rock type and moist climate, as indicated by the cover of Yellow Pine rather than sagebrush or Desert Mahogany, which are typical of other canyons.

Boulders on Tenaya deposits are weathered to an intermediated degree between boulders on both Tahoe and Tioga deposits at Parker and Grant Lakes, justifying consideration of the Tenaya glaciation as distinct and separable from the Tahoe and Tioga glaciations. However, variability within Tenaya deposits is often quite high, making it important to draw samples from at

least three sites.

Tenaya deposits were poorly differentiable from Tahoe deposits but were distinct from Tioga deposits at June Lake, based on RD techniques. Moreover, stratigraphic relationships at June Lake demonstrate that the glacier retreated at least back to the southern end of present-day June Lake between Tioga and Tenaya times, and therefore that Tenaya deposits are separated from Tioga deposits by at least a partial recession of the glacier.

Estimated ages of deposits

Crook and Gillespie (1986) found the glacial time scale in Table 1-1 to be strongly correlated with mean V_p from eastern Sierra Nevada moraines in several locales. CSV data in this study fit well with their glacial chronology in some localities, but poorly in others. Estimated age and mean V_p correlated strongly at Parker Canyon and Grant Lake. At June Lake and Lundy Canyon, poor results can be attributed to readily noticeable features of the boulder samples. At Lee Vining Canyon, the reason for weak correlation between mean V_p and age is not clear -- both lithology and climate are similar to those at Bloody and Parker Canyons, where significant correlations were observed. One possible explanation of the discrepancy is that moraines V and VI at Lee Vining Canyon are older than the Mono Basin moraines of Bloody Canyon, implying that Mono Basin moraines are completely overlain by Tahoe till and are inaccessible. Another possibility is that moraine V at Lee Vining may be Mono Basin age, and moraine VI may be older. Thus, the use of a Mono Basin age for moraine VI in the regression may skew it and weaken the results. In some respects, moraine VI appears to be more profoundly weathered and therefore significantly older than moraine V, indicating that further CSV

or RD sampling would probably improve the V_p vs. age regression by requiring moraines V and VI to be considered separately.

The goodness of fit of the regressions of mean V_p against age, especially at Parker Canyon, reinforces the hypothesis that Tahoe, Tenaya and Tioga deposits should be correlated to oxygen isotope stages two through four (Table A-1). Furthermore, no data suggested the correlation of Mono Basin deposits to anything earlier than oxygen isotope stage six, in agreement with Gillespie (1982) and Mathieson (1984). The results are therefore consistent with the suggestions of Sharp and Birman (1963), Gillespie (1982) and Mathieson (1984) that Wisconsin deposits (isotope stages 2 to 4) can be distinguished one from another, and are inconsistent with those of Burke and Birkeland (1979), who were unable to observe weathering differences among Wisconsin moraines.

CONCLUSIONS

Relative weathering features and CSV suggest that the canyons of the Mono Basin contain the records of at least four distinct late Pleistocene glacial advances. In contrast to the conclusion reached by Burke and Birkeland (1979), Tenaya and Mono Basin deposits are distinctly different in weathering characteristics from Tioga and Tahoe deposits. The findings agree with those of Sharp and Birman (1963), Birman (1964), Gillespie (1984) and Mathieson (1984), all of whom were able to distinguish at least three separate late Pleistocene advances at Bloody Canyon.

With exceptions, regression of mean V_p against estimated glacial ages, based on pluvial and marine records as well as absolute dates, revealed a good

correlation between the two variables. The CSV data are therefore compatible with correlation of the glacial record in the Mono Basin to the pluvial records of Lake Russell and Searles Lake, and to the marine oxygen isotope record.

CHAPTER 2

DETERMINATION OF AGES OF MORAINES AT LEE VINING CANYON FROM LANDFORM DEGRADATION

INTRODUCTION

Differential weathering of soils and boulders on the surfaces of glacial moraines has been used by previous workers in the Sierra Nevada as an indicator of moraine age. Blackwelder (1931) was the first to discuss systematic differences in morainal landforms, and in the degree of weathering of boulders and soils among moraines of different ages in the Sierra Nevada. Sharp and Birman (1963), following Blackwelder (1931), quantified measurements of the differential weathering of boulders and soils by noting such features as the number of boulders in a given area, the percentage of granitic boulders with glacially abraded surfaces and the degree to which grains within soils had been broken down. Since the measurements could not be statistically treated or related directly to age, Sharp (1969) called the measurements "semiquantitative." Burke and Birkeland (1979) and Gillespie (1982) devised a number of new semiquantitative methods based on more rigorous observations.

Although the weathering of boulders and soils has been used extensively as a semiquantitative measure of moraine age, little work has been done to use degradation of the morainal landform as an age indicator, in spite of recent advances in modelling landform evolution. Burke and Birkeland (1979) merely recorded slope angle measurements, which showed that in any group of moraines, the outer, older moraines generally have noticeably more shallow slopes than

the inner, younger moraines.

In this chapter, I investigate a simple method by which observations of moraine degradation can be quantified and used to distinguish moraines of different ages. The parameters used to quantify moraine shape can be derived from a linear-diffusion model of slope degradation. Use of model-related parameters makes it possible to study not only the relationship between moraine age and form, but also the processes that dominate degradation.

Bucknam and Anderson (1979) and Nash (1980) have shown that fault and river terrace scarps degrade approximately according to the diffusion equation, after initial steep slopes have become sufficiently shallow for downslope transport to be dominated by creep or rain splash. The success of these and later workers suggests that moraine degradation might also be approximated with a linear diffusion model. I have tested a diffusion model on the late Pleistocene moraines at Lee Vining Canyon, California (Figure 2-1).

Several workers have assessed age differences among the moraines of Lee Vining Canyon. Russell (1889) was the first to note that the nested moraines record at least four separate glacial advances. Blackwelder (1931) suggested a number of relative dating techniques for discerning age differences among these and other moraines, and named latest Pleistocene deposits "Tioga" after the pass at the head of Lee Vining Canyon. Moraine I in Figure 2-1 is the Tioga moraine of Blackwelder (1931). Deposits correlative to the Lee Vining Canyon Tioga moraine have been found throughout the eastern Sierra Nevada. Birman (1964) correlated some of the other moraines of Lee Vining Canyon to glacial deposits mapped at other eastern Sierra Nevada locales, using relative dating techniques such as granitic boulder surface roughness and the
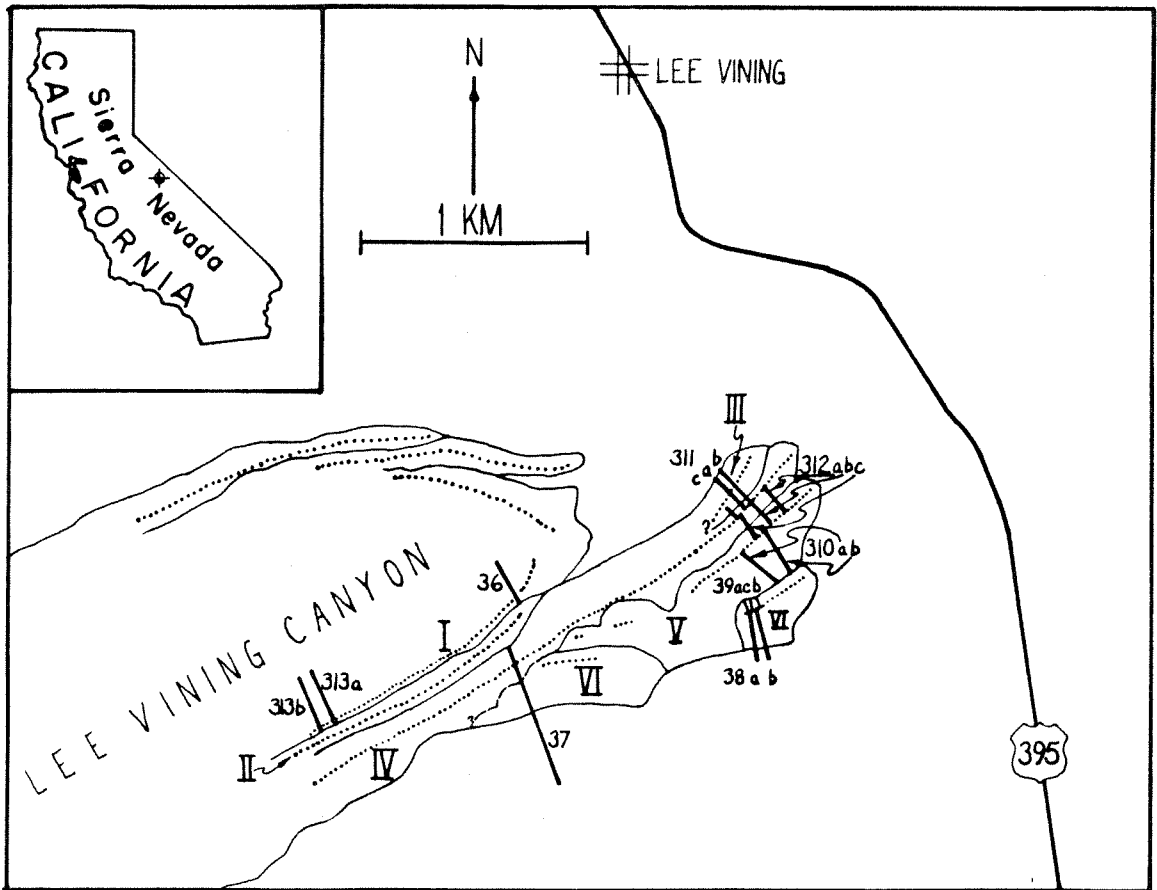
Figure 2-1. Profiles measured at Lee Vining Canyon. Profile and moraine numbers are same as in Table 2-1. Moraine I is the type Tioga moraine of Blackwelder (1931). Moraine II was correlated to the Tenaya glaciation by Birman (1964). Moraines III and IV are Tahoe moraines. Moraines V and VI are Mono Basin moraines. Inset map shows location of Lee Vining Canyon.

percentage of granitic boulders on the moraine surface. The moraine profiles used here were measured on some of the same moraines studied by Birman (1964). I have extended the dating work of Birman (1964) to include all moraines on which profiles were measured. Estimated ages based on quantitative measurements of weathering serve as a basis for testing the applicability of the diffusion model to the evolution of moraine profile shape.

DATA

Data collection and errors

A two-person team surveyed profiles of moraines with a Wild-Heerbrugg TC-2000 Total Station (EDM and theodolite). A rod-person walked up the flank of each lateral moraine, perpendicular to the moraine crest, with a reflector. Distance and angle measurements were made to the reflector from the Total Station, which was set up on the moraine crest or on a surface adjacent to the moraine. Shots were spaced one to twenty meters apart, depending on the rate at which the moraine slope changed.

There are three possible sources of error in the profiles: 1) instrumental and natural measurement uncertainty caused by atmospheric conditions and unsteadiness of instruments, 2) error caused by non-collinear target sites, and 3) error caused by deviation of profile from perpendicularity to moraine crest.

Measurement uncertainty (number (1) above) is negligible, since closure errors were several orders of magnitude smaller than the quantities measured.

Profile errors caused by non-collinear target sites (number (2) above) and

by the rod-person's not following a fall-line (number (3) above) are probably also negligible, since moraine slope changes slowly in the direction parallel to the moraine crest and since the instrument-person helped guide the rod-person to follow fall-lines down moraine slopes.

Description of profiles

Data consist of two to three cross-sectional profiles on each of five right- lateral moraines with estimated ages of 10^4 to 10^5 years. Most of the profiles were surveyed across both inner and outer moraine flanks. Figure 2-2a illustrates the nomenclature that will be used to discuss the various slope segments of the profiles, and Table 2-1 lists each profile, with separate entries for halves of profiles measured on inner and outer flanks. In both figures that illustrate profiles (Figures 2-2 and 2-3), the flank that initially faced the glacier is to the left.

Profiles on young moraines are characterized by sharp crests, long, straight upper-slope segments, and gently curving lower-slope breaks joining to adjacent landforms. Old moraines have broad crests, and flanks that lack long, straight, slope segments. Even though all profiles were measured at right angles to the crestal trend, those on older moraines obliquely cross salients and broad swales in the flanks, thus accounting in part for their lack of extensive straight slope segments. Field observations indicate that some profiles of older moraines have been resteepened by streams that flowed on the lower surface and undercut the moraines near their base.

I measured profiles on sections of moraines in five geomorphic settings, as determined by relationships to surrounding landforms, to obtain an idea of the effect of different initial conditions on the evolution of profile shape.
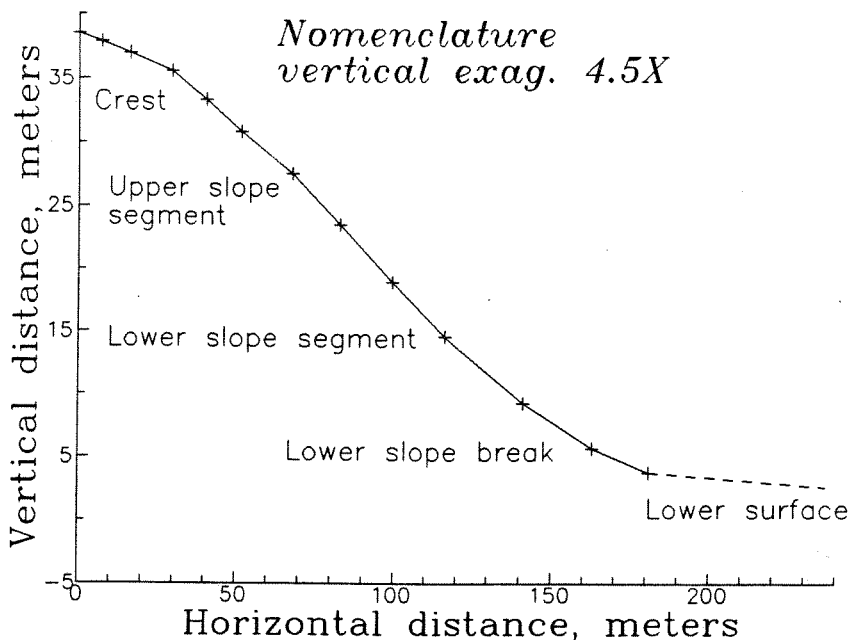
Figure 2-2a
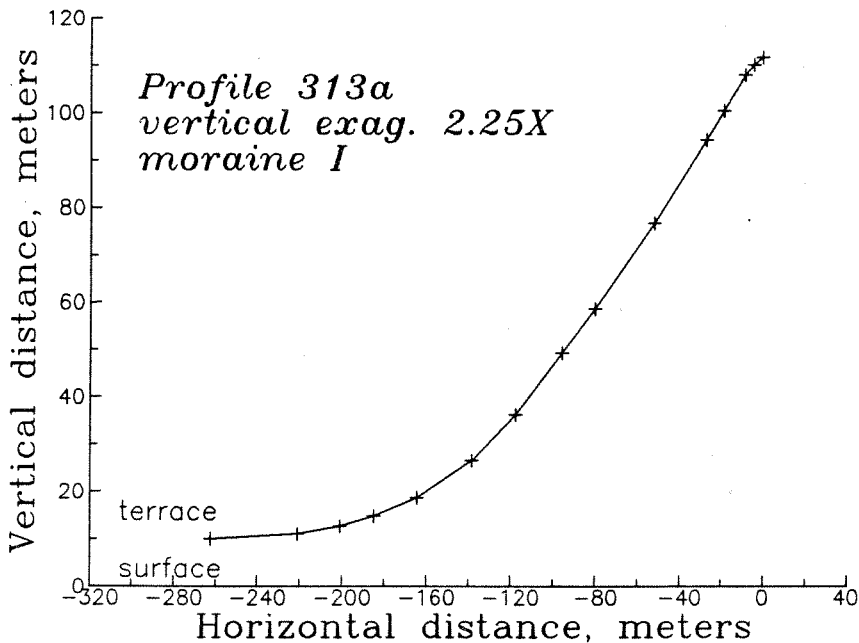
Figure 2-2b

Figure 2-2. Geomorphic settings of moraine cross-sectional profiles. Distance measurements are from an arbitrary origin. 2a) nomenclature of profiles, 2b) lateral moraine grading into outwash and stream terrace within Lee Vining Canyon, 2c) lateral moraines grading into bench. Below benches are outwash surfaces, 2d) nested lateral moraines, 2e) lateral moraine highly modified by stream undercutting, 2f) composite lateral moraine. Profiles of moraines were made in the different settings to study relatioship of degradation to varying initial conditions.

Figure   2-2c

Figure   2-2d

Profiles 38a and b
vertical exag. 2.25X
moraine VI

— Erosion surface
slope break (?)

38a

38b

Slope break of
wave–cut cliff (?)

Lake terrace

Stream
channel
off plot

Figure   2-2e

Profile 37
vertical exag. 4.6X

37a

Lower slope break of
overlying moraine
(moraine IV)

37b

Lower slope break of
underlying moraine
(moraine V (?))
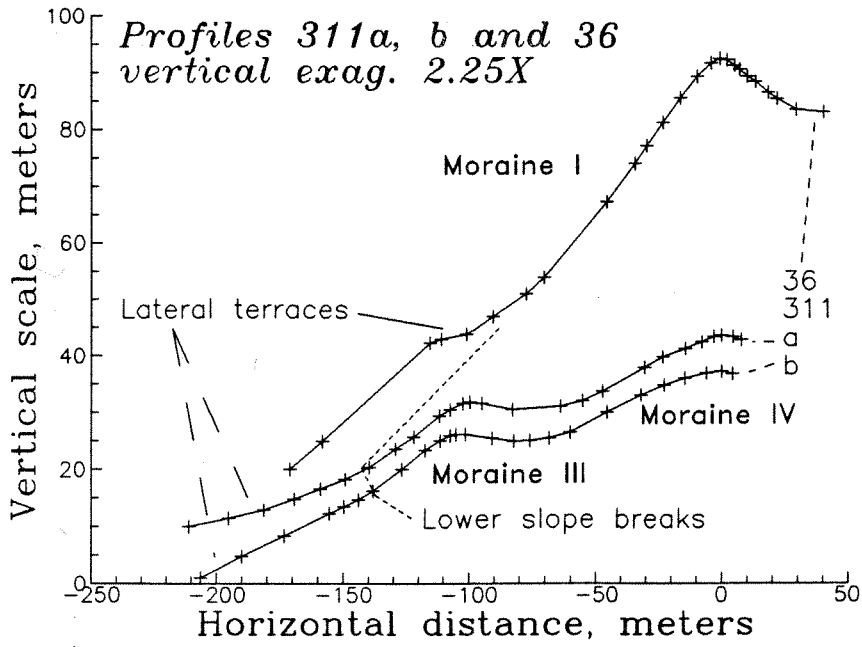
Rod–person
not
visible

Figure   2-2f

Table 2-1. Maximum slope angles and widths of profiles.

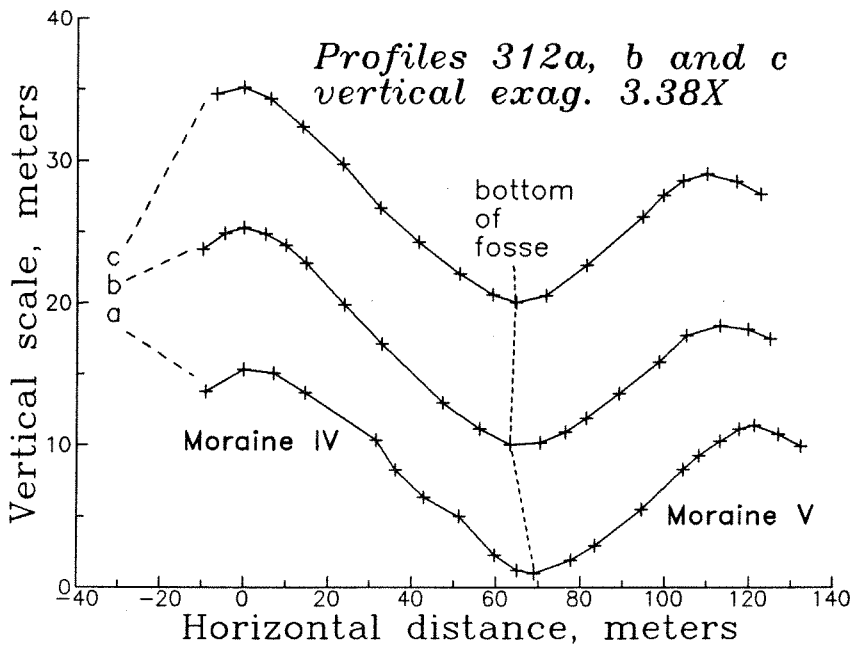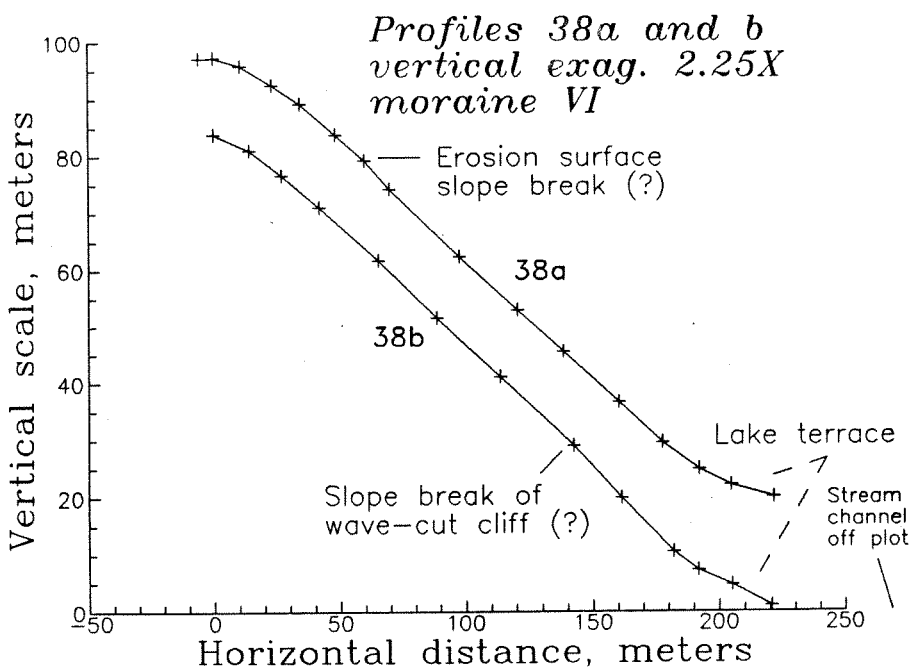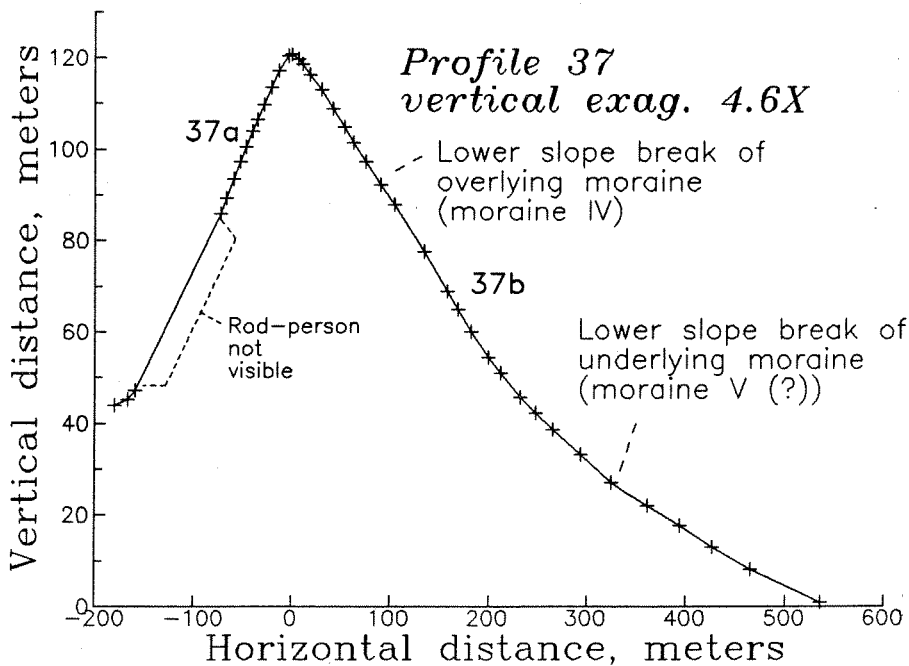| Profile	Moraine	Max. slope angle	Apparent height[a]	$w^2-A_0/3\tan\phi_i$, m^2	$F(1/\tan\phi_{max})$, m^2	R^2 [b]	Max. fract'l deviation	Fract'l gaussian use	Inner/outer[c]	Setting[d]
313a	I	36.5	102.1	-210	-60	0.9980	0.10	0.99	i	1
313b	I	36.3	104.0	560	-40	0.9981	0.11	0.99	i	1
36-1	I	21.2	9.4	160	40	0.9937	0.04	0.99	o	3
36-2	I	32.7	51.4	260	110	0.9971	0.07	0.96	i	2
311a-1	III	19.6	22.5	2360	370	0.9883	0.14	0.96	i	2
311b-1	III	20.1	14.5	460	130	0.9987	0.03	0.87	i	2
37a	III	30.0	79.5	890	570	0.9992	0.05	0.96	i	3
37b	IV	20.0	39.5	2870	890	0.9973	0.05	0.82	o	5
311a-2	IV	14.8	13.2	800	260	0.9952	0.06	0.99	i	3
311b-2	IV	13.5	12.8	1140	350	0.9900	0.08	0.98	i	3
311c	IV	17.9	14.3	1190	220	0.9693	0.03	0.80	i	3
312b-1	IV	17.8	16.9	920	250	0.9995	0.02	0.90	o	3
312a-1	IV	24.1	17.5	1640	170	0.9938	0.03	0.83	o	3
312c-1	IV	18.6	16.3	890	220	0.9990	0.04	0.92	o	3
310a	V	15.3	38.5	8850	2200	0.9998	0.02	0.90	o	4
310b	V	16.5	38.2	8920	1770	0.9927	0.09	0.90	o	4
312a-2	V	15.9	11.1	590	160	0.9996	0.03	0.93	i	3
312b-2	V	16.2	8.6	370	100	0.9892	0.04	0.98	i	3
312c-2	V	16.4	9.5	360	110	0.9970	0.04	0.96	i	3
39a	VI	13.5	16.4	3055	640	0.9988	0.02	0.79	i	4
39b	VI	13.8	17.4	1970	550	0.9909	0.02	0.89	i	4
39c	VI	12.3	11.8	1550	370	0.9853	0.03	0.96	i	4
38a	VI	26.9	84.7	---	---	0.9981	0.03	0.91	o	6
38b	VI	26.0	94.1	---	---	0.9975	0.04	0.84	o	6

[a] The height of the moraine assigned by least-squares regression.

[b] Correlation coefficient for fit of profile to Gaussian curve.

[c] i=inner, o=outer moraine flank.

[d] 1=outwash terrace; 2=lateral terrace; 3=unentrenched fosse; 4=entrenched fosse; 5=composite moraine; 6=lake terrace+channel.

Examples from each of the settings are shown in Figures 2b-f: 1) lateral moraines grading into outwash or stream terraces (Figure 2-2b), 2) lateral moraines grading into benches on their inner flanks (Figure 2-2c), 3) nested lateral moraines (Figure 2-2d), 4) lateral moraines grading into stream channels (Figure 2-2e), and 5) "composite" lateral moraines that consist of younger moraines overlying older moraines (Figure 2-2f).

Only the innermost of the lateral moraines grades into an outwash or fluvial terrace at its base (Figure 2-2b). Profiles measured in this setting (313a and 313b) are characterized by sharp crests, straight upper-slope segments, and gently curving lower-slope breaks that join with almost flat terrace surfaces. Profiles 313a and 313b were measured in avalanche chutes because the rod-person was unable to climb the narrow regions between chutes. Mass-wasting is therefore in part responsible for the present form of these profiles. Material on the upper, straight slope segment is loose and at the angle of repose. The lower-slope segment and break are composed in part of colluvial material initially transported by rockfalls and avalanches originating on the upper-slope segment. These profiles provide a worst-case comparison with the diffusion model, since mass-wasting processes that degrade the upper-slope segments of the chutes are not diffusive processes. Nevertheless, much of the data from these profiles is explained by the diffusion model.

Several profiles were measured on lateral moraines that grade into benches perched above outwash surfaces (Figure 2-2c). Profile 36b, on the youngest moraine, grades into a narrow-treaded bench and has a well-defined slope break separating the bench from the lower-slope segment of the moraine. Profiles 311a and 311b grade into a broad-treaded bench. The slope break between bench

and moraine is difficult to locate precisely. The bench tread dips only

slightly less steeply than the moraine flank.

Some profiles were measured into fosses between adjacent moraines (Figure

2-2d). Profiles 312a, b and c were measured upstream from a channel within a

fosse. The head of the channel is migrating up the fosse, but has not yet

reached the point crossed by the lowest profile. Therefore, the fosse floor

is a constructional landform where the profiles were measured. The

asymmetrical position of the fosse bottom suggests that most of the original

landform of the older moraine has been preserved. The lowest points in the

fosse floor are characteristically offset toward moraine IV (the younger

moraine), and the lower-slope segment on moraine V is concave-upward,

therefore, the lower surface to which moraine V graded, prior to construction

of moraine IV, is probably not far below the present fosse bottom.

Presumably, if moraine IV had been built up to the level of the upper-slope

segment of moraine V, then the lowest point in the fosse would be either

symmetrical or offset toward moraine V.

Profiles 310a and b, and 39a, b and c on the two outermost moraines, also

terminate at the base of a fosse. These profiles are not illustrated in

Figure 2-2. All these profiles are characterized by a sharp change in slope

angle at the bottom of the lower-slope break. On stereoscopic aerial

photographs, it is clear that stream entrenchment is the cause of the angular

lower-slope break.

The outer flank of the outermost lateral moraine grades into a lake

terrace perched above a deep, active stream channel (Figure 2-2e). The steep,

straight, upper and lower slope segments of the two profiles measured on this

flank suggest that it was modified by transport of material cascading into the

undercutting stream, before the lake terrace was deposited. A slope break

that may be associated with this parallel-slope retreat is visible near the

top of profile 38a. The slope break at the top of the wave-cut cliff above

the lake-terrace tread is noticeable in profile 38b. These profiles were not

used in the following analysis because of their extensively modified forms.

Profile 37b records the morphology of a composite moraine formed by the

superposition of two or perhaps three separate moraines (Figure 2-2f). The

lower surface below uppermost moraine IV, which is part of the flank of the

underlying moraine, has a minimum slope angle of 17 degrees, making it the

most steeply dipping lower surface. Particularly characteristic of this

profile are long, straight slope segments separated by barely distinct slope

breaks between the superposed landforms. Only the uppermost portion of this

profile, which comprises the overlying moraine and its lower slope break, was

used in the analysis.

Although profiles were measured in a number of different settings, all

were used to obtain an idea of whether certain settings yield better results.

Only profiles 38a and 38b, both of which are heavily modified by stream

undercutting, were not used.

Independent measure of moraine ages

Because Birman (1964) did not study relative weathering features on all

moraines for which I measured profiles, a relative-age dating method was used

to establish a basis of comparison between degree of degradation and age. I

used the clast-sound velocity (CSV) technique to correlate the moraines of Lee

Vining Canyon to the eastern Sierra Nevada glacial chronology shown in Table

1-1. The CSV technique consists of measuring the sound (p-wave) speed in

boulders on moraine crests. Sound speed in boulders decreases as they become more pervasively riddled with microcracks during mechanical weathering. Boulders on old moraines have been weathering for a longer time than boulders on young moraines, contain denser microcrack networks and, therefore, have lower average p-wave speeds. Crook and Gillespie (1986) applied the method to granitic boulders in Quaternary clastic deposits in southern California and the eastern Sierra Nevada, and found results to be internally consistent, reproducible and compatible with absolute-age information. Results for boulders sampled on the late Pleistocene moraines of Lee Vining Canyon are presented in Table 2-2.

The CSV data are statistically compatible with dividing the five moraines studied in Lee Vining Canyon into three separate glacial episodes -- Tioga, Tahoe and Mono Basin -- which may correspond to $\delta^{18}O$ stages 2 through 6, and to pluvial periods in Searles and Mono Lakes (Table 1-1). The estimated ages are 14,000 (range: 11,000 to 21,000) for Tioga; 66,000 (range: 60,000 to 85,000) for Tahoe, and 130,000 (range: 130,000 to 200,000) years old for Mono Basin stage deposits. Moraine profile results regressed against these estimated ages were used to test the validity of the degradation model presented below.

ANALYSIS

Treatment

From each cross-sectional profile, I measured two parameters to compare with estimated moraine ages. The two parameters were 1) maximum slope angle,

Table 2-2. CSV data for Lee Vining Canyon right-lateral moraines.

Moraine	$\overline{V_p}$[a,b]	Stage	Estimated age, yr BP[c]
I	1.582 ± 0.053	Tioga	14,000 (11,000–21,000)[*]
III	1.450 ± 0.065	younger Tahoe	
IV	1.461 ± 0.076	older Tahoe	
III+IV	1.455 ± 0.050	Tahoe	66,000 (60,000–85,000)
V	1.254 ± 0.072	younger Mono Basin	
VI	1.197 ± 0.047	older Mono Basin	
V+VI	1.222 ± 0.041	Mono Basin	130,000 (130,000–198,000)

[a] Error bars are one standard deviation of the mean.
[b] Coefficient of determination for regression of mean V_p against estimated age is 0.86.
[c] From Table 1-1.
[*] Age in parentheses is range of estimated age.

and 2) a characteristic width determined by fitting each profile with a Gaussian curve.

The profiles were fit to Gaussian curves from the point on each profile nearest the base of the lower slope break, to the top of the moraine crest.

Profiles measured on inner and outer flanks of the same moraine were treated separately because inner and outer flanks had different initial shapes, were deposited in different geomorphic settings and in some instances, seem to have degraded locally by different slope processes. Outer flanks formed at or below the angle of repose, and initially graded into older moraines or outwash terraces. Inner flanks, however, were initially oversteepened and degraded by parallel-retreat slope processes because they formed in contact with, and were supported by, glacial ice (Small, 1983). In addition, all inner flanks initially graded into a terrace surface.

Diffusion model

To approximate the evolution of the form of lateral moraines, a reasonable starting point is a simple analytical solution to the diffusion equation (Nash, 1980):

$$\partial^2 z/\partial x^2 + \partial^2 z/\partial y^2 - (1/\kappa)\partial z/\partial t = 0, \qquad (2.1)$$

where x is the horizontal coordinate perpendicular to the moraine crest, with origin at the crest and positive direction away from the glacial trough, y is the coordinate parallel to the moraine crest, z is the vertical coordinate, t is time and κ is the coefficient of slope diffusion. The properties sought in the solution are: 1) that its validity can be checked by testing whether it

correctly predicts moraine form, 2) that it facilitate a statistical analysis of the relative ages of moraines, and 3) that it can be used to derive calibrated or estimated moraine ages.

Transport in the y-direction is negligible, since little material is moved across moraine flanks rather than down them. For this situation, equation (2.1) reduces to:

$$\partial^2 z/\partial x^2 = (1/\kappa)\partial z/\partial t,$$

which simply states that the change in elevation of a point with time $(\partial z/\partial t)$ is equal to the change in the amount of material flowing through the point in the x-direction $(\partial/\partial x(\kappa \partial z/\partial x))$.

For an arbitrary continuous function $f_0(x)$ and for the boundary conditions:

$$z = f_0(x) \quad \text{at} \quad t = 0,$$

$$\text{and}$$

$$z \to 0 \quad \text{as} \quad x \to \pm\infty,$$

which correspond approximately to the conditions of lateral moraines, Andrews and Hanks (1985) have shown that the solution approaches:

$$z = \{A_0/[4\pi\kappa(t-t_0)]^{1/2}\}exp[-x^2/4\kappa(t-t_0)],$$

as $t \to \infty$. In this equation, A_0 is the area under the curve $f_0(x)$ and t_0 is "initial apparent age" (Andrews and Hanks, 1985). For simplicity, I assume

that the centroid of $f_0(x)$ remains at $x = 0$ through time. This equation suggests that profiles of moraines that degrade by diffusive processes converge toward Gaussian forms with time.

If the initial shape of the moraine profiles $(f_0(x))$ is furthermore assumed to be triangular, with initial inner and outer slopes of $tan(\varphi_i)$, then it can be shown that $t_0 = A_0/12\kappa tan(\varphi_i)$ (Appendix C), so that:

$$z = \frac{A_0 exp(-x^2/\{4\kappa t-[A_0/3tan(\varphi_i)]\})}{\{4\pi\kappa t-[\pi A_0/3tan(\varphi_i)]\}^{1/2}}. \qquad (2.2)$$

Equation (2.2) can be put in a more readily useable form by recognizing that $A_0/\{4\pi\kappa t-[\pi A_0/3tan(\varphi_i)]\}^{1/2}$ is the height of the Gaussian curve, $h(t)$, and that $4\kappa t-[A_0/3tan(\varphi_i)]$ is the $1/e$-width, $w(t)$, of the Gaussian curve, so that:

$$z(x, t) = h(t)exp\{-[x/w(t)]^2\}. \qquad (2.3)$$

I have used equation (2.3) as the basis for comparing moraine profiles to the diffusion model. The first step in the comparison was to fit moraine profiles to curves derived from equation (2.3). For each profile, I found the best-fit Gaussian curve with a linear-regression routine that solved for $h(t)$ and $w(t)$ (Press *et al.*, 1986). Because the height of the lowest point in each profile with respect to each Gaussian curve was also unknown, the linear regression routine was run with different choices for the height of the lowest point -- at 0.1 m increments -- until the values for $h(t)$ and $w(t)$ were found that maximized the coefficient of determination, r^2. Figure 2-3 illustrates
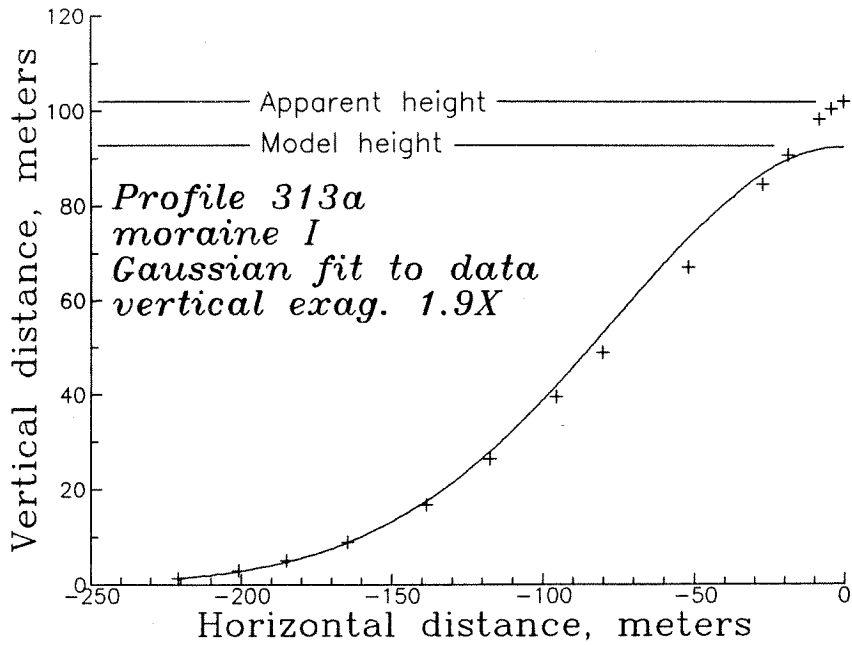
Figure 2-3a
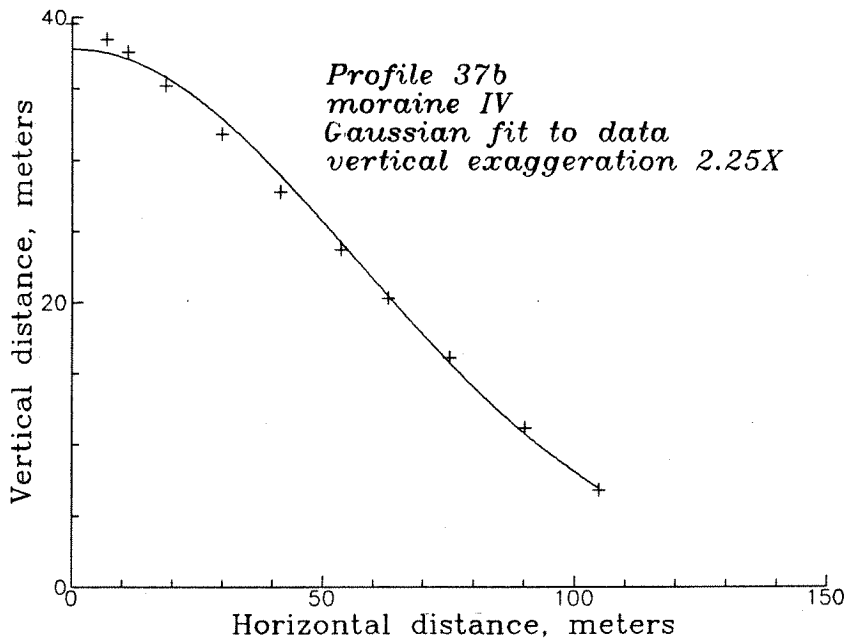
Figure 2-3b

Figure 2-3. Fit of Gaussian curves to data, order of profiles is
youngest to oldest, (a)-(d). If moraines degrade by diffusive
processes, then profiles should approach Gaussian form with time.
Deviations between model and data do seem to decrease and become less
systematic from (a) to (d).

Profile 310a
moraine V
Gaussian fit to data
vertical exag. 3.75X

Figure 2-3c

Profile 39c
moraine VI
Gaussian fit to data
vertical exag. 7X

Figure 2-3d

examples of Gaussian curves fit to moraine profiles.

After the least-squares best-fit curves were found for each profile, I tested for systematic deviations between model and data with three parameters, the coefficient of determination, and what I call the "Fractional vertical error" and the "Fractional Gaussian use". The results of these tests are discussed below.

Coefficients of determination for the Gaussian fits, listed in Table 2-1, are all very near unity, suggesting that Gaussian shapes closely approxima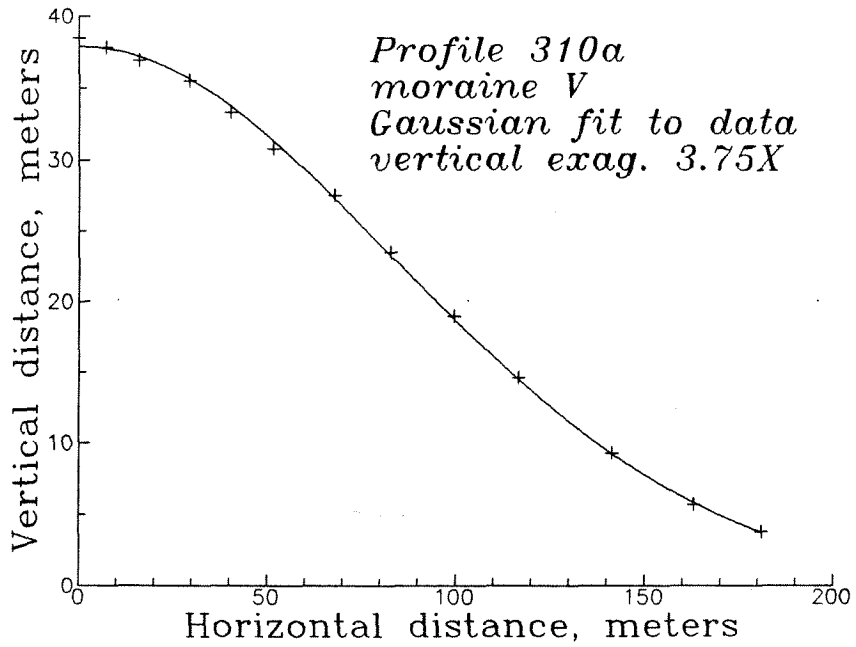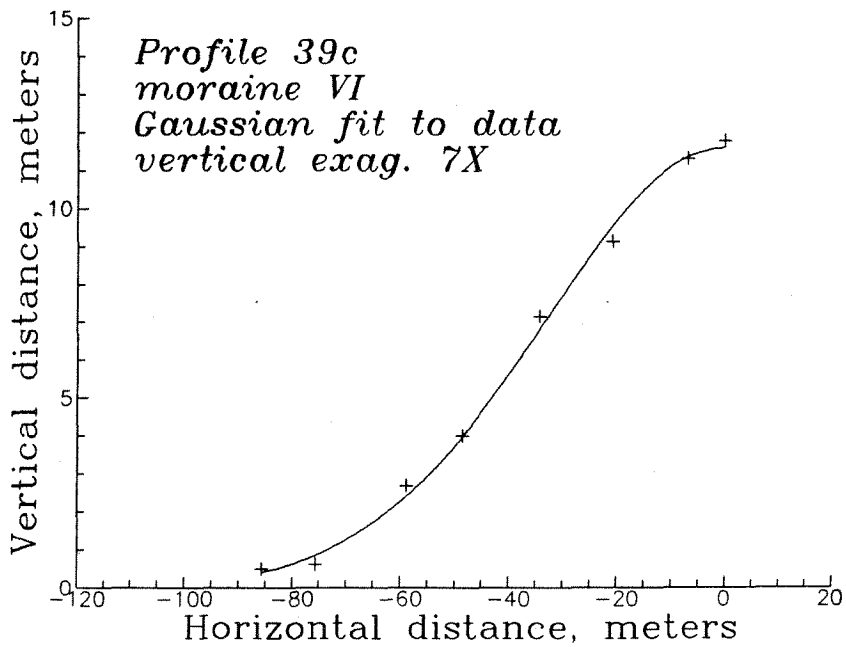te profiles of moraines, even though the moraines initially had local features that diverged markedly from Gaussian form, in particular, angular crests and nearly vertical slopes (Small, 1983).

Coefficients of determination do not noticeably improve with age, as might be expected if profiles continuously approach Gaussian form with time. However, maximum fractional vertical deviations, which are maximum differences in elevations of points between model and data divided by model height, $h(t)$, do decrease with age, falling from about ten percent for 10^4 year-old moraines, to less than five percent for 10^5 year-old moraines (Figure 2-4). In addition, examples in Figure 2-3 illustrate that mis-fitting becomes less systematic with age, since consecutive data points have a weaker tendency to lie toward one side of the Gaussian curve on profiles from older moraines.

The fraction of the total height of each Gaussian curve used by the curve-fitting procedure is another measure of the compatibility of the Gaussian approximation with the data. This fraction measures how much of the Gaussian curve is fit to each profile. Table 2-1 shows that over 90% of the height of each Gaussian curve is used in fitting most profiles. For some profiles with terraces or fosses as lower surfaces, the fractional use is about 99%.
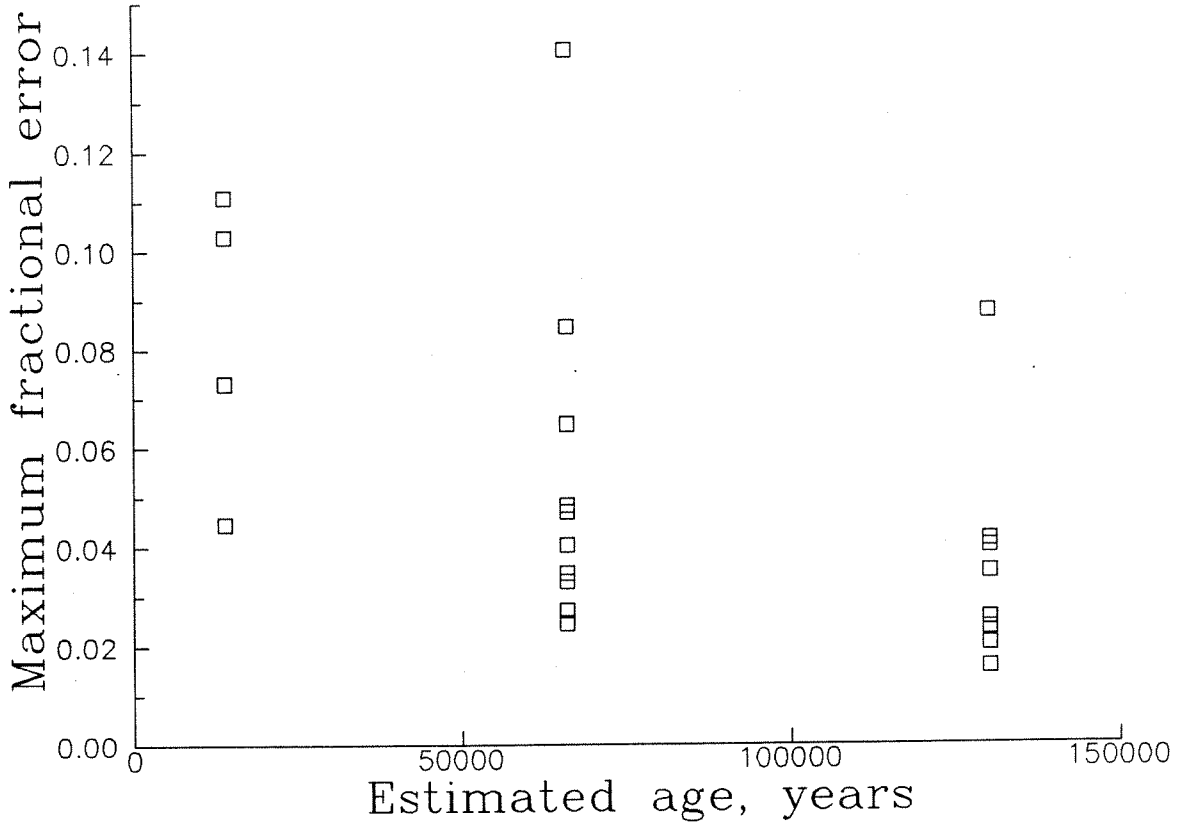
Figure 2-4. Maximum fractional error of model from data vs. moraine age. Maximum fractional error is the absolute value of the maximum difference between profiles measured in the field and the Gaussian curve fit to the profiles normalized by model profile height, and measures how well diffusion model fits data. Error decreases with age, on average, suggesting that moraine profiles do become more like Gaussian curves in form with time.

Therefore, profiles are fit to a large fraction of each Gaussian curve, rather than to a small fraction near the top of each curve, which is not particularly representative of Gaussian shape.

DISCUSSION

Since the diffusion model predicts moraine form reasonably well, it may be possible to use it as the basis for a relative-dating method. Following are two techniques that use predictions of the diffusion model about profile width and maximum slope angle to differentiate between moraines of different ages.

Characteristic profile width

The least-squares parameters of the diffusion model are the $1/e$-width, w, and the model height, h. The $1/e$-width is a measure of how "flattened" each profile is. The model height is the height of the Gaussian curve used in each regression of model against data (Figure 2-3a).

The $1/e$-width can be used to obtain a measure of the degree of degradation, which I will call the characteristic width. Directly from equating arguments in equations (2.2) and (2.3):

$$w^2 = 4\kappa t + [A_0/3tan(\varphi_i)],$$

or

$$w^2 - [\pi^{1/2}wh/3tan(\varphi_i)] = 4\kappa t, \tag{2.4}$$

since $A_0 = \pi^{1/2}wh$ (Beyer, 1980).

$w^2 - [\pi^{1/2}wh/3tan(\varphi_i)]$ was calculated for a number of values of $tan(\varphi_i)$ between 0.3 and 0.7 (φ_i = 17 to 35 degrees), because its value is very sensitive to initial slope. A plot of $w^2 - [\pi^{1/2}wh/3tan(\varphi_i)]$ versus $tan(\varphi_i)$ showed that a minimum in the scatter of data from moraines I, and III and IV occurs near $tan(\varphi_i) = 0.5$. Therefore, assuming that all profiles of the same age should yield the same model age, 0.5 was chosen as the best estimate for $tan(\varphi_i)$, since it reduced the scatter in the model age estimates for two of the groups of profiles.

Figure 2-5 illustrates results with characteristic widths of moraines grouped according to age. Characteristic widths of moraines III and IV are statistically separable from those of moraine I, but not from those of moraines V and VI at the 10% significance level, using the Kolmogorov-Smirnov test. However, if the profiles from moraine V with extremely low apparent heights -- 312a-, 312b- and 312c-2 (Table 2-1) -- are not used, then the characteristic widths of moraines III and IV are distinct from those of moraines V and VI at the 10% significance level. This improvement in the separability of samples suggests that it may be important to use profiles of approximately the same height in comparisons among moraines.

The regression of mean characteristic width against estimated age (Table 2-3; Figure 2-5) shows that characteristic width increases approximately linearly with age, as required by equation (2.4). Since the evolution of characteristic width follows equation (2.4) and since widths of moraines of different ages are statistically distinct (if profile heights are similar), the diffusion model can be used as the basis for a relative-dating technique.
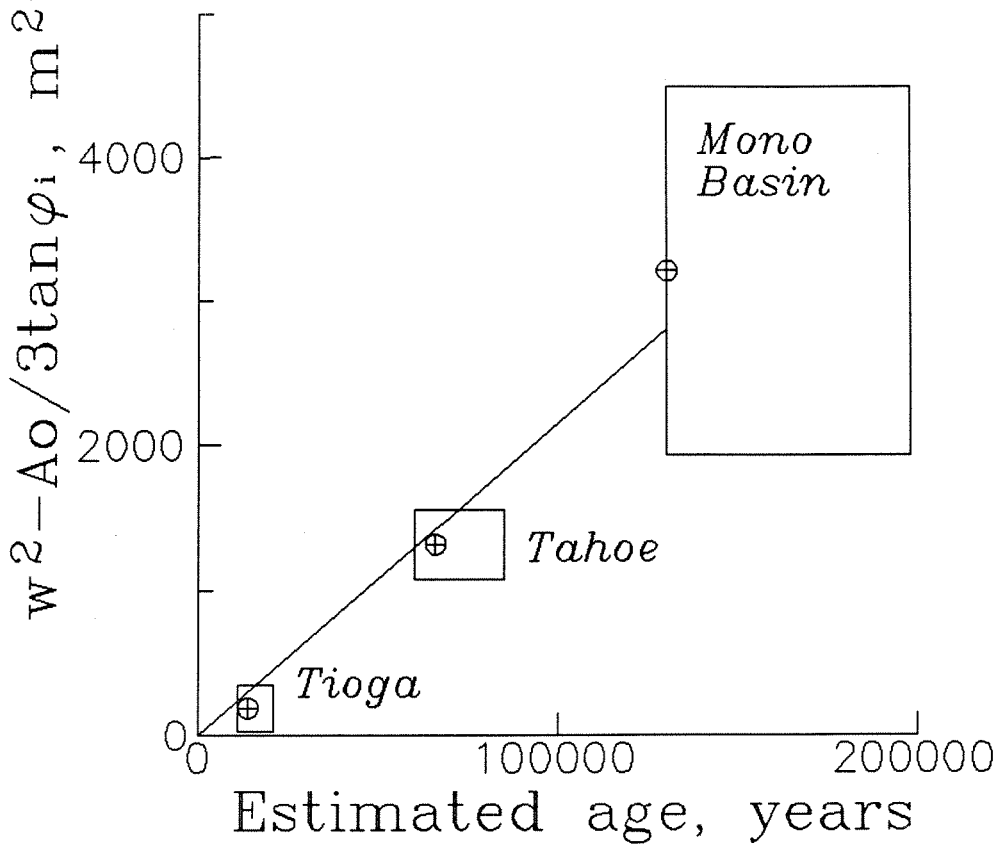
Figure 2-5. Characteristic Gaussian profile width as a function of age. Vertical error bars are one standard error of the mean. Horizontal error bars are ranges of estimated moraine ages. Curve is constrained to go through origin. Straight line does fit through error boxes, suggesting that moraine degradation is a diffusion-dominated process that can be approximated by the large-time solution to the diffusion equation.

Table 2-3. Correlation of characteristic width with estimated age.

Moraine	Stage	Estimated age, yr BP	$\overline{w^2 - A_0/3\tan\phi_i}$ [a,b]
I	Tioga	14,000	190 ± 160
III+ IV	Tahoe	66,000	1320 ± 240
V+ VI	Mono B.	130,000	3210 ± 1280

[a] Error bars are one standard deviation of the mean.
[b] Coefficient of determination is 0.98.

Maximum slope angle

Another characteristic of the profiles, the maximum slope angle, can be related to age with the diffusion model.

Table 2-1 and Figure 2-6a show that maximum slope angle decreases monotonically with estimated age. Error bars in Figure 2-6a illustrate that differences in mean maximum slope angle are significant, and that the data are separable into three distinct groups. The results compare well with those of Wallace (1977), who found that maximum slope angles of fault scarps decrease monotonically with age and that angles decrease fastest in the early part of the degradation history, as in Figure 2-6a.

An expression defining the relationship between maximum slope angle and age can be derived from equation (2.2) by solving for the tangent of maximum slope angle. Since the tangent of maximum slope angle is the same as the maximum value of the derivative of z with respect to x, equation (2.2) can be differentiated with respect to x to obtain:

$$tan(\varphi_{max}) = (\partial z/\partial x)_{max} = A_0/((8e\pi)^{1/2}\{\kappa t + [A_0/12tan(\varphi_i)]\}), \quad (2.5)$$

or, after rearranging terms:

$$F[1/tan(\varphi_{max})] = wh(\{1/[(8e)^{1/2}tan(\varphi_{max})]\} - \{\pi^{1/2}/12tan(\varphi_i)\}) = \kappa t,$$

where φ_{max} is maximum slope angle. Appendix C contains a complete derivation of equation (2.5). Equation (2.5) states that maximum slope angle is inversely proportional to age. Figure 2-6b, which shows the results of the regression of $F[1/tan(\varphi_{max})]$ against age for φ_{max} taken from Table 2-1, w and h taken from Gaussian fits, and $tan(\varphi_i) = 0.5$, suggests that the relationship between maximum slope angle and age is compatible with the simple diffusion
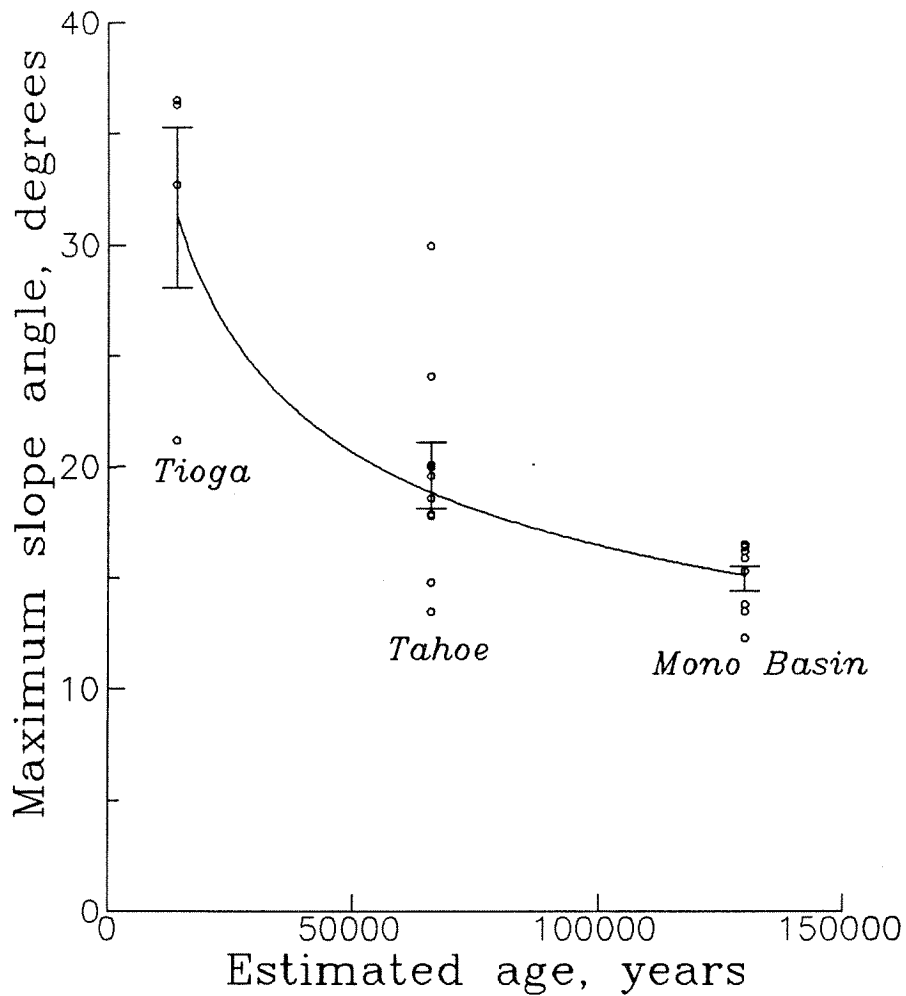
Figure 2-6a

Figure 2-6. Slope angle as a function of age: 6a) maximum slope angle measured along each moraine profile. Error bars are one standard error of the mean. As Wallace (1977) found with scarp profiles, maximum slope angle changes more slowly as age increases; 6b) Regression of $\tan(\varphi_{max})$ against inverse age. Vertical error bars are one standard error of the mean. Horizontal error bars are ranges of estimated moraine ages. Curve is best-fit line. Straight line fits through error boxes, indicating that slope angle evolution is compatible with the diffusion model.

Figure   2-6b

model. Data for moraines III and IV are distinguishable from data from both moraine I, and moraines V and VI at the 10% significance level, if profiles 312a-, 312b- and 312c-2 are discarded. The compatibility of the slope angle data with the diffusion model is another indication that sufficient time has passed for the moraines to have been degraded to near-Gaussian forms.

Variations from the diffusion approximation

There are several factors that play an important role in moraine degradation which are not considered in the approximate diffusion solution used above. I will d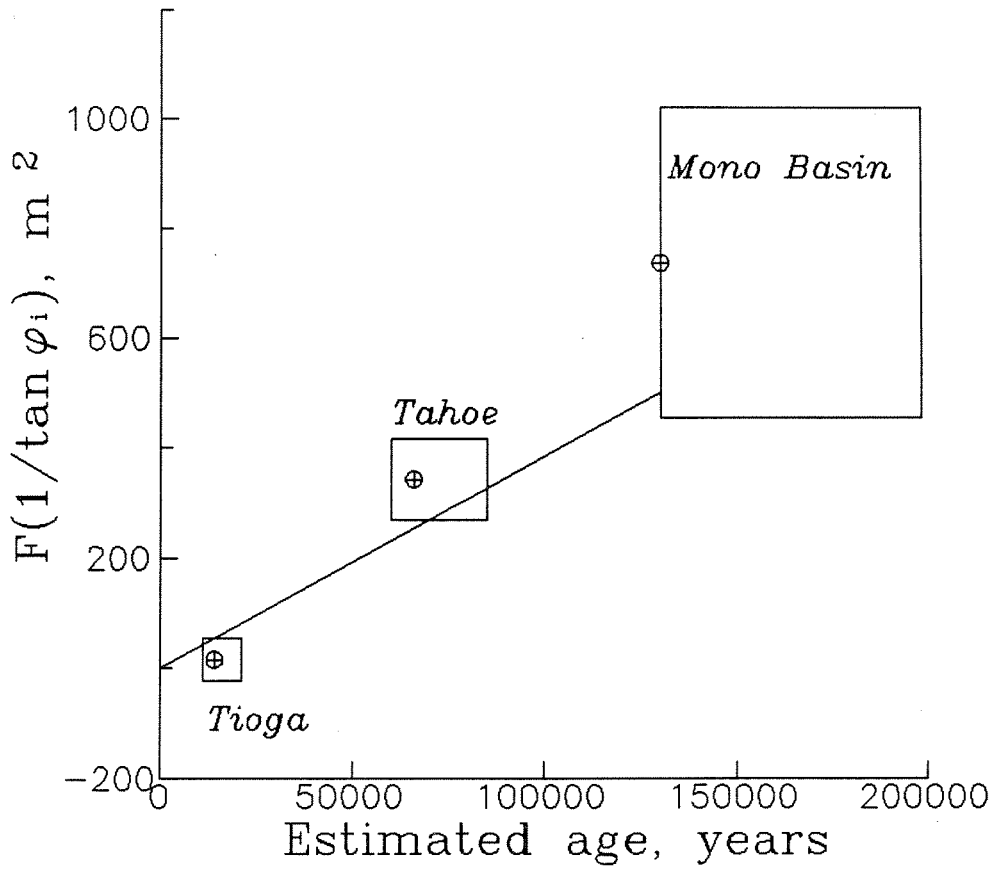iscuss these factors in an order related to how they affect the diffusion equation: 1) differences in initial shape of inner and outer flanks, 2) differences between moraines caused by construction in different settings, and 3) processes poorly modeled by the diffusion equation.

Different initial conditions on inner and outer flanks

Since inner moraine flanks are initially steeper than outer flanks, one might expect a significant difference in slope parameters between inner and outer flanks if a moraine is young enough to retain features of the initial configuration. Figure 2-7 shows that maximum slope angles are steeper on the inner flank of the youngest moraine. However, maximum slope angle seems to assume about the same value on the inner and outer flanks of moraines III to VI, indicating that differences caused by initial conditions persist for about 10^5 years. This suggests that less scatter in the data could be obtained by measuring profiles on inner or outer flanks alone.

Inner and outer moraine flanks are not necessarily the same height, since they are adjacent to different surfaces. To account for this height
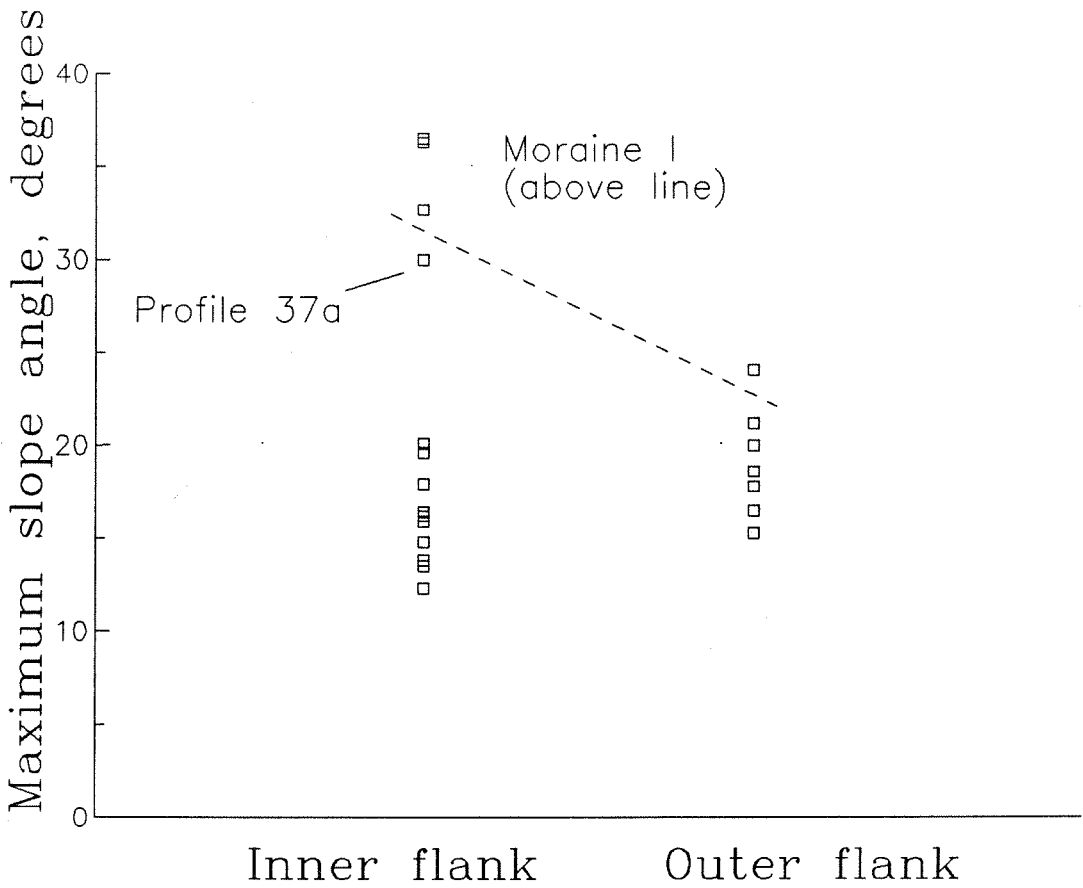
Figure   2-7

Figure 2-7. Correlation of slope angle with direction in which moraine flank faces. Inner flank = initially faced glacier, outer flank = initially faced away from glacier. There are systematic differences between slope angle for inner and outer moraine flanks of the youngest moraine, indicating that errors could be minimized by measuring profiles only on one flank.

difference, an error function term should be introduced into equations (2.2) and (2.3), and both flanks should be modeled simultaneously (D.J. Andrews, pers. comm.). The effect of neglecting the error function term was not evaluated for this study, but the results indicate that its effect is negligible in comparison with the scatter of the data.

Variations caused by setting

The degree to which data from different geomorphic settings fit the diffusion model is illustrated by plotting errors against setting. Fractional use was found to be the only measure of error that correlates with setting. Figure 2-8 shows the relationship between the fractional Gaussian use in the regressions and setting.

Some profiles that have fosses or outwash terraces as lower surfaces use about 99% of the Gaussian curve. Since the fractional use correlates directly with the slope angle of the lowest slope segment --it measures how far down, along the Gaussian curve, data can be fit -- the correlation between setting and fractional use reflects that fosses, as well as outwash terraces, are flatter than other lower surfaces. The two moraine-to-fosse profiles having the highest fractional use are on young moraines (profiles 36-1 and 311a-2 in Table 2-1). Material from the moraine flanks adjoining these fosses has not coalesced to transform initially flat fosse bottoms into U-shapes, nor have the fosses been entrenched.

The results suggest that the best settings in which to measure profiles are outwash terraces and broad fosses.

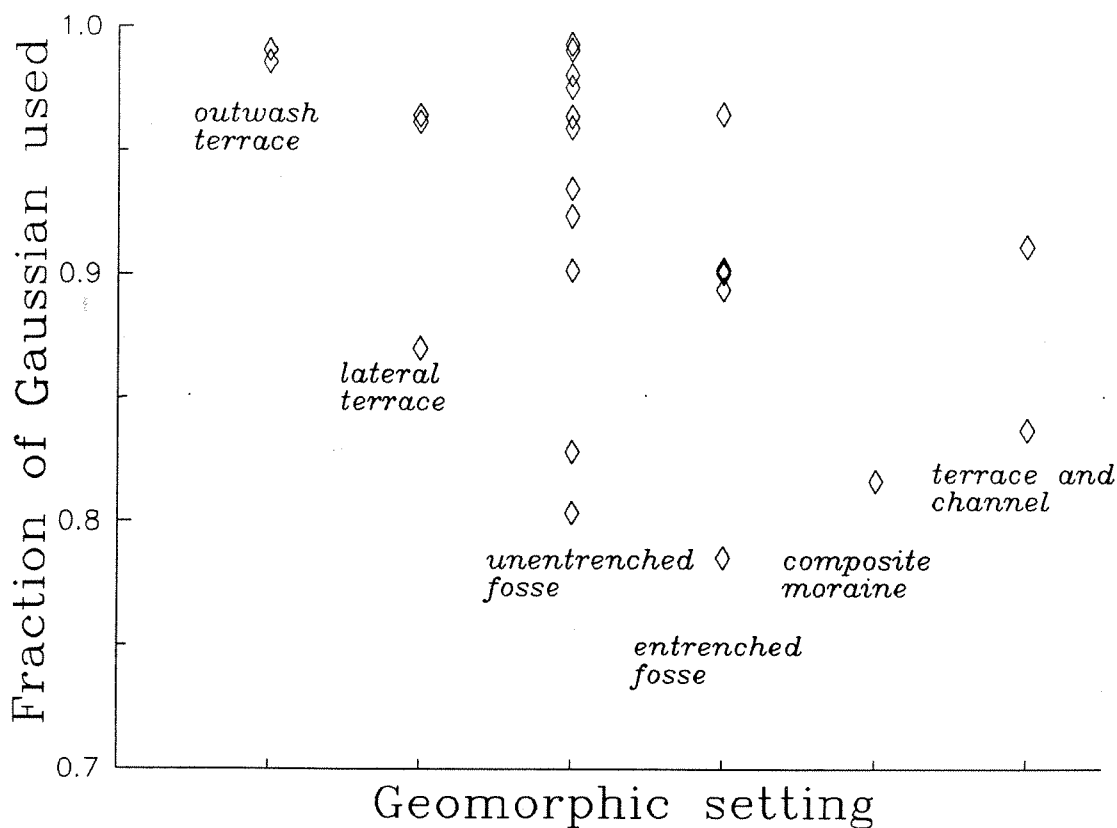**Figure 2-8.** Correlation of geomorphic setting and fractional Gaussian use. A high value for the fractional Gaussian use generally indicates that the overall shape of the profile is similar to a Gaussian curve. Large fractions of Gaussian curves are used by moraine profiles adjacent to outwash terraces and unentrenched fosses, indicating that these are the best environments in which to measure profiles.

Processes not described by the diffusion equation

The rate of slope degradation must be initially faster on inner moraine flanks because characteristic widths and maximum slope angles start from different values on inner and outer flanks and end with similar values after 10^5 years. The diffusion equation can be modified in two ways to express different transport rates on inner and outer flanks: 1) make the coefficient of slope diffusion a function of the spatial coordinate, x, to account for different material properties, or 2) modify the dependence of the diffusion equation on slope angle $(\partial z/\partial x)$ or make it dependent on other factors, such as slope length, to account for non-diffusive transport processes (Ahnert, 1976).

It is not possible to determine precisely the applicability of either alternative (1) or (2) above. However, non-linear transport processes, such as landslides, debris and snow avalanches, sheetwash and gullying (modeled by using alternative (2)), clearly play a role in degradation. Obliquely trending inactive gullies, avalanche chutes, and weathered landslide scarps (?), formed by the above processes, were a few of the features noted in the field and on aerial photographs along some of the profiles. For example, profile 313a (Figure 2-2a) was measured in an avalanche chute down which debris-falls, debris and snow avalanches, and perhaps landslides have transported material. In its upper mid-section, the profile is quite straight and steep, indicating that mass-wasting has resulted in parallel-retreat of slopes, proceeding at the angle of repose in the material. Even so, the profile fits a Gaussian curve with a coefficient of determination of 0.998 and a maximum model-to-data fractional deviation of about 10%, suggesting that diffusive, as well as parallel-retreat processes, play an important role in downslope transport, particularly in the lower half of the profile. The

obvious local importance of non-diffusive processes suggests that a physically meaningful modification to be made to the diffusion equation in the future is to use alternative (2) above and to change the dependence of the equation on slope angle.

Since maximum model-to-data deviations decrease with age, diffusive processes seem to become more important in transporting material as parallel-retreat slope processes -- landslides, debris-falls and avalanches -- become less important. Deviations from Gaussian form in younger profiles are related to initial conditions and parallel-retreat slope processes. Deviations from Gaussian form in older profiles are related mostly to gullying at oblique trends to the down-moraine direction, and undercutting in fosses by entrenching streams. Deviations caused by undercutting and gullying are relatively small because diffusive processes proceed at faster rates than gullying processes.

CONCLUSIONS

Characteristic moraine profile widths, derived from fitting Gaussian curves to profiles, increase approximately linearly with age, as predicted by a diffusion model. Mean maximum slope angles decrease monotonically with age, in a manner similar to fault and river terrace scarps, and roughly in the manner expected from the diffusion model.

Profiles of moraines that are approximately 10,000 years old deviate a greater amount from Gaussian best-fit curves than do profiles measured on moraines that are 100,000 years old, indicating that the time taken for

initial geometry and non-linear degradation processes to become subordinate to diffusive-degradation processes in determining slope form is on the order of 10^5 years.

The ease with which long topographic profiles across moraines can be measured with modern electronic surveying instruments makes it possible to use moraine profiles to correlate moraines to established glacial chronologies, and suggests that, if calibrated with absolute ages, profiles can be used to date lateral moraines for which no absolute age control is available.

CHAPTER 3

EVOLUTION OF THE SIERRA NEVADA RANGE FRONT IN THE MONO BASIN AND THE RELATIONSHIP OF RANGE-FRONT FAULTING TO VOLCANISM

INTRODUCTION

Relationship between volcanic and tectonic processes

Objectives and previous work

Although it has long been known that volcanism and tectonism are related, the nature of the link between the two processes is poorly understood. Anderson (1951) was the first to note that both intrusion of magma and faulting act as mechanisms of strain relief. Ode (1957), Muller and Pollard (1977), Delaney and Pollard (1979), Fink and Pollard (1983), Nakamura (1977), Roquemore (1980), Bacon et al. (1980) and Fink (1985) have given clear examples from the field of eruption centers or dikes that were formed in response to regional tectonic stresses. Lachenbruch and Sass (1978) have suggested that dike intrusion as well as normal faulting is a mechanism for strain relief throughout the Basin Ranges.

In spite of the wealth of information outlined above, only Bacon (1982) has attempted to link a measure of the rate of volcanic activity to tectonic extension rates. Therefore, I began this study of the Mono Craters and the Sierra Nevada range front to understand how the construction of a volcanic chain and underlying intrusion of magma might be quantitively related to tectonic forces responsible for range-front faulting.

The Mono Basin lies on the western margin of the Basin Ranges, east of

the central Sierra Nevada (Figure 3-1). In this study, the Mono Basin is considered that area bounded by the Bodie Hills, Cowtrack Mountain, Long Valley Caldera and the Sierra Nevada on north, east, south and west. The area has been the site of extensive volcanic and tectonic activity in late Quaternary time (Bailey *et al.*, 1976).

The Mono Basin is an ideal laboratory in which to compare the geologic record of active volcanic and tectonic processes for these reasons: 1) The record of volcanism at the Mono Craters has been extensively studied, so that constraints can be placed on the ages and styles of dome formation, 2) The record of surficial fault slip along range- bounding faults is relatively complete over the past hundred-thousand years, and 3) Obvious lack of latest Quaternary faulting on the section of the range front directly opposite the Mono Craters suggests that intrusions which feed the Mono Craters are accomodating strain that was once taken up by range-front normal faulting. The test of this hypothesis of the relief of regional strain by dike intrusion served as motivation for my work.

Structure of the Mono Basin

Before plunging into the active tectonics of the basin, a review of the structural setting is necessary to familiarize the reader with the area.

Huber (1981) hypothesized that the Mono Basin--Long Valley region began downdropping relative to the Sierra Nevada about 3 m.y. ago. Since that time differential motion between the Hartley Springs area (Figure 3-1) and the crest of the Sierra Nevada has been about 1100 m. Huber (1981) was unable to extrapolate his work to the north and south along the range front, but the conclusion of Gilbert *et al.* (1968), that much of the movement on the Cowtrack

Figure 3-1. The Mono Basin is situated east of the Sierra Nevada, between
Long Valley Caldera and the Bodie Hills. HSF = Hartley Springs Fault, RPF =
Reversed Peak Fault. Lettered localities are referred to in the text.
Faulted glacial moraines (stipple) reveal some of the history of faulting in
the basin and its relationship to volcanism. All faults that break mid-
Pleistocene or younger material are shown, except those within the volcanic
edifices. The Silver Lake Fault and the fault at Virginia Creek are not
mapped into terrain where they do not form bedrock escarpments. See Plate 3-1
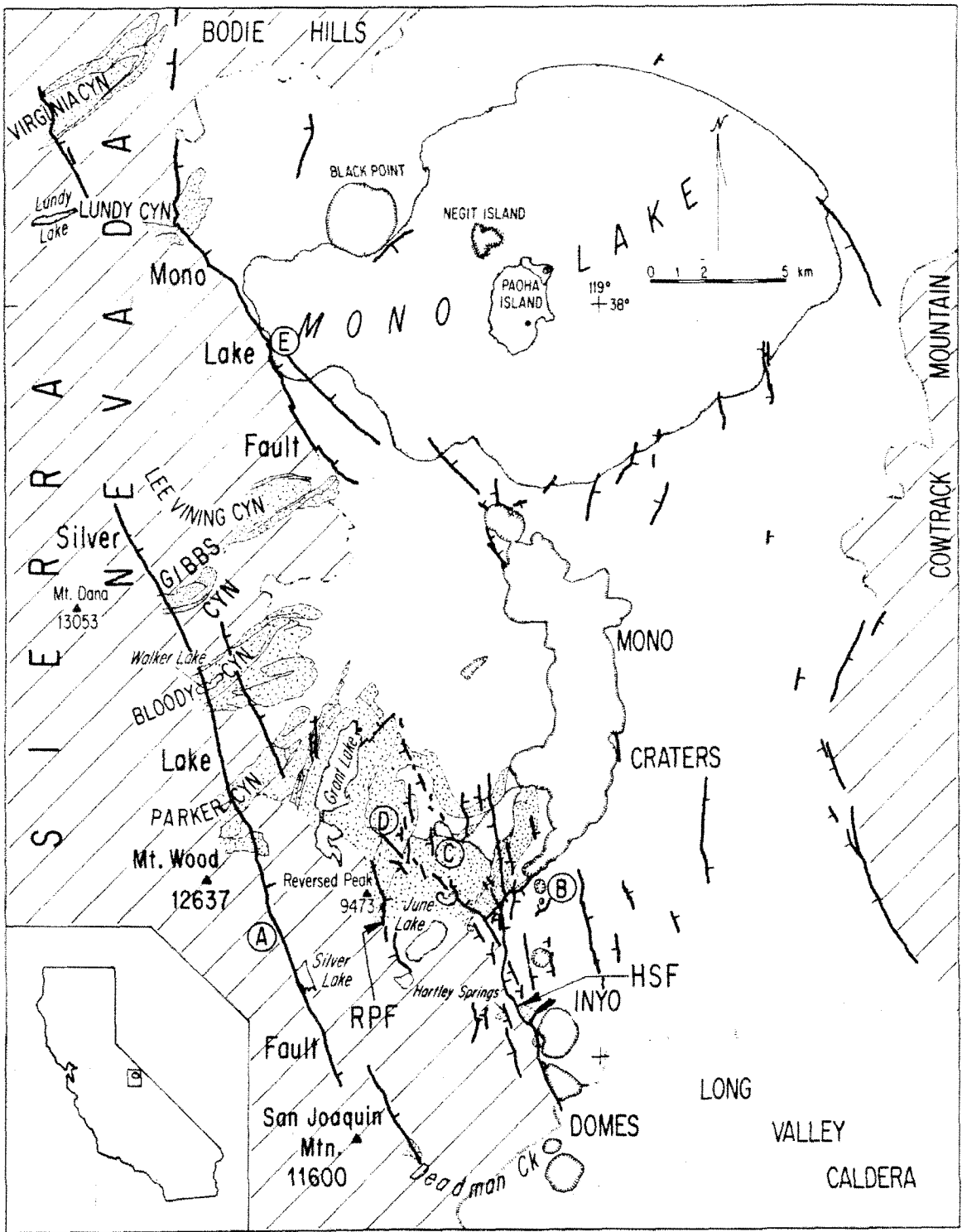for more detailed map of faults.

Figure 3-1

Mountain range front (Figure 3-1) also occurred after 3-4 m.y. ago, supports Huber's hypothesis.

The great amount of subsidence which Pakiser *et al.* (1960) found underneath Mono Lake led them to speculate that the basin is a volcano-tectonic depression or caldera. Pakiser *et al.* (1960) used mostly gravity data to show that 6 km of subsidence had occurred on a set of nearly vertical faults roughly underlying the shore of Mono Lake. They were, however, unable to find enough volcanic material in the region to account for the large amount of subsidence, which, in the case of calderas, is thought to occur in response to evacuation of a large magma chamber.

Gilbert *et al.* (1968) showed that the gravity anomalies of Pakiser *et al.* (1960) could be explained with a basin only 1 km deep, by assuming more reasonable values for the density contrast between Cenozoic sediment and basement rock. Based on detailed mapping of the area, Gilbert *et al.* (1968) found that the Mono Basin is a northward-plunging graben from the northern boundary of Long Valley Caldera to the center of Mono Lake, and a west-trending homocline, with subordinate faulting, that dips southward from the Bodie Hills to the center of Mono Lake. The lack of voluminous volcanic rock around the basin fit their interpretation that the basin is not a volcano-tectonic depression.

Pakiser (1976) returned to the Mono Basin and ran seismic refraction profiles to resolve the discrepancy between the two earlier models. He concluded that the Mono Basin is 2 to 2.5 km deep and that the southern and northern margins of the volcano-tectonic depression that he had earlier hypothesized were formed by flexure as well as by faulting. His (1976) model was essentially the same as that of Gilbert *et al.* (1968), except for the

depth of sediment in the center of the basin.

Although the depth to basement is 1 to 2 km in the center of Mono Basin, depending on interpretation, all workers agree that the depth to basement is much shallower in the rest of the basin. For example, it is less than 300 m underneath the Mono Craters (Gilbert *et al.*, 1968; Putnam, 1949; Hill *et al.*, 1985).

The Mono Basin, therefore, seems to be a shallow structure less than 3 m.y. old. South of Mono Lake, between the Sierra Nevada and Cowtrack Mountain, it is essentially a graben with a northward-plunging floor. North of Mono Lake, the crust is faulted and gently flexed from the Bodie Hills into the basin. The minimum differential uplift between the basin and the Sierra Nevada is 1100 m.

Outline of present work

Data presentation is organized in order of reliability of the data. The first section treats the amount of offset by range-front and intrabasinal faults of dated late Quaternary features. The offsets are used to assess vertical slip rates of active faults. The next section treats what can be inferred concerning the ages and amounts of deformation associated with the volcanoes of the Mono Basin. Following this, I combine information on rates of crustal extension by faulting and by intrusion of dikes underneath the Mono Craters for different time slices in the late Quaternary period. Lastly, I present extension direction data from this study and others.

The discussion section is arranged in a hierarchy similar to the data presentation, with different subsections based on the degree of support from the data for the hypotheses being forwarded.

AMOUNT AND TIMING OF OFFSETS ON THE RANGE-FRONT FAULTS

Data

My primary goal has been to constrain the amount and timing of slip along the faults of the Mono Basin. To accomplish this, it was necessary both to map faults and to measure offsets of dated late Quaternary features or deposits. Therefore, data consist of a tectonic map of the Mono Basin, and approximately 50 profiles of scarp slopes and measurements of scarp heights across faults active in middle-to-late Quaternary time.

The fault map (Plate 3-1) was constructed by field mapping and checking of fault scarps initially mapped in the office from U. S. Forest Service aerial photographs with a nominal scale of 1:20,000. Only faults with known or possible offset in the middle-to-late Quaternary period are depicted in the plate.

After the map was completed, I measured topographic profiles of fault scarps to quantify offsets. Most scarp profiles were made along moraine crests for three important reasons: 1) Glacial moraines issue from the mouths of all major canyons in the study area and cross the frontal fault system, providing dateable late Quaternary features that can be correlated throughout the area; 2) scarps are better preserved on moraine crests than on any other landform, and 3) it is easier to estimate the ages of moraines than the ages of any other landforms. Scarp-profile data are compiled in Table 3-1, and scarp profiles are in Appendix B. Moraine ages are estimated in Chapter 1.

Generally, fault scarps have a morphology unlike any other landform. They are characterized by a laterally extensive slope facet that cuts across other landforms with a relatively constant height. In this respect, they

Table 3-1. Scarp profiles.

Profile	Age of offset surfaces	Best estimate of vertical separation, meters[a]	Scarp height, meters[b]	Vertical slip, meters			Comments
				vert. fault	50 deg. fault	mean	
11	Tioga		8.7				
12	Sherwin		120				
21	Tioga	19.0		19.0	19.6	19.3	
22	Tioga	23.0		23.0	23.9	23.5	Near junction of 2 traces, fault trend changes rapidly.
23	Mono Basin	131		131	148	139	Minimum. Near junction of 2 traces, fault trend changes rapidly.
24	Sherwin	242		242	267	255	Minimum. Near junction of 2 traces, fault trend changes rapidly.
25	Ti.-Holo.		7.5				
33	Tioga	3.7		3.7	4.0	3.8	
nd	late Ti.	0.376		0.4	0.4	0.4	Stratigraphic offset measured in trench along U. S. Highway 120.
41	pre-Mono Basin II	105		105	109	107	Age from Gillespie (1982).
42	Mono Basin	63		63	72	68	Maximum. No scarp. Height of moraine below Tahoe moraine.
43	Tahoe	0					
51	Tahoe	43		43	49	46	
52	Tioga	0					
53	Tenaya	0					
61	Tenaya	16.3		16.3	17.1	16.7	
62	Tahoe	21.1		21.1	22.5	21.8	
63	Tioga	3.8		3.8	4.0	3.9	
71	Tioga	5.5		5.5	6.0	5.7	

Table 3-1. Cont.

Profile	Age of offset surfaces	Best estimate of vertical separation, meters[a]	Scarp height, meters[b]	Vertical slip, meters			Comments
				vert. fault	50 deg. fault	mean	
72	Tahoe	20.9		20.9	21.6	21.2	
73	Tahoe	10.7		10.7	10.9	10.8	
74	Mono Basin	0					
75	Tahoe	10.4		10.4	10.0	10.2	Mono Basin moraine probably not offset more than Tahoe.
76	Tenaya	14.8		14.8	14.4	14.6	A short fault. Similar offset of Tahoe and Tenaya moraines.
77	Tioga	0					
78	Tenaya	7		7	7.8	7.5	Height of Tenaya crest below Tioga. Std. dev. of seven
79	Tenaya	4.2		4.2	4.4	4.3	
710	Mono Basin	62		62	64.1	62.9	Maximum. Glacier may have overridden pre-existing scarp.
711	Mono Basin	63		63	63	63	Maximum. Glacier may have overridden pre-existing scarp.
712	Mono Basin	78		78	79	79	Maximum. Glacier may have overridden pre-existing scarp.
715	Tioga	1.2		1.2	1.2	1.2	Offset of Tenaya moraine probably greater.
716	Bishop Tuff		3.4				
717	Tioga	2.8		2.8	2.8	2.8	Maximum. Part of scarp is stream-channel wall.
719	Tahoe	4.43		4.4	4.4	4.4	
720	Tenaya	3.0		3.0	3.0	3.0	
81	Tahoe	36.3		36.3	31.5	33.9	Minimum, since till has been eroded from upthrown block.
82	Tahoe	28		28	34	31	
83	Bishop Tuff		13.5				
91	Tioga	2.8		2.8	2.8	2.8	

Table 3-1. Cont.

| Profile | Age of offset surfaces | Best estimate of vertical separation, meters[a] | Scarp height, meters[b] | Vertical slip, meters | | | Comments |
				vert. fault	50 deg. fault	mean	
92-mx	late Ti.		4.2				
94	Holocene		5.2				
95	Ti.-Te.		12				Offset beds of Wilson Creek Formation.
96	Bishop Tuff		11.5				
97	Bishop Tuff		7				
98	Bishop Tuff		77				
99	Bishop Tuff	85		85	85	85	Dips of surfaces are approximate.

[a] This is the separation at midpoint of steepest profile segment or at top of bedrock exposed by fault, if available. If not, it is the mean of mininimum and maximum measurements (not tabulated).

[b] Definition of Bucknam and Anderson (1979). Only tabulated where profile was not measured.

resemble lacustrine terrace risers. These two landforms can be distinguished one from another because lacustrine terrace risers generally maintain a constant elevation along strike, whereas fault scarps cut across topographic contours. Several other landforms can also be confused with fault scarps, especially where exposure of the feature is poor because of thick vegetation or weathering. Most important of these features are landslide head scarps, bedrock knolls and small glacial moraines or mounds. Landslide head scarps can generally be distinguished from fault scarps by their lack of continuity across sets of moraines, and from the presence of a toe or colluvial deposit at their base. Bedrock knolls, over which till is sometimes deposited to form a slope discontinuity along a moraine crest, generally can be distinguished from fault scarps because they are not continuous across sets of moraines. Fault scarp-like glacial moraines or hummocks can be distinguished from fault scarps by carefully mapping landform relationships to gain a detailed understanding of glacial flow and geometry. Generally, if a suspect landform is a fault scarp, it will be discordant with landforms caused by glacial action. A mound or ridge of glacial origin will have an orientation that fits into a larger pattern of glacial-geological features.

When I decided that a particular landform was a fault scarp, I profiled it with a Wild-Heerbrugg TC-2000 Total Station or with a 2 or 4 m stadia rod and Abney level. Fault scarps on the order of 50 to 100 meters high, at June Lake, Hartley Springs and Lundy Canyon, were profiled from U.S. Geological Survey 7.5-minute topographic maps with 40-foot contour intervals. I profiled the large fault scarp in the pre-Mono Basin II right-lateral moraine at Sawmill Canyon from the 15-minute map of the Mono Craters quadrangle, which has an 80-foot contour interval. I walked out and noted features along all

scarps profiled from topographic maps, both to ensure that upper and lower surfaces were correlative and to note what fraction of the scarp heights could reasonably be attributed to faulting.

Nomenclature of fault scarp profiles is depicted in Figure 3-2. Note in particular that vertical offset and vertical slip are the same only for vertical faults.

Errors in scarp-profile measurements

The uncertainty in the degree to which slip measurements derived from scarp profiles differ from true fault slips cannot be measured with precision. However, there are two important types of error that can be associated with fault scarp measurements: 1) measurement uncertainty in the instruments, 2) uncertainty of fault, slip vector and offset surface orientation.

Measurement uncertainty in Total Station, rod-and-level and map-profile measurements are much smaller than uncertainties in fault orientation and will not be discussed further.

Uncertainties in orientation can be resolved into four components: 1) dip of fault plane, 2) dip of upper and lower offset surfaces, 3) position of intersection of fault plane and scarp, and 4) strike and dip of slip vector. Below, I address each of these uncertainties.

True dips of fault planes for all profiles measured in this study are unknown. However, other studies of new scarps, and subsurface and bedrock exposures in the Basin Ranges indicate that pristine fault scarps dip 50-90 degrees in unconsolidated material, and that faults in bedrock dip 55-75 degrees (Page, 1934; Lubetkin, 1980; Slemmons, 1957; Myers and Hamilton, 1964; Swan *et al.*, 1980); Witkind, 1964; Wallace, 1977). All vertical slips were
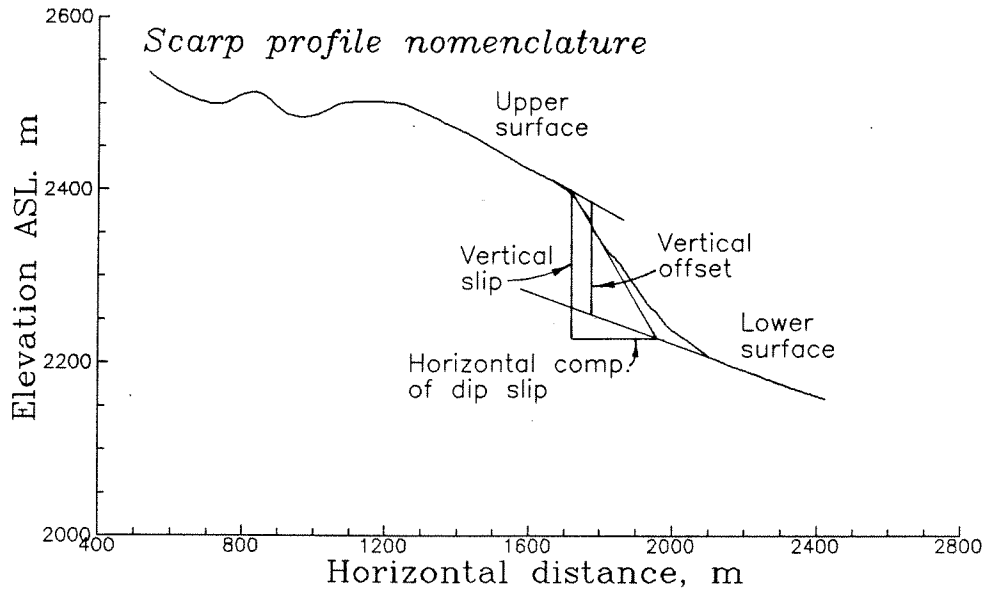
Figure 3-2. Nomenclature of scarp-profile measurements. Vertical offset is the vertical distance between the upper and lower surfaces measured at the midpoint of the steepest segment of the profile, or at the midpoint of the profile if the steepest segment is poorly defined. Vertical slip is the vertical component of dip slip. It is the same as the vertical offset for a vertical fault.

therefore calculated assuming fault dips of 50-90 degrees at the surface. The average of the vertical slips calculated assuming fault dips of 50 and 90 degrees was used as the best estimate of vertical slip. All horizontal slips (extensions) were calculated assuming fault dips at depth of 50 to 75 degrees, as suggested by the subsurface data. The best estimate of horizontal slip was assumed to be that calculated using a fault dip of 60 degrees at depth, as suggested by theoretical studies of tensile failure.

Swan *et al.* (1980) showed examples from the Hobble Creek site along the Wasatch Fault of uncertainty in the dips of offset surfaces. The most serious uncertainty that can arise when estimating the position and dip of the offset surfaces occurs where there is a zone of back-tilting near the main scarp. If offsets are measured within this zone, slips can be overestimated by more than 100%. All profiles from this study were therefore measured beyond any possible back-tilted zone. Even where back-tilted zones are properly taken into consideration, an error is inherent in estimating the dip of offset surfaces. The error in estimating the dips of offset surfaces is small, as suggested by Figure 11 of Swan *et al.* (1980), and is somewhat subjective. This error was therefore not assessed.

For profiles in which the upper and lower surfaces have slightly different dips, an uncertainty in the amount of slip will arise if the position of the intersection of the fault plane and the scarp is not known. Best estimates were made of the position of the intersection by assuming that fault planes intersect scarps in the middle of the most steeply dipping slope segment. For profiles in which the position of the most steeply dipping segment was not known, for example in some of the profiles measured from topographic maps, the fault was assumed to intersect the midpoint of the

scarp, as suggested by Nash (1980). The error in location of the intersection of fault and scarp cannot be evaluated at this time, for lack of sufficient sites at which both scarp profiles and subsurface fault exposures are available.

The most egregious errors in deriving horizontal-slip rates from scarp profiles are caused by ignorance of the orientation of the slip vector. For a few profiles in this study, the position of the moraine crest, in map view, could be measured carefully enough to estimate the strike of the average slip vector. However, these values cannot be used throughout the entire region. Therefore, when I evaluated horizontal slips, I calculated their values orthogonal to the average trend of each fault.

In the tables and figures below, only the uncertainties related to different fault dips are reported, as these are probably the largest uncertainties that can be estimated. It should be noted that other uncertainties are probably locally as large or larger than fault dip uncertainties.

Discussion of scarps

General

In this subsection, I discuss the general features of the map pattern of scarps in the study area as shown in Plate 3-1. Later subsections will focus on offsets of units at specific locales.

The Hartley Springs Fault between Long Valley Caldera and the southern end of the Mono Craters is a broad zone, up to five kilometers wide, consisting mostly of normal faults and some fissures. Most activity is concentrated in a narrow band of faults at the steep range front. Most offset is on east-

dipping faults, but there are notable exceptions. Opening of fissures and perhaps some offset on faults are related to intrusion of magma underneath the southern Mono Craters and the Inyo Craters (Fink, 1985).

At its northern end, the Hartley Springs Fault splays into a complicated group of faults, with similar amounts of offset, between Reversed Peak and June Lake. Movement on some of these structures, especially the faults near the southern end of the Mono Craters and a graben near the cinder cone at June Lake, may be related to volcanic intrusions. Others of the smaller fault splays are probably similar to those discussed by Bateman (1965) in the Volcanic Tableland south of Long Valley. These are structures preserved against degradation on the resistant surface of the Bishop Tuff and may be quite ancient. This region of distributed faulting, up to seven kilometers wide, ends abruptly on its west side at the Reversed Peak Fault, a short normal fault that marks the range front, and on its south side along the strand of the range-front fault underlying the June Lake cinder cone. No structure clearly delineates the northern limit of this zone.

The range front steps to the west north of Reversed Peak. The section of range front at Parker and Bloody Canyons is simple when compared to that to the south, since it is not comprised of a myriad of fault splays. The Sierra Nevada are separated from Mono Basin by two range-front faults. Topographic offsets on these two faults, one of which has been named the Silver Lake Fault, seem to die out to the north near Lee Vining Canyon (Kistler, 1966a; Chesterman, 1975).

The range front makes a right en echelon step between Bloody and Lee Vining Canyons. From Lee Vining Canyon northward a single range-front fault crops out discontinuously to Lundy Canyon, forming the steep, dramatic scarp next to

Mono Lake. The fault is here called the Mono Lake Fault.

North of Lundy Canyon, the range front enters a complicated terrane where it separates the Bodie Hills from the Sierra Nevada. There appears to be a narrow graben between the Bodie Hills on the east and the Sierra Nevada to the west.

Within the Mono Basin itself, numerous faults crop out, especially near the shore of Mono Lake and in the zone of distributed faulting north of June Lake. Offsets on most of the faults near Mono Lake are probably exaggerated by shoreline erosion and deposition.

The east side of Mono Basin is delineated by the Cowtrack Mountain range front. Only in the southern part of the escarpment are Pleistocene deposits noticeably offset.

In the following subsections, I discuss offsets of dateable features, mostly glacial moraines, derived from measurements of scarp profiles across the faults described above.

Hartley Springs Fault

Hartley Springs

Two strands of the Hartley Springs Fault offset Tahoe till(?) at Hartley Springs. The western strand forms a spectacular, nearly vertical, west-facing scarp in Bishop Tuff. The upper surface of this scarp consists of Bishop Tuff on top of which lie Tahoe erratics. The eastern escarpment consists of several east-facing slope facets, only the lowest of which seems to have been formed during post-Tahoe faulting. The upper facets dip at sufficiently low angles that they are probably pre-existing scarps over which the Tahoe glacier cascaded. Total vertical offset across both strands is 64 m, corresponding to

an average total vertical slip rate since Tahoe time of at least 1 mm/yr. However, net motion of the Sierra Nevada relative to Mono Basin on these two strands alone has been downward. The slip rate may be a minimum value because only erratics and not the entire offset glacial moraine crop out on the upthrown horst between the two faults, indicating that the moraine that may once have existed there has been removed by erosion.

In the bedrock plateau west of Hartley Springs, several normal faults offset June Lake Granite. These faults may be quite young, since one is bordered by steep-walled collapse pits tens of meters in diameter and several meters deep. Some of the pits are shown in Plate 3-1. Although the bedrock scarps are locally prominent, offsets die out rapidly along strike.

June Lake

Three major strands of the range-front fault displace right lateral moraines near June Lake (Plate 3-1) down to the east. These faults (F_1 to F_3) together may down-drop the Mono Basin moraine 210 meters. This figure must be taken as a maximum because a fraction of the vertical separation may have occurred previous to the Mono Basin glaciation. The Mono Basin glacier may have flowed over an escarpment cut in resistant Bishop Tuff -- which directly underlies the Mono Basin moraine -- and deposited till that roughly conformed to the offset surfaces of Bishop Tuff.

A fourth obliquely trending strand (F_4) may displace Mono Basin material as much as several tens of meters. F_4 is visible in a roadcut along U.S. Highway 395. In the roadcut, Mono Basin till overlies Bishop Tuff on the northwest side of the fault. On the southwest, down-dropped side of the fault, only colluvium crops out. The lack of till on the down-dropped side

indicates that the till may be offset as much as several tens of meters. Again, part of the offset on this fault could have occurred before the moraine was deposited.

Inboard of the Mono Basin moraine, F_1 and F_2 cross a group of Tahoe moraines. Twenty meters of vertical displacement are visible on the western scarp (F_1), and 10 m on the eastern scarp.

Faults F_5 and F_6 offset the Tahoe moraines down to the west. The scarp of F_5 is visible only on aerial photographs, because it was destroyed by construction of U.S. Highway 395. F_6 offsets the Tahoe moraines 7 m.

Faulting of Tenaya and Tioga moraines by F_1 is somewhat problematic. Two models explain the outcrop relationships between Tenaya and Tioga moraines, and F_1 equally well. The models are shown in Figure 3-3.

According to model 1, Tenaya moraines were offset 7 ± 4 m by F_1 before Tioga moraines were deposited. Seven meters is the elevation of the Tenaya moraine crest below the adjacent Tioga crest. In unfaulted locales, Tenaya moraines are as high or higher than Tioga moraines. Therefore, the lower height of the Tenaya moraine is caused by post-Tenaya but pre-Tioga faulting. In addition to the faulting that caused the height difference between the moraines, Tioga and Tenaya moraines were down-dropped another 6 m in post-Tioga time, forming the scarp now visible in the Tioga moraine. Therefore, according to model 1, the Tenaya moraine has been offset 13 m and the Tioga moraine has been offset 6 m by F_1.

In model 2, the fault scarp in the Tioga moraine and the 7 ± 4 m morainal height difference are both ascribed to the same pre-Tioga faulting. Model 2 assumes that no faulting has occurred since Tioga time, and the scarp in Tioga material is caused by draping of till in a uniform layer over the pre-existing
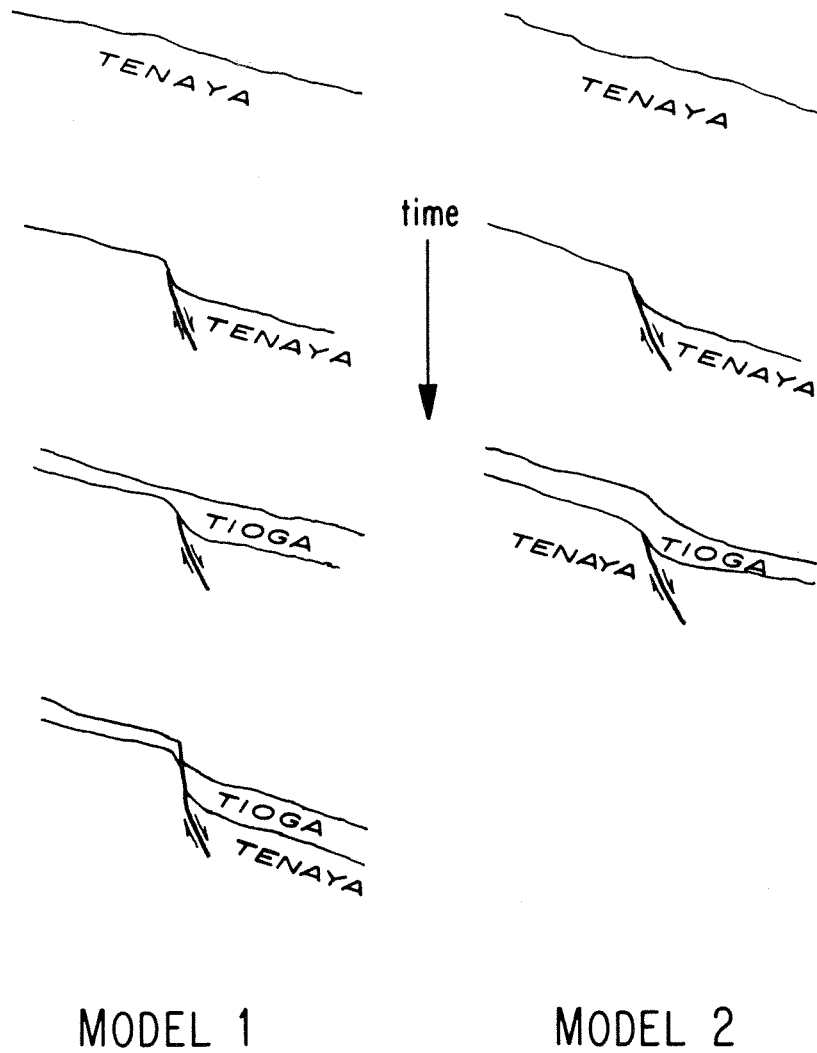
MODEL 1   MODEL 2

Figure 3-3. Two models explain the relationship between the Tenaya and Tioga moraines and fault 1 at June Lake. Model 1 suggests that 7 m of offset of the Tenaya moraine occurred before deposition of the Tioga moraine, and that 6 m of offset occurred after Tioga time. Model 2 posits that all faulting was pre-Tioga, and that the Tioga moraine was merely deposited in a uniformly thick layer over a pre-existing scarp. Both models explain present-day geomorphic relationships.

scarp. In model 2, the Tenaya moraine has been offset 7 ± 4 m by F_1, and the Tioga moraine is unfaulted. Given the available data, it is not possible to discern which of the two models or any intermediate case is correct.

In addition to the offset by F_1, the Tenaya moraine is offset 4 m by F_2, 15 m by F_5 and 3 m by F_6.

Tioga moraines are not offset by F_2 through F_5. F_6 does not seem to offset the basaltic flow northeast of June Lake, which is between Tioga and Tenaya till in age.

Northwest of the Tioga right-lateral moraine, F_1 can be projected across the north side of the cinder cone at June Lake. This cinder cone, like the basaltic flow, was erupted between Tenaya and Tioga time. A complicated group of morainal embankments and glacial flutes surrounds the cone. The complex glacial features render measurement of the displacement of the cone impossible.

Figure 3-4 summarizes the total vertical slip on all strands of the Hartley Springs Fault at June Lake. Given the uncertainties in the ages of the moraines, the data are compatible with a constant vertical slip rate of about 0.9 mm/yr since Mono Basin time, assuming model 1 is correct. Use of best estimates for ages of the moraines, however, suggests that the slip rate has been steadily decreasing from at least Tahoe time to the present. The total slip rate is zero since Tioga time, if model 2 is correct.

Reversed Peak Fault

North and east of Reversed Peak, a prominent strand of the range-front fault offsets Tahoe, Tenaya and Tioga moraines of Grant and June Lake 21, 16 and 4 m, respectively (Plate 3-1). To the south, the fault crosscuts Tioga
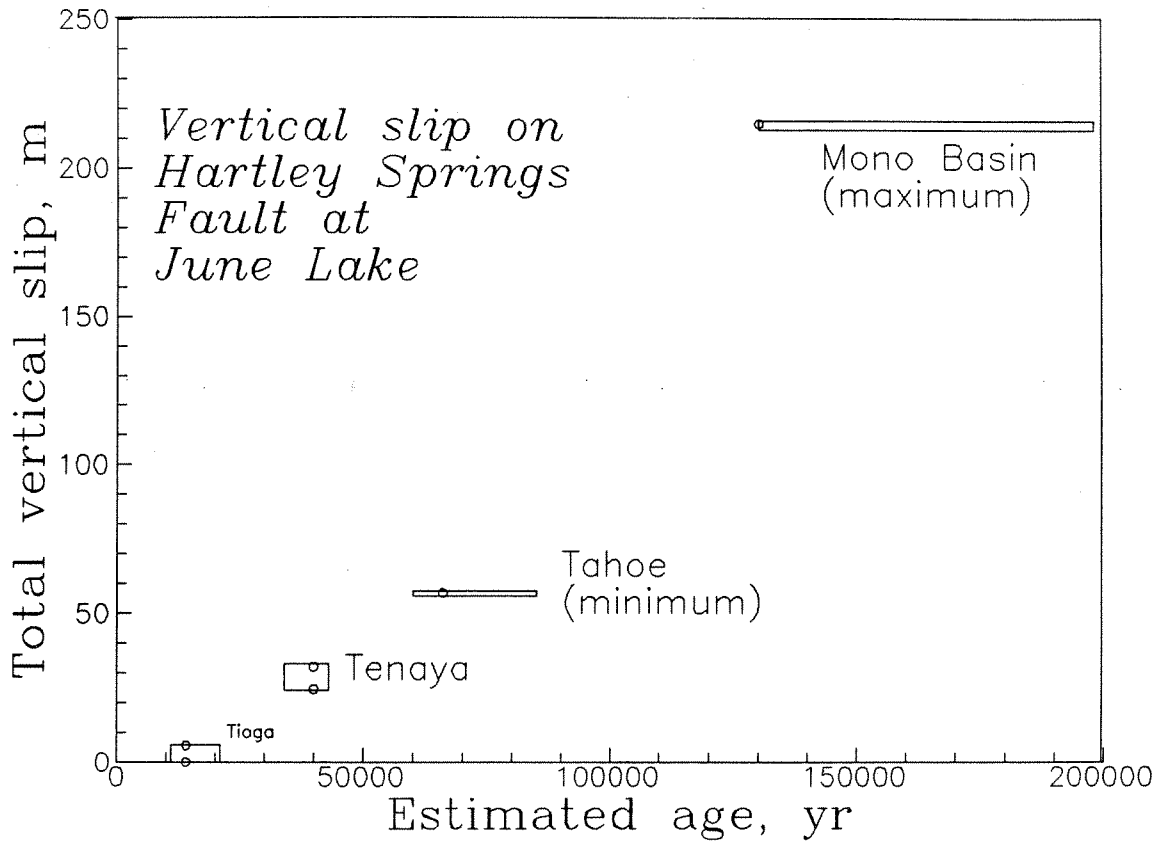
Figure 3-4. Total vertical slip on all strands of the range-front fault at June Lake. Best estimates of slip for both models 1 and 2 are included for Tenaya and Tioga moraines. Small open circles are best estimates. Error boxes enclose ranges in ages of glaciations and in vertical slips assuming different fault dips. Error boxes for Tenaya and Tioga slips also enclose intermediate cases between models 1 and 2. Data are compatible with a constant rate of slip since Mono Basin time, although the best estimates for the ages of the moraines suggest a decreasing rate of faulting.

recessional moraines before dying out(?) in ground moraine northwest of June Lake. Farther south, a conjugate strand of this fault may offset recessional Tioga outwash north of Gull Lake. The small Reversed Peak massif has been uplifted primarily along this structure, so I refer to it as the Reversed Peak Fault.

As shown in Figure 3-5, the data suggest that the rate of faulting along the Reversed Peak Fault increased between Tenaya and Tioga time over that prevailing during Tahoe to Tenaya time. The data do not rule out the possibility that this rate of faulting has continued to the present day, since all measurements in the period from Tioga time to the present should be considered minima (a 3-m faulting event may occur tomorrow, for example). Even at its fastest vertical slip rate of 0.5 mm/yr, however, the Reversed Peak Fault accomodated only about one-half the strain of other range-front faults.

The range front between Parker Canyon and Bloody Canyon

The moraines of Parker and Bloody Canyons cross two major range-front structures. One of these has been named the Silver Lake Fault. It extends north-northwest from the western boundary of Long Valley Caldera. The topographic expression of this fault dies out near Lee Vining Canyon (Kistler, 1966a; Chesterman, 1975). The range-front fault at Virginia Creek may be a splay of the Silver Lake Fault (Kistler, 1966a; Chesterman and Gray, 1975). The other fault defines the range front proper. It is a relatively short structure, the topographic expression of which dies out somewhere near Lee Vining Canyon, like that of the Silver Lake Fault.
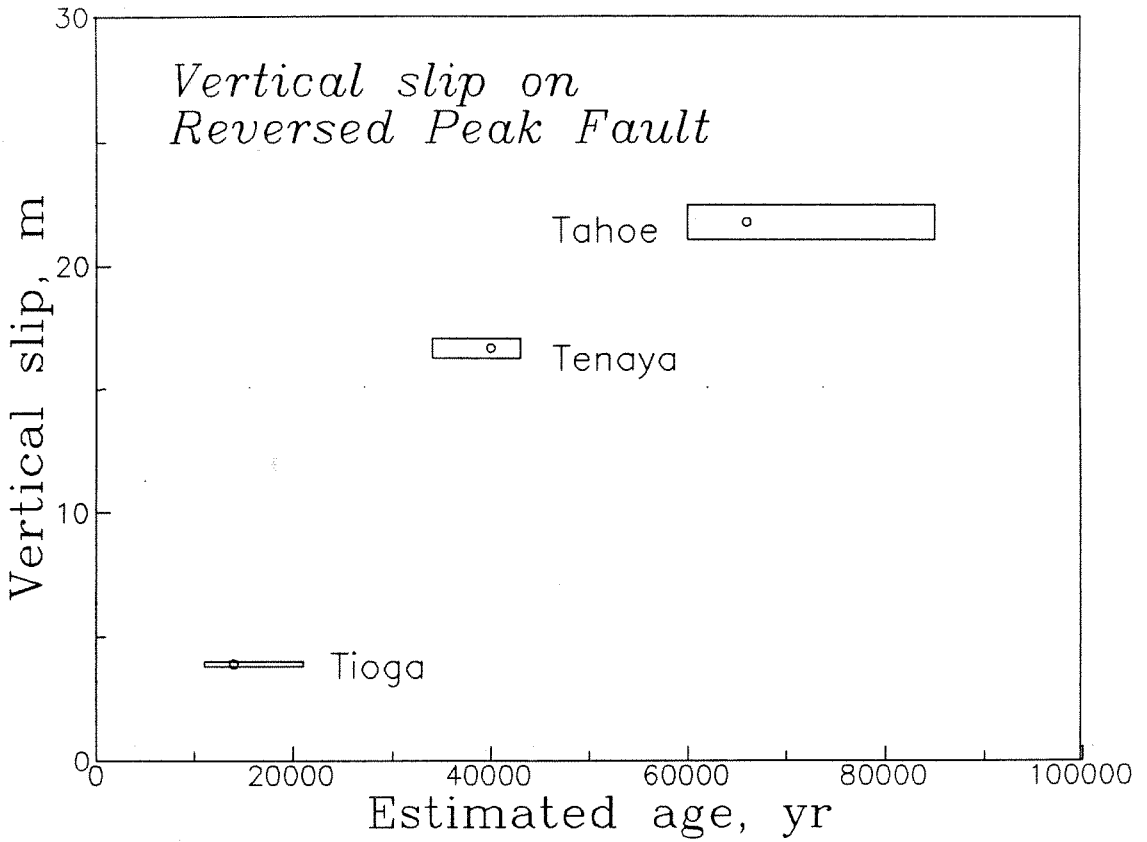
Figure 3-5. Vertical slip on the Reversed Peak Fault. Small open circles are best estimates. Error boxes enclose ranges in ages of glaciations and in vertical slips assuming different fault dips. The Reversed Peak Fault accommodates only a fraction of the slip that is accommodated by other range-front faults. The data suggest that there was an increased slip rate between Tenaya and Tioga time, and that the slip rate may have slowed since Tioga time.

Parker Canyon and the Silver Lake Fault

In this subsection, I first discuss the Silver Lake Fault from Long Valley Caldera to Parker Canyon, before treating relationships at Parker Canyon.

The most prominent fault not bounding the present-day range is the Silver Lake Fault. Rather than bound the range, this fault divides the peaks and plateaux of the High Sierra on the west from a lower plateau on the east, which has been uplifted along the Hartley Springs and Reversed Peak Faults.

Nowhere along its length from its intersection with Long Valley Caldera to Silver Lake does the Silver Lake Fault convincingly offset late Quaternary material. One locale in particular needs to be mentioned in this respect. At Deadman Creek (Figure 3-1), glaciers issuing from a cirque on the east face of San Joaquin Mountain crossed the fault where it joins the western limb of the Long Valley Caldera ring fracture. The upper surface of an escarpment in the left-lateral moraine crest is probably a heavily weathered bedrock knoll overlain with a thin veneer of till. The coarse matrix and angularity of the clasts on the upper surface of the scarp are dissimilar to the fine-grained matrix and more rounded clasts that make up the material on the lower surface. The two surfaces probably do not represent one original surface that was separated by faulting.

North of Silver Lake the fault crosses Tioga through Tahoe (?) lateral moraines at point A in Figure 3-1, but does not seem to displace any of them. However, colluvium and slumping complicate geomorphic relationships in this area, and it is not possible to make a convincing argument.

North of these moraines, the fault crosses the east face of Mt. Wood, which is a long colluvial slope south of Parker Canyon (Figure 3-1). Most of

the talus wedges that combine to form this slope have gentle, concave-upward slopes in down-slope sections. However, some of the wedges end abruptly with convex-upward profiles along the path of the fault. These older colluvial wedges may be faulted. Also along this section of the fault, a rock-glacial moraine of Tioga age appears to have overridden a pre-existing scarp but is itself unfaulted. The relationships here may indicate that the fault has been inactive since Tioga time, but had been active not long before.

A scarp that crosscuts the right-lateral Tahoe moraine at Parker Canyon may have been formed by faulting (Figure 3-1). Springs flow from its base and the feature is steep and relatively free of vegetation. The scarp cannot be projected into the Tioga moraine to the north along the strike of the Silver Lake Fault, and is difficult to trace into the bedrock directly to the south, but it is collinear with the scarps in the colluvial apron of Mount Wood. Upstream from the scarp, steep Tahoe and Tioga moraines are at approximately the same elevation. Directly next to the scarp but on the down-dropped side, the Tahoe moraine is overlain by a meadow, suggesting sagging or back-tilting next to the fault. Downstream, where the Tahoe moraine is not overlain by meadow, it is about 45 m below the Tioga moraine. This is peculiar, because in all canyons where both Tioga and Tahoe moraines are unfaulted, Tahoe moraines are as high or higher than Tioga moraines. The low height of the Tahoe moraine therefore suggests that it is offset at least 45 m (Clark, 1979).

Although it does not crop out alongside the Tioga moraine, the Tenaya moraine crest projects to approximately the same height as the Tioga moraine, except at the Tioga terminus, which is anomalously high. Such a relationship is consistent with either a lack of faulting or very little faulting in the

period between Tioga and Tenaya time.

The above information was used to construct the slip curve displayed in Figure 3-6. From Tahoe to Tenaya time, the data are consistent with a typical uplift rate of as much as 2 mm/yr. From Tenaya to Tioga time, a low or zero slip rate is suggested. No faulting has occurred since Tioga time.

The range-bounding fault does not offset any of the moraines of Parker Canyon. There are no scarps in the moraines along the path of the fault.

Bloody Canyon

Both the Silver Lake Fault and the range-bounding fault at Parker Canyon can be projected into the moraines of Bloody Canyon.

There is, however, a paucity of scarps in the Bloody Canyon moraines. The 200,000(?)-year-old pre-Mono Basin II moraine (Gillespie, 1982) is probably offset by the range-bounding fault (Plate 3-1), since it terminates abruptly along the path of that fault. A Sierra-facing slope at the up-canyon end of the Mono Basin right-lateral moraine may be caused by back-tilting on the down-dropped side of the range-front fault. No fault scarps can be seen in lateral moraines of Tioga through Tahoe ages.

Clark (1979) hypothesized that the low elevation of the Mono Basin moraines relative to the Tahoe moraines was caused by faulting. It is pertinent to give a brief synopsis of his arguments. Clark noted that the Mono Basin moraines extend down-valley a distance intermediate between that of the Tioga and Tahoe moraines. In most canyons where moraines have down-valley extents similar to one another, their crests are within 15 m of one another in height, except at termini. At Bloody Canyon, the crests of the Mono Basin moraines are an average of 60 m below the crest of the Tahoe right-lateral
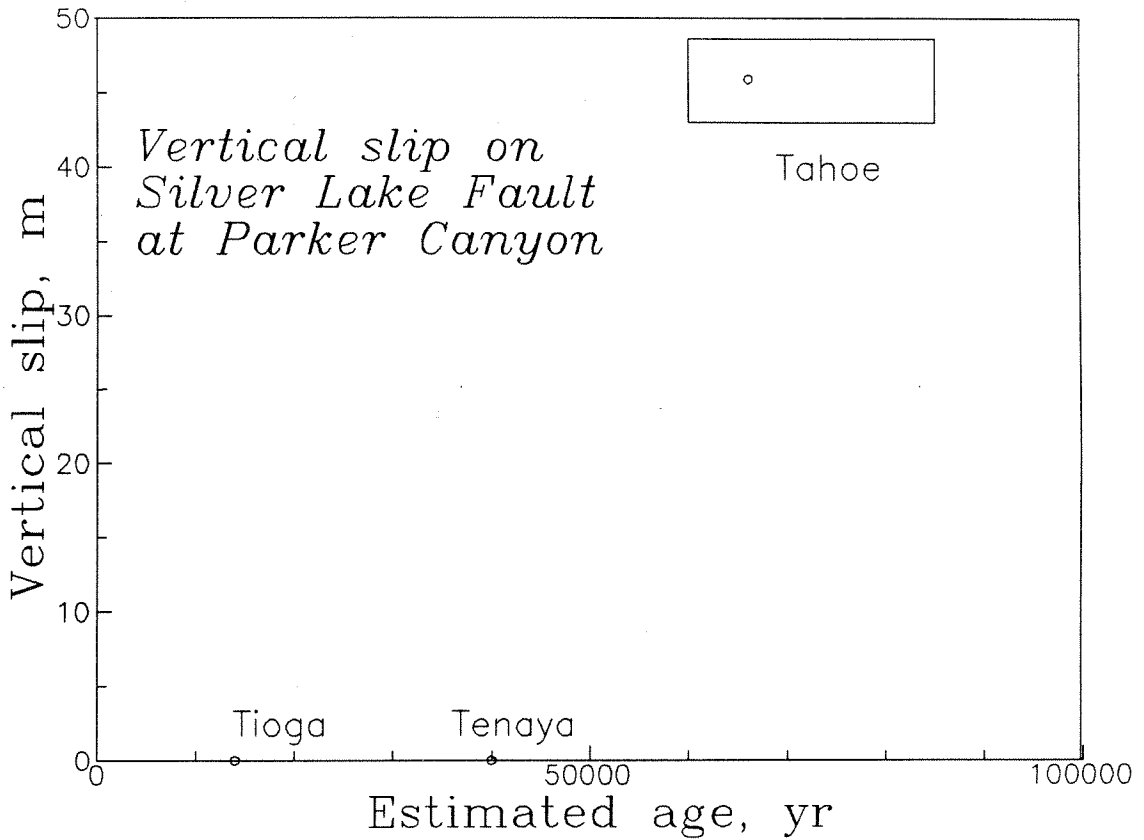
Figure 3-6. Vertical slip on the Silver Lake Fault at Parker Canyon. Small open circles are best estimates. Error boxes enclose ranges in ages of glaciations and in vertical slips assuming different fault dips. The Tioga moraine is definitely not offset and the Tenaya moraine may not be offset. The data are compatible with no faulting since Tenaya time, but a typical range-front slip rate between Tahoe and Tenaya time.

moraine, indicating that something unusual has happened. The simplest and most reasonable explanation is that faulting between Tahoe and Mono Basin time down-dropped the Mono Basin moraines so that later moraines were deposited with crestal elevations considerably higher. Since it is likely that the anomalous height is caused by faulting, the 60 m vertical separation between Mono Basin and Tahoe moraines can be used as an estimate of fault offset.

Figure 3-7 illustrates the possible vertical slip on both Silver Lake and range-bounding faults at Bloody Canyon. Offset of the pre-Mono Basin moraine is taken as a minimum, since possible offset by the Silver Lake Fault is not included, and since the lower surface of the scarp may not be till, but colluvium. As the figure shows, both faults have been inactive at least since Tahoe time, even though they may have had a typical range-front vertical slip rate of about 0.8 mm/yr between Tahoe and pre-Mono Basin II time.

Both the Silver Lake Fault and the range-front fault appear to die out north of Bloody Canyon. Small Tioga and Tahoe moraines at Gibbs Canyon (Figure 3-1) appear to be unfaulted along the path of the Silver Lake Fault, although there is a prominent bedrock escarpment. Tahoe moraines at Lee Vining Canyon are unfaulted along the path of the range-bounding fault.

Mono Lake Fault

Lee Vining Canyon

Offsets of moraines along the Mono Lake Fault at Lee Vining Canyon are not measurable because latest Pleistocene lacustrine terraces have covered the down-dropped sections of Tahoe and Mono Basin moraines. Offset of one lacustrine terrace can be measured. This Tioga-stage terrace is displaced 4 m along a fault scarp trending obliquely to terrace risers at the canyon mouth
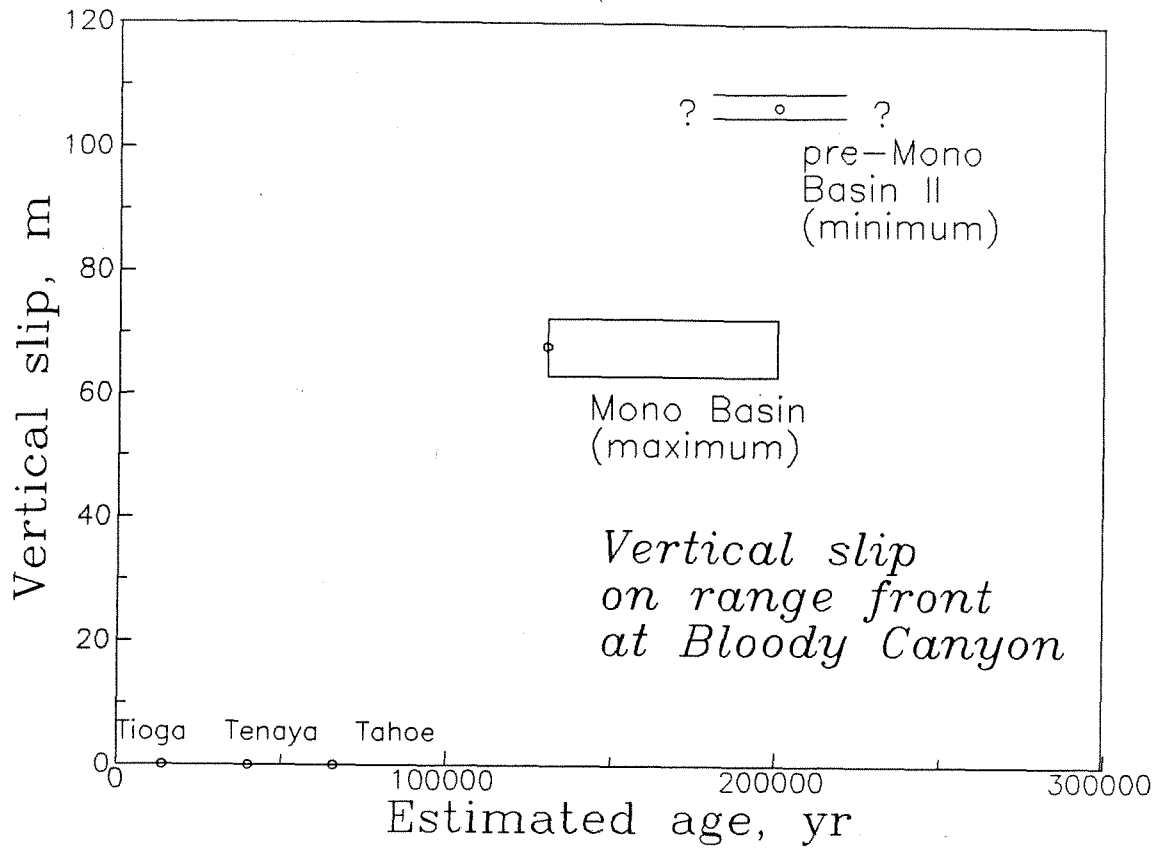
Figure 3-7. Vertical slip on the Silver Lake Fault and the range-bounding fault at Bloody Canyon. Small open circles are best estimates. Error boxes enclose ranges in ages of glaciations and in vertical slips assuming different fault dips. Offset of pre-Mono Basin II moraine is a minimum, since possible offset by Silver Lake Fault cannot be estimated. No faulting has occurred since Tahoe time, even though data suggest a typical range-front rate of offset from pre-Mono Basin II to Tahoe time.

(Figure 3-8).

In addition to the geomorphic scarp, the fault itself crops out in a road cut along California State Highway 120. The offset of the silty bottom-set beds visible in the roadcut is only 0.4 m. This is only 10% of the topographic offset. The difference between the stratigraphic and topographic offsets suggests that the scarp may have been formed during at least two events, only the latter of which broke the relatively young strata visible in the roadcut.

To the south of Lee Vining Canyon, the scarp does not crosscut a prominent 13,000 year old terrace at about 2090 m (6880 feet; Lajoie and Robinson, 1982; Lajoie, 1968), suggesting either that the fault dies out rapidly southward as it skirts the canyon mouth (Figure 3-8), or that no offset has occurred over the past 13,000 years.

Offset of Tahoe and Mono Basin moraines cannot be measured because of modification by the Tioga-age terraces. However, since the older moraines end abruptly along the path of the fault, they are probably offset several tens of meters.

Lundy Canyon

The range-front fault scarp at Lundy Canyon has long been appreciated for its pristine appearance (Russell, 1889). The fault displaces Tioga stage moraines 21 meters across a scarp that is clearly visible in ground moraine and outwash as well as in the right-lateral moraine.

Mono Basin and Sherwin moraines outboard of the Tioga moraines are buried on the basin side of the frontal fault. Therefore, the vertical separations between their crests and the valley floor of 150 and 270 m, respectively,

Figure 3-8. Offset terraces at the mouth of Lee Vining Canyon. Terraces are marked by lines with "T's" on terrace tread. Alluvial fans (arrows), colluvial fans (crescents) and head scarps (serrated lines) are also shown. Offset Tioga recessional terrace shown in stipple. Fault does not seem to break the 13,000-year-old terrace just above 6,800 feet, suggesting either that offset dies out rapidly to the north of Lee Vining Canyon or that offset occurred prior to 13,000 years ago.
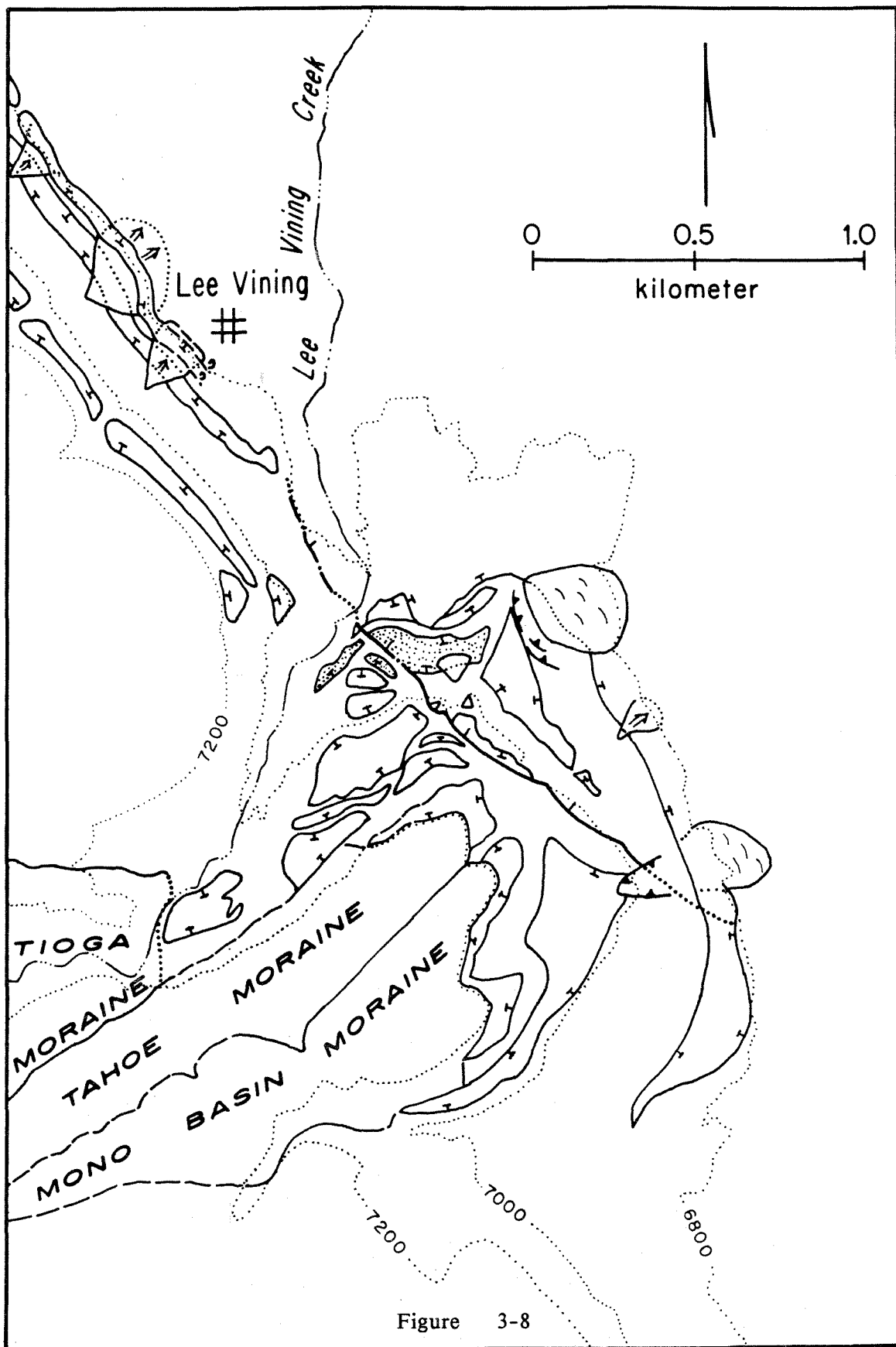
Figure   3-8

place constraints on the minimum amounts of offset.

The vertical slip versus age data shown in Figure 3-9 suggest that range-front faulting at Lundy Canyon may have been continuous and substantial throughout late Quaternary time, with an uplift rate of 1 to 2 mm/yr.

Between Lee Vining and Lundy Canyons

A number of Pleistocene alluvial fans and lacustrine terraces along the shore of Mono Lake between Lundy and Lee Vining Canyons are truncated by scarps. Many of these scarps are arcuate and exhibit a large displacement over a short map length. These features are probably the head scarps of landslides or slumps and may have destroyed some evidence of faulting. However, the lack of obvious landslide debris at the base of the scarps suggests that the landslide deposits may have been down-dropped by faulting and covered by lacustrine deposits. I infer that most of the evidence of late Quaternary history along the steep mountain front has been destroyed by slumping and lacustrine transport.

Two sections of this portion of the range front merit special attention. One scarp, at point E in Figure 3-1, has a small and relatively constant offset along its length. It was probably formed by a fault that displaces late Pleistocene terraces. It can be projected to the south into Mono Lake, and farther still, into a fault that Pakiser (1976) defined in refraction profiles underneath the Pleistocene delta of Lee Vining Creek. It is possible, then, that a major range-front fault lies to the east of the current range front at Lee Vining Canyon.

North of point E, the path of the Mono Lake Fault crosses the Pleistocene delta of Mill Creek. Two possible fault scarps are shown in Plate 3-1 along
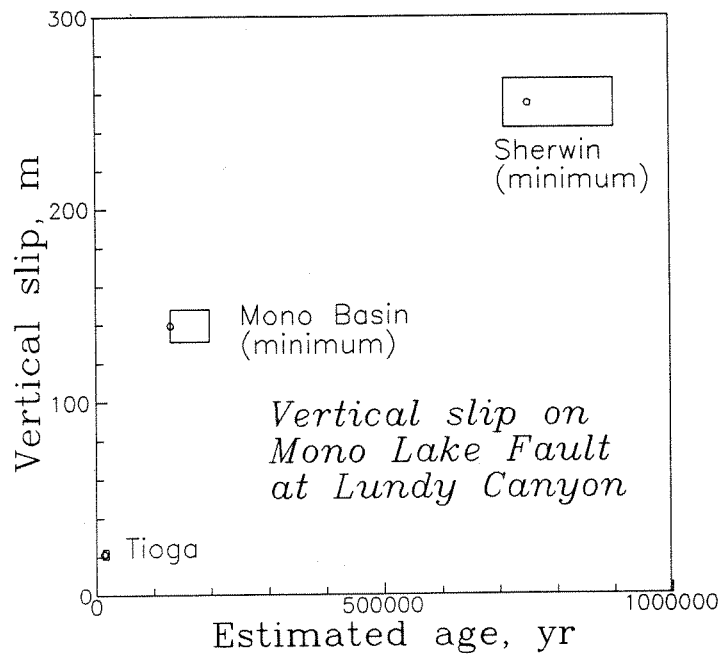
Figure 3-9. Vertical slip on Mono Lake Fault at Lundy Canyon. Small open circles are best estimates. Error boxes enclose ranges in ages of glaciations and in vertical slips assuming different fault dips. Offsets of Mono Basin and Sherwin moraines are minima because lower surfaces are below present-day ground level. Data are compatible with a constant rate of slip for the last 700,000 years.

this section of range front. However, the two scarps may well be wave-cut cliffs formed during two of the higher lake stands, since they crop out at approximately the same elevations as two prominent lacustrine terraces. The apparent lack of faulting between point E and Lundy Canyon suggests that the post-Tioga faulting so prominent at Lundy Canyon dies out rapidly to the south, before possibly resuming at point E and continuing southward.

Intrabasinal Faults

A number of scarps crop out within the Mono Basin. Many of these structures can be ascribed either to volcanic activity or to anomalous preservation in resistant materials. Only a few were clearly formed by late Quaternary tectonic activity. Characteristic examples of each type of feature are discussed below.

Many of the intrabasinal faults north of June Lake probably predate the glacial deposits which they appear to break. However, several faults do appear to offset late Pleistocene drift. One example of a fault that probably breaks late Pleistocene till is the one approximately three kilometers east of Grant Lake (Figure 3-1). The fault appears to offset a Tahoe-stage lateral moraine down to the west. At its north end, Bishop Tuff crops out in the scarp, although the upper and lower scarp surfaces are till. The relationships are compatible with offset occurring before Tahoe time, followed by Tahoe till spilling over and partially covering the scarp. The relationships at the north end of the fault are misleading, however, because the fault continues to the south in a series of en echelon scarps with similar offsets through the Tahoe and perhaps into Tioga moraines (Plate 3-1). No Bishop Tuff crops out where the scarps cross moraine flanks, as would be

expected if the scarps were formed by till deposited atop faulted Bishop Tuff, as is the case at the northern end of the fault. The outcrop pattern therefore suggests that offsets did occur during late Pleistocene time, although the till may have been locally draped over a pre-existing scarp. North of the Tahoe moraine, the fault crosses a fluvial terrace that grades into Tioga lake terraces. Here, the scarp is collinear with a stream channel wall, and therefore part of its height may be the product of channel erosion. The inferred rate of slip on this and another fault that probably breaks Tioga and Tenaya till at point C on Figure 3-1 are much lower than range-front offset rates.

Some of the other faults north of June Lake do not seem to break late Pleistocene material. The most prominent of these faults is discussed next. At the northeast edge of Grant Lake, a northeast trending scarp crosscuts Tioga and Tenaya moraines. The scarp is probably related to the scarp in Bishop Tuff visible on the inner side of the Tioga lateral moraine near the shore of Grant Lake. Because the Tioga moraines and crestal boulder fields drape the scarp rather than being displaced along it, the offset that produced the scarp probably predates the Tioga glaciation. The Tenaya moraine terminates at the scarp, probably because a prominent Tioga-stage terrace cuts the moraine, not because of faulting.

Other intrabasinal faults in the area are probably associated with volcanic activity. East of F_3 at June Lake, a small hill is uplifted along northeast and north-trending faults (Point B in Figure 3-1). Some of the short scarps on the faces of the hill are probably quite young, judging from their rather steep slopes. Part or all of the offset on these faults may have been caused by dikes that underlie the southern part of the Mono Craters.

This is especially true of the fault that was the guiding fracture for the eruption of the craters at the southern end of the chain (Plate 3-1). This fault clearly offsets Bishop Tuff at least 30 meters where it has been exposed in the southernmost crater. Based on relationships near point B, it is apparent that part of the offset on fault F_3 at June Lake may have been caused by magmatic intrusion near the southern end of the Mono Craters. Along the south and north shores of Mono Lake, and on the islands within the lake, numerous scarps and lineaments show that deformation has occurred in the center of Mono Basin. However, the largest amounts of deformation are clearly associated with the volcanic uplift or extrusive volcanism of the islands of Mono Lake or the Mono Craters.

Faults on the eastern edge of Mono Basin

Range-front faults along the southwest edge of Cowtrack Mountain offset Bishop Tuff no more than about 90 m. This implies a relatively low slip rate if it has remained constant since the Bishop Tuff was deposited 700,000 years ago. To the north along the range front, a paucity of late Quaternary deposits renders it difficult to say whether the range front has been active in late Quaternary time.

HISTORY OF CONSTRUCTION OF THE MONO CRATERS

Now that I have outlined the available information on the late Quaternary tectonic history of the Mono Basin, I must do the same for the volcanic history, since my goal is to compare range-front tectonism with deformation

associated with volcanic activity. In order to characterize deformation associated with the craters, it is necessary to estimate both the timing and the amounts of deformation that can be related to them.

The third variable that characterizes the deformation associated with the volcanic activity is the shape of intrusions that feed the volcanoes. If the intrusive bodies are dikes, then a relatively straightforward way to relate faulting and volcanic deformation is by comparing extension rates that are due to each process.

What is the evidence for the shape of underlying intrusions? Sieh and Bursik (1986) showed that the last eruption from the Mono Craters had a dike source that extended for 6 km from North Coulee to Panum Crater (Figure 3-20). Miller (1985) and Fink (1985) showed that the products of the latest Inyo Craters eruption issued from an 11-km-long dike that extended from the southwestern perimeter of Long Valley Caldera to the Inyo Domes. As shown in Figure 3-20, flow foliations and lineaments on other domes within the Mono Craters suggest that these were also erupted from dikes. Finally, the edifice of the Mono Craters is elongated north-south. Taken together, the above data suggest that dike intrusion has occurred repeatedly over the lifetime of the Mono Craters, and is probably the most prevalent intrusive form from which the domes comprising the craters have been erupted. Therefore, extension rates related to faulting and volcanism can be compared. The task, then, is to estimate dike intrusion rates underneath the Mono Craters.

This analysis consists of an attempt to understand the spatial and temporal distribution of dikes based on surficial information. To understand spatial distribution, I have divided the Mono Craters into segments, according to the number of dikes that may underlie each segment. The number of dikes

underlying a segment is assumed constant along the length of that segment, but varies from segment to segment. This is only a rough estimate of dike distribution. A better understanding of dike number and thickness would require a great deal of subsurface exploration.

I have used available ^{14}C and hydration-rind data to constrain the temporal distribution of dikes that have fed the Mono Craters. Ages of some of the domes are known much more precisely than is needed for present purposes. Because I seek to compare dike intrusion with faulting rates, I need only resolve the timing of intrusions to the degree to which I have resolved the timing of fault offsets. So, although some eruptions and their dike intrusions have been dated precisely with ^{14}C, these data will be used only to relate intrusion ages to the glacial chronology that was used to determine fault-slip rates.

In the following analysis, I first discuss the constraints that can be placed on the ages of the volcanoes of the Mono Basin, then I discuss the ages of segments of the Mono Craters, and finally, the number of dikes per segment. From these data I can then estimate extension rates.

Ages of the volcanoes of Mono Basin

In this section I cover the available evidence on the ages of the volcanoes in the Mono Basin.

Late Pleistocene volcanism appears to have started in the Mono Basin less than 40,000 years ago. The oldest eruptions are recorded in the beds of Pleistocene Lake Russell (Mono Lake) and at the June Lake cinder cone. Lajoie (1968) studied a section of lacustrine silt beds that crop out throughout the Mono Basin. These silts are from 12,000 to 36,000 years old and were named

the Wilson Creek Formation by Lajoie (1968). Lajoie (1968) and Lajoie and Robinson (1982) found that all rhyolitic ash layers in the Wilson Creek Formation were chemically similar to the domes of the Mono Craters. However, none of the ash layers sampled by Lajoie (1968) in older lake beds that crop out on Paoha Island were of Mono Craters affinity. Lajoie's data therefore suggest that no rhyolitic volcanism is greater than 36,000 years old. As discussed in Chapter One, the basalt of June Lake is probably older than Tioga till but younger than Tenaya till. Since the Tenaya glaciation is tentatively thought to have occurred 35,000 to 45,000 years ago, the basalt of June Lake erupted between about 40,000 years and 20,000 years ago.

Where are the domes that correlate to the ash layers of the Wilson Creek Formation? Although Mono Craters rhyolitic volcanism seems to have initiated about 40,000 years ago, very few of the currently exposed domes are more than about 20,000 years old, as discussed in detail below. The exposed domes constitute only half the total 8.5 km^3 volume of the Mono Craters. Therefore, most of the 19 rhyolitic ash beds in the Wilson Creek Formation were erupted in association with domes that are now buried. Most of the buried domes probably lie underneath the central section of the Mono Craters near Crater Mountain (Figure 3-11) because much of the unexposed volume of the edifice lies in this section.

The ages of most of the exposed domes and flows of the Mono Craters are constrained by obsidian hydration-rind data from Wood (1977). The obsidian hydration-rind dating method consists of measuring the thickness of rinds of hydrated glass, which form on all obsidian fragments as atmospheric moisture diffuses into the glass. Although hydration-rind dating is not an absolute dating method, it is the only method available at present to estimate the ages

of the domes of the Mono Craters. A suite of hydration-rind thicknesses measured on different domes can be transformed to ages by calibration against one measurement of thickness for which an absolute age is also available. If an absolute date is not available, then the hydration rate must be assumed for calibration. Because Wood (1977) calibrated his hydration-rind thicknesses with the less satisfactory method of assuming a hydration rate, I have recalibrated his hydration-rind curve by tentatively correlating dome 11 to a 13,320 year old ash layer in the Wilson Creek Formation with a similar, distinct phenocryst assemblage (Denham and Cox, 1971; M. Fahnestock, pers. com.). The recalibrated hydration rind-age curve is shown in Figure 3-10.

As a confirmation of the validity of the recalibration, the new hydration-rind curve fits new ^{14}C ages on some of the younger domes and a gap in deposition of tephra recorded in the sediments of Black Lake (Batchelder, 1970) better than does the curve of Wood (1977). Four domes sampled by Wood (1977), which comprise the North Mono eruption of 605 ± 20 yr BP (Sieh and Bursik, 1986), have a mean hydration-rind age of 900 ± 400 years using the new calibration, and a mean age of 1,500 ± 700 using Wood's calibration (all (?) ^{14}C ages are ± 2σ; all hydration-rind ages are ± 1σ). Domes 22 and 26 have hydration-rind ages of 1,800 ± 300 and 1,900 to 2,500 years based on the new calibration or 3,200 ± 500 and 3,300 to 4,400 based on the old. New ^{14}C ages for tephra layers correlative to these domes suggest that they were erupted between about 1,200 and 1,700 years ago (K. Sieh, pers. com.). A gap in the deposition of Mono Craters ash at Black Lake, east of the Mono Basin, occurs between layers with (corrected (?)) ^{14}C ages of 11,350 ± 350 and 5,230 ± 110 yr BP. Using Wood's calibration, many domes have ages that fall within this time gap. Using the new calibration, a gap in hydration-rind ages of domes

occurs between about 5,800 and 13,000 years. I conclude that the new hydration-rind calibration yields reasonable ages for the domes of the Mono Craters.

The hydration-rind curve shown in Figure 3-10 suggests that only dome 6, at the north end of the chain, may be older than the Tioga glaciation. Dome 24 may have been erupted at about the same time as dome 11, that is, at the time of maximum Tioga glaciation. All other currently exposed domes from which Wood (1977) measured hydration rinds seem to be Holocene in age.

One dome which Wood (1977) did not sample is, like dome 6, probably quite old. Dome 12 is cut by a 12,000- to 14,000-year-old shoreline of Lake Russell (Lajoie, 1968; Lajoie and Robinson, 1982), is chemically unevolved (Kelleher, 1986), and, therefore, probably predates the Tioga glaciation.

A number of volcanic edifices lie outside the Mono Craters proper. The ages of Black Point and the Mono Lake volcanic islands are well constrained by ^{14}C-dated ash layers. Ash that erupted from Black Point occurs just above a ^{14}C-dated ostracod-bearing horizon in the Wilson Creek Formation (Denham and Cox, 1971). Black Point ash is approximately 13,000 years old and is therefore late Tioga in age. Stine (1984) showed that the oldest part of the Mono Lake Islands, the "platform" of Negit Island, is slightly older than the 2,000 ± 200 ^{14}C-year-old ash that mantles it. No older ash overlies it. The rest of Negit Island and the volcanoes on Paoha Island are not overlain by the 2000 ^{14}C-year-old ash and therefore postdate it. All of the Inyo Craters appear to be late to mid-Holocene in age (Miller, 1985).

Ages of domes in segments

The maximum age of domes in all segments except segment 5 (Figure 3-11)

Figure 3-10. Ages of the Mono Craters determined by the hydration-rind method. Hydration-rind thicknesses are from Wood (1977). Numbers are dome numbers shown in Figure 3-11. Line is drawn through hydration-rind data (small boxes) and shows the relationship that relates hydration-rind thickness to age. Curve is calibrated by assuming that dome 11 (small filled box) correlates with ash layer 3 of Lajoie (1968), which is 13,320 years old (Denham and Cox, 1971). Typical error bars for hydration rinds are ±0.3 microns (± 1σ measurement precision). Boxes with filled lower-right corners correlate to 605± 20-year-old tephra (small filled circle; Sieh and Bursik, 1986). Boxes with filled upper-left corners correlate to ash layers with corrected radiocarbon ages ranging from 1200 to 1700 yr BP (large filled box). Early-to-middle Holocene gap in hydration-rind ages correlates to gap in deposition of Mono Craters tephra at Black Lake from 11,350 ± 350 yr BP to 5,230 ± 110 yr BP (large open box). The above correlations suggest that the calibration of the hydration-rind curve is reasonable. Hydration-rind thickness of dome 6 is compatible with a pre-Tioga age. Dome 12, not shown, is cut by a Tioga shoreline, so it must also be pre-Tioga in age. All other exposed domes are of Tioga age or younger.

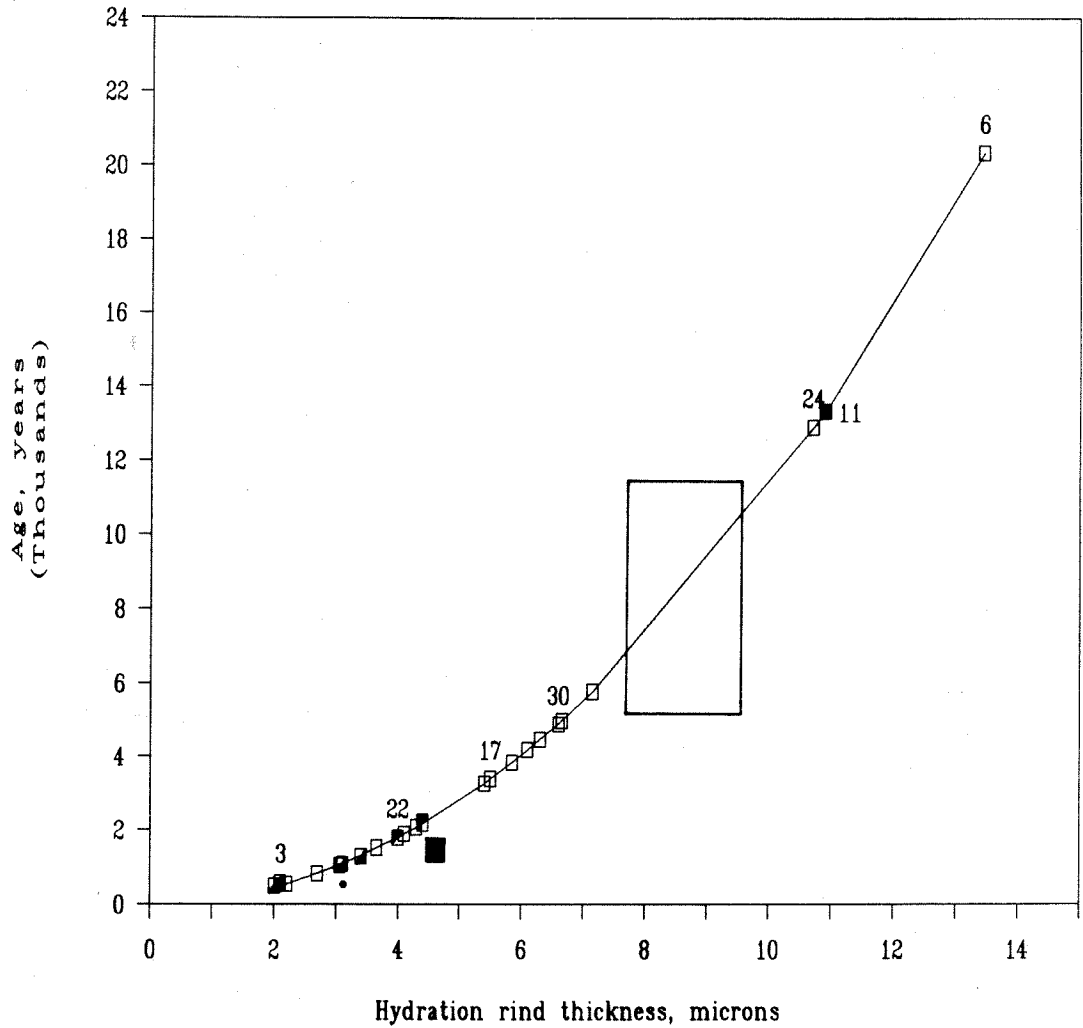# Hydration rind ages of the Mono Craters

Figure 3-10

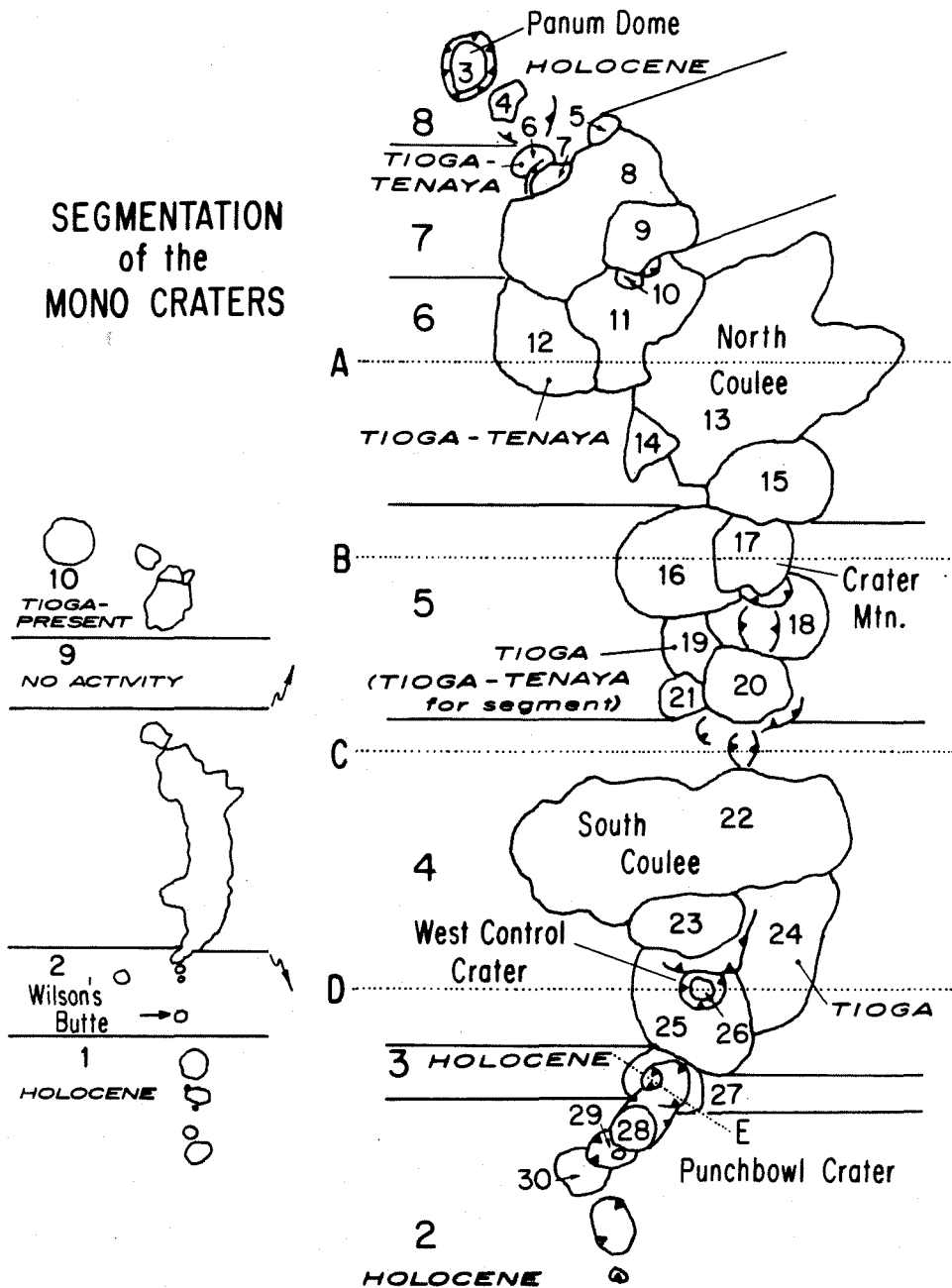
SEGMENTATION of the MONO CRATERS
Panum Dome
HOLOCENE
8
TIOGA-TENAYA
7
6
A
12
TIOGA - TENAYA
North Coulee
13
1
2
3
4
5
6
7
8
9
10
11
14
15
B
16
17
Crater Mtn.
18
5
TIOGA
(TIOGA - TENAYA for segment)
19
20
21
C
South Coulee
22
4
West Control Crater
23
24
D
TIOGA
25
26
3 HOLOCENE
27
29
28
E
Punchbowl Crater
30
2
HOLOCENE
10
TIOGA-PRESENT
9
NO ACTIVITY
2
Wilson's Butte
1
HOLOCENE

Figure 3-11. Segmentation of the Mono Craters according to number of underlying dikes. Cross sections A-E are shown in Figure 3-12. Inset shows segments not in the Mono Craters proper. Segments are chosen so that the number of dikes along the trend of each is constant. Dividing the volcanic features into segments allowed the calculation of rates of extension caused by dike intrusion.

are probably well represented by domes currently exposed, so I give only a brief summary of the age of initiation of volcanism in most segments. All domes in segments 1 to 3 are well-exposed and most have Holocene hydration-rind or ^{14}C ages (Miller, 1985; Figure 3-10). Segment 4 contains dome 24, which is about 13,000 years old, and the segment is therefore considered to have formed completely from Tioga time to the present. Segment 6 contains the dacitic dome 12, and, as discussed above, has probably been active since Tioga to Tenaya time. Segment 7 includes dome 6, which has a hydration-rind age of about 20,000 years. I estimate the segment to have become active in Tioga to Tenaya time.

Segment 8 contains only two domes, the oldest of which (dome 4) may have been erupted during the same event as domes 7 and 8 (K. Sieh, pers. com.). Dome 4 is overlain by 600 year old tephra but not by any older tephra. It may correlate to a 1200 ± 200 year old pyroclastic flow in Rush Creek. All volcanism in segment 8 has therefore occurred from Tioga time to the present. No volcanism has been known to occur in segment 9 (Figure 3-11), although some crater-like forms can be seen in bathymetric maps made by Pelagos Corporation (1987). The oldest volcanism in segment 10 (Figure 3-11) is the 13,300 year old Black Point volcano, and therefore all dike intrusions in the segment occurred from Tioga time to the present.

The age of segment 5 is probably underestimated by the age of the oldest dome in that segment, because of burial of a large number of older domes by the younger, exposed domes. The oldest dome in segment 5 is probably dome 19. It is geochemically similar to domes 11 and 24, both of which are about 13,000 years old. Since dome 19 crops out rather high in the edifice of the central Mono Craters, it probably overlies at least two older domes (Figure 3-12).

Figure 3-12. Cross sections through the Mono Craters. Cross sections taken at locales shown in Figure 3-11. Number of dikes underlying segments with buried domes is estimated by filling the cross sections with domes of average cross-sectional area. Using this technique, greatest density of dikes is found underneath segments 5 and 6 (cross-sections A and B). Note that there are probably at least three dikes underlying craters in cross section E, even though material in it has less cross-sectional area than one average dome. If this situation is common, then the number of dikes in some sections is underestimated. On the other hand, if flows the size of Northern Coulee are contained in cross section B, then the number of dikes is overestimated. The number of dikes counted in these cross sections was used to estimate the rate of extension caused by dike intrusion for the numbered segment in which each cross section was made.

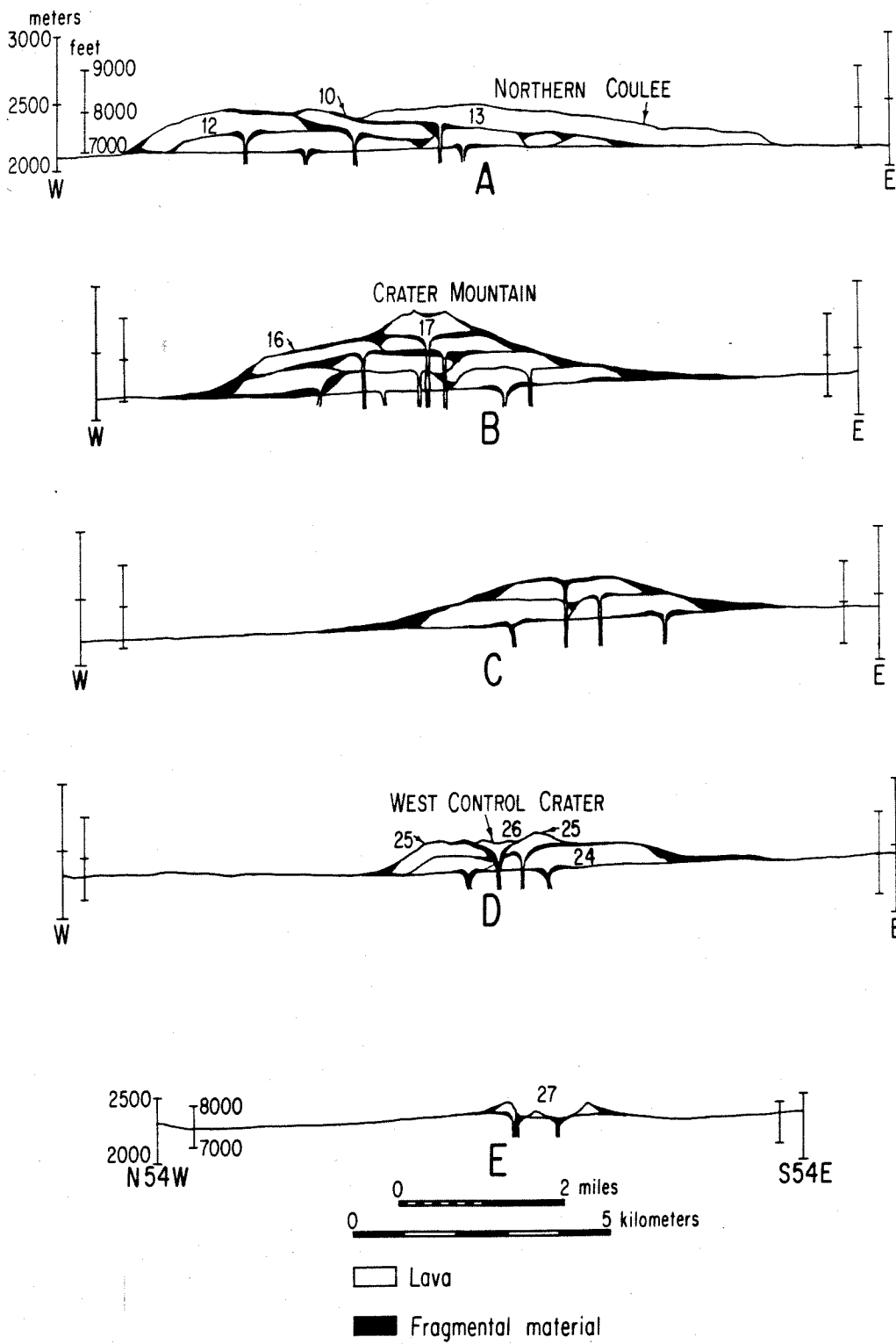# CROSS SECTIONS THROUGH THE MONO CRATERS

Figure   3-12

Therefore, eruptions from segment 5 probably initiated between Tioga and Tenaya time.

The general temporal pattern of latest Quaternary volcanism in the Mono Basin can be summarized as follows: Initial eruptions occurred in the central and north-central parts of the Mono Craters (segments 5 and 6) and at June Lake between Tioga and Tenaya time. During maximum Tioga time, eruptions occurred at Black Point and began in the south-central Mono Craters (segment 4). In Holocene time, volcanic activity has extended south to the Inyo Domes and north to the islands of Mono Lake.

Number of dikes

Now that I have estimated ages of segments of the Mono Craters, I estimate the number of dikes underlying each segment. With these data, I can then estimate extension rates over the lifetime of each crater segment. The following discussion summarizes the number of dikes which I have estimated to underlie each segment.

There is no simple way in which to estimate the number of dikes that are intruded underneath the Mono Craters. In the only previous comparable study, Bacon (1982) assumed that the volume of domes erupted in the Coso Volcanic Field during a given time interval was proportional to the thickness of dikes and therefore to extension. Two approaches, both of which differ from that of Bacon (1982), will be used here, depending on the outcrop pattern of domes in the segment under consideration.

The first approach is applicable to those segments in which buried domes probably exist, and is based on the observation that there is an "average" dome size for the Mono Craters -- about the size of Panum Dome or Crater

Mountain (Figure 3-11). If cross-sectional slices are made through the Mono Craters, then a certain number of average-size domes will be intersected by each slice. If a dike is connected to each average dome in the cross section, then the extension caused by dike intrusion in that cross section can be estimated, assuming a certain thickness for each dike. This is the method illustrated in Figures 3-11 and 3-12. Figure 3-11 is a map view showing exposed domes and positions of cross sections in Figure 3-12. Figure 3-12 shows the cross sections filled with average-size domes and fragmental debris to satisfy outcrop patterns and subsurface data, which consist of three logs of exploratory shafts drilled near South Coulee for the Mono Craters Tunnel of the Los Angeles Department of Water and Power. These logs show that there are up to 100 m of fragmental material on the flanks of the Mono Craters (Berkey, 1935).

Also shown in Figure 3-11 are the numbered segments of the Mono Craters. The segments encompass the length along the craters over which the lettered cross sections are thought to provide reasonable estimates of the number of dikes. So, segment 5 includes that section of the craters under which I have estimated there to be eight feeder dikes. Segment 4 is constrained by two cross-sections, both of which can be filled with four average-size domes. Similar situations hold for segments 6 and 3.

The second approach was used to estimate the number of dikes in the remaining segments, in which all domes are currently exposed, so cross sections were not useful. In some of these segments, ages of eruptive events during which separate domes were extruded are known. In others, reasonable assumptions about the number of events of dome formation and dike intrusion were made based on available chronological and petrological data as well as

stratigraphic relationships between the domes and dated tephra layers. The following is a summary of the estimated number of dikes in each of these segments.

Segment 1 contains domes that may have been formed during only two separate intrusion events, if the small dome at Glass Creek and Sampson's Dome (Sampson, 1987) are the same age as the North Deadman Dome. It seems reasonable that these domes were erupted during the same episode since, as Miller (1985) showed, all other Inyo domes, except Wilson's Butte, formed during a single eruptive event. The ranges over which the domes of the two generations crop out along strike overlap, so, I estimate that two sub-parallel dikes underlie the entire segment.

Segment 2 also contains domes that formed during at least two eruptions. Wilson's Butte is 1,350 to 1,200 ^{14}C years old (Miller, 1985). The domes at the southern end of the Mono Craters (domes 28 to 30) are petrologically similar to one another, and dome 30 has an obsidian hydration-rind age of 4,900 ± 500 years. Therefore, there may have been only two eruptive events in this segment 1,300 years ago and 4,900 years ago. The craters between Wilson's Butte and dome 30 may have formed during either of these events. Although the domes and craters of this segment formed during at least two events, the ranges over which the domes of the separate events crop out do not overlap, so I estimate that the segment has been extended by only one dike-thickness in two distinct extensional events. Wilson's Butte is underlain by one dike, and the southern Mono Craters are underlain by another. I infer that the tips of these dikes do not overlap because the outcrop areas of the extrusions formed from them do not overlap.

Segment 7 includes domes of three distinct ages. Domes 5 and 9 formed

during the North Mono eruption of 600 yr BP (Sieh and Bursik, 1986). Domes 7 and 8 are both overlain by tephra from the 600-year old eruption, but are not overlain by any older tephra. They both may be correlative with the 1200 ± 200 yr old pyroclastic flow in Rush Creek. Early explosive phases of the eruption associated with domes 7 and 8 blasted through part of dome 6 in the north and part of dome 12 in the south, so the outcrop areas of domes formed during three separate eruptions overlap, hence, three dikes may underlie this segment.

Segment 8 contains only two overlapping domes, and therefore two sub-parallel dikes may underlie it.

Segment 9 contains no known volcanic edifice, so I have estimated that no dikes underlie it.

Segment 10 is unusual. The dikes that fed Black Point and Negit Island clearly trend approximately orthogonal to the overall trend of the volcanic features (Plate 3-1). If the intrusion underlying Paoha Island (Pakiser, 1976) is a body elongated between the crater at the south end of the island and the tuff ring in the northeastern corner, then the Paoha Island intrusion also trends orthogonal to the overall trend of the volcanoes. Therefore, I have considered each edifice separately, because there are probably no dike-filled fractures at depth, which link the vents, as is the case in other segments. Black Point seems to be the product of a single dike; Paoha Island may be the product of two dikes, and Negit Island may be the product of up to three overlapping dikes (Stine, 1984).

Since it is off the trend of the other volcanoes, I have not assigned the June Lake cinder cone to a numbered segment. A graben north of the cone (Figure 3-13) may be the fissure from which it erupted. The fissure has been
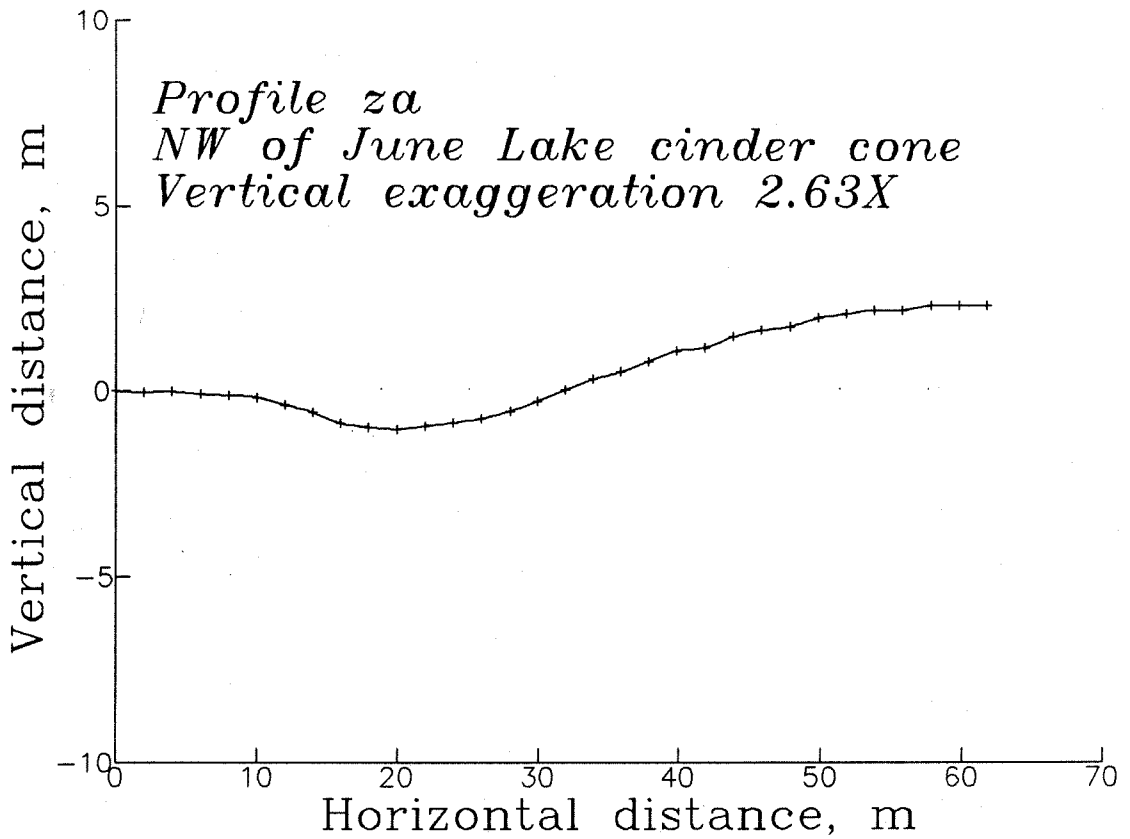
Figure 3-13. Profile Za, northwest of June Lake cinder cone. Although there is net vertical offset across this scarp, the presence of a prominent swale between up-thrown and down-dropped sides suggests that a fissure filled with pyroclastic material is present. It may be the fissure along which the cinder cone was erupted.

filled with glacial outwash and pyroclastic material since its formation. The length of the graben suggests the lateral extent of the dike underlying the cinder cone. This dike seems to have erupted along F_1 of the Hartley Springs Fault. There is probably only one dike underlying the cone, since most cinder cones form during a single eruptive pulse (Williams and McBirney, 1979).

As stated above, the central segment, segment 5, must have the greatest number of feeder dikes underlying it. Since it is reasonable for the greatest number of dikes to overlie the source of magma, the great bulk of the central segment is consistent with the finding of Achauer *et al.* (1986) that a body of seismically slow material (perhaps a magma chamber) lies beneath it.

Cross sections A and E give some idea of possible errors in dike number estimates. If one or more of the buried flows under segment 5 has the same area as North Coulee in cross section A, then the number of dikes is overestimated. On the other hand, if some dikes did not breach the surface and formed explosion pits instead, as in cross section E, then the number of dikes is underestimated. Errors in the estimates of the number of dikes may therefore be rather large in segments 4 to 6, perhaps on the order of 50%, because of the lack of exposure. Errors in segments 1 through 3 and 8 through 10 are probably rather small because of complete exposure.

Note in Table 3-2 that the number of dikes in segments 6 through 8 had to be apportioned between Tenaya to Tioga time, and Tioga time to the present. The apportionment of dikes in each period was based on the cross sections, giving the minimum number of dikes possible to the Tenaya to Tioga period because there seems to be a steady increase in the rate of Mono Craters volcanism through time (Wood, 1984; Sieh, unpub. data).

I now have the data necessary to estimate extension rates in every

Table 3-2. Numbers of dikes and dike extension rates in crater segments.

Crater segment	Number of dikes	Extension, meters[a]			Length of time interval			Extension rate, m/Kyr or mm/yr[b]		
		minimum	best	maximum	minimum	best	maximum	minimum	best	maximum
1	2	10	16	20	11000	14000	21000	0.5	1.1	1.8
2	1	5	8	10	11000	14000	21000	0.2	0.6	0.9
3	3	15	24	30	11000	14000	21000	0.7	1.7	2.7
4	4	20	32	40	11000	14000	21000	1.0	2.3	3.6
5	8	40	64	80	34000	40000	43000	0.9	1.6	2.4
Tenaya-Tioga		20	32	40	13000	26000	32000	0.6	1.2	3.1
Tioga-present		20	32	40	11000	14000	21000	1.0	2.3	3.6
6	5	25	40	50	34000	40000	43000	0.6	1.0	1.5
Tenaya-Tioga		10	16	20	13000	26000	32000	0.3	0.6	1.5
Tioga-present		15	24	30	11000	14000	21000	0.7	1.7	2.7
7	3	15	24	30	34000	40000	43000	0.4	0.6	0.9
Tenaya-Tioga		5	8	10	13000	26000	32000	0.2	0.3	0.8
Tioga-present		10	16	20	11000	14000	21000	0.5	1.1	1.8
8	2	10	16	20	11000	14000	21000	0.5	1.1	1.8
9	0									
10-Negit	3	15	24	30	11000	14000	21000	0.7	1.7	2.7
10-Paoha	2	10	16	20	11000	14000	21000	0.5	1.1	1.8
10-Black Pt.	1	1	2	5	11000	14000	21000	0.05	0.1	0.5
June L. cone	1	1	2	5	13000	26000	32000	0.03	0.08	0.4

[a] Minimum, best and maximum => 5, 8 and 10 m widths, respectively, for silicic dikes (Sieh and Bursik, 1986) and 1, 2 and 5 m for trachyandesitic dikes under Black Point and the June Lake cinder cone, limiting thicknesses for which are estimated from Walker (1986) and from the maximum 5 m opening of the Black Point fissures.

[b] Minimum extension rate, e.g., assumes minimum dike width and maximum time interval for calculation.

segment of the volcanic chain of the Mono Basin. In the following section, I tie these data together with the faulting data to assess the evolution and interrelationships of tectonic and volcanic extension.

EXTENSION RATES

Estimates of range-front faulting and dike intrusion rates allow the computation of the rate of extension caused by faulting and by dike intrusion. I display data in Figures 3-14 to 3-17, which are maps that show rate of extension caused by both faulting and dike intrusion for different time slices. Tables 3-2 and 3-3 contain information about the range of extension rates possible using different values for fault dips, ages of glaciation and dike widths.

The maps were constructed by plotting the extension rate averaged over each time interval. Where displacement rates were not available for a particular time slice, rates are averaged over the next longest available interval.

For faults, extension rate was computed by dividing the horizontal component of dip slip for the time interval, assuming a 60-degree fault dip, by the best estimate for the length of time in each interval. Table 3-3 shows how the extension rates change when making extreme assumptions about ages and fault dips. For dikes, I multiplied the estimated number of dikes in a time interval by average dike width, then divided the result by the length of the time interval. The average width of a silicic dike was taken to be 8 m, since this is the width of the dike that was intersected by drilling underneath the

Table 3-3. Extension rate in time intervals for faults in the Mono Basin.

Locality	Fault dip, degrees ->	Present to Tioga			Tioga to Tenaya			Tenaya to Tahoe			Tahoe to Mono Basin		
		75	60	50	75	60	50	75	60	50	75	60	50
	Length of time interval[a]												
Lundy	Maximum	0.3	0.6	0.9	0.2	0.4	0.5	0.2	0.4	0.5	0.2	0.4	0.5
	Best	0.4	0.9	1.3	0.3	0.6	0.9	0.3	0.6	0.9	0.3	0.6	0.9
	Minimum	0.5	1.1	1.6	0.3	0.6	0.9	0.3	0.6	0.9	0.3	0.6	0.9
Lee Vining		0.05	0.1	0.2									
		0.07	0.2	0.2									
		0.09	0.2	0.3									
Bloody		0	0	0	0	0	0	0	0	0	0.1	0.3	0.4
		0	0	0	0	0	0	0	0	0	0.3	0.6	0.9
		0	0	0	0	0	0	0	0	0	0.4	0.9	1.3
Parker		0	0	0	0	0	0	0.2	0.5	0.8			
		0	0	0	0	0	0	0.5	1.0	1.5			
		0	0	0	0	0	0	0.7	1.6	2.3			
Reversed Peak		0.05	0.1	0.2	0.1	0.2	0.3	0.03	0.06	0.08			
		0.07	0.2	0.2	0.1	0.3	0.4	0.05	0.1	0.2			
		0.09	0.2	0.3	0.3	0.6	0.8	0.08	0.2	0.3			

Table 3-3. Cont.

Locality	Fault dip, degrees ->	Present to Tioga			Tioga to Tenaya			Tenaya to Tahoe			Tahoe to Mono Basin		
		75	60	50	75	60	50	75	60	50	75	60	50
	Length of time interval[a]												
June Lake		0.07	0.2	0.2	0.06	0.1	0.20	0.04	0.09	0.1	0.08	0.2	0.3
Fault 1		0.1	0.2	0.3	0.08	0.2	0.2	0.08	0.2	0.3	0.2	0.4	0.6
Model 1[b]		0.1	0.3	0.4	0.2	0.3	0.5	0.1	0.3	0.4	0.3	0.5	0.8
June Lake		0	0	0	0.05	0.1	0.2	0.08	0.2	0.3	0.08	0.2	0.3
Fault 1		0	0	0	0.06	0.1	0.2	0.2	0.3	0.5	0.2	0.4	0.6
Model 2[b]		0	0	0	0.1	0.3	0.4	0.2	0.5	0.8	0.3	0.5	0.8
June Lake		0	0	0	0.04	0.08	0.1	0.03	0.07	0.1	0.1	0.2	0.3
Fault 2		0	0	0	0.04	0.1	0.1	0.07	0.1	0.2	0.2	0.5	0.7
		0	0	0	0.09	0.2	0.3	0.1	0.2	0.3	0.3	0.7	1.0
June Lake		0	0	0	0	0	0	0	0	0	0.2	0.3	0.5
Fault 3		0	0	0	0	0	0	0	0	0	0.3	0.7	1.0
		0	0	0	0	0	0	0	0	0	0.5	1.0	1.5
June Lake		0	0	0	0.1	0.3	0.4						
Fault 5		0	0	0	0.2	0.3	0.5						
		0	0	0	0.3	0.7	0.9						

Table 3-3. Cont.

Locality	Fault dip, degrees ->	Present to Tioga			Tioga to Tenaya			Tenaya to Tahoe			Tahoe to Mono Basin		
		75	60	50	75	60	50	75	60	50	75	60	50
	Length of time interval[a]												
June Lake Fault 6		0	0	0	0.03	0.05	0.08	0.04	0.08	0.1			
		0	0	0	0.03	0.07	0.1	0.07	0.2	0.2			
		0	0	0	0.06	0.1	0.2	0.1	0.2	0.4			
June Lake Profile 715		0.02	0.03	0.05									
		0.02	0.05	0.07									
		0.03	0.06	0.09									
June Lake Profiles 717 and 719		0.04	0.08	0.1	0.01	0.01	0.02	0.01	0.01	0.02			
		0.05	0.1	0.2	0.01	0.02	0.03	0.01	0.02	0.03			
		0.07	0.2	0.2	0.01	0.02	0.03	0.01	0.02	0.03			
Hartley Springs Profile 81 Model 1[c]		0.06	0.1	0.2	0.1	0.2	0.3	0.09	0.2	0.3			
		0.09	0.2	0.3	0.1	0.3	0.4	0.2	0.4	0.6			
		0.1	0.2	0.4	0.3	0.5	0.8	0.3	0.6	0.9			
Hartley Springs Profile 81 Model 2[c]		0	0	0	0.09	0.2	0.3	0.1	0.3	0.4			
		0	0	0	0.1	0.2	0.3	0.2	0.5	0.8			
		0	0	0	0.2	0.5	0.7	0.4	0.8	1.2			

Table 3-3. Cont.

Locality	Fault dip, degrees ->	Present to Tioga			Tioga to Tenaya			Tenaya to Tahoe			Tahoe to Mono Basin		
		75	60	50	75	60	50	75	60	50	75	60	50
	Length of time interval[a]												
Hartley Springs		0.05	0.1	0.2	0.09	0.2	0.3	0.08	0.2	0.3			
Profile 82		0.08	0.2	0.3	0.1	0.2	0.4	0.2	0.4	0.5			
Model 1[c]		0.1	0.2	0.3	0.2	0.5	0.7	0.3	0.5	0.8			
Hartley Springs		0	0	0	0.08	0.2	0.3	0.1	0.2	0.4			
Profile 82		0	0	0	0.1	0.2	0.3	0.2	0.5	0.7			
Model 2[c]		0	0	0	0.2	0.4	0.6	0.3	0.7	1.0			
N of Black Point		0.04	0.08	0.1									
Profile 91		0.05	0.1	0.2									
		0.07	0.2	0.2									

Table 3-3. Cont.

Locality	Fault dip, degrees ->	Present to Tioga			Tioga to Tenaya			Tenaya to Tahoe			Tahoe to Mono Basin		
		75	60	50	75	60	50	75	60	50	75	60	50
	Length of time interval[a]												
Cowtrack Mountain[d]		0.03	0.07	0.1	0.03	0.07	0.1	0.03	0.07	0.1	0.03	0.07	0.1
Profile 99		0.03	0.07	0.1	0.03	0.07	0.1	0.03	0.07	0.1	0.03	0.07	0.1
		0.03	0.07	0.1	0.03	0.07	0.1	0.03	0.07	0.1	0.03	0.07	0.1

[a] Lengths of time intervals are the estimates from Table 1-1.

[b] Model 1 assumes no slip since Tioga time, and Tioga till was deposited over pre-existing scarp in a uniformly thick layer. Model 2 assumes scarp caused by offset of Tioga material.

[c] Since only Tahoe till crops out at Hartley Springs, the slip on the fault was divided proportionately into time intervals as at June Lake, assuming the same model for slip on F_1. F_5 was not used because slip in Tahoe-Tenaya time is not known.

[d] Offset unit is Bishop Tuff. Slip rate was assumed constant in all time intervals. Min., mean, and max. ages used are from Bailey et al. (1976).

Inyo Domes (Heiken *et al.*, 1988). Minimum and maximum widths of 5 and 10 m

are plausible extrema, based on the considerations discussed in Sieh and

Bursik (1986). Assumed widths of mafic dikes are discussed in Table 3-2.

Table 3-2 shows how extension rate changes under different assumptions about

intrusion age and dike width. I now discuss each map and its implications.

Figure 3-14 illustrates the rate of extension between Mono Basin and

Tahoe time, from 130,000 years ago to 66,000 years ago. Data are available

from only three locales (shown by stippling), and all data are minima or

maxima. However, they are compatible with a constant extension rate along the

entire range front in the Mono Basin of approximately 0.6 mm/yr. There is no

evidence for volcanism in the basin during this period.

From Tahoe to Tenaya time, 66,000 to 40,000 years ago, data are more

complete than for the preceding interval (Figure 3-15). These data are

compatible with continued extension on the range front in a left-stepping en

echelon zone from June Lake to Parker Canyon, and along the Mono Lake Fault.

Fault 3 at June Lake (shown by open circles) seems to have become inactive, or

dies out rapidly to the north before reaching the Tahoe moraine. Tectonic

activity seems to have ceased around Bloody Canyon. Some activity is obvious

on the intrabasinal faults north of June Lake. The pattern, amount of offset

and sense of motion (down to the west) on these faults suggests that they are

secondary features, perhaps related to flexure between the en echelon range-

front segments at June Lake and Reversed Peak. Currently available data

suggest that there was not yet any volcanism in the basin.

Between Tenaya and Tioga time, 40,000 to 14,000 years ago, faulting seems

to have ceased at Parker Canyon, as well as at Bloody Canyon (Figure 3-16).

Data are consistent with a somewhat lower extension rate along the Hartley

Figure 3-14. Extension rate orthogonal to trend of faults and craters during Mono Basin to Tahoe time, c. 130,000 to 66,000 yr BP. Extension-rate values are in mm/yr. Moraines used for slip-rate measurements are stippled. GC = Gibbs Canyon. i = interpolated from slip rate measured over a time interval longer than that depicted. 700,000-year-old Bishop Tuff is material offset along Cowtrack Mountain range front. Data are compatible with a constant slip rate along the entire Sierra Nevada range front in the Mono Basin, and a lack of volcanic activity.

205
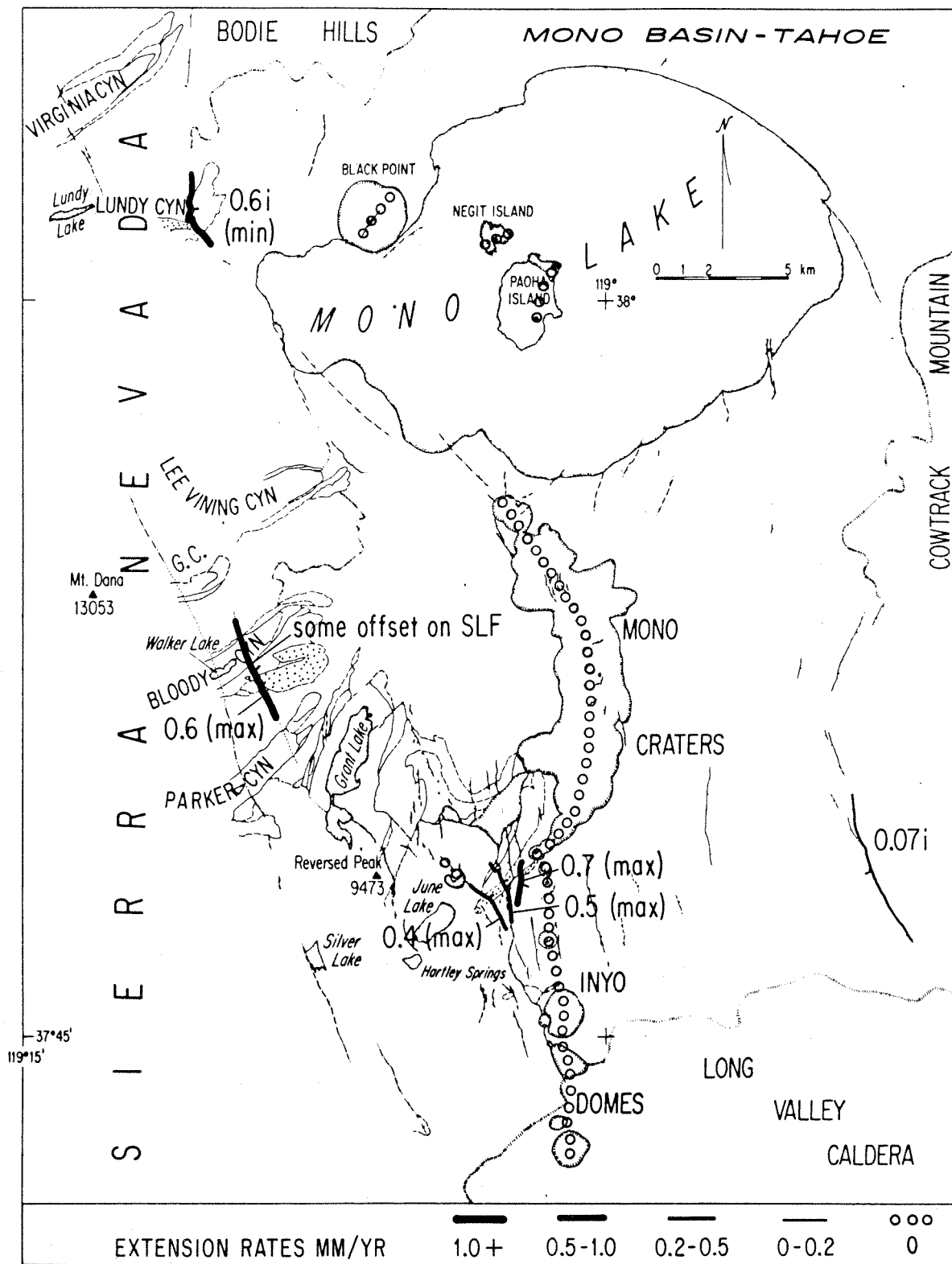
Figure 3-14

Figure 3-15. Extension rate during Tahoe to Tenaya time, c. 66,000 to 40,000 yr BP. Extension-rate values are in mm/yr. Moraines used for slip-rate measurements are stippled. GC = Gibbs Canyon. i = interpolated from slip rate measured over a time interval longer than that depicted. Range in slip rate at Hartley Springs is based on using the two models for slip along F_1 at June Lake. Since data for Hartley Springs are interpolated, slip has been divided into time intervals in the same proportions as at June Lake. Figure suggests that range-front faulting has ceased at Bloody Canyon, but has continued along the rest of the range-front faults and along the Silver Lake Fault to the south. There is evidence for activity along the Reversed Peak Fault and small splays of the Hartley Springs Fault north of June Lake, all of which die out to the north. Available data suggest no volcanism in this time interval, unless a minimum value is assumed for the age of the Tenaya glaciation. If there was volcanic activity, then it would probably have been in the central segment of the Mono Craters (queried).
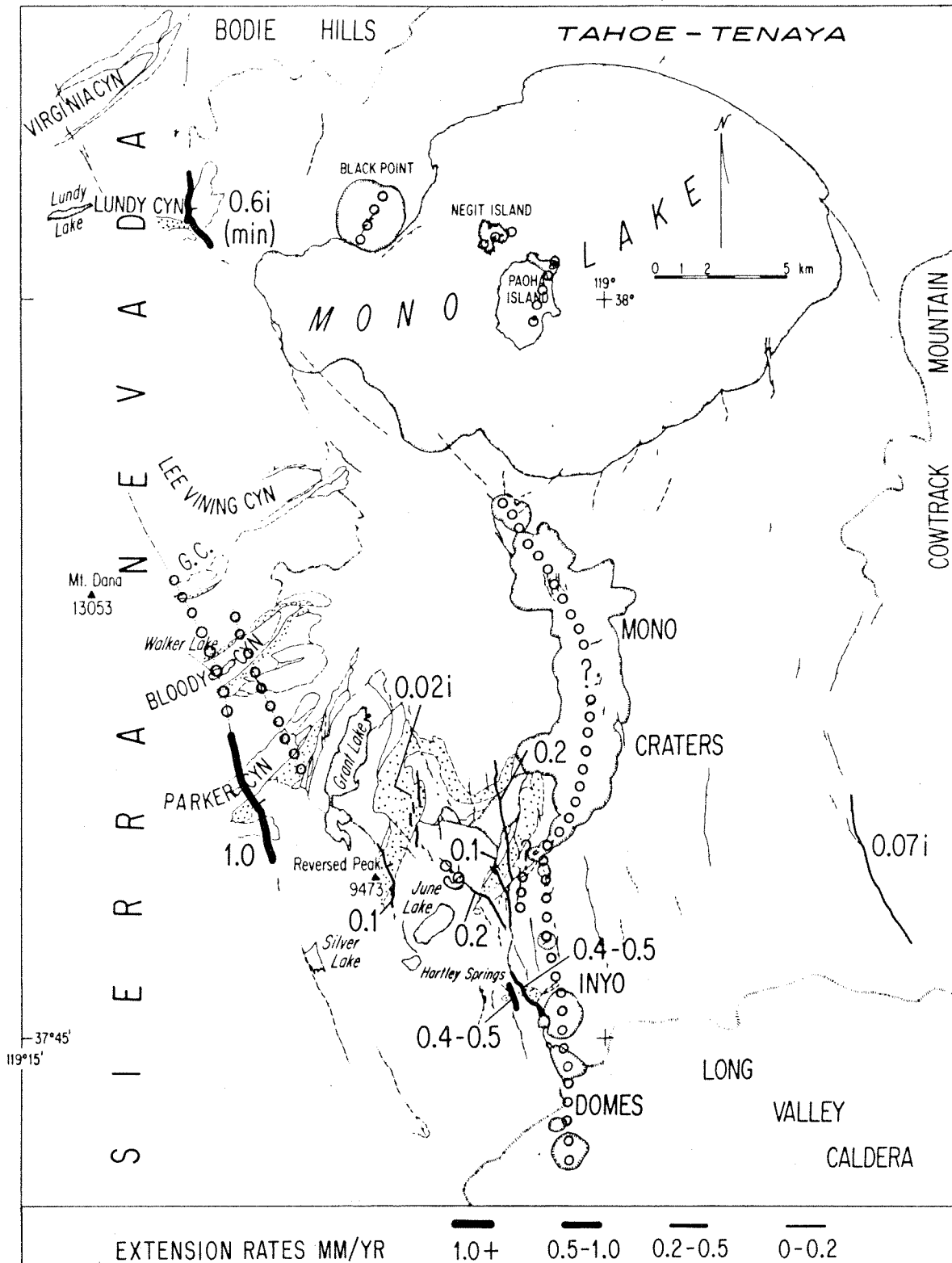
Figure 3-15

Figure 3-16. Extension rate during Tenaya to Tioga time, c. 40,000 to 14,000 yr BP. Extension-rate values are in mm/yr. Moraines used for slip-rate measurements are stippled. GC = Gibbs Canyon. i = interpolated from slip rate measured over a time interval longer than that depicted. e = extrapolated from later time interval based on air-photo interpretation. Range in slip rate at Hartley Springs is based on using the two models for slip along F_1 at June Lake. Since data for Hartley Springs are interpolated, slip has been divided into time intervals in the same proportions as at June Lake. Faulting at Parker Canyon as well as at Bloody Canyon has now ceased, although data are consistent with similar slip rates along the Mono Lake Fault and the Hartley Springs Fault. A low level of fault activity persists on intrabasinal faults between the Hartley Springs and Reversed Peak Faults. Dikes intrude underneath the central and northern segments of the Mono Craters and underneath the cinder cone at June Lake.
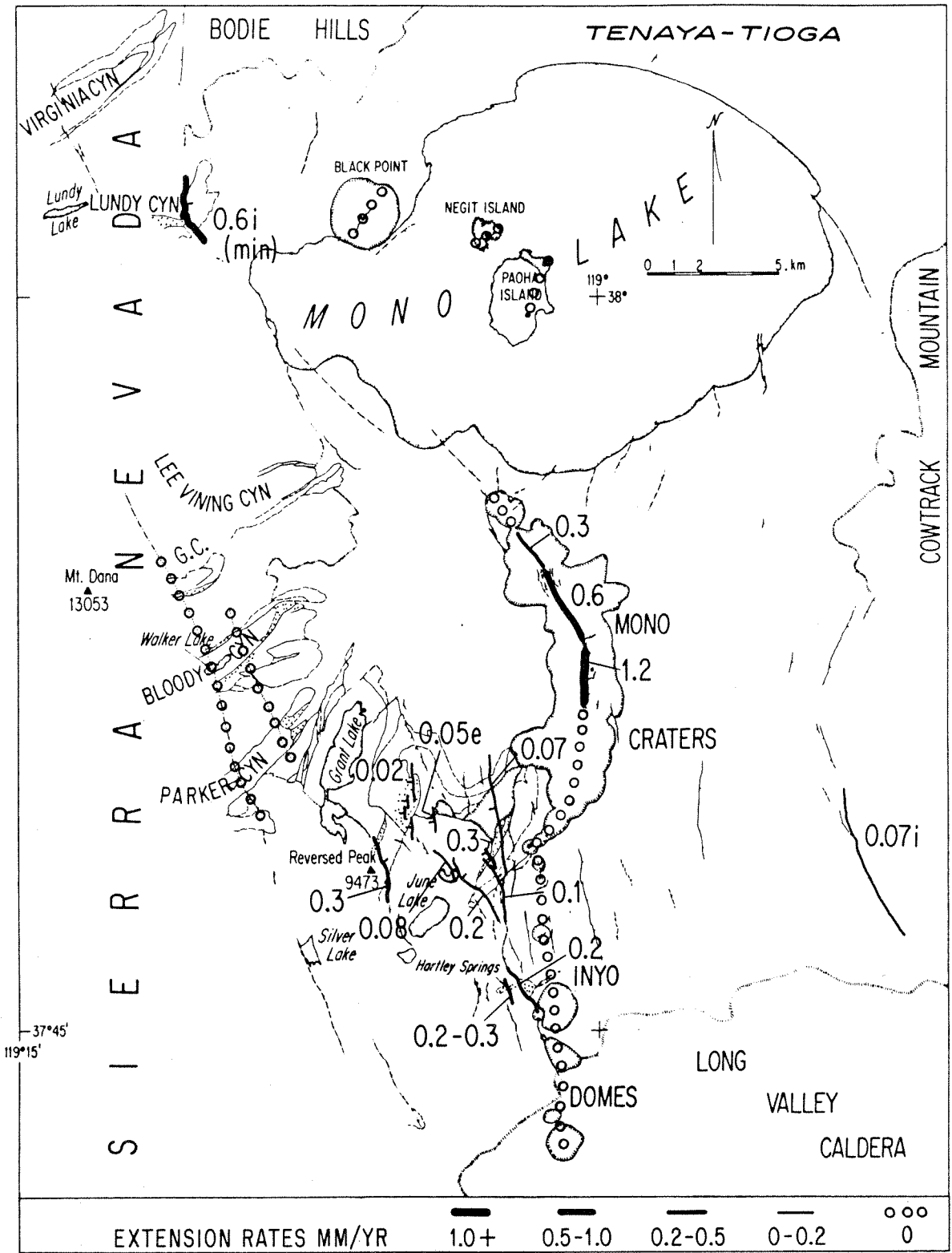
Figure 3-16

Springs Fault, but an increased extension rate along the Reversed Peak Fault, although it still accommodated less extension than other range-front faults. Volcanism began in the central and northern Mono Craters, with most activity occurring in the central segment. The volcanic activity in the northern Mono Craters may have been localized by a buried range-front fault hypothesized by Pakiser (1976) underneath this region. The June Lake cinder cone also erupted at this time, possibly from a fissure that followed F_1 at June Lake.

From Tioga time to the present, only one strand (F_1) of the Hartley Springs Fault at June Lake seems to have been active (Figure 3-17). There has been a decrease in activity on the Reversed Peak Fault and on the intrabasinal faults north of June Lake. Along the Mono Lake Fault, extension has continued at a typical range-front rate of 0.9 mm/yr only at Lundy Canyon. The height of the scarp in Tioga till at Virginia Canyon (Table 3-1) suggests that faulting has continued to the north of Lundy Canyon at typical rates. However, directly south of Lundy Canyon, there is evidence that no faulting has occurred since Tioga time. Still farther south, at Lee Vining Canyon, the fault is again active, but at a much lower rate than at Lundy Canyon. In contrast to reduced rates of faulting, volcanic activity has dramatically increased over the preceding period. Activity is concentrated in the central and southern segments of the Mono Craters, but there are high rates of extension caused by dike intrusion from Long Valley Caldera to the islands of Mono Lake. Segments 2 and 9 (Table 3-2) are the least active. The concentrations of volcanic activity may reflect the hypothesized positions of magma bodies under the Mono Lake islands, central Mono Craters and Long Valley Caldera (Bailey, 1982; Pakiser, 1976; Achauer et al., 1986; Sanders, 1984).

Figure 3-17. Extension rate from Tioga time to the present.
Extension-rate values are in mm/yr. Moraines used for slip-rate
measurements are stippled. GC = Gibbs Canyon. i = interpolated from
slip rate measured over a time interval longer than that depicted.
Range in slip rate at Hartley Springs and for F_1 at June Lake is based
on using the two models for slip along F_1 at June Lake. Since data for
Hartley Springs are interpolated, slip has been divided into time
intervals in the same proportions as at June Lake. Although faulting
at Lundy Canyon has continued at typical range-front rates, extension
rates are lower at Lee Vining Canyon and perhaps at June Lake.
Activity on the Reversed Peak Fault may also have slowed since the
preceding interval. Extension from Lee Vining Canyon south to the Inyo
Domes is largely taken up by dikes which are concentrated underneath
the central Mono Craters and the southern Inyo Domes. There is also a
large amount of activity on a west-northwest-trending group of
northeast-trending faults and dikes from Paoha Island to Black Point.
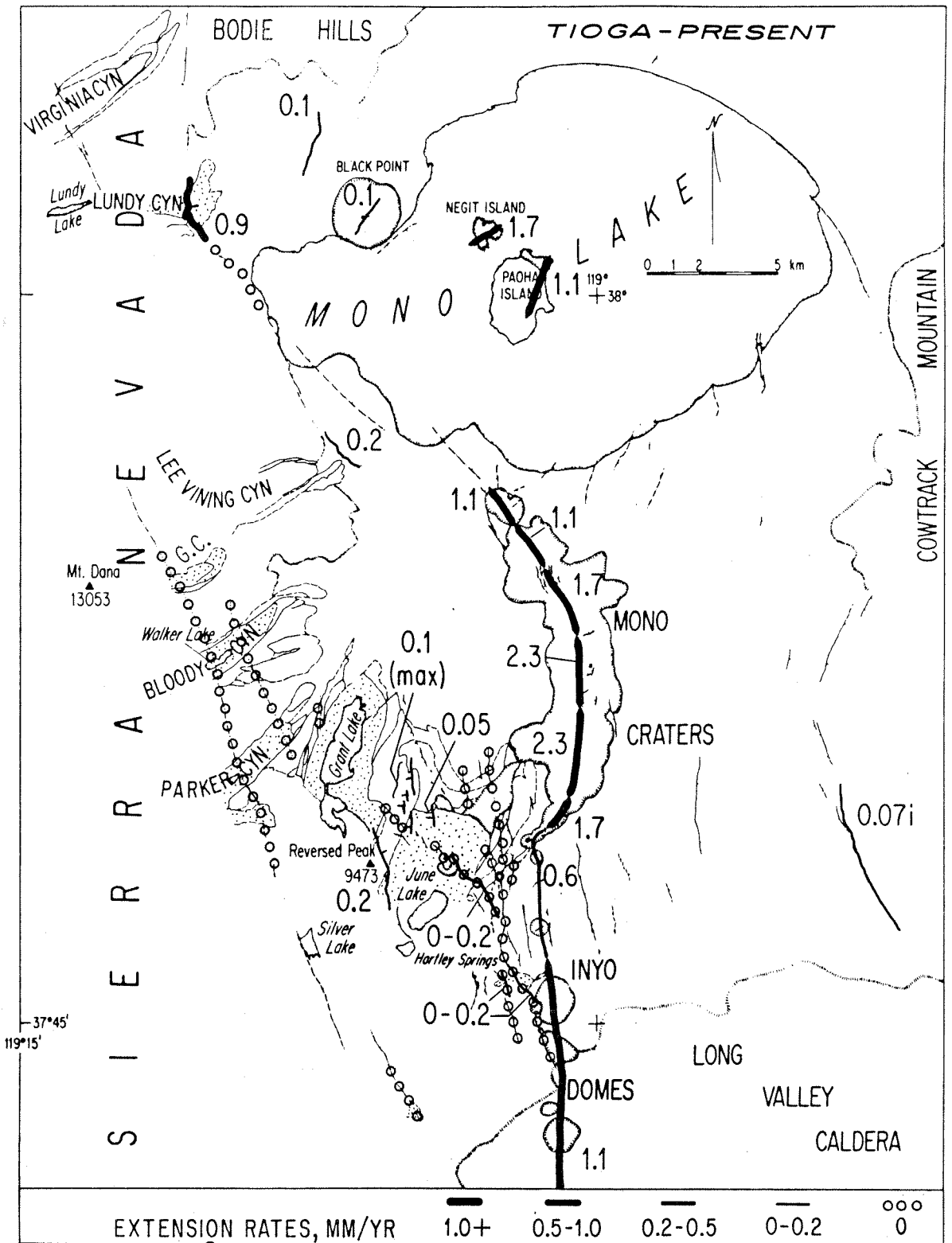
Figure 3-17

DIRECTION OF EXTENSION

In the preceding sections, I discussed extension as measured orthogonal
to average dike and fault trends, that is, without reference to the regional
strain pattern into which it fit. To completely characterize the deformation
in Mono Basin, however, the direction, as well as the amount, of extension
must be specified. Therefore, in this section I discuss the available
evidence on direction of extension in the Mono Basin region.

Previous geological studies

Wright (1976) and Slemmons *et al.* (1979) have compiled evidence that the
western Basin Ranges between Walker Lane and the Sierra Nevada is a zone of
coeval strike-slip and normal faulting. Although the sense of motion on
faults of the Sierra Nevada range front is poorly constrained by geological
data, Walker Lane is known to be a zone of right-lateral, strike-slip faulting
with perhaps 48 km of cumulative offset and a slip rate on the order of 2
mm/yr (Slemmons *et al.*, 1979). Within the western Basin Ranges, right-lateral
strike-slip faults, such as the Death Valley and Las Vegas Valley Faults,
trend northwest, subparallel to the Walker Lane and the Sierra Nevada range
front. Left-lateral faults, such as the Carson Lineament and the Olinghouse
Fault, trend northeast. Slemmons *et al.* (1979) therefore consider the western
Basin Ranges to be a broad zone of conjugate (Reidel) lateral faulting bounded
by the en echelon faults of the Sierra Nevada on the west and by Walker Lane
on the east. As Wright (1976) points out, these data are consistent with
active north-south compression causing east-west extension.

A small amount of evidence gathered near the Sierra Nevada frontal fault

zone to the south of the Mono Basin corroborates the regional patterns outlined by Slemmons *et al.* (1979) and Wright (1976). The most salient information is discussed below.

Bateman (1965) noted that numerous normal faults of the Volcanic Tableland, southeast of Long Valley Caldera, are arranged in left-stepping echelons associated with broad warps. He showed that northwest-trending, distributed right-lateral shear could account for all the structural features of the Tableland.

In July, 1986, earthquakes of the Chalfant Valley Sequence occurred underneath the Volcanic Tableland. Lienkaemper *et al.* (1987) noted right-lateral slip on faults of the White Mountains frontal fault zone, and left-stepping en echelon fractures in the Volcanic Tableland. Trilateration measurements by Gross and Savage (1987) were compatible with 1.3 m of right-lateral slip and 0.7 m of dip-slip on a fault that dips 50 to 55 degrees southwest underneath the Tableland.

South of the Tableland, the Owens Valley Fault accommodates right-lateral shear as well as extension along the Sierra Nevada range front, as shown by oblique-slip ground breakage caused by the 1872 Owens Valley Earthquake and previous earthquakes (Lubetkin and Clark, 1987).

The above works suggest that the northwest-trending normal faults of the Mono Basin may have a component of right-lateral slip.

Previous geophysical studies

The tension axes of composite focal mechanisms for earthquakes in the region around the Mono Basin vary somewhat, but are directed west-northwest on average. Composite focal mechanisms that are probably representative of the

Mono Basin are those from the Chalfant Valley Earthquake Sequence, which has a tension axis striking nearly east-west (Vetter, unpub. ms.), or, better yet, a composite focal mechanism for the eastern Mono Lake region, for which the tension axis strikes between N50W and N70W (Vetter and Ryall, 1983). However, there is an important exception to the common east-west to west-northwest trends of regional focal mechanisms. The maximum extension axis for earthquake focal mechanisms in the Mammoth region strikes about N60E (Vetter and Ryall, 1983). This trend is probably the result of stresses localized around the large magma chamber underlying Long Valley Caldera, which may not propagate as far as the Mono Basin.

Trilateration measurements support the inference that maximum extension trends west-northwest in the Mono Basin. Data from the Excelsior trilateration network, east of Mono Lake, suggest a N81 $\pm$ 7W maximum extension axis, and data from the Owens network, southeast of Mono Basin, suggest a N69 $\pm$ 11W axis (Savage, 1983).

The above mentioned focal mechanism and trilateration data suggest that the maximum extension axis within the Mono Basin strikes slightly north of west. This orientation is compatible with the geological work outlined in the preceding section.

Geological evidence from this study

Several pieces of evidence from this study give some indication of the extension direction in the Mono Basin: 1) The horizontal component of slip can be measured from two moraines offset by the range-front fault and 2) trends of some volcanic features can be used to infer extension direction.

Offset moraine crests can be used to measure horizontal as well as

vertical components of offset, if the position of the crests are adequately resolved. Because most moraine crests are tens of meters wide, lateral offsets are frequently too small to be resolved, even though vertical offsets are easily measured.

At two localities in the basin, data are sufficiently well-resolved to estimate horizontal components of slip. At Lundy Canyon, the Tioga moraine crest does not appear to be offset laterally. Since the fault trends approximately N3E, the maximum extension direction inferred at this locale is N87W. A better estimate of extension direction can be made at Reversed Peak. The N23E trending Tahoe morainal bench is offset 21 m vertically and 30 m horizontally by the Reversed Peak Fault, which trends N23W. Depending on the fault dip, then, the slip vector strikes N27W to N60W. The attitudes of these slip vectors suggest that there is a component of right-lateral slip on north-northwest-trending range-front faults of the Mono Basin, and, therefore, that structures which trend north-south to north-northeast accommodate pure extension.

One additional indicator of right-lateral slip on the range front is the fault at point D in Figure 3-1. In the aerial photograph shown in Figure 3-18, the northwest-striking fault seems to offset a Tahoe moraine as much as 50 m in a right-lateral sense. A profile of this fault made from the topographic map of the area (Figure 3-19) suggests that it has little vertical displacement. The data therefore suggest that it may have a large right-lateral, strike-slip component.

Attitudes of dikes that fed the Mono Craters is probably controlled at depth by the orientation of the cataclasized border of the Aeolian Buttes pluton (Kistler, 1966b) or by the orientation of range-front structures.

Figure 3-18. Vertical aerial stereo-photograph of the left lateral moraines of June Lake and the right lateral moraines of Grant Lake. Nadir of photo on left-hand side is marked with a cross. The crest of an offset moraine is marked with a dotted line. Morphology of the delineated fault which offsets this moraine is compatible with a large component of right-lateral, strike-slip motion. The horizontal offset of the moraine crest may be as much as 50 m.
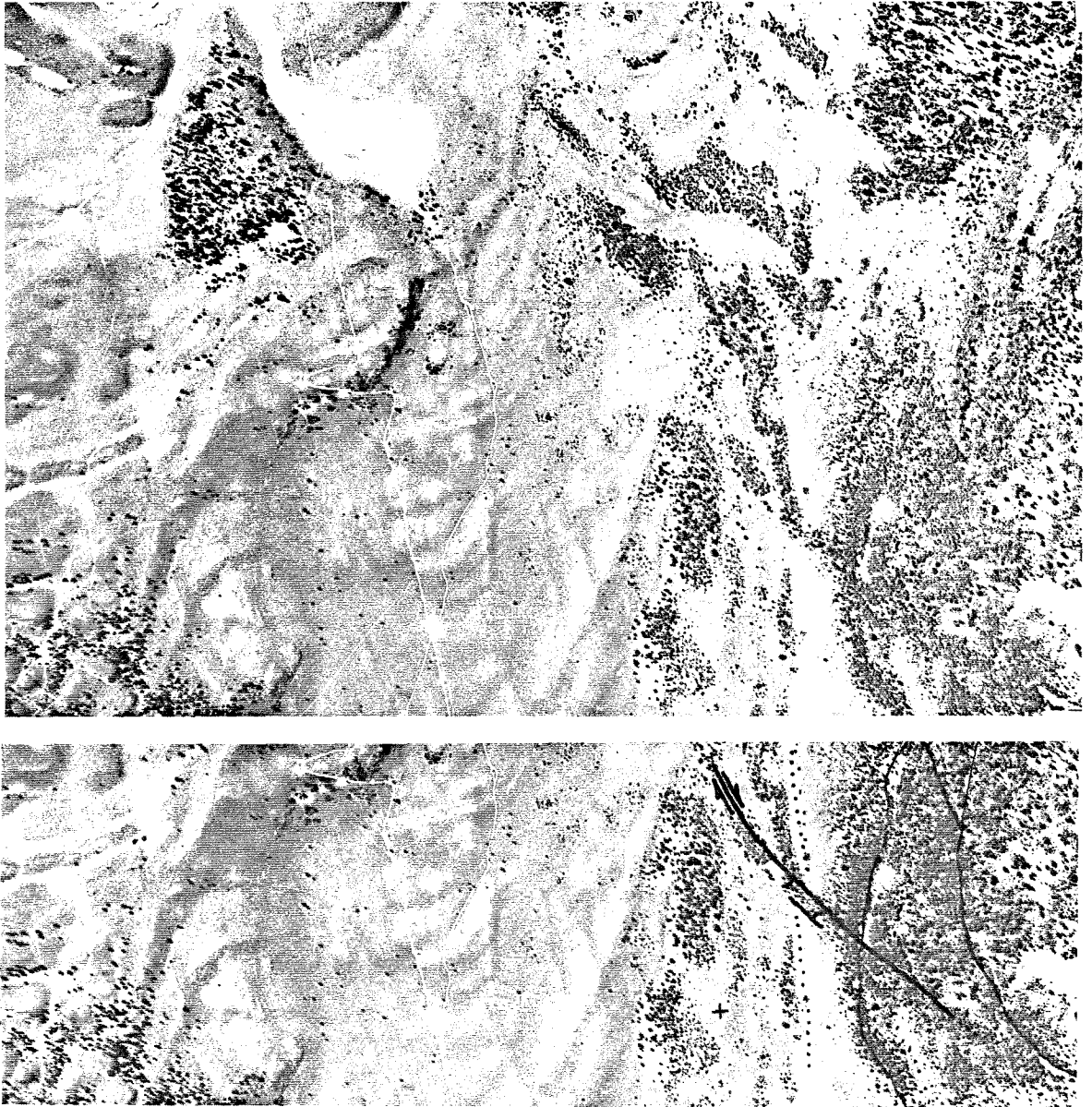
Figure 3-18
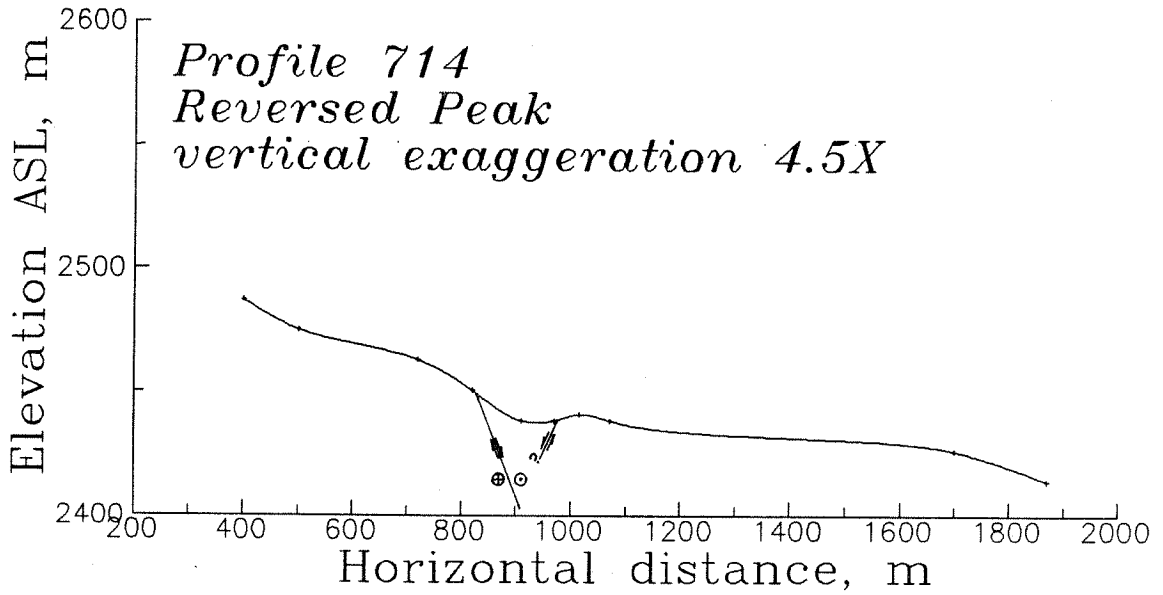
Figure 3-19. Profile 714, drawn from a 1:24,000 scale topographic map with a 40 foot contour interval. Profile is of the moraine crest, which is dotted on Figure 3-18. To the right of the graben (?), the crest of the moraine is somewhat low in elevation because of glacial phenomena, not necessarily because of faulting. Profile is compatible with no net vertical offset of the moraine crest, suggesting that fault is almost pure strike-slip.

Above bedrock, however, some dikes may have rotated and aligned themselves in response to the regional stress field. Domes 15 and 20, and Wilson's Butte (Mayo *et al.*, 1936) issued from dikes which clearly were not aligned parallel to bedrock structures (Figures 3-1, 3-20). Vent structures and flow foliations on these domes trend northeast. Therefore, the feeder dikes may have rotated in the shallow subsurface to the northeast from the trends of the range-front normal faults and the plutonic border that probably controlled their orientations at depth. This interpretation is consistent with the work of Fink (1985), who hypothesized that the dikes from which the Inyo Craters erupted rotated from north-northwest to north-northeast in the shallow subsurface in response to regional stresses.

Fissures atop Black Point volcano have been thought to be caused by sediment compaction and adjustment (Custer, 1973), but their trends are, in fact, consistent with regional tectonics, and were perhaps formed by a late-stage injection of a dike that did not erupt. The N27E-trending fracture zone opened along slip vectors that strike N24W to N35W, based on the separation of two corners in the walls of the fissures.

To summarize, then, there is evidence for a right-lateral component of offset on range-front faults that strike north-northwest to northwest, indicating that the axis of maximum extension lies in the northwest quadrant. Vent structures in the Mono Craters also show evidence for west-northwest- to northwest-directed extension. At Black Point, the direction of opening of northeast-trending fissures is also compatible with northwest-directed extension. Lastly, regional geological and geophysical studies suggest that the Mono Basin may be extending along a west-northwest- to northwest-trending axis.

Figure 3-20. Probable trends of dikes underneath Mono Craters. Data for dome north of Crater Mountain from Kelleher (1986), for North Coulee and Panum Dome from Sieh and Bursik (1986) and for South Coulee from Loney (1968). Rose diagrams show strikes of flow foliations in domes mapped for this study. Dikes are schematically depicted as tapering black lines inside the flows. Two common trends of dikes exist, a north-northwest trend roughly parallel to most range-front faults and a NE trend that may be close to the azimuth of the regional extensional strain axis.
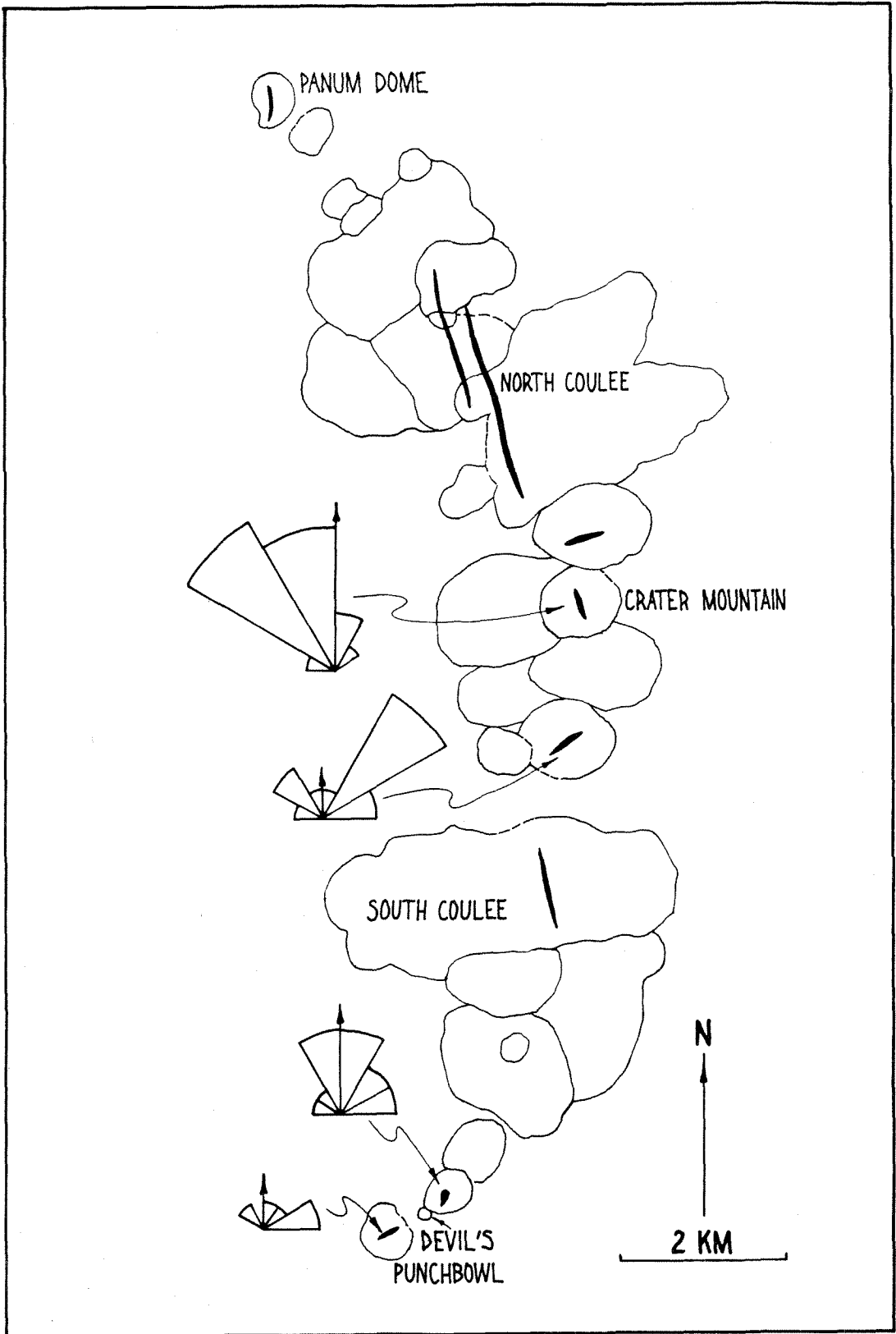
Figure 3-20

DISCUSSION

The following discussion is organized according to the reliability of the data upon which each section is based. The first section, therefore, treats extension rates in time slices and makes no reference to more speculative extension directions. The second section deals with the implications of the inferred regional extension direction when coupled with the extension rates. The final section speculates on the possible implications of this work to the formation of large calderas.

Extension rate

In this section, I discuss only the evolution of extension rate patterns, beginning with a brief résumé of the data.

Figures 3-14 to 3-17 suggest that before about 70,000 years ago, late Quaternary extension in the Mono Basin took place rather uniformly on normal faults at or very near the range front. However, since about 70,000 years ago, faulting has progressively ceased or slowed on range-front segments from Bloody Canyon to the Hartley Springs Fault. Between 70,000 and 40,000 years ago, the range front became inactive at Bloody Canyon. Between 40,000 and 14,000 years ago, the range front became inactive at Parker Canyon, and faults at June Lake were less active than during the preceding period. For the past 14,000 years, extension at June Lake and at Lee Vining Canyon has proceeded at only a fraction of typical range-front rates. Many splays of the Hartley Springs Fault have become inactive.

The first indications of volcanism at the Mono Craters occurred a few tens of thousands of years after the first signs of range-front inactivity at

Bloody Canyon. As range-front extension decreased or ceased from Bloody Canyon south, volcanic activity increased roughly proportionally.

Changes in extension rate along the range front and at the Mono Craters suggest that crustal stretching, which was once accommodated by range-front faulting, may now be accommodated by dike intrusion underneath the Mono and Inyo Craters. The result of accommodating crustal stretching with dikes rather than range-front faults is a slip gap in the range front.

On the other hand, it could be argued that dikes are intruding in response to forces other than regional crustal stretching, and that therefore, the range-front slip gap is not related to the Mono Craters. The most reasonable alternative is that dike intrusion is the relief mechanism for stretching above an inflating or overpressurized magma chamber rather than for tectonic crustal stretching. I argue against this possibility in the following paragraphs.

Two lines of reasoning suggest that dikes are forming in response to crustal stretching rather than magma chamber inflation: 1) lack of surficial doming associated with the Mono Craters, and 2) similar values for range-front and dike-extension rates.

I first discuss the lack of structural doming around the Mono Craters. If the dikes underneath the Mono Craters formed by intrusion of magma into tensile fractures above an inflating magma chamber, then the height of the structural dome needed to accommodate the dikes can be found geometrically, if it assumed that the crust above the magma chamber does not thin. For a total dike width of 64 m, as may be the case underneath the central Mono Craters, and a wedge-shaped magma chamber with a width of 4 km (Achauer *et al.*, 1986), the surface uplift should be about 350 m. Such uplift clearly has not

occurred in the region surrounding the Mono Craters. Thus, dikes do not seem to be intruding in direct response to inflation of a magma chamber.

The proposition that dikes are intruding in response to crustal stretching rather than inflation is also supported by comparable rates for extension accommodated by both faulting and dike intrusion. Reasonable values for dike widths, numbers of dikes and fault dips, only slightly different from those used to construct Figures 3-14 to 3-17 (Tables 3-2 and 3-3), can be used to make rates of extension due to dike intrusion the same as rates of extension due to faulting. This suggests that dike intrusion and range-front faulting are both accommodating the same uniform regional stretching.

The available data support the hypothesis that the Mono Craters are forming in response to regional crustal extension and are, therefore, accommodating extension which was previously taken up by range-front normal faulting.

Although the evidence does not support the proposition that dikes are intruding in response to magma chamber overpressurization and inflation, overpressurization may modify the response of the magmatic system to regional stretching. For example, the degree of overpressurization, as well as the amount of elastic strain energy stored in rock surrounding the magma chamber, may control the timing of dike-intrusion events.

If it is accepted that dikes are being intruded in response to regional crustal stretching, then the process of dike intrusion underneath the Mono Craters may be envisioned as follows. Smith and Bruhn (1984) have shown that most of the stress relief by earthquakes in the Basin Ranges province nucleates at about ten kilometers depth. Achauer et al. (1986) have suggested that the roof of the Mono Craters magma chamber is also at a depth of ten

kilometers. Moreover, their work indicates that the chamber is situated under the central segment of the Mono Craters. If the crust at a depth of ten kilometers fails, then a magma-filled fracture is likely to propagate where magma pressure is greater than the effective normal stress across the initial break, as may often be the case underneath the central Mono Craters, directly above the magma chamber. A normal fault is likely to propagate from the initial break where magma pressure is low or magma is not present, such as along the Mono Lake or the Hartley Springs Fault. As a consequence of the preferential propagation of dikes over normal faults in response to regional stretching near the magma chamber, offset events (earthquakes) along the frontal fault are forestalled, and after many dikes have been intruded, a measurable slip gap develops in the range-front fault system. Conversely, segments of the volcanic edifice are built up by extrusions in proportion to the number of dikes intruded and, therefore, in proportion to the magnitude of the slip gap in the range front. Along segments of the range front progressively more remote from the magma chamber, dikes propagate progressively less frequently than normal faults, until the situation is reached where all extension is accommodated by faulting and no volcanic activity occurs.

Relationship of Mono Basin to regional tectonic patterns

In this section I discuss how volcanism at the Mono Craters may be related to what is known of extension direction as well as extension rate.

The available geological and geophysical evidence indicates that the maximum extension axis trends about west-northwest and, therefore, that the north-northwest-striking faults of the Sierra Nevada range front in the Mono

Basin are oblique-slip faults with a right-lateral component. The only segments of the range front that may trend orthogonally to the maximum extension direction are those north of and including Bloody Canyon, and north of and including Lundy Canyon. The south-central Mono Craters may also trend perpendicular to the maximum extension axis.

The hypothetical sense of motion on faults is illustrated in Figure 3-21. In this figure, the northwest-trending segment of the Mono Lake Fault, the fault of Pakiser (1976) near the northern Mono Craters, the Hartley Springs Fault, the Reversed Peak Fault and the range-front fault between Parker and Bloody Canyons are shown as right-lateral, oblique-slip structures. Among these faults, the Hartley Springs Fault, Reversed Peak Fault and the range-front fault between Parker and Bloody Canyons comprise one group of left-stepping echelons. The Mono Lake Fault and the fault near the northern Mono Craters comprise another left-stepping echelon. The range-front fault at and to the north of Bloody Canyon, and the south and central Mono Craters are features that accommodate extension alone. They transfer motion between faults from the two left-stepping groups. The range front near Bloody Canyon and the south and central Mono Craters are therefore opposite limbs of a structure similar to a pull-apart basin. Activity seems to have "traded off" between these limbs of the pull-apart zone about 40,000 to 60,000 years ago -- when the Mono Craters became active and the range front near Bloody Canyon became inactive. It was this shift in extensional activity that resulted in the slip gap discussed in the preceding section.

I suggest that the southern Mono Basin is similar to a pull-apart basin (Burchfiel and Stewart, 1966), which is a down-dropped extensional structure that links echelons in a strike-slip fault zone. The Mono Craters area

228

Figure 3-21. Schematic diagram of hypothetical sense of motion on groups of faults and fractures in the Mono Basin during the lifetime of the Mono Craters. Data are compatible with extensional motion on north-south- to north-northeast-trending structures and right-lateral oblique-slip motion on northwest- to north-northwest-trending structures.
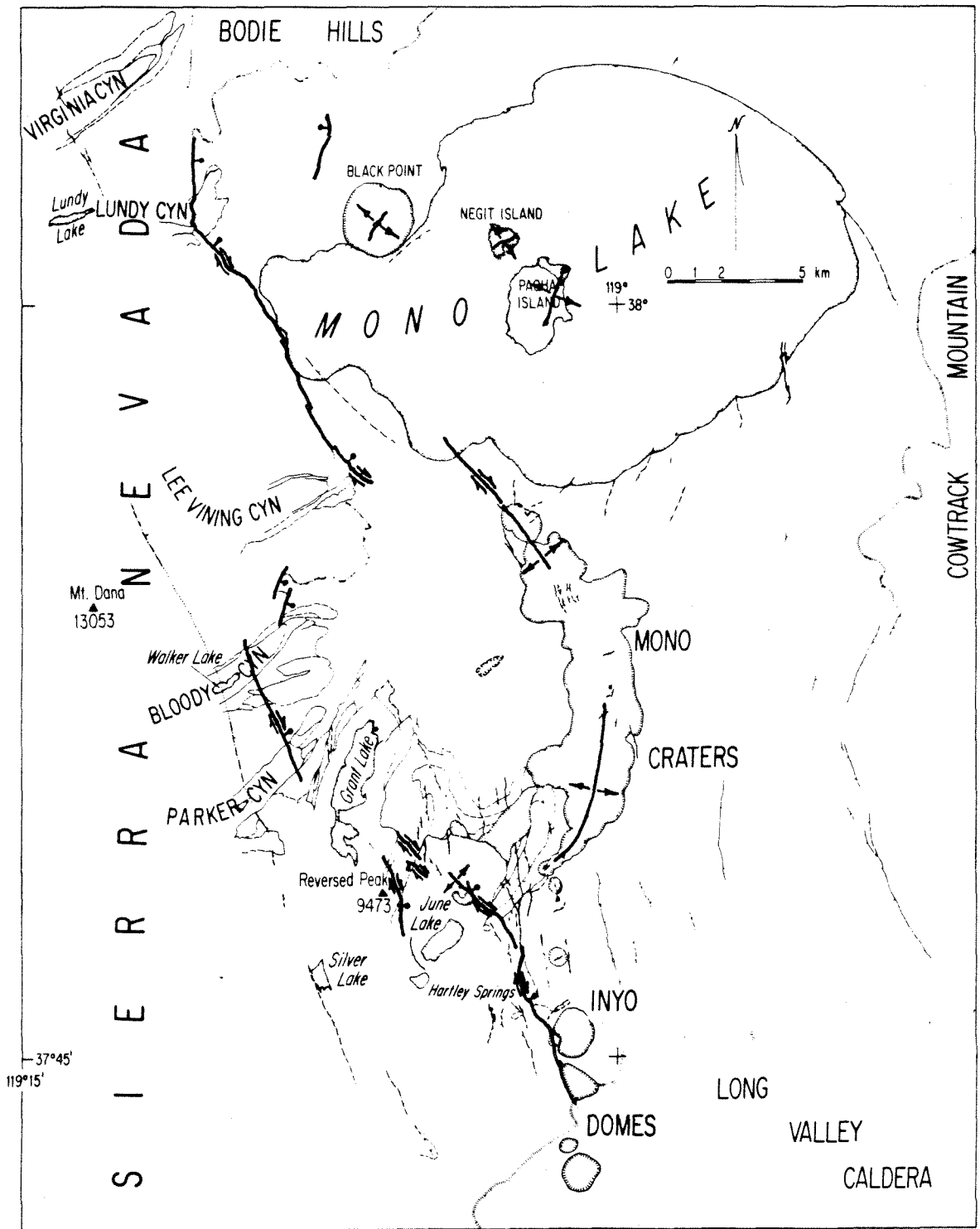
Figure 3-21

differs from a pull-apart basin as described by Burchfiel and Stewart (1966)
in three significant ways: 1) It occurs between en echelon oblique-slip rather
than strike-slip faults; 2) it is asymmetric, since it has been down-dropped
on only one edge, and 3) the extensional limbs, near Bloody Canyon and at the
Mono Craters, have not been active simultaneously.

The volcanic islands of Mono Lake and Black Point are outside the
hypothesized pull-apart zone. Gilbert *et al.* (1968) have explained the
locations of volcanoes and structures in this region in a manner that is
compatible with the inferred direction of regional extension. Gilbert *et al.*
(1968) suggested that the volcanoes of Mono Lake are related to the
"structural knee" of the western Basin Ranges. The "knee" is a region in
which bedrock structures rotate progressively from north-northwest trends to
northeast trends as they are followed from south to north. The Cowtrack
Mountain range front is an example (Figure 3-1). The north-northwest-trending
faults seem to have accommodated right-lateral strain and the northeast-
trending faults seem to have accommodated left-lateral strain. The trends of
lineaments related to active volcanism and faulting in Mono Lake are parallel
to bedrock faults in the "structural knee" of the eastern Mono Basin.
Gilbert *et al.* (1968) concluded that Black Point and the volcanoes of Mono
Lake are localized at the apex of the "knee," where there should be almost
pure extension (Figure 3-21), as exhibited by the Black Point fissures. The
north-trending section of the Mono Lake Fault is probably also located near
the apex of the knee, since it too accommodates almost pure extension.

Based on the above evidence, I suggest a simple model for the
relationship between volcanic activity in the Mono Basin and regional
tectonics. The model is illustrated in Figure 3-22. The Sierra Nevada range
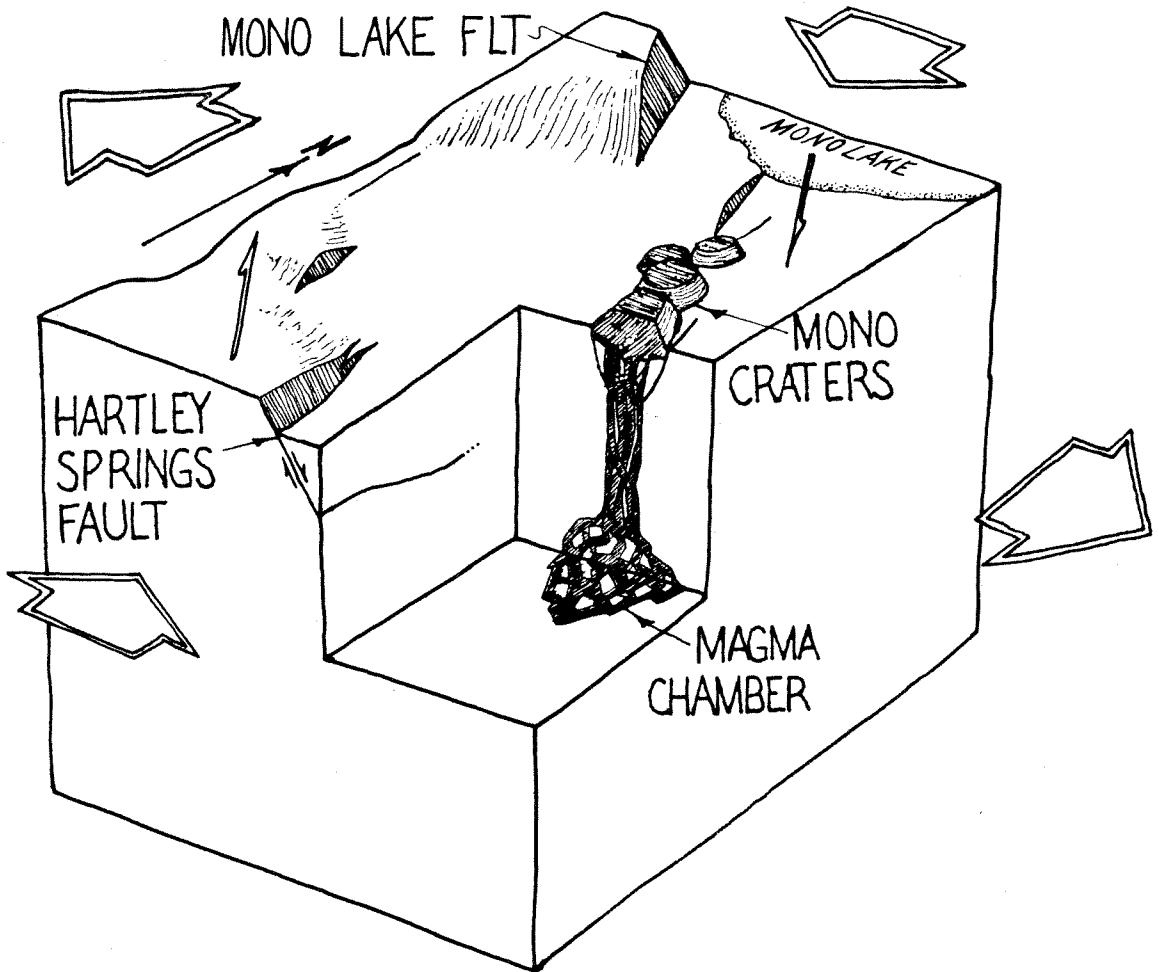
Figure 3-22. Block diagram illustrating current tectonic relationships in the Mono Basin. Dikes intruding underneath the craters have caused a slip gap in the range front of the Sierra Nevada, because the dikes now accommodate extension that was once accommodated by range-front normal faults. North-northeast-directed compression results in oblique-slip on north-northwest-trending range-front faults, and in almost pure extension underneath the south and central Mono Craters. The region may be similar to a pull-apart basin, if the Hartley Springs Fault and the Mono Lake Fault are right-stepping, right-lateral, oblique-slip echelons.

front is actively shortening in the north-northeast direction. The principle manifestation of this strain field is the system of range-front normal faults arranged in left-stepping echelons which accommodate right-lateral shear. Right-steps occur in this system between the range-front fault at Bloody Canyon and the Mono Lake Fault, and between the Hartley Springs Fault and structures underlying the northern Mono Craters. The Mono Craters and the magma chamber which underlies them are therefore localized by a concentration of extension between echelons, along the border of a structure similar to a pull-apart basin.

Implications for caldera formation

Bailey (1982) noted that the Mono Craters are structurally and petrologically analogous to Glass Mountain on the northeast rim of Long Valley Caldera. This led him to hypothesize that the craters represent an early phase of caldera formation, since the construction of Glass Mountain directly preceded the formation of Long Valley Caldera. If this is so, then the current tectonic state of Mono Basin is a "snap-shot" of one phase in the early evolution of a Long Valley-type caldera. This "snap-shot" suggests that some calderas may form in en echelon portions of wide shear zones. Early products from the magma chamber are erupted along one limb of a pull-apart basin between two en echelon fault segments. Caldera collapse structures may later follow the trends of the boundary faults of the pull-apart basin.

CONCLUSIONS

The lack of late Quaternary faulting along the Sierra Nevada range front in the Mono Basin may result from stress relief by dikes feeding the Mono and Inyo Craters. Dike intrusion may therefore play some role in the "earthquake" cycle in volcanic regions. Overpressurization of the source magma chamber may modify the response of the dike intrusion system so that dikes are injected aperiodically, in contrast to more periodic release of strain by tectonic earthquakes.

Late Quaternary faults define two oblique-slip fault zones along the eastern Sierra Nevada range front in the Mono Basin. The area within the overlap of the two oblique-slip zones is a pull-apart basin. The Mono Craters have erupted along one extensional bounding structure of the pull-apart basin.

If the Mono Craters represent an early phase of caldera formation (Bailey, 1982), then some large ash-flow tuff calderas may have been preferentially localized at pull-apart basins in broad shear zones, in analogy with the setting of the Mono Craters.

REFERENCES

Achauer, U., Greene, L., Evans, J.R. and Iyer, H.M. (1986) Nature of the magma chamber underlying the Mono Craters area, eastern California, as determined from teleseismic travel time residuals, *Jour. Geophys. Res.*, 91, 13873.

Ahnert, F. (1976) Brief description of a comprehensive three-dimensional process-response model of landform development, *Zeits. Geomorph.*, Sup. 25, 29.

Andrews, D.J. and Hanks, T.J. (1985) Scarp degraded by linear diffusion: Inverse solution for age, *Jour. Geophys. Res.*, 90, 10208.

Anderson, E.M. (1951) *The Dynamics of Faulting and Dyke Formation*, Oliver and Boyd, London, 206pp.

Bacon, C.R. (1982) Time-predictable bimodal volcanism in the Coso Range, California, *Geology*, 10, 65.

Bacon, C.R., Duffield, W.A., Nakamura, K. (1980) Distribution of Quaternary rhyolite domes of the Coso Range, California: Implications for extent of the geothermal anomaly, *Jour. Geophys. Res.*, 85, 2425.

Bailey, R.A. (1982) Volcanic evolution and potential hazards in the Long Valley-Mono, Coso, and Clear Lake, volcanic areas, California, *Calif. Div. Mines Geol. Spec. Pub. 63*, 17.

Bailey, R.A., Dalrymple, G.B. and Lanphere, M.A. (1976) Volcanism, structure, and geochronology of Long Valley Caldera, Mono County, California, *Jour. Geophys. Res.*, 81, 725.

Bailey, R.A. and Koeppen, R.P. (1977) Preliminary geologic map of Long Valley Caldera, Mono County, California, *U.S. Geol. Surv. Open-file Rpt. 77-468*, 20pp. and map.

Batchelder, G.L. (1970) Postglacial ecology at Black Lake, Mono County,

California, *Ph.D. Thesis*, Arizona St. Univ., Tempe, 180pp.

Bateman, P.C. (1965) Geology and Tungsten Mineralization of the Bishop District, California, *U.S. Geol. Surv. Prof. Paper 470*, 208pp.

Berkey, C.P. (1935) Revised geologic section of Mono Basin based on later exploration, *Memorandum no. XII*, L. A. Dept. Water and Power, 31pp.

Beyer, W.H. (1980) *CRC Standard Mathematical Tables*, CRC Press, Boca Raton, Florida, 613pp.

Birkeland, P.W. (1964) Pleistocene glaciation of the northern Sierra Nevada, north of Lake Tahoe, California, *Jour. Geol.*, 72, 810.

Birkeland, P.W., Burke, R.M., Walker, A.L. (1980) Soils and subsurface rock-weathering features of Sherwin and pre-Sherwin glacial deposits, eastern Sierra Nevada, California, *Geol. Soc. Amer. Bull.*, 91, 238.

Birman, J.H. (1964) Glacial geology across the crest of the Sierra Nevada, California, *Geol. Soc. Amer. Spec. Paper 75*, 80pp.

Blackwelder, E. (1931) Pleistocene glaciation in the Sierra Nevada and Basin Ranges, *Geol. Soc. Amer. Bull.*, 42, 865.

Bradley, J.V. (1968) *Distribution-Free Statistical Tests*, Prentice-Hall, Inc., Englewood Cliffs, NJ, 388pp.

Bucknam, R.C. and Anderson, R.E. (1979) Estimation of fault-scarp ages from a scarp-height-slope-angle relationship, *Geology*, 7, 11.

Burchfiel, B.C. and Stewart, J.H. (1966) "Pull-apart" origin of the central segment of Death Valley, California, *Geol. Soc. Amer. Bull.*, 77, 439.

Burke, R.M. and Birkeland, P.W. (1979) Reevaluation of multiparameter relative dating techniques and their application to the glacial sequence along the

eastern escarpment of the Sierra Nevada, California, *Quat. Res.*, 11, 21.

Chesterman, C.W. (1975) Geology of the Matterhorn Peak Quadrangle, Mono, and Tuolomne Counties, California, *Calif. Div. Mines Geol. Map Sheet 22.*

Chesterman, C.W. and Gray, C.H. Jr. (1975) Geology of the Bodie Quadrangle, Mono County, California, *Calif. Div. Mines Geol. Map Sheet 21.*

Clark, M.M. (1967) Pleistocene glaciation of the drainage of the West Walker River, Sierra Nevada, California, *Ph.D. Thesis*, Stanford Univ., 130pp.

Clark, M.M. (1979) Range-front faulting: Cause of the difference in height between Mono Basin and Tahoe moraines at Walker Creek, in Field Guide to Relative Dating Methods Applied to Glacial Deposits in the Third and Fourth Recesses and along the Eastern Sierra Nevada, California, with Supplementary Notes on Other Sierra Nevada Localities (Burke, R.M. and Birkeland, P.W., eds.), *Field Trip Guidebook for Friends of the Pleistocene Pacific Cell*, p.54.

Clark, M.M. and Gillespie, A.R. (1981) Record of Late Quaternary faulting along the Hilton Creek Fault in the Sierra Nevada, California, *Earthquake Notes* (abstr.), 52, 46.

Clark, M.M., Harms, K.K., Lienkaemper, J.J., Harwood, D.S., Lajoie, K.R., Matti, J.C., Perkins, J.A., Rymer, M.J., Sarna-Wojcicki, A.M., Sharp, R.V., Sims, J.D., Tinsley, J.C., Ziony, J.I. (1984) Preliminary slip-rate table for late Quaternary faults of California, *U.S. Geol. Survey, Open-file Rpt. 84-106*, 12pp. and maps.

Conca, J.L. and Rossman, G.R. (1985) Core softening in cavernously weathered tonalite, *Jour. Geol.*, 93, 59.

Crook, R. (1986) Relative dating of Quaternary deposits based on p-wave velocities in weathered granitic clasts, *Quat. Res.*, 25, 281.

Crook, R. and Gillespie, A.R. (1986) Weathering rates in granitic boulders measured by p-wave speeds, in *Rates of Chemical Weathering of Rocks and*

Minerals (Colman, S.M. and Dethier, D.P., eds.), Academic Press, Orlando, p.395.

Curry, R.R. (1971) *Glacial and Pleistocene History of the Mammoth Lakes Area, California -- A Geologic Guidebook*, Geol. Ser. Publ., no. 11, Dept. of Geol., Univ. Montana, Missoula, 53pp.

Custer, S.G. (1973) Stratigraphy and sedimentation of Black Point Volcano, Mono Basin, California, *M.S. Thesis*, Univ. Calif., Berkeley, 114pp.

Delaney, P. and Pollard, D. (1979) Deformation of host rocks and flow of magma during growth of minette dikes and breccia-bearing intrusions near Ship Rock, New Mexico, *U.S. Geol. Survey Prof. Paper 1202*, 61pp.

Denham, C.R. and Cox, A. (1971) Evidence that the Laschamp polarity event did not occur 13,300-30,400 years ago, *Earth Planet. Sci. Let.*, 13, 181.

Dixon, W.J. and Massey, F.J. Jr. (1957) *Introduction to Statistical Analysis*, McGraw-Hill, New York, 488pp.

Dorn, R.I., Turrin, B.D., Jull, A.J.T., Linick, T.W., Donahue, D.J. (1987) Radiocarbon and cation-ratio ages for rock varnish on Tioga and Tahoe morainal boulders of Pine Creek, eastern Sierra Nevada, Calif., and their paleoclimatic implications, *Quat. Res.*, 28, 38.

Edwards, R.L., Chen, J.H., Ku, T.-L. and Wasserburg, G.J. (1987) Precise timing of the last interglacial period from mass spectrometric determination of Thorium-230 in corals, *Science*, 236, 1547.

Fink, J.H. (1985) Geometry of silicic dikes beneath the Inyo Domes, California, *Jour. Geophys. Res.*, 90, 11127.

Fink, J.H. and Pollard, D.D. (1983) Structural evidence for dikes beneath silicic domes, Medicine Lake Highland Volcano, California, *Geology*, 11, 458.

Fullerton, D.S. (1986) Chronology and correlation of glacial deposits in the Sierra Nevada, California, in *Quaternary Glaciations in the Northern Hemisphere* (Sibrava, V., Bowen, D.Q. and Richmond, G.M., eds.), Quat. Sci. Revs., 5, 161.

Gilbert, C.M., Christensen, M.N., Al-Rawi, Y., and Lajoie, K.R. (1968) Structural and volcanic history of Mono Basin, California-Nevada, *Geol. Soc. Amer. Memoir 116*, p.275.

Gillespie, A.R. (1982) Quaternary glaciation and tectonism in the southeastern Sierra Nevada, Inyo County, California, *Ph.D. Thesis*, Calif. Inst. Technology, 689pp.

Gillespie, A.R. (1984) Evidence for both Wisconsin and Illinoian ages for the Tahoe glaciation, Sierra Nevada, California, *Geol. Soc. Amer. Abstr. Programs*, p.519.

Gross, W.K. and Savage, J.C. (1987) Deformation associated with the 1986 Chalfant Valley Earthquake, eastern California, *Bull. Seismo. Soc. Amer.*, 77, 306.

Hanks, T.C., Bucknam, R.C., Lajoie, K.R. and Wallace, R.E. (1984) Modification of wave-cut and faulting-controlled landforms, *Jour. Geophys. Res.*, 89, 5771.

Heiken, G., Wohletz, K. and Eichelberger, J. (1988) Fracture fillings and intrusive pyroclasts, Inyo Domes, California, *Jour. Geophys. Res.*, 93, 4335.

Hill, D.P., Kissling, E., Luetgert, J.H. and Kradolfer, U. (1985) Constraints on the upper crustal structure of the Long Valley -- Mono Craters volcanic complex, eastern California, from seismic refraction measurements, *Jour. Geophys. Res.*, 90, 11135.

Huber, N.K. (1981) Amount and timing of late Cenozoic uplift and tilt of the central Sierra Nevada, California -- Evidence from the upper San Joaquin River Basin, *U.S. Geol. Survey, Prof. Paper 1197*, 28pp.

Huber, N.K. and Rinehart, C.D. (1965) Geologic Map of the Devils Postpile Quadrangle, Sierra Nevada, California, *U.S. Geol. Surv. Quad. Map GQ-437.*

Jennings, C.W. (1975) Fault map of California, *Calif. Div. Mines and Geol. Geol. Data Map no. 1.*

Jones, J.G. (1970) Intraglacial volcanoes of the Laugarvatn region, southwest Iceland, II, *Jour. Geol.,* 78, 127.

Kelleher, P. (1986) The geology, petrology, and geochemistry of the Mono Craters -- Mono Lake Islands volcanic complex, eastern California, *M.S. Thesis,* Univ. of Calif., Santa Cruz, 111pp.

Kistler, R.W. (1966a) Geologic Map of the Mono Craters Quadrangle, Mono and Tuolomne Counties, California, *U.S. Geol. Surv. Quad. Map GQ-462.*

Kistler, R.W. (1966b) Structure and metamorphism in the Mono Craters quadrangle, Sierra Nevada, California, *U.S. Geol. Surv. Bull. 1221-E,* 53pp.

Kistler, R.W. and Swanson, S.E. (1981) Petrology and geochronology of metamorphosed volcanic rocks and a middle Cretaceous volcanic neck in the east-central Sierra Nevada, California, *Jour. Geophys. Res.,* 86, 10489.

Lachenbruch, A.H. and Sass, J.H. (1978) Models of an extending lithosphere and heat flow in the Basin and Range province, in *Cenozoic Tectonics and Regional Geophysics of the Western Cordillera* (Smith, R.B. and Eaton, G.P., eds.), Geol. Soc. Amer., Memoir 152, p.209.

Lachmar, T.E. (1977) Glacial geology of Lundy, Virginia, and Green Canyons, Mono County, California, *M.S. Thesis,* Purdue Univ., 88pp.

Lajoie, K.R, (1968) Late Quaternary stratigraphy and geologic history of Mono Basin, eastern California, *Ph.D. Thesis,* Univ. Calif., Berkeley, 271pp.

Lajoie, K.R. and Robinson, S.W. (1982) Late Quaternary glacio-lacustrine

chronology, Mono Basin, California, *Geol. Soc. Amer. Abstr. Programs*, 14, 179.

Lienkaemper, J.J., Pezzopane, S.K., Clark, M.M. and Rymer, M.J. (1987) Fault fractures formed in association with the 1986 Chalfant Valley, California, Earthquake Sequence: preliminary report, *Bull. Seismo. Soc. Amer.*, 77, 297.

Loney, R.A. (1968) Flow structure and composition of the Southern Coulee, Mono Craters, California -- a pumiceous rhyolitic flow, in *Studies in Volcanology* (Coates, R.R., Hay, R.L. and Anderson, C.A., eds.), Geol. Soc. Amer. Memoir 116, p.415.

Lubetkin, L.K.C. (1980) Late Quaternary activity along the Lone Pine Fault, Owens Valley Fault Zone, California, *M.S. Thesis*, Stanford Univ., 85pp.

Lubetkin, L.K.C. and Clark, M.M. (1987) Late Quaternary fault scarp at Lone Pine, California; location of oblique slip during the great 1872 earthquake and earlier earthquakes, *Geol. Soc. Amer. Cent. Field Guide -- Cordilleran Section*, p. 151.

Marchand, D.E. and Allwardt, A. (1981) Late Cenozoic stratigraphic units, northeastern San Joaquin Valley, California, *U.S. Geol. Surv., Bull. 1470*, 70pp.

Martel, S.J., Harrison, T.M. and Gillespie, A.R. (1987) Late Quaternary vertical displacement rate across the Fish Springs Fault, Owens Valley Fault Zone, California, *Quat. Res.*, 27, 113.

Mathews, W.H. (1947) "Tuyas," flat-topped volcanoes in northern British Columbia, *Am. Jour. Sci.*, 245, 560.

Mathieson, S.A. (1984) Comparison of glacial sequences between the Yuba-Feather Divide, northern Sierra Nevada and Mono Basin, central Sierra Nevada, California: Evidence for and Illinoian Tahoe glaciation, *Geol. Soc. Amer. Abstr. Programs*, 320.

Mayo, E.B., Conant, L.C. and Chelikowsky, J.R. (1936) Southern extension of the Mono Craters, California, *Am. Jour. Sci.*, 32, 81.

McKenzie, D.P. (1969) The relation between fault plane solutions for earthquakes and the directions of the principal stresses, *Bull. Seismo. Soc. Amer.*, 59, 591.

Mezger, E.B. (1986) Pleistocene glaciation of Cottonwood Basin, southeastern Sierra Nevada, California, *M.S. Thesis*, Univ. S. Calif., 149pp.

Miller, C.D. (1985) Holocene eruptions at the Inyo volcanic chain, California: implications for possible eruptions in Long Valley Caldera, *Geology*, 13, 14.

Mono Basin Ecosystem Study Committee (1987) *The Mono Basin Ecosystem: Effects of Changing Lake Level*, National Academy Press, Washington, D.C., 272pp.

Muller, O.H. and Pollard, D.D. (1977) The stress state near Spanish Peaks, Colorado determined from dike pattern, *Pageoph.*, 115, 69.

Myers, W.B. and Hamilton, W. (1964) Deformation accompanying the Hebgen Lake Earthquake of August 17, 1959, in The Hebgen Lake, Montana, Earthquake of August 17, 1959, *U.S. Geol. Surv. Prof. Paper 435*, 55.

Nakamura, K. (1977) Volcanoes as possible indicators of tectonic stress orientation -- principle and proposal, *Jour. Volc. Geot. Res.*, 2, 1.

Nash, D.B. (1980) Morphologic dating of degraded normal fault scarps, *Jour. Geol.*, 88, 353.

Nash, D.B. (1984) Morphologic dating of fluvial terraces scarps and fault scarps near West Yellowstone, Montana, *Geol. Soc. Amer. Bull.*, 95, 1413.

Ode, H. (1957) Mechanical analysis of the dike pattern of the Spanish Peaks area, Colorado, *Geol. Soc. Amer. Bull.*, 68, 567.

Page, B.M. (1934) Basin-Range faulting of 1915 in Pleasant Valley, Nevada, *Jour. Geol.*, 43, 690.

Pakiser, L.C. (1976) Seismic exploration of Mono Basin, California, *Jour. Geophys. Res.*, 81, 3607.

Pakiser, L.C., Press, F. and Kane, M.F. (1960) Geophysical investigation of Mono Basin, California, *Geol. Soc. Amer. Bull*, 71, 415.

Pelagos Corp. (1987) *A Bathymetric Map and Geologic Survey of Mono Lake*, California, 38pp., with appendices and maps.

Pierce, K.N. and Colman, S.M. (1986) Effect of height and orientation (microclimate) on geomorphic degradation rates and processes, late-glacial terrace scarps in central Idaho, *Geol. Soc. Amer. Bull.*, 97, 869.

Press, F. (1966) Seismic velocities, in *Handbook of Physical Constants* (Clark, S.P. Jr., ed.), Geol. Soc. Amer. Memoir 97, p.195.

Press, W.H., Flannery, B.P., Teukolsky, S.A. and Vetterling, W.T. (1986) *Numerical Recipes: the Art of Scientific Computing*, Cambridge Univ. Press, Cambridge, 818pp.

Putnam, W.C. (1949) Quaternary geology of the June Lake district, California, *Geol. Soc. Amer. Bull.*, 60, 1281.

Putnam, W.C. (1950) Moraine and shoreline relationships at Mono Lake, California, *Geol. Soc. Amer. Bull.*, 61, 115.

Rabassa, J., Rubulis, S. and Suarez, J. (1979) Rate of formation and sedimentology of (1976-1978) push-moraines, Frias Glacier, Mount Tronador (41°10'S; 71°53'W), Argentina, in *Moraines and Varves: Origin/ Genesis/ Classification* (Schluchter, Ch., ed.) A.A. Balkema, Rotterdam, p.65.

Richmond, G.M. and Fullerton, D.S. (1986) Summation of Quaternary glaciations

in the United States of America, in *Quaternary Glaciations in the Northern Hemisphere* (Sibrava, V., Bowen, D.Q. and Richmond, G.M., eds.), Quat. Sci. Revs., 5, 183.

Roberts, J.L. (1971) The intrusion of magma into brittle rocks, in Mechanism of Igneous Intrusion (Newhall, G. and Rast, N., eds.) *Geol. Jour. Spec. Issue 2*, p.287.

Roquemore, G. (1980) Structure, tectonics, and stress field of the Coso Range, Inyo County, California, *Jour. Geophys. Res.*, 85, 2434.

Russell, I.C. (1889) Quaternary history of the Mono Valley, California, *U.S. Geol. Surv. Eighth Ann. Rpt.*, p.267 (reprinted by Artemisia Press, Lee Vining, California, 1984).

Sampson, D.E. (1987) Textural heterogeneities and vent are structures in the 600 year old lavas of the Inyo volcanic chain, eastern California, *Geol. Soc. Amer. Spec. Paper 212*, 89.

Sanders, C.O. (1984) Location and configuration of magma bodies beneath Long Valley, California, determined from anomalous earthquake signals, *Jour. Geophys. Res.*, 89, 8287.

Savage, J.C. (1983) Strain accumulation in the western United States, *An. Rev. Earth. Plan. Sci.*, 11, 11.

Sharp, R.P. (1968) Sherwin till -- Bishop Tuff relationship, Sierra Nevada, California, *Geol. Soc. Amer. Bull.*, 74, 1079.

Sharp, R.P. (1969) Semiquantitative differentiation of glacial moraines near Convict Lake, Sierra Nevada, California, *Jour. Geol.*, 77, 68.

Sharp, R.P. (1972) Pleistocene glaciation, Bridgeport Basin, California, *Geol. Soc. Amer. Bull.*, 83, 2233.

Sharp, R.P. and Birman, J.H. (1963) Additions to the classical sequence of Pleistocene glaciations, Sierra Nevada, California, *Geol. Soc. Amer. Bull.*, 74, 1079.

Sieh, K.E. and Bursik, M.I. (1986) Most recent eruption of the Mono Craters, eastern central California, *Jour. Geophys. Res.*, 91, 12539.

Slemmons, D.B. (1957) Geological effects of the Dixie Valley-Fairview Peak, Nevada, Earthquake of December 16, 1954, *Bull. Seismo. Soc. Amer.*, 49, 251.

Slemmons, D.B., Van Wormer, D., Bell, E.J., and Silberman, M.L. (1979) Recent crustal movements in the Sierra Nevada -- Walker Lane region of California -- Nevada: part I, rate and style of deformation, *Tectonophysics*, 52, 561.

Small, R.J. (1983) Lateral moraines of Glacier de Tsidjiore Nouve: form, development, and implications, *Jour. Glaciol.*, 29, 250.

Smith, R.B. and Bruhn, R.L. (1984) Intraplate extensional tectonics of the eastern Basin-Range: Inferences on structural style from seismic reflection data, regional tectonics and thermal-mechanical models of brittle/ductile deformation, *Jour. Geophys. Res.*, 89, 5733.

Smith, G.I. (1979) Subsurface stratigraphy and geochemistry of late Quaternary evaporites, Searles Lake, California, *U.S. Geol. Surv. Prof. Pap. 1043*, 130pp.

Sparks, R.S.J., Pinkerton, H. and Hulme, G. (1976) Classification and formation of lava levees on Mount Etna, *Geology*, 4, 269.

Stine, S. (1984) Late Holocene lake level fluctuations and island volcanism at Mono Lake, California, in *Geologic Guide to Aspen Valley, Mono Lake, Mono Craters, and Inyo Craters*, Genny Smith Books, Palo Alto, Calif., p.21.

Swan, F.H. III, Schwartz, D.P. and Cluff, L.S. (1980) Recurrence of moderate to large magnitude earthquakes produced by surface faulting on the Wasatch Fault Zone, Utah, *Bull. Seismo. Soc. Amer.*, 70, 1431.

Taylor, G.C. and Bryant, W.A. (1980) Surface rupture associated with the Mammoth Lakes earthquakes of 25 and 27 May, 1980, *in* Mammoth Lakes, California earthquakes of May 1980, *Calif. Div. Mines. Geol. Spec. Rpt. 150*, p.49.

Vetter, U.R., Characterization of regional stress patterns in the western Great Basin using grouped earthquake focal mechanisms, ms. submitted to *Tectonophysics*.

Vetter, U.R. and Ryall, A.S. (1983) Systematic change of focal mechanism with depth in the western Great Basin, *Jour. Geophys. Res.*, 88, 8237.

Walker, G.P.L. (1986) Koolau dike complex, Oahu: intensity and origin of a sheeted dike complex high in a Hawaiian volcanic edifice, *Geology*, 14, 310.

Wallace, R.E. (1977) Profiles and ages of young fault scarps, north-central Nevada, *Geol. Soc. Amer. Bull.*, 88, 1267.

Williams, H., and McBirney, A.R. (1979) *Volcanology*, Freeman, Cooper, San Francisco, 397pp.

Witkind, I.J. (1964) Reactivated faults north of Hebgen Lake, in The Hebgen Lake, Montana, Earthquake of August 17, 1959, *U.S. Geol. Surv., Prof. Pap. 435*, 37.

Wood, S.H. (1977) *Chronology of late Pleistocene and Holocene volcanics, Long Valley and Mono Basin geothermal areas, eastern California*, Final Tech. Rpt., U.S. Geol. Surv. Geot. Res., Extramural Prog., 78pp. (reprinted as U. S. Geol. Surv., Open File Rpt. 83-747, 76pp., 1983).

Wood, S.H. (1984) Obsidian hydration-rind dating of the Mono Craters, in *Geologic Guide to Aspen Valley, Mono Lake, Mono Craters, and Inyo Craters*, Genny Smith Books, Palo Alto, Calif., p.82.

Wright, L. (1976) Late Cenozoic fault patterns and stress fields in the Great Basin and westward displacement of the Sierra Nevada block, *Geology*, 4, 489.

APPENDIX A

SOME OBSERVATIONS ON DATING TECHNIQUES

In this appendix, I present several observations on the techniques used in Chapter One to date moraines. After a brief note on the minimum number of sites necessary to characterize a moraine, I discuss the effects of climate, vegetation and rock type on boulder weathering in the Mono Basin. Following this, I make some observations on important factors that affect the usefulness of the CSV technique.

Number of sites

It was found useful to observe relative weathering features on boulders from at least three sites on each moraine, since variability in weathering characteristics between sites on one moraine is occasionally as large as that between moraines.

Factors that affect boulder weathering

There has been some disagreement about the effect of vegetation on granitic boulder weathering (Burke and Birkeland, 1979; Gillespie, 1982). In this study, where there were vegetational differences between moraines, they seemed to have a minor effect on weathering characteristics. This is especially noticeable at Grant Lake, where even though some moraines north of Reversed Peak are exclusively pine-covered, and others exclusively sagebrush-covered, reasonable correlations between the two groups were possible with RD. On the other hand, the presence of vegetation locally plays an important role in the development of weathering features. Some boulders at Hartley Springs

are covered with "fire flakes" (cobble-sized, plate-shaped boulder shards) that clearly crosscut oxidation fronts within affected boulders, and probably have "erased" weathered surfaces and weathering pits. Obviously, fire flakes could not develop where there is insufficient fuel in the form of vegetation.

Climatic differences may be important to the evolution of weathering features. The large degree of case-hardening at June and Grant Lakes may have been caused by fast, abrading winds there in glacial time, since the case-hardening is accompanied by ventifaction. Another factor that may contribute to case-hardening is greater rainfall. The June Lake area seems to receive more precipitation than other areas (Mono Basin Ecosystem Study Committee, 1987).

Lithology is as important as climate in influencing the style of boulder weathering. At June Lake and Reversed Peak, under both sagebrush- and pine-covered conditions, the coarse-grained Wheeler Crest Quartz Monzonite is clearly more susceptible to the development of weathering pits than other lithologies. Weathering-pit depths are therefore the relative-dating parameter most sensitive to age for this lithology. At Parker Canyon, medium-grained granite of Lee Vining Canyon is susceptible to granular disintegration, and therefore, grain-scale surface roughness is the RD parameter most diagnostic of age for that lithology.

Observations on the CSV technique

Mean CSV at Lundy Canyon, as well as at Green Creek in the Bridgeport Basin (Gillespie, 1982), reaches a minimum in Mono Basin stage deposits, and at Grant Lake, reaches a minimum in Tahoe stage deposits. This indicates that the CSV method arrives at the limit of its useful application in deposits

that are about 10^5 years old, because of case-hardening (at Green Creek and Grant Lake) and attrition of normally weathering boulders (at Lundy Canyon). Thus, the method locally does not seem to reach the 10^6-year limit envisioned by Crook (1986).

Crook and Gillespie (1982) found that the moraines of Bloody Canyon were anomalous relative to other deposits in terms of the regression coefficients of CSV vs. time (Table A-1). Notice that the time intercept and rate of decrease of CSV with time at Bloody Canyon are different from those at other sites in their study. They speculated that the difference was caused by lithology or climate. From this study, the values of the regression coefficients for Grant Lake and Parker Canyon seem to be similarly unusual, whereas the values for Lundy Canyon and Lee Vining Canyon are not. Since the main rock type at Bloody Canyon is not the same as that at Grant Lake but is the same as that at Lee Vining Canyon, these data suggest that climate rather than lithology influences CSV to follow a certain time history.

Table A-1. Comparison of CSV/age regression results with Crook and Gillespie (1986).[a]

Study area	$V_p(0)$, km/s[b]	$\frac{dV_p}{dt}$, km/s/log(yr)	r^2
San Gabriel Valley	3.148 ± 0.039	-0.353 ± 0.009	0.999
Cajon Pass	3.228 ± 0.294	-0.387 ± 0.072	0.991
Little Onion Valley	3.367 ± 0.118	-0.330 ± 0.026	0.997
Onion Valley	3.474 ± 0.183	-0.394 ± 0.044	0.986
Bloody Canyon	5.333 ± 0.019	-0.773 ± 0.004	0.999
Green Creek	3.979 ± 0.178	-0.446 ± 0.038	0.999
Parker Canyon	4.807 ± 0.049	-0.675 ± 0.100	0.978
Grant Lake	4.775 ± 0.073	-0.682 ± 0.103	0.956
June Lake	3.995 ± 0.058	-0.534 ± 0.083	0.977
Lee Vining Canyon	3.017 ± 0.098	-0.340 ± 0.140	0.855
Lundy Canyon	2.958 ± 0.161	-0.320 ± 0.132	0.856

[a] Parker Canyon, Grant Lake, June Lake, Lee Vining Canyon and Lundy Canyon from this study. All other data from Crook and Gillespie (1986). Errors from this study are one standard error (68% confidence interval). Others are 70% confidence interval.

[b] $V_p(0)$ is the value of V_p at $t = 0$. dV_p/dt is the rate of change of V_p. r^2 is the coefficient of determination for the regression of V_p vs. age.

APPENDIX B

FAULT-SCARP PROFILES

This appendix contains all scarp profiles used as data for Chapter Three. Each profile is plotted with the west side to the left.
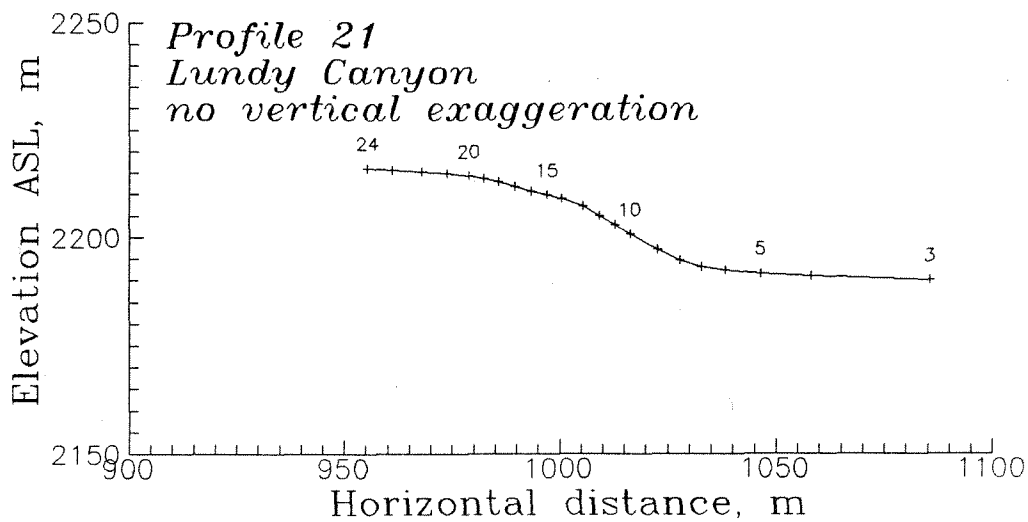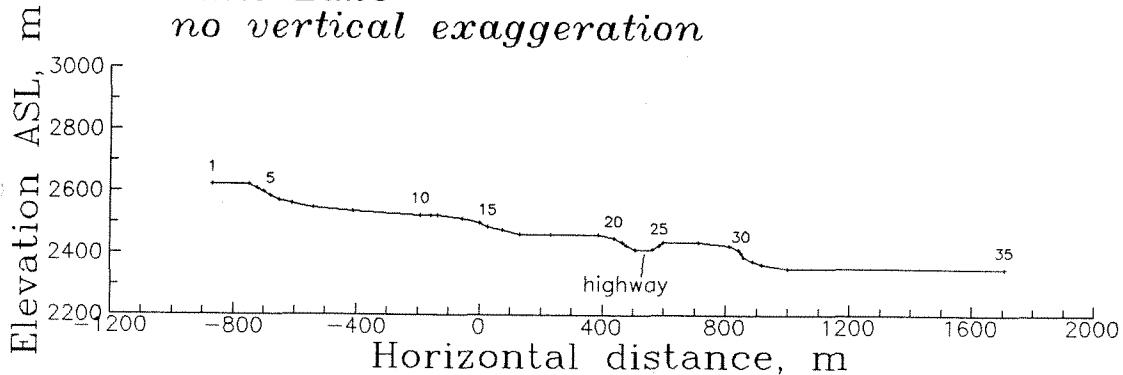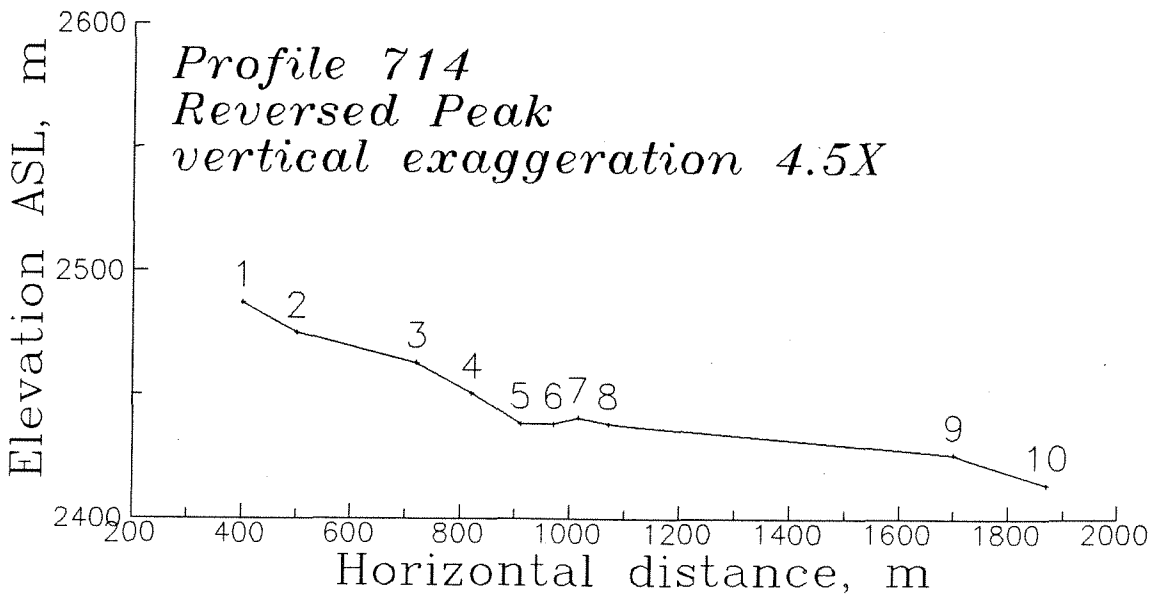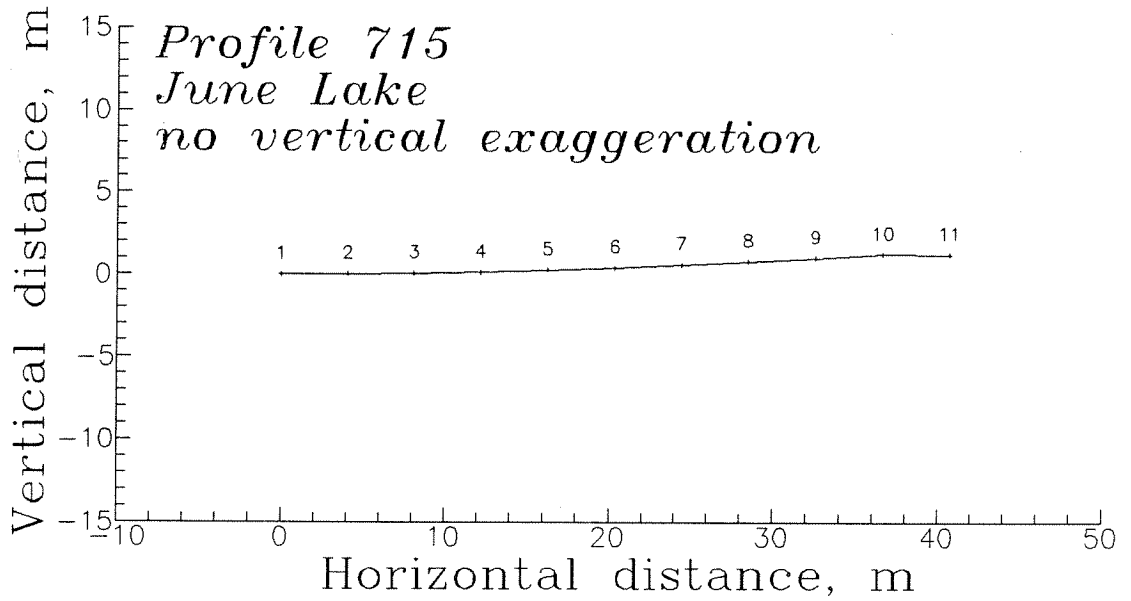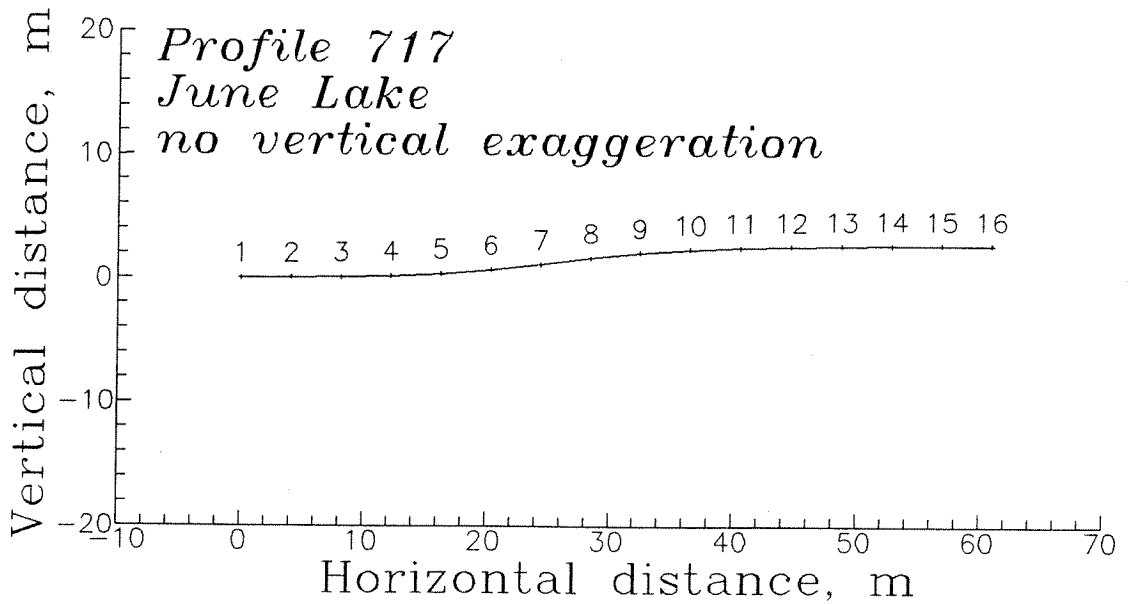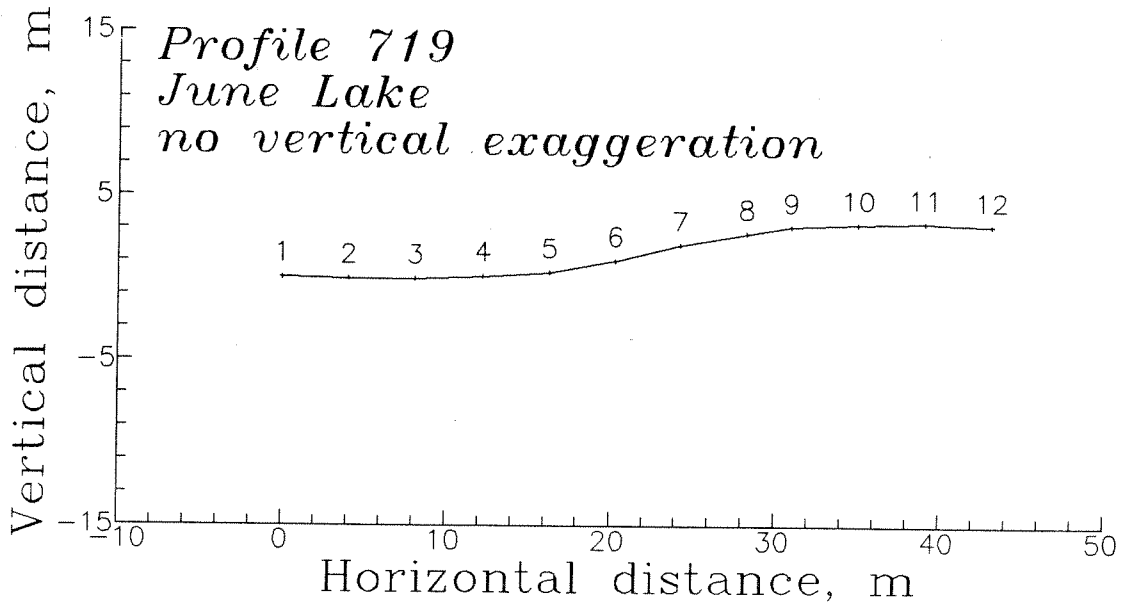
Figure B-1
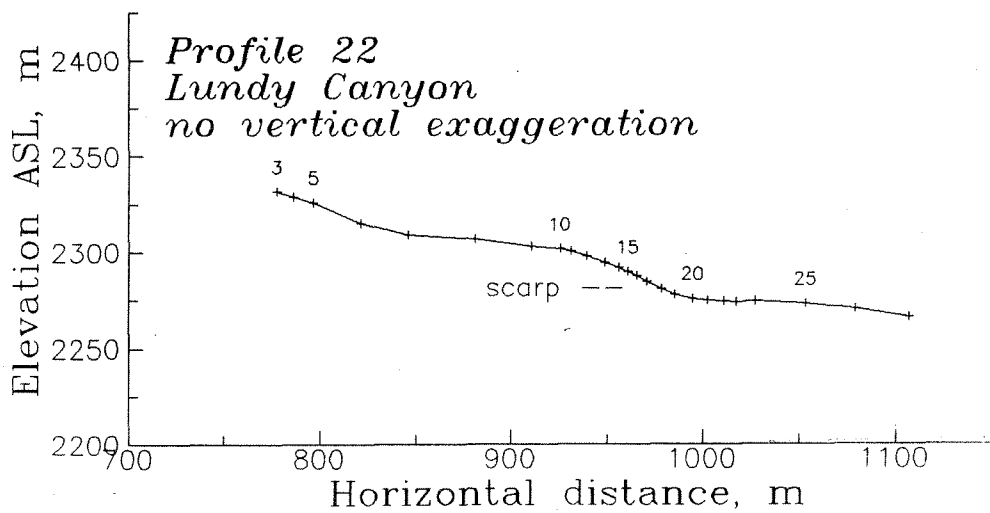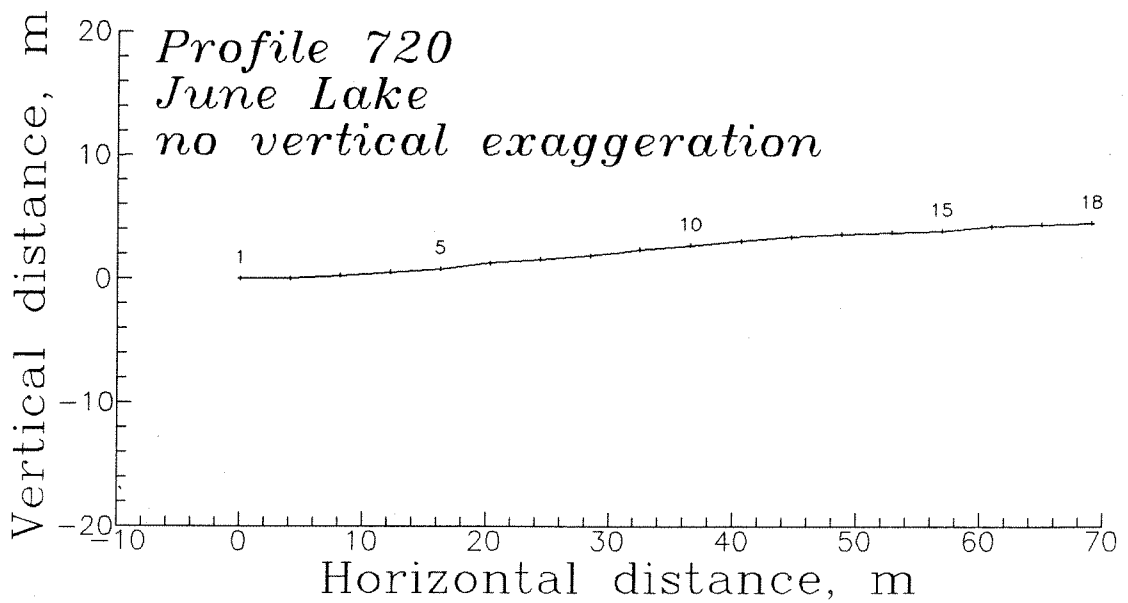

Figure B-2
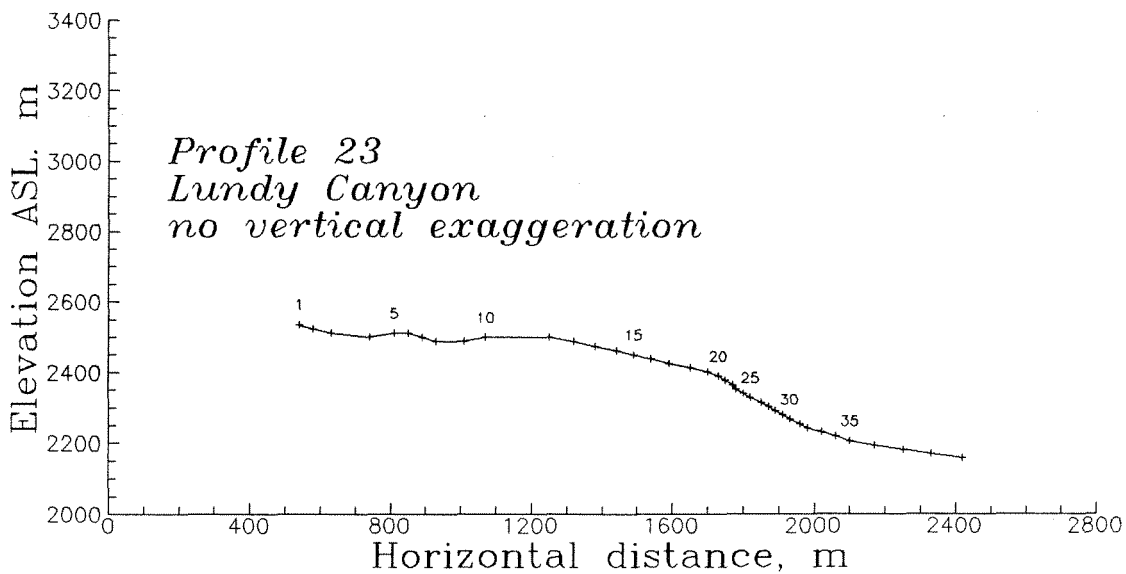
Figure B-3

Figure B-4

Figure B-5

Profile 41
Bloody Canyon
vertical exaggeration 3.25X

Horizontal distance, mi.

Figure B-6

Profiles 42 and 43
Bloody Canyon
vertical exaggeration 3.25X

TIOGA

43(MONO BASIN)

42(TAHOE)

Horizontal distance, mi.

Figure B-7

255
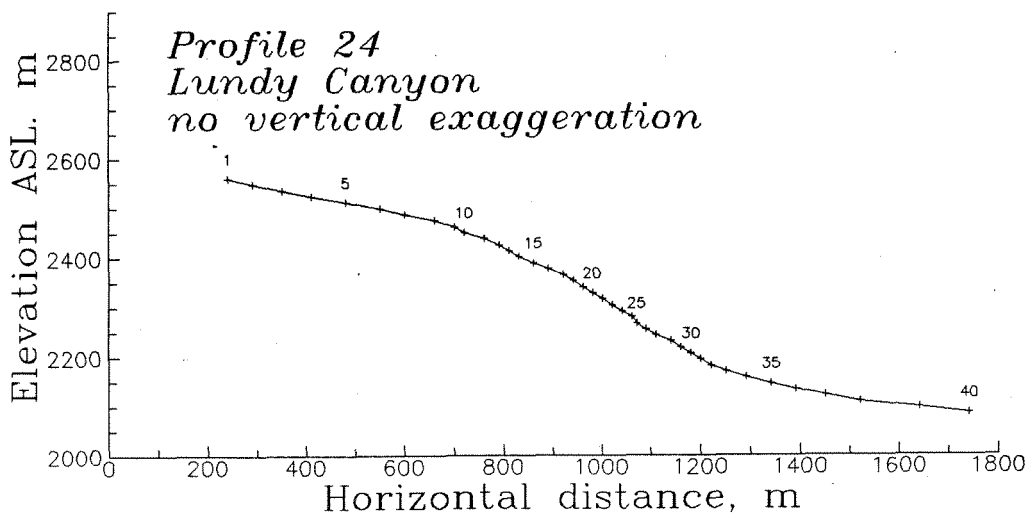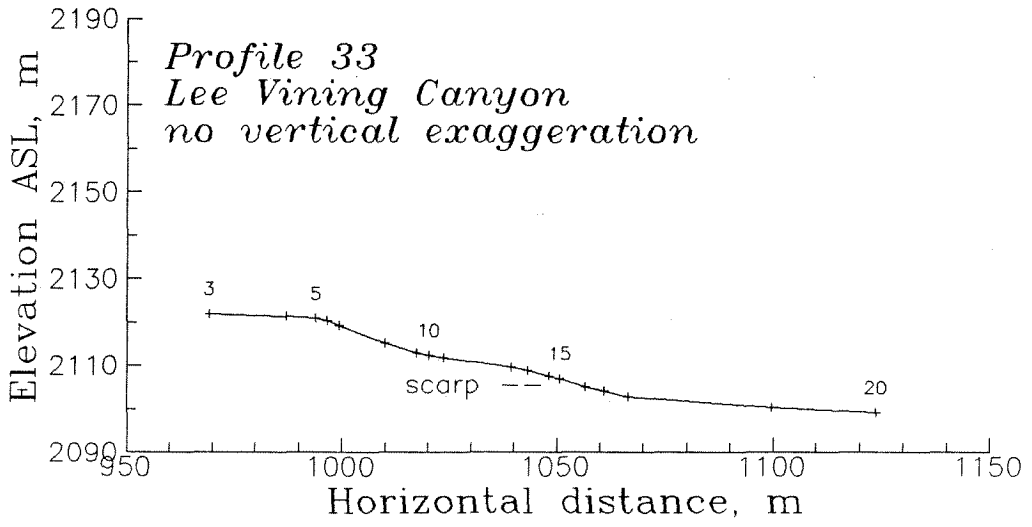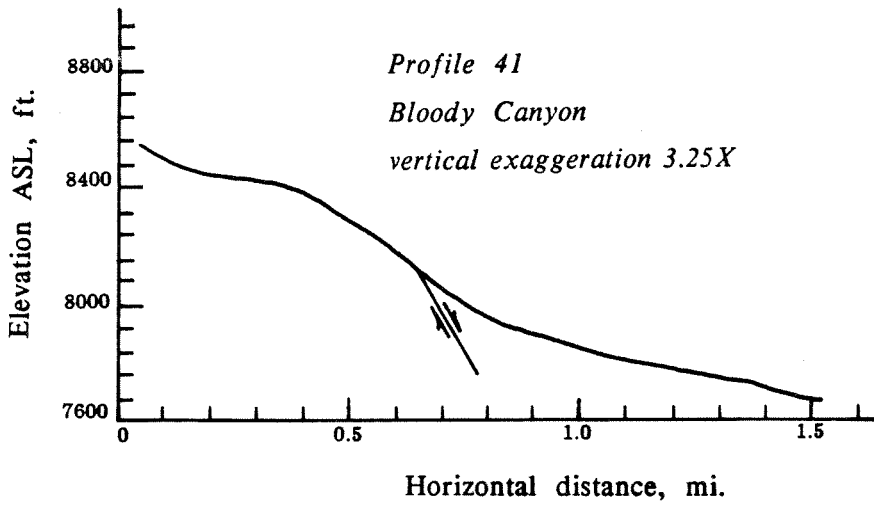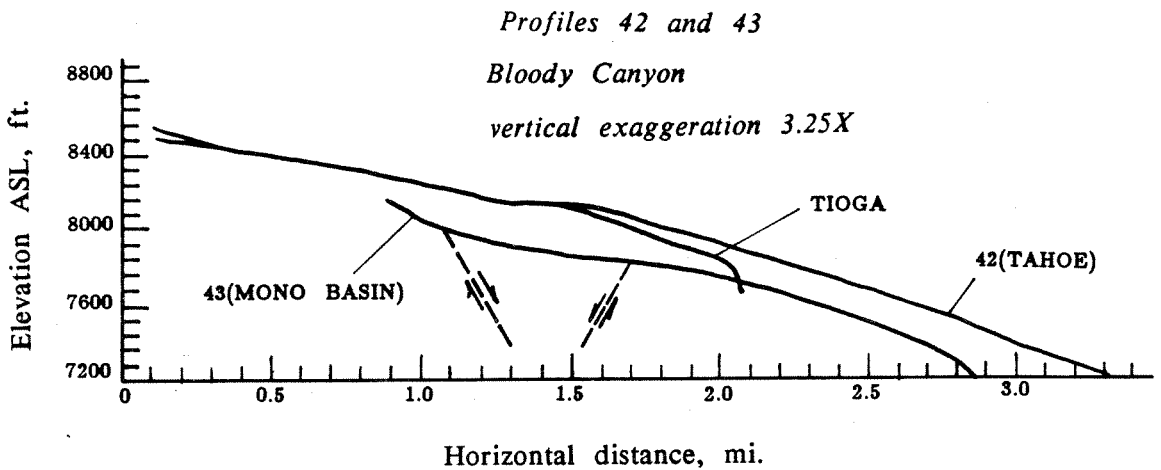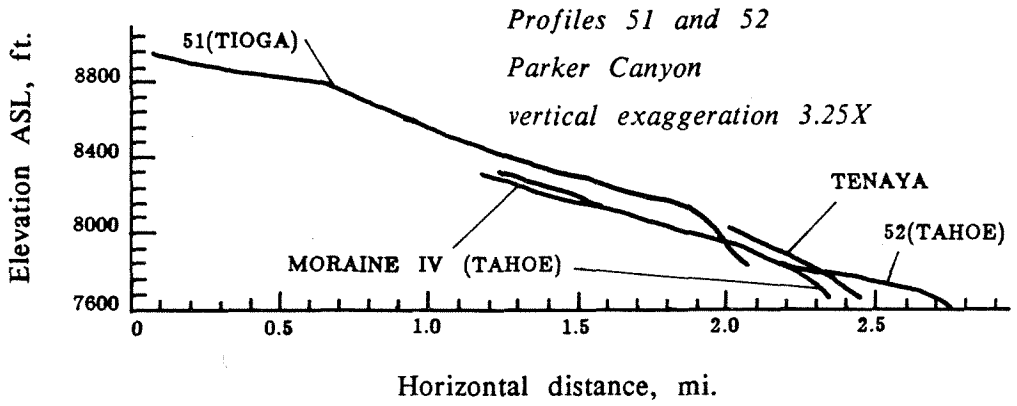
Figure B-8

Figure B-9

256
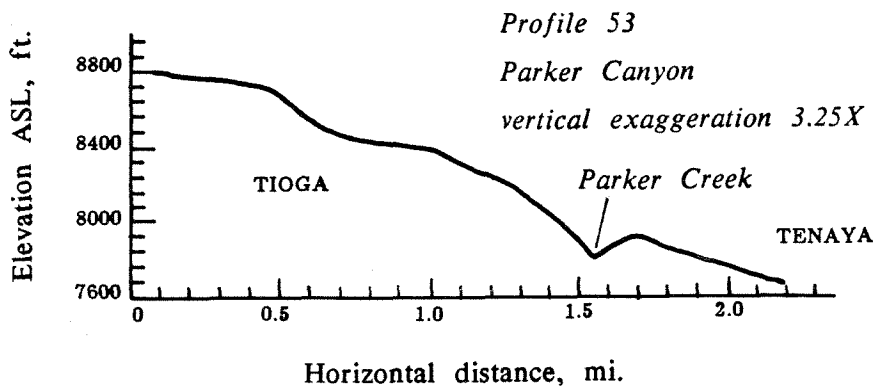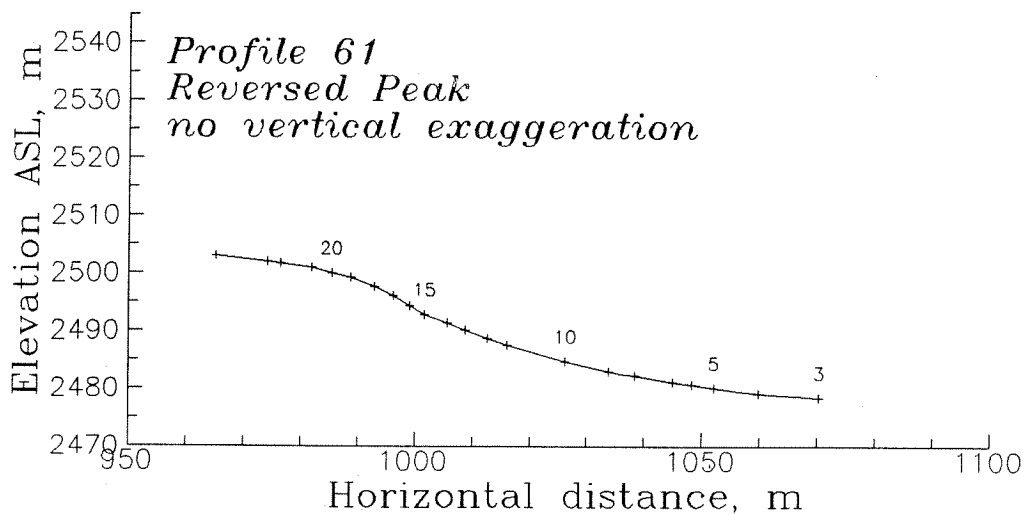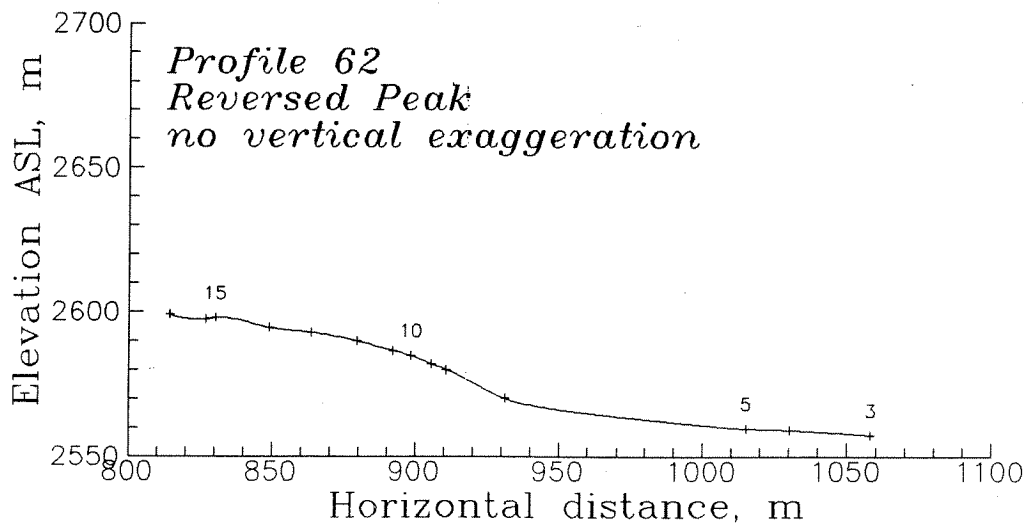
Figure B-10

Figure B-11

Figure B-12

Figure B-13

Profile 72
June Lake
no vertical exaggeration

Figure B-14
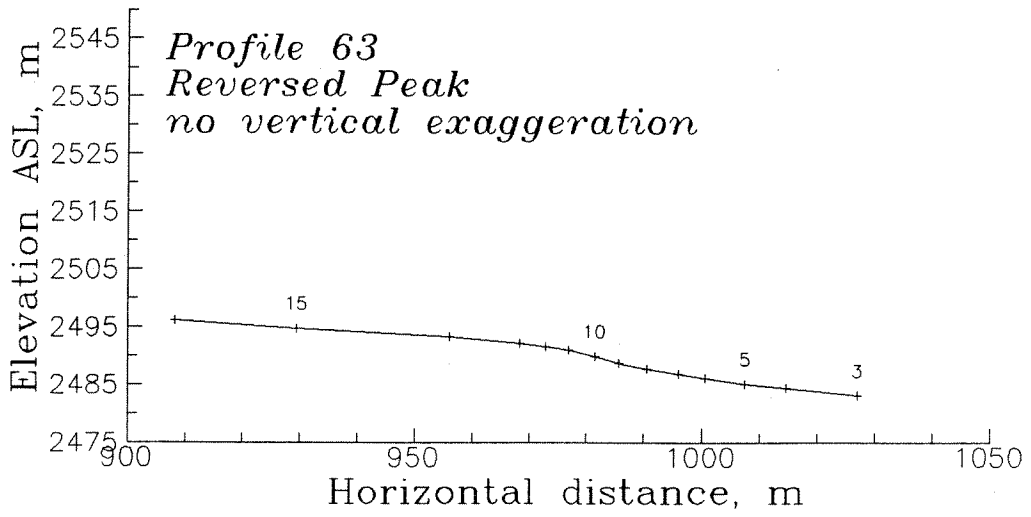
Profile 73
June Lake
no vertical exaggeration
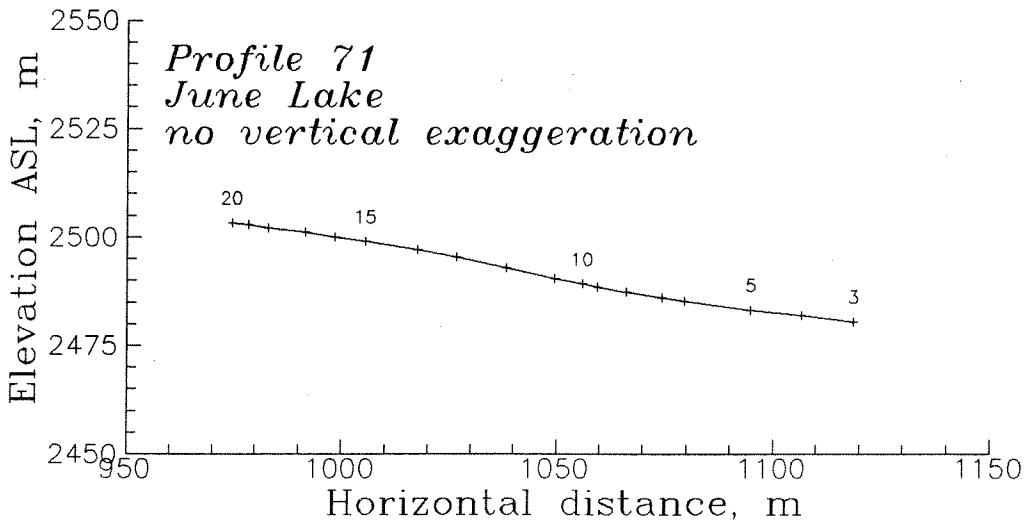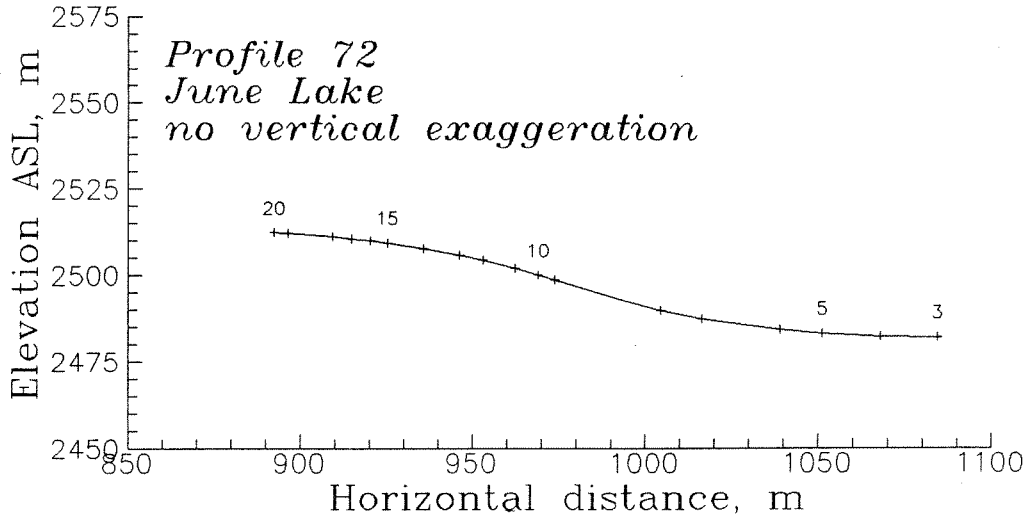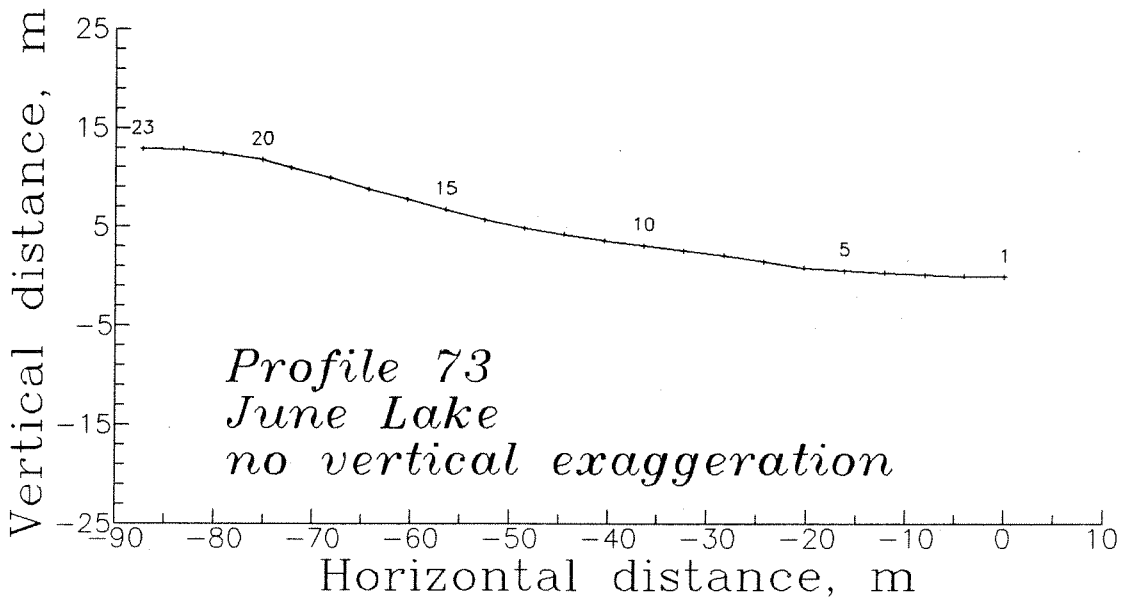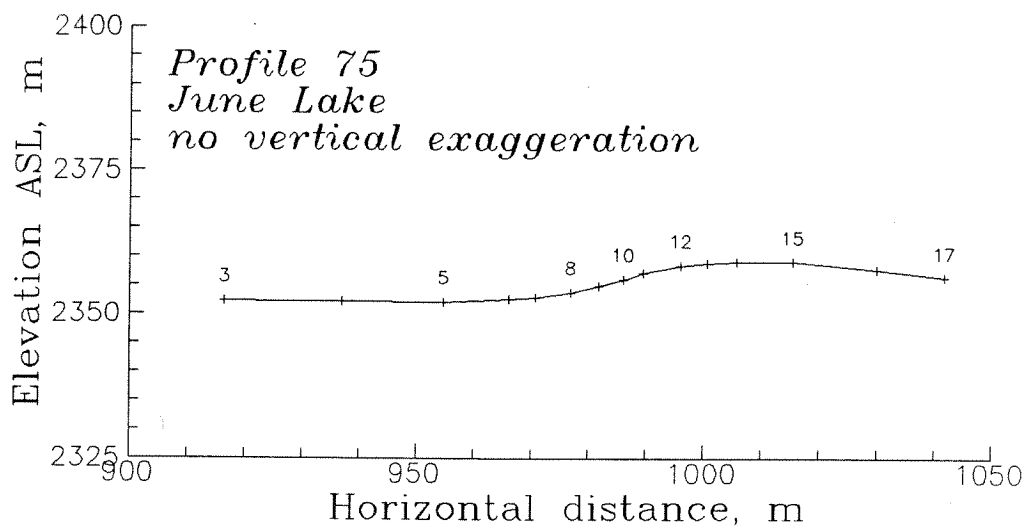
Figure B-15
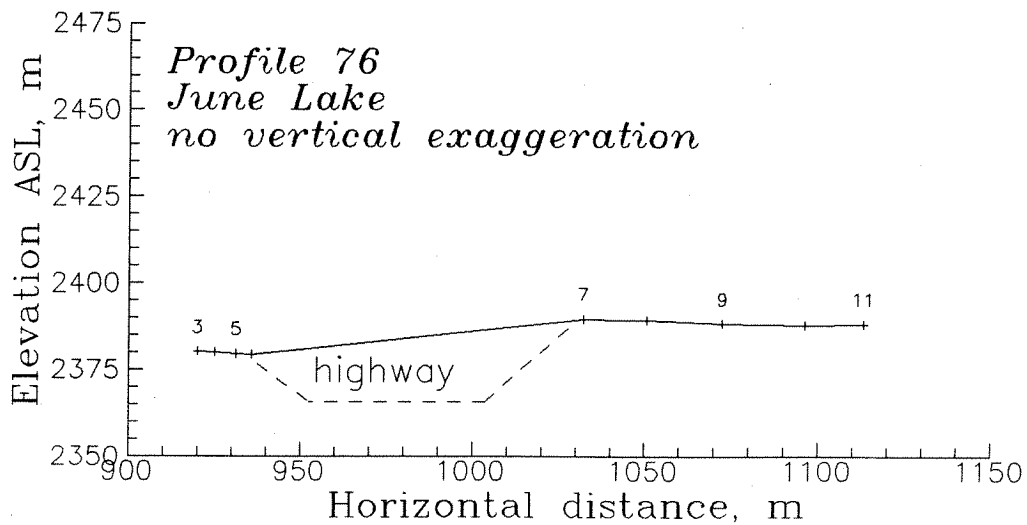
Figure B-16

Figure B-17
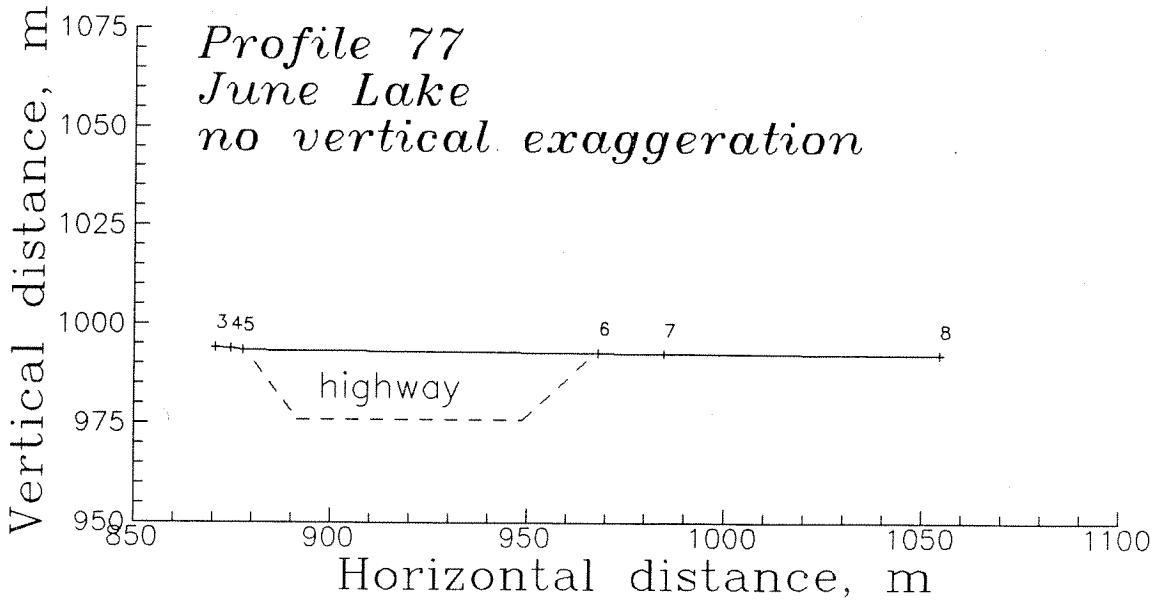
Figure B-18
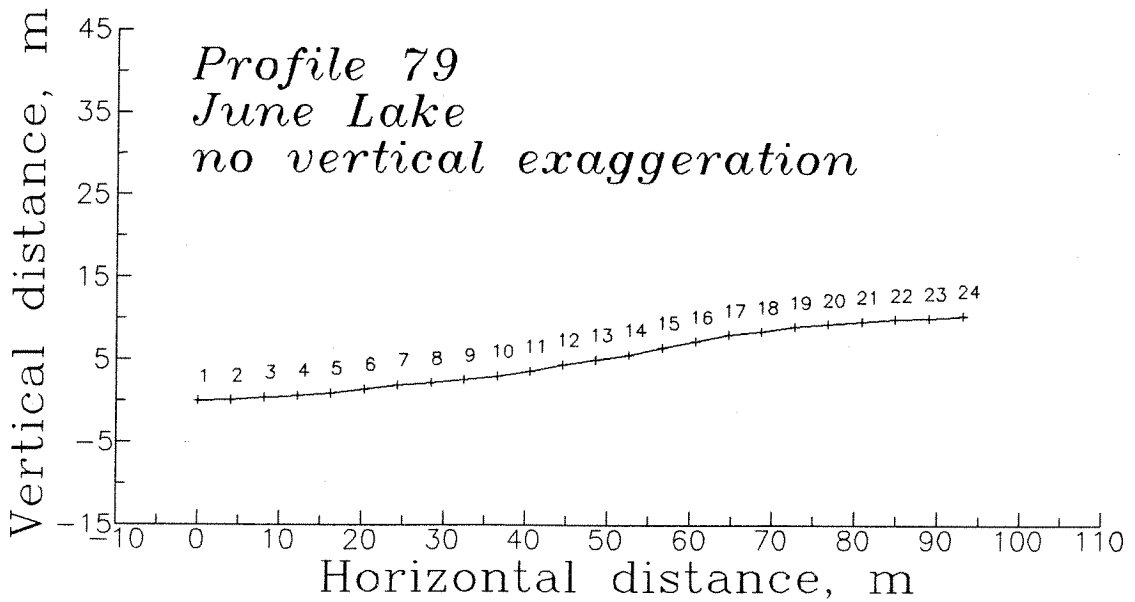
Figure B-19

Profiles 710, 711, 712
June Lake
no vertical exaggeration

Figure B-20

Profile 714
Reversed Peak
vertical exaggeration 4.5X

Figure B-21

Figure B-22

Figure B-23
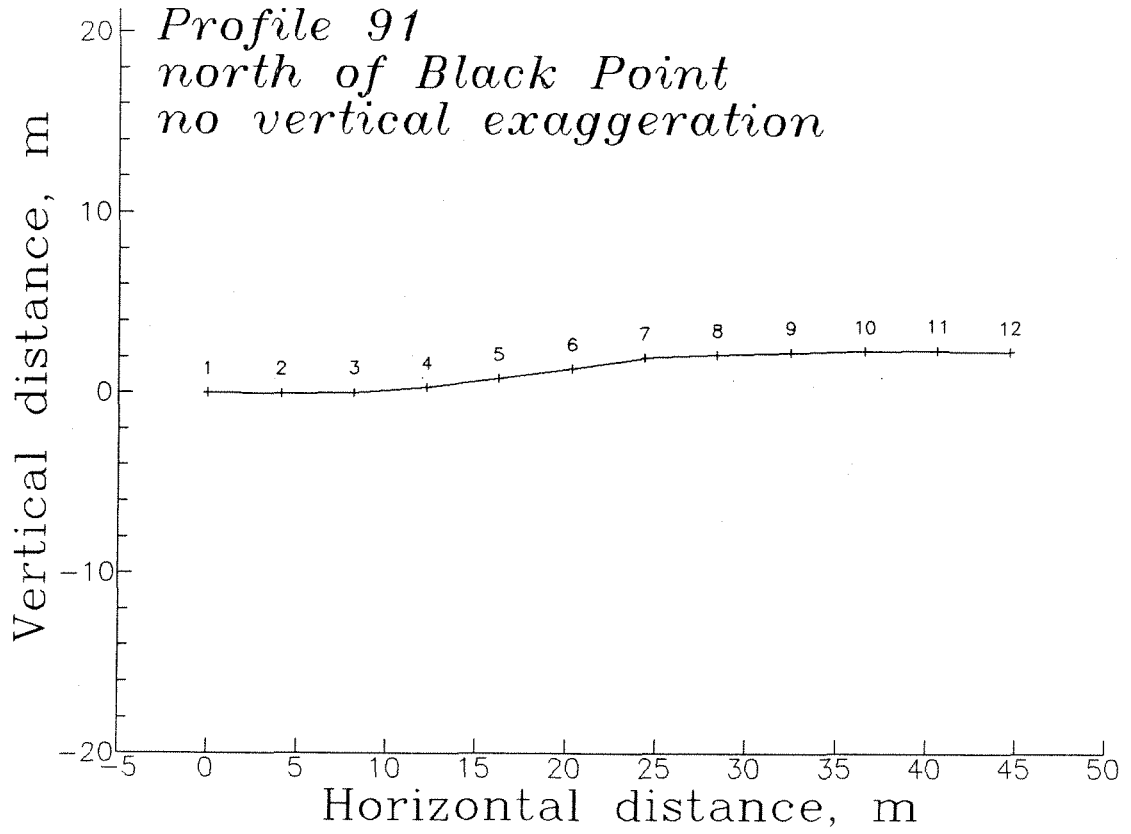
Figure B-24

Figure B-25
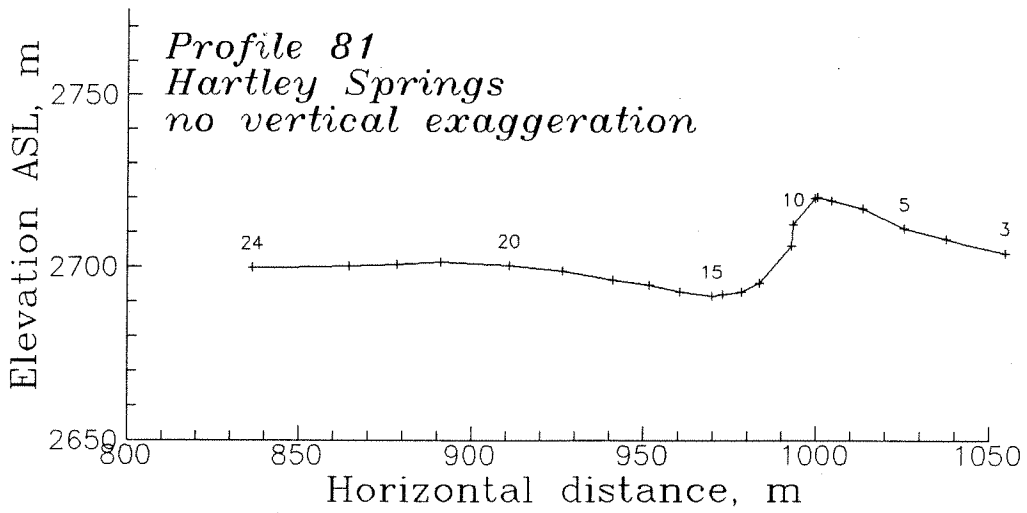
Figure B-26
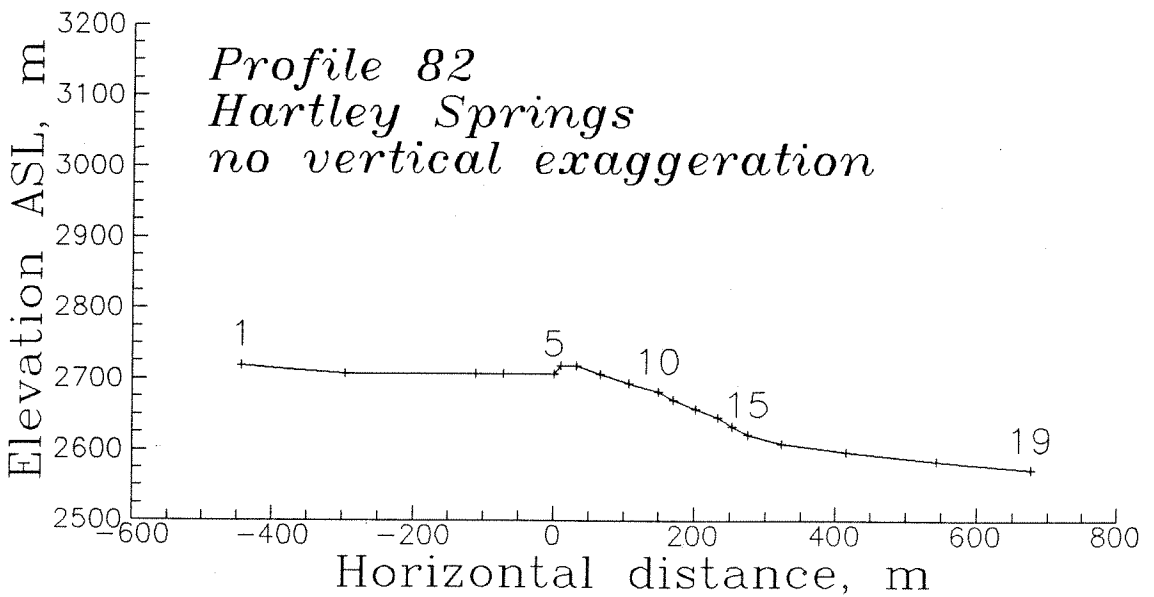
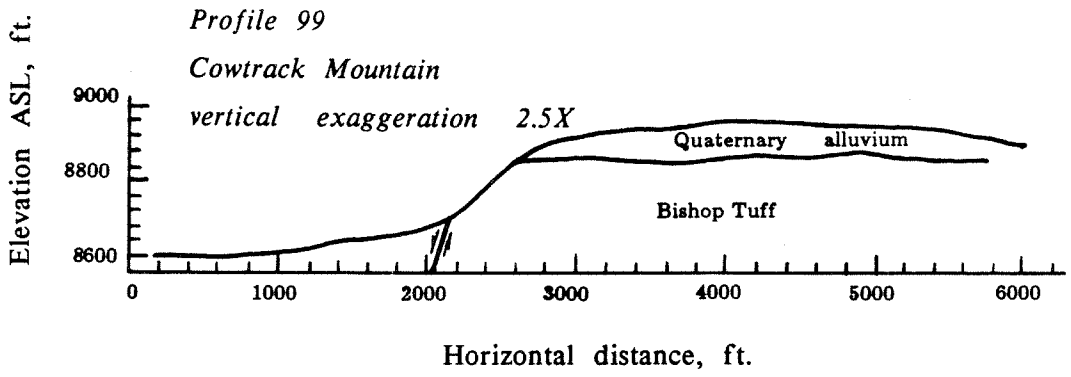**Figure B-27**

Figure B-28

Figure B-29

APPENDIX C

DERIVATION OF EQUATIONS IN CHAPTER 2

In this appendix, I derive two of the important equations that form a basis for the discussion in Chapter 2.

Derivation of the equation for t_0

From Andrews and Hanks (1985):

$$\kappa t_0 = M_2(0)/M_0,$$

where

$$M_n(\kappa t) = (1/n!) \int_{-\infty}^{\infty} x^n f(x, \kappa t) \ dx,$$

$M_n(\kappa t)$ is called the nth moment of the function $f(x, \kappa t)$. So, if $f_0(x)$ (Chapter 2) is a triangle, with slopes of $tan(\varphi_i)$, area A_0, x intercepts at $\pm a$ and z intercept at b, then:

$$M_0 = \int_{-\infty}^{\infty} f_0(x) \ dx$$

$$= \int_{-\infty}^{-a} 0 \ dx + \int_{-a}^{0} tan(\varphi_i)x + b \ dx + \int_{0}^{a} -tan(\varphi_i)x + b \ dx + \int_{a}^{\infty} 0 \ dx$$

$$= [tan(\varphi_i)x^2/2 + bx]\big|_{-a}^{0} + [-tan(\varphi_i)x^2/2 + bx]\big|_{0}^{a}$$

$$M_0 = -tan(\varphi_i)a^2/2 + ab - tan(\varphi_i)a^2/2 + ab$$

or, since $tan(\varphi_i)=b/a$,

$$M_0 = -(ab/2) + ab - (ab/2) + ab$$

$$= ab$$

$$M_0 = A_0.$$

Similarly, for $M_2(0)$:

$$M_2(0) = (1/2!)\int_{-\infty}^{\infty} x^2 f_0(x)\ dx$$

$$= \{\int_{-\infty}^{-a} 0\ dx + \int_{-a}^{0} x^2[tan(\varphi_i)x+b]dx + \int_{0}^{a} x^2[-tan(\varphi_i)x+b]dx$$

$$+ \int_{a}^{\infty} 0\ dx\}/2$$

$$= [\int_{-a}^{0} tan(\varphi_i)x^3+bx^2\ dx + \int_{0}^{a} -tan(\varphi_i)x^3+bx^2\ dx]/2$$

$$= \{[tan(\varphi_i)x^4/4 + bx^3/3]|_{-a}^{0} + [-tan(\varphi_i)x^4/4 + bx^3/3]|_{0}^{a}\}/2$$

$$= [-tan(\varphi_i)a^4/4 + ba^3/3 - tan(\varphi_i)x^4/4 + ba^3/3]/2$$

$$M_2(0) = -tan(\varphi_i)a^4/4 + ba^3/3.$$

But, since $a=[A_0/tan(\varphi_i)]^{1/2}$ and $b = [A_0 tan(\varphi_i)]^{1/2}$,

$$M_2(0) = -tan(\varphi_i)A_0^2/4[tan(\varphi_i)]^2 + A_0^2/[3tan(\varphi_i)]$$

$$= -A_0^2/[4tan(\varphi_i)] + A_0^2/[3tan(\varphi_i)]$$

$$M_2(0) = A_0^2/[12tan(\varphi_i)].$$

So:

$$\kappa t_0 = M_2(0)/M_0$$

$$\kappa t_0 = A_0/[12tan(\varphi_i)]$$

and

$$t_0 = A_0/[12\kappa tan(\varphi_i)].$$

Derivation of the equation for $tan(\varphi_{max})$

Differentiating equation (2.3),

$$z = hexp(-x^2/w^2),$$

yields

$$\partial z/\partial x = (-2x/w^2)hexp(-x^2/w^2)$$

$$\partial z/\partial x = -(2hx/w^2)exp(-x^2/w^2)$$

and

$$\partial^2 z/\partial x^2 = -(2h/w^2)exp(-x^2/w^2) - (2hx/w^2)(-2x/w^2)exp(-x^2/w^2)$$

$$\partial^2 z/\partial x^2 = (-2h/w^2 + 4hx^2/w^4)exp(-x^2/w^2).$$

Where $\partial^2 z/\partial x^2 = 0$, $\partial z/\partial x$ is at a maximum (or a minimum), so:

$$\partial^2 z/\partial x^2 = 0 = -2h/w^2 + 4hx^2/w^4$$

$$4hx^2/w^4 = 2h/w^2$$

$$x^2 = w^2/2$$

$$x = \pm\ w/2^{1/2}.$$

These are the values of x for which $\partial z/\partial x$ is at a maximum. Choosing $tan(\varphi_{max}) \geq 0$ yields:

$$tan(\varphi_{max}) = (\partial z/\partial x)_{max} = [2h(w/2^{1/2})/w^2]exp[-(w^2/2)/w^2]$$

$$= (2^{1/2}/w)he^{1/2}$$

$$tan(\varphi_{max}) = (2/e)^{1/2}(h/w).$$

Substituting the values for h and w from equation (2.2) results in:

$$tan(\varphi_{max}) = (2/e)^{1/2}.$$

$$[A_0/(4\pi\kappa\{t+[A_0/12\kappa tan(\varphi_i)]\})]^{1/2}(4\kappa\{t+[A_0/12\kappa tan(\varphi_i)]\})^{1/2}]$$

$$= (2/e)^{1/2}[A_0/(4\pi^{1/2}\kappa\{t+[A_0/12\kappa tan(\varphi_i)]\})]$$

$$tan(\varphi_{max}) = A_0/((8e\pi)^{1/2}\{\kappa t+[A_0/12 tan(\varphi_i)]\}).$$